# Natural Attenuation of Organic Contaminants: Integral Mass Flux Estimation and Reactive Transport Modelling in Heterogeneous Porous Media

Dissertation

zur Erlangung des Grades eines Doktors der Naturwissenschaften

der Geowissenschaftlichen Fakultät

der Eberhard-Karls-Universität Tübingen

vorgelegt von

Alexander Bockelmann

aus Hamburg

2002

# Natural Attenuation of Organic Contaminants:
# Integral Mass Flux Estimation and
# Reactive Transport Modelling in
# Heterogeneous Porous Media

ALEXANDER BOCKELMANN[1]

**Abstract:** Groundwater from porous media is an important resource for the drinking water supply and provisions more than one and a half billion people in the urban areas of the world alone. Nowadays, organic compounds originating from landfills, leaking underground storage tanks and pipelines, accidental spills, improper disposal techniques, and industrial discharges often contaminate groundwater resources. During the last decade it was shown that the remediation of contaminated groundwater using active remediation approaches was unable to achieve cleanup goals at many field sites. Consequently, passive remediation approaches were investigated, which are based on the natural attenuation and degradation of organic contaminants without human interference (natural attenuation approach). As a remediation strategy, this approach includes a detailed monitoring program (monitored natural attenuation) and requires the documentation of the reduction in contaminant concentrations or mass fluxes at field scale, as well as the identification of the mass flux reducing processes. Conventional mass flux investigation methods using a screen of multilevel wells quantify contaminant mass fluxes based on regionalized point-scale data and are hence subject to uncertainties in the results that increase with the spatial changes in contaminant concentrations and hydraulic parameters in the investigated aquifer. To overcome these limitations, this thesis documents the field scale application of a new **I**ntegral **G**roundwater **I**nvestigation **M**ethod (IGIM) that allows the estimation of field scale mass fluxes without the regionalization of point-scale data and which requires only a reduced number of monitoring wells for the site investigation. A comparison of the of new IGIM with a conventional multilevel mass flux estimation method at a field site with a dense monitoring network, showed a good agreement in the mass flux respective mass flux estimations. This demonstrates that the integral groundwater investigation can be a good alternative for the investigation of field scale contaminant mass fluxes. The IGIM was extended in this study to directly quantify field scale natural attenuation rates by measuring contaminant mass fluxes at two control planes located at different distances from a contaminant source. This approach was applied at a former **M**anufactured **G**aswork **P**lant (MGP) in Germany ("Testfeld Süd") which is contaminated by a complex mixture of monoaromatic and polyaromatic hydrocarbons since around 100 years. At the MGP site, the application of the integral groundwater investigation at two control planes allowed the identification of the major groundwater contaminants, the quantification of the compound-specific mass fluxes at different distances from the source, the estimation of the respective natural attenuation rate constants for the targeted compounds, and the localisation of the major contaminant plumes at the field site. In a second step, the contaminant transport between the investigated control planes was simulated utilizing a new modelling code that accounts for the diffusion limited intra-particle sorption of contaminants. The numerical transport modelling indicated that the biodegradation of the organic contaminants is nowadays the dominating mass flux reducing process at the MGP site. The reactive transport modelling was also used to investigate the sensitivity of the IGIM on the contaminant plume displacement during the pumping at a monitoring well. The results show that sorption / desorption processes occurring during the contaminant transport towards a pumping well can, under certain conditions, have an influence on the IGIM by changing the mobile mass flux that is measured at the monitoring well. This influence, however, decreases with the age of the investigated contaminant plume. It increases with the distance between the pumping well and the main contaminated aquifer region.

---

**Kurzfassung:** Grundwasser aus Sand- und Kiesaquiferen stellt in vielen Regionen der Welt eine wichtige Trinkwasserressource dar. Diese versorgt alleine in den urbanen Gebieten der Erde mindestens 1,5 Milliarden Menschen mit Trinkwasser. Gleichzeitig werden diese Trinkwasserressourcen durch Kontaminationen mit insbesondere organischen Schadstoffen bedroht. Potentielle Kontaminationsquellen für diese Schadstoffe sind u.a. undichte Mineralöltanks und Leitungen, Müllhalden, industrielle Unfälle sowie ungeeignete Entsorgungsmethoden oder Industrieabwässer und –emissionen.

In den letzten 10 Jahre zeigte sich bei der Sanierung kontaminierter Standorte, dass aktive Sanierungsmethoden häufig nicht die gewünschten Sanierungsziele erreichen konnten. Aus diesem Grunde wurden u.a. passive Sanierungsmethoden entwickelt, welche auf dem natürlichen Rückhalte- und Abbaupotential des Untergrundes aufbauen und auf dem natürlichen Schadstoffabbau im Grundwasser ohne menschliches Eingreifen basieren („Natural Attenuation Ansatz"). Dieser Ansatz beinhaltet im Rahmen einer Sanierung ein detailliertes Messprogramm, welches zum Ziel hat, die Reduktion der Schadstofffrachten in Fließrichtung in Raum und/oder Zeit zu dokumentieren. Des weiteren müssen begleitende Modellierungen und/oder Experimente den biologischen Abbau der organischen Schadstoffe am Standort nachweisen, um zu demonstrieren, dass die Schadstoffe effektiv abgebaut und nicht nur sorbiert bzw. retardiert werden.

Konventionelle Feldmethoden zur Bestimmung der Schadstofffracht verwenden dabei Multilevel-Messstellen, welche entlang einer Kontrollebene installiert sind. Die gemessenen punktuellen Schadstoffkonzentrationen werden im Rahmen der Frachtenbestimmung regionalisiert, wodurch eine Methodenunsicherheit entsteht, welche mit der räumlichen Variabilität der Schadstoffkonzentrationen und Aquifereigenschaften um die jeweiligen Multilevel-Messpunkte herum ansteigt.

Um diese Unsicherheiten zu überwinden wurde eine neue integrale Grundwasser-Erkundungsmethode (INGWER) entwickelt, welche im Gegensatz zum Multilevel-Ansatz keine Punktwerte regionalisiert, sondern die Schadstoffmassenflüsse integral bestimmt und eine im Vergleich deutlich reduzierte Anzahl von Messstellen zur Felderkundung benötigt. An einem ehemaligen Gaswerkstandort („Testfeld Süd") wurde der integrale Ansatz im Rahmen dieser Dissertation zur Quantifizierung von Schadstoffmassenflüssen und Natural Attenuation-Raten implementiert und erlaubte die Identifikation der Hauptschadstoffe am Standort sowie eine Darstellung ihrer wahrscheinlichen Verteilung im Untergrund. Darüber hinaus wurde INGWER erweitert, um erstmalig Abbauratenkonstanten basierend auf integral ermittelten Schadstofffrachten direkt im Feldmaßstab zu quantifizieren. Dafür wurden zwei Kontrollebenen in unterschiedlicher Entfernung zum Schadensherd installiert und die gemessene Reduktion der stoffspezifischen Massenflüsse zur Berechung der Abbauratenkonstanten verwendet.

Eine anschließende Transportmodellierung im Feldmaßstab ermöglichte die Identifizierung des biologischen Schadstoffabbaus als den dominierenden Prozess, welcher heutzutage an diesem Standort für die gemessene Frachtenreduktion verantwortlich ist. Die Modellierung des Sorptionsverhaltens basierte dabei auf einem diffusionslimitierten Sorptionsprozess im Intrapartikelraum des Aquifermaterials.

Die reaktive Transportmodellierung wurde darüber hinaus für die Untersuchung des Einflusses der Schadstofffahnenverschiebung auf die integrale Massenflussbestimmung verwendet, welche während des Pumpens einer Grundwassermessstelle durch die Veränderung der Grundwasserströmung im Aquifer auftritt. Numerische Experimente zeigten dabei, dass Sorptions- / Desorptionsprozesse unter bestimmten Bedingungen durch die Veränderung der transportierten mobilen Schadstofffracht einen Einfluss auf die integrale Schadstofffrachtbestimmung haben können. Es zeigte sich, dass dieser Einfluss mit dem Alter der Schadstofffahne abnimmt und mit der Entfernung des Pumpbrunnens zur Schadstofffahne zunimmt.

# Acknowledgements

# Table of Contents

v

# List of Tables

# List of Figures

# Nomenclature

Dimensions: Length [L], Mass [M], Pressure [P], and Time [T]

| | | |
|---|---|---|
| A | Area in a cross-section | $[L^2]$ |
| b | Aquifer thickness | [L] |
| C | Concentration of a compound in a medium | $[ML^{-3}]$ |
| $C_a$ | Concentration of a compound in soil gas | $[ML^{-3}]$ |
| $C_{aq}$ | Dissolved contaminant concentration | $[ML^{-3}]$ |
| $C_g$ | Concentration of a contaminant in groundwater | $[ML^{-3}]$ |
| $C_{pi}$ | Concentration measured at a pumping well | $[ML^{-3}]$ |
| $C_s$ | Equilibrium concentration on a solid phase | $[ML^{-3}]$ |
| $C_{si}$ | Contaminant concentration in a streamtube | $[ML^{-3}]$ |
| $C_{xi}$ | Theoretical average concentration of two streamtubes | $[ML^{-3}]$ |
| D | Diffusion coefficient | $[L^2T^{-1}]$ |
| $D^*$ | Molecular diffusion coefficient | $[L^2T^{-1}]$ |
| $D_a$ | Apparent diffusion coefficient | $[L^2T^{-1}]$ |
| $D_l$ | Longitudinal dispersion coefficient | $[L^2T^{-1}]$ |
| $d_{10}$ | Mesh sieve size where 90% of the sample mass is retained | [L] |
| $d_{60}$ | Mesh sieve size where 40% of the sample mass is retained | [L] |
| E | Total error of an estimation | [%] |
| $f_{oc}$ | Fraction of organic carbon in a media | [-] |
| F | Diffusive mass flux | $[ML^{-2}T^{-1}]$ |
| $F_t$ | Total mass flux of a compound at a groundwater fence | $[MT^{-1}]$ |
| G | Facies type: gravel | |
| Gm | Facies type: bimodal gravel with a fine grain matrix | |
| h | Elevation of the hydraulic head | [L] |
| H | Henry's Law constant | $[PML^{-3}]$ |
| $I_t$ | Integral mass discharge | $[MT^{-1}]$ |
| K | Hydraulic conductivity of a porous media | $[LT^{-1}]$ |
| k | Overall attenuation rate constant | $[T^{-1}]$ |
| $K_d$ | Equilibrium distribution coefficient | [-] |
| $K_{Fr}$ | Freundlich coefficient | $[(L^3M^{-1})^{1-1/N}]$ |
| $K_L$ | Langmuir equilibrium coefficient | $[MM^{-1}]$ |
| $K_{ow}$ | Octanol-water partition coefficient | [-] |
| l | Distance between two measuring points | [L] |
| MF | Integral contaminant mass flux across a control plane | $[MT^{-1}]$ |
| $M_d$ | Total mass discharge from a source zone | $[MT^{-1}]$ |
| $n_e$ | Effective porosity of a porous media | [-] |
| 1/N | Feundlich exponent | [-] |
| N | Number of isochrones in a well capture zone | [-] |
| q | Specific discharge or volumetric flow rate per unit area | $[LT^{-1}]$ |
| Q | Volumetric flow rate | $[L^3T^{-1}]$ |
| $Q^0$ | Maximum sorptive capacity | [M] |
| R | Retardation factor | [-] |
| r | Radius of an isochrone | [L] |
| S | Facies type: sand | |
| t | Time | [T] |
| T | Transmissivity | $[L^2T^{-1}]$ |
| v | Linear groundwater velocity | $[LT^{-1}]$ |
| $v_c$ | Average velocity of a solute in a porous media | $[LT^{-1}]$ |

## Acronyms

| | |
|---|---|
| ACE | Acenaphthene |
| ANY | Acenaphthylene |
| ANT | Anthracene |
| BTEX | Benzene, Toluene, Ethylbenzene, o,m,p-Xylene |
| CHR | Chrysene |
| CSIA | Compound-specific Stable Isotope Analysis |
| CP | Control Plane |
| FLR | Fluorene |
| FTH | Fluoranthene |
| IGIM | Integral Groundwater Investigation Method |
| MGP | Manufactured Gas Plant |
| MNA | Monitored Natural Attenuation |
| MTBE | Methyl Tert-Butyl Ether |
| NA | Natural Attenuation |
| NAP | Naphthalene |
| NAPL | Non Aqueous Phase Liquids |
| PAH | Polycyclic Aromatic Hydrocarbons |
| PCE | Tetrachloroethane |
| PHE | Phenanthrene |
| RMS | Root Mean Squared error |
| TCE | Trichloroethane |
| TMB | Tri-Methyl-Benzenes |
| UST | Underground Storage Tank |
| VC | Vinyl Chloride |
| VOC | Volatile Organic Compounds |

## Greek Symbols

| | | |
|---|---|---|
| $\nabla$ | Directional derivative of a variable (Nabla operator) | |
| $\alpha$ | Capacity factor | [-] |
| $\alpha_l$ | Dispersivity | [L] |
| $\rho$ | Bulk density of a porous media | [$ML^{-3}$] |
| $\lambda$ | First-order natural attenuation rate constant | [$T^{-1}$] |
| $\varepsilon$ | Effective intra-particle porosity | [-] |
| $\tau_f$ | Tortousity factor | [-] |
| $\mu$ | Dynamic viscosity | [$ML^{-1}T^{-1}$] |
| $\omega$ | Empirical coefficient for the calculation of $D_a$ | [-] |

# 1 Introduction

## 1.1 Research significance

Groundwater represents about 97% of the existing fresh-water resources, excluding fresh water stored in polar ice caps. These groundwater resources are used for the drinking water supply of more than one and a half billion people in the urban parts of the world alone (World Bank, 1999; Shiklomanov, 1997). Reasons for the extensive use of groundwater resources include the relatively small investment costs required for their development and their higher reliability compared to the often seasonally changing quantity and quality of surface waters. Moreover, due to the filtration of percolating water by geological media, groundwater is generally of a higher quality then surface water.

Inasmuch as groundwater provides drinking water for so many people, its sustainable development, protection and remediation is of paramount importance. Groundwater can fail to meet drinking water standards due to dissolved constituents originating from either natural or anthropogenic sources. Typical examples of constituents coming from natural sources are dissolved solids, sulfate, and chloride. However, at a large scale and from a public health point of view, groundwater quality is more severely threatened by anthropogenic influences.

Anthropogenic sources of groundwater contamination such as landfills, improper disposal techniques of industrial wastes, industrial discharges, accidental spills and leaking underground storage tanks primarily contaminate groundwater resources with organic compounds (Schiedek et al., 1997

and Figure 1.1). In the United States alone there is a reported number of 412.000 leaking underground storage tanks spilling petroleum hydrocarbons into the subsurface (U.S. EPA, 2000a).

Industrial processes can often be linked to groundwater contamination. Since the early 1800s for example, gas was the main energy source for many cities and towns. It was mostly manufactured locally through the capture of combustible gas generated from coke, coal or oil. Former **M**anufactured **G**as **P**lants (MGPs) are hence a common feature in many large towns and cities. Fischer et al. (1999) estimate that between the 1920s and the 1930s about 10.000 MGPs were in operation throughout North America and Europe.

In the gas manufacturing process, however, large quantities of waste were produced. Today such wastes can be found in the soil and groundwater at virtually every major MGP (Merkel, 1996). The subsurface contamination at such sites usually comprises a complex mixtures of PAH (**P**olycyclic **A**romatic **H**ydrocarbons) and often BTEX (**B**enzene, **T**oluene, **E**thylbenzene and **X**ylenes) compounds. Many of these compounds have been shown to act carcinogenic, toxic, and/or mutagenic, thus generating a considerable hazard to the environment in general and mankind in particular.

In the next 30 years, the clean up costs for the former MGPs in the United States could add up to between $25-75 billion (Murarka, 1995) and reach around DM10 billion for former MGPs in West-Germany.
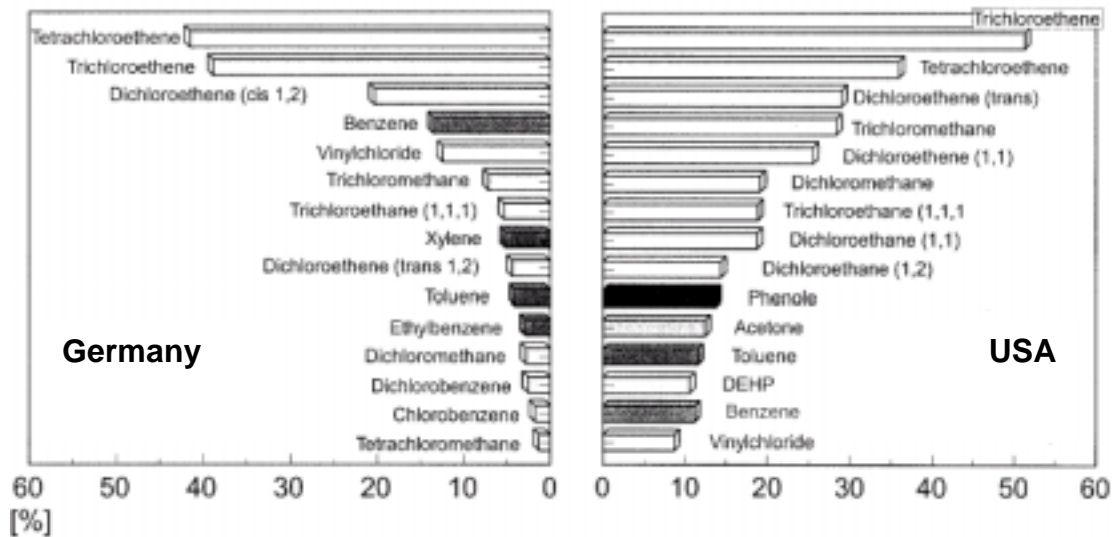
Figure 1.1: The 15 most frequently detected organic compounds at contaminated sites in Germany and the Unites States (modified from Teutsch, 1999)

Confronted with severe public health and environmental problems and the immense remediation costs associated with site cleanups, it is not surprising that subsurface investigation techniques, remediation technologies and groundwater risk assessments became a focus of today's research in hydrogeology and related environmental sciences.

In this context, the scale-dependencies of different investigation technologies and approaches are problematic. Especially the up-scaling of data obtained from controlled laboratory experiments to the field scale can introduce significant uncertainties into the data interpretation. Reliable site-specific quantifications of environmental processes such as contaminant degradation in groundwater are therefore only possible through in-situ investigation approaches, which quantify the studied processes at the field scale under field conditions. But this is often difficult to perform especially in heterogeneous systems, where conditions and environmental parameters vary spatially and/or temporally at small scales. Under such conditions conventional point scale investigation techniques are difficult to

employ because the obtained data is only representative for a small volume around the sampling location and individual data point have to be regionalized. This can lead to erroneous results if heterogeneous conditions are encountered. Due to the limitations inherent to such investigation and measuring techniques, the development of new and reliable site investigation techniques is one of the current research needs in the field of hydrogeology.

This thesis focuses on the development and field scale application of new field scale investigation and modelling techniques (Figure 1.2), which can provide reliable information about the contaminant fate and transport in homogeneous and heterogeneous aquifer systems without the need of data regionalization. The investigation and modelling techniques employed can for example be used for the documentation of the natural contaminant reduction at a field site, as well as during active and passive remediation projects, which require (a) the documentation of field scale mass flux reductions in a contaminated aquifer and (b) require a reactive transport model concept to predict contaminant transport at the field site.
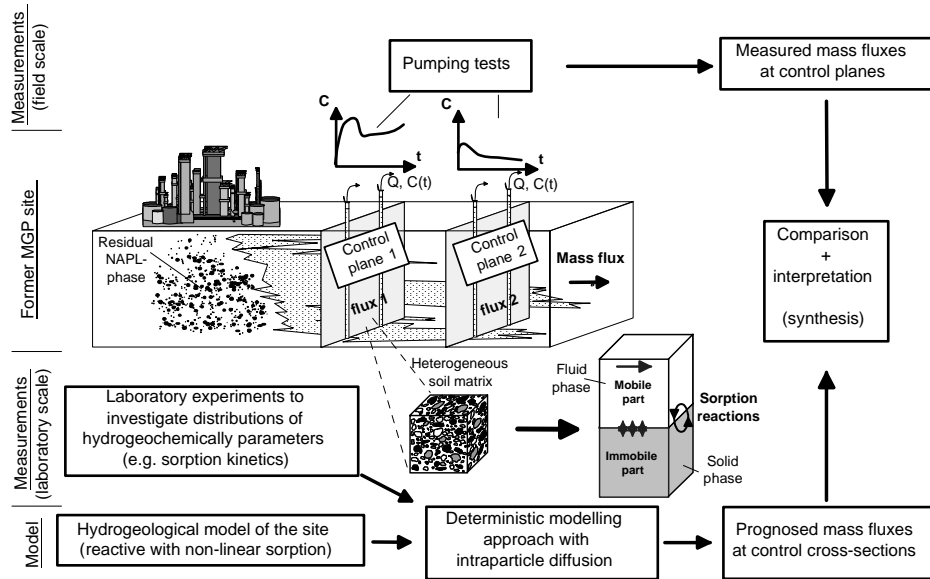
Figure 1.2: Concept of the conduced research at a former manufactured gas plant in south-west Germany. Research included field measurements (integral groundwater investigation), laboratory scale experiments (estimation of sorption kinetics with aquifer material), and reactive transport modelling of acenaphthene as the model contaminant (modified from Herfort et al., 1999).

## 1.2   Research objectives

In order to understand and quantify the fate and transport of organic contaminants in groundwater and to allow for the selection and implementation of cost-effective remediation schemes, it is necessary to develop reliable site investigation techniques that allow to measure and monitor contaminant mass fluxes and their spatial distributions in the groundwater.

This thesis focuses on the development and application of such new investigation and modelling techniques at the field scale.

These new techniques are applied during this study at a former manufactured gas plant ("Testfeld Süd") located in the Neckar river valley in south-west Germany (Figure 1.3) to investigate the transport and natural attenuation of organic groundwater contaminants, including BTEX and PAH compounds.

The investigated alluvial sand and gravel aquifer system is typical for many river valley aquifer systems in southern Germany.
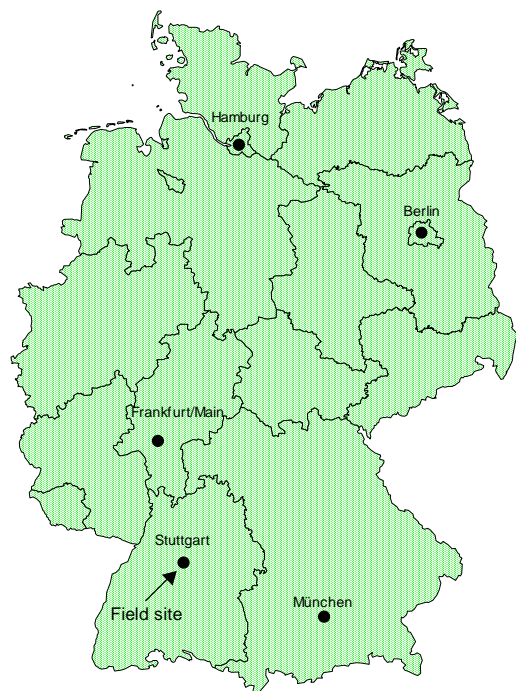


Figure 1.3: Location of the field site.

A special research focus in this thesis was on:

1. The first-time field scale application of a novel groundwater investigation technique utilizing two control planes situated at increasing distances downstream of contaminant source zones at a former manufactured gas plant (MGP) site in Germany.

2. The quantification of compound-specific field scale mass fluxes of the organic groundwater contaminants at the former MGP site and the identification of the persistent mobile contaminants that pose the greatest environmental hazard to downgradient receptors.

3. The estimation of field scale natural attenuation rate constants for the target contaminants based on the in-situ measured reduction of contaminant mass fluxes in flow direction at the MGP site.

4. The characterisation and localisation of the contaminant plumes migrating downgradient from the source zone at the MGP site.

The exact localisation and characterization of the contaminant sources using conventional investigation approaches is not possible at the site (Zamfirescu, 2000). The information gained through this research allows for the development of efficient remediation strategies, which require an extensive knowledge about the location and composition of the contaminant plumes in the groundwater.

5. The independent determination of the importance of sorption and biodegradation processes on the reduction of contaminant mass fluxes in flow direction.

If sorption is the dominant factor the migration of the contaminant mass at the site would only be retarded, causing severe public health and environmental concern in the future. On the other hand, biodegradation as the major transport controlling factor would cause an effective reduction in contaminant mass, reducing also the environmental hazard caused by the groundwater contamination.

6. Modelling of the field scale transport of organic groundwater contaminants at the MGP site, accounting for diffusion limited non-linear sorption of the groundwater contaminants during the transport in flow direction.

This thesis documents the first-time field scale application of a new transport model code at a real world field site, which utilizes a facies approach in which independent sorption parameters can be attributed to individual geological facies that make up the aquifer at the studied field site. The transport code was numerically tested by Herfort (2001) utilizing artificial aquifer scenarios and laboratory-scale column tests.

7. A high resolution application of the new integral groundwater investigation approach at an underground storage tank (UST) site at the Canadian Forces Base in Ontario, Canada, and a comparison of the integral mass flux estimations with the results from a conventional high resolution multilevel mass flux estimation method that was simultaneously applied at the field site.

8. Characterization of the impact of sorption on the integral groundwater investigation technique employed throughout this study.

If sorption / desorption processes significantly influence the mobile contaminant mass that is transported towards a pumping well, the integral groundwater investigation could yield erroneous results with regard to the field scale mass flux estimation.

The information gained in this research through the numerical transport modelling and the simulation of long-term pumping tests in homogeneous and heterogeneous porous aquifers allows to quantify the possible influence of reactive transport processes occurring during the plume displacement initiated by an extensive pumping test. These effects are numerically investigated for different plume and aquifer conditions.

## 1.3 Outline of the thesis

Following this introductory chapter, Chapter 2 illustrates the limitations of engineered remediation strategies that focus on the active removal of contaminants from aquifers using the commonly used pump-and-treat system as an example.

The failure of these active remediation systems to meet cleanup goals at a large number of sites nourished the development of passive remediation approaches, like the concept of natural attenuation. Chapter 2 highlights the stages in which natural attenuation was introduced into legislative regulations and illustrates the research needs connected with the documentation of natural attenuation at field sites, which are then further addressed later in this thesis.

Chapter 3 discusses the main processes of natural attenuation and describes the major factors that control the fate and transport of organic contaminants in groundwater.

The application of a new groundwater investigation method at a former MGP in Germany and the analytical interpretation of the measured field data are presented in Chapter 4.

Chapter 5 introduces a case study focusing on the applicability and limitations of different investigation methods if applied at a field site with a limited monitoring network.

Chapter 6 portrays the field scale application of the integral investigation technique at a fuel hydrocarbon contaminated field site in Ontario, Canada, where a leaking underground storage tank (UST) resulted in a BTEX contamination of the local sand aquifer.

At this site, the integral groundwater investigation was conducted simultaneously with a conventional point-scale mass flux estimation method (groundwater fence approach). In Chapter 6 the results of the two different investigation methods are presented and discussed.

Chapter 7 deals with the numerical interpretation of the data gathered at the MGP site in Germany. In addition, this chapter compares the numerical interpretation of the integral groundwater data with the analytically derived results and explains the influence of aquifer heterogeneities on the mass flux quantification process.

Finally, Chapter 8 introduces the field scale numerical transport modelling for the MGP site, using acenaphthene as the model contaminant. This chapter also demonstrates the influence of diffusion limited non-linear sorption on the contaminant transport towards a pumping well and, hence, the sensitivity of the integral mass flux quantification process on reactive transport processes in heterogeneous and homogeneous porous media.

# 2 Site remediation and investigation approaches

## 2.1 Pump-and-treat

Following the 1978 Love Canal incident in the United States (e.g. U.S. EPA, 2000b), large-scale site restoration projects were initiated to remediate hazardous waste sites. These projects mainly employed engineered systems that attempted to remove contaminants from groundwater and soil. "Pump-and-treat" systems were the most common remedial technologies, which were and are used to (a) hydraulically contain contaminated groundwater, and/or (b) restore groundwater quality to meet defined standards such as drinking water quality standards (U.S. EPA, 1994).

A pump-and-treat remedial action involves the extraction of contaminated groundwater followed by its subsequent ex-situ treatment for contaminant removal with, for example, air stripping, carbon adsorption, biological reactors, or chemical precipitation. The extracted groundwater is then either disposed off site or reinfiltrated into the subsurface.

In different studies in the late 1980s and early 1990s (e.g. Mackay and Cherry, 1989; National Research Council (NRC), 1994) remediation projects at sites with operating pump-and-treat systems in the United States were studied, of which only a small percentage achieved the defined cleanup goals within the expected time frames. The key reasons for the failure of the pump-and-treat systems were:

- Difficulties in characterising the subsurface

- Physical heterogeneities in the sub-surface, making groundwater pathways difficult to predict
- Sorption of the contaminants
- Migration of contaminants into low permeability zones like clays or pores of the aquifer matrix
- Presence of NAPLs, creating long-time sources

These factors lead to characteristic tailing- and rebound-phenomena of dissolved contaminant concentrations during site cleanup as illustrated in Figure 2.1.
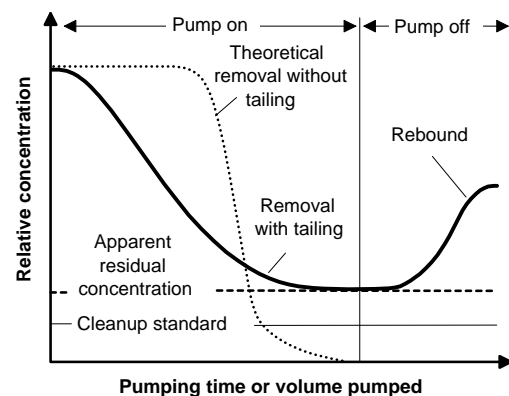


Figure 2.1: Tailing and rebound behaviour of pump-and-treat systems (modified from Keely, 1989).

Tailing refers to the progressively slower rate of reduction in dissolved contaminant concentrations during the pumping, leading to extensive treatment times (up to centuries) and possibly to residual contaminant concentrations in excess of the required cleanup standards. Rebound is the relatively fast increase in dissolved contaminant concentrations that can occur after the shut-off of the pump-and-treat system. Re-

bound effects are especially problematic if the contaminant concentration increases to a level exceeding the attained cleanup standard after the discontinuation of the pump-and-treat system.

Remediation costs for pump-and-treat systems can easily reach several million U.S. dollars per site (Kelley et al., 1996). In a recent study, the U.S. Environmental Protection Agency analysed the remediation costs of 32 pump-and-treat systems and estimated an average cost of US $ 3.6 to 8.9 million for the cleanup of mainly chlorinated solvents or a combination of organic contaminants, respectively (U.S. EPA, 2001).

The high costs of engineered cleanup systems and the disappointing performance of a large number of pump-and-treat systems lead to the conclusion that pump-and-treat approaches often cannot remove all contamination from a site (National Research Council (NRC), 1994) and that it is a *"simple fact"* that *"contaminated aquifers cannot be restored by pumping and treating"* (Travis and Doty, 1990).

During the last few years, the growing awareness of the limitations of engineered systems therefore initiated a search for alternative remediation strategies and a rethinking of remediation goals and time frames. In this context, the potential of the natural removal of contaminants from an aquifer system without human interference evolved and lead to a remediation strategy known as natural attenuation.

## 2.2 Natural attenuation

In practice, natural attenuation is also referred to as intrinsic bioremediation or passive bioremediation. Natural attenuation refers to the observed reduction in contaminant concentration and mass

during the migration from a source through a subsurface environment down to concentrations that are protective of human health and the environment. This decrease in groundwater contaminant concentrations and mass is due to a number of natural physical, chemical, and biological processes.

Natural attenuation processes are contaminant specific. Each contaminant tends to be unique in the way different natural processes affect its fate. Especially significant is the difference between organic and inorganic contaminants. This thesis focuses exclusively on the natural attenuation of selected organic contaminants, which include benzene, ethylbenzene, toluene and the xylene isomers (BTEX), as well as polycyclic aromatic hydrocarbons (PAHs). The major processes controlling the transport and natural attenuation of these organic contaminants are further discussed in Chapter 3. Natural attenuation of metals, which is limited to an alternation of the metals mobility and/or toxicity, is not within the scope of this thesis.

When natural attenuation (NA) processes are shown to be capable of attaining site-specific remediation goals in a time frame that is reasonable compared to other alternatives, monitored natural attenuation (MNA), the combination of natural attenuation processes and long time monitoring, can alone or in combination with other (more active) remedies be the preferred remediation alternative for the cleanup of contaminated sites.

The United States Environmental Protection Agency Office of Solid Waste and Emergency Response (OSWER) defines MNA as (USEPA, 1999):

*"The reliance on natural attenuation processes (within the context of a carefully controlled and monitored clean-up approach) to achieve site-specific reme*

*diation objectives within a time frame that is reasonable compared to that offered by other, more active methods. The "natural attenuation processes" that are at work in such a remediation approach include a variety of physical, chemical, or biological processes that, under favourable conditions, act without human intervention to reduce the mass, toxicity, mobility, volume, or concentration of contaminants in soil and groundwater. These in-situ processes include biodegradation; dispersion; dilution; sorption; volatilisation; radioactive decay; and chemical or biological stabilization, transformation, or destruction of contaminants."*

The main advantages of MNA as a remediation strategy are that it is non-intrusive and does not interfere with on-going site operation. It is furthermore cost-effective and cheaper than active remediation approaches. Typical MNA costs for the remediation of sites contaminated with fuel hydrocarbons without the use of additional treatment technologies have been estimated as $200.000 (Kelley et al., 1996; US Air Force, 1999). These costs typically increase to $600.000 respective $800.000 if MNA is coupled to one or two additional treatment technologies like source removal or bioventing (U.S. Air Force, 1999). Additional treatment technologies can be installed and operated to reduce the required time frame for acceptable site cleanup.

In addition, MNA applications have minimal technical requirements, do focus on the destruction rather than the transfer of the contaminants into another medium or phase, and can be used in conjunction with or as a follow-up to conventional remedial technologies.

However, MNA also has its disadvantages. These include for example that MNA is not a "quick-fix" solution, but that the timeframe for complete remediation may be long. Moreover, MNA can be sensitive to natural or an-thropogenic changes of the groundwater flow conditions, geochemical situation and/or to potential future spills and releases of contaminants into the subsurface. Furthermore, intermediate products (e.g. vinyl chloride (VC)) formed during the biodegradation of organic compounds can be more toxic than the parent compound (e.g. trichlorethene (TCE)) and the potential exists for continued contaminant migration, and/or cross-media transfer of the contaminants during the natural attenuation process. In addition, aquifer characterisation and the documentation of NA at a site is more complex and may be difficult to achieve especially in the presence of spatial or temporal heterogeneities in the subsurface.

## 2.2.1 NA and governmental regulations

Since the early 1990s, monitored natural attenuation (MNA) as a remediation strategy has been introduced into different technical protocols and legislative regulations in a number of countries and regulatory bodies in the world.

In the United States the use of natural attenuation as a remediation strategy was discussed and defined by a number of state agencies like the Florida Department of Environmental Regulation (FDER, 1990), the New Jersey Department of Environmental Protection (NJDEP, 1996), the Minnesota Pollution Control Agency (MPCA, 1997), the Wisconsin Department of Natural Resources (WDNR, 1997, 1999), the New Hampshire Department of Environmental Services (NHDES, 1999), and the North Carolina Division of Waste Management (NCDWM, 2000), as well as by private oil companies such as Amoco (Caldwell et al., 1992; Yang et al., 1995a, 1995b), Chevron (Buscheck and O'Reilly, 1995, 1997) and the Mobil Oil Corporation (MOC, 1995), which were and are problem

owners of a large number of fuel hydro-carbon contaminated sites and who are interested in alternative remediation technologies for the cleanup of these sites.

Research in the field of monitored natural attenuation was also conducted and published in reports by the American Society for Testing and Materials (ASTM, 1997), and the American Petroleum Institute (API, 1997). The U.S. Air Force initiated research programs and published extensive technical protocols for the application of MNA at U.S. Air Force sites contaminated with petroleum hydrocarbons and jet fuel (Wiedemeier et al., 1995) and later for sites contaminated with chlorinated solvents (Wiedemeier et al., 1997). Similar protocols were developed for MNA applications at contaminated sites owned by the U.S. Navy (Wiedemeier and Chapelle, 1998), and the U.S. Department of Energy (USDOE, 1998). For MNA remediation of explosives in groundwater, the U.S. Army Corps of Engineers published a technical report in 1999 (Pennington et al., 1999).

On a federal level in the United States, MNA is dealt with in a number of regulations from the U.S. Environmental Protection Agency (e.g., USEPA, 1997; Wiedemeier et al., 1998). However, the key U.S. EPA policy document pertaining natural attenuation is the directive entitled *Use of Monitored Natural Attenuation at Superfund, RCRA Corrective Action, and Underground Storage Tank Sites* finalized and published in 1999 (USEPA, 1999). This directive governs the application of MNA in the United States and also had a huge impact on the development of MNA regulations in other parts of the world.

In Europe, there is no single European framework dealing with MNA as a remediation strategy yet. However, in-dividual governmental bodies have developed local regulations. In England, the Environment Agency has recently published a general MNA regulation (Carey et al., 2000) and in the Netherlands, a Decision Support System (Sinke et al., 1999) is available, which allows the regulation of MNA applications at contaminated sites.

In Denmark, MNA is dealt with in the framework of the Danish Soil Protection Law (Dahlstrohm, 1999). However up to now no framework exists which specifically regulates and exclusively deals with the use of MNA in Denmark.

In Germany, technical guidelines for the utilization of MNA are not yet available on the federal level. MNA can therefore only be applied on a case-to case basis and after individual site assessment. At a state level however, the first studies about the possibilities of NA and MNA have been initiated, for example in Baden-Wuertemberg (e.g., Schiedek et al., 1997).

In a critical review of the MNA protocols and regulations in the United States, the National Research Council (NRC, 2000) concluded, that one of the main research needs in the context of natural attenuation is to study the influences and impacts of subsurface heterogeneities on the NA potential in the groundwater and on the required site characterization process.

### 2.2.2 NA documentation requirements

In nearly all regulations, protocols, and reports about the implementation of MNA at contaminated sites, it is emphasised that the decision to employ MNA as a remediation alternative should be thoroughly and adequately supported with site-specific characterisation data and analysis. Site specific conditions might also call for a source control strategy were appropriate to minimize the

ongoing mass flux output from the source. However, for MNA a suitable long-term monitoring program is mandatory to observe the plume development with time.

After an extensive site investigation it is important to reliably evaluate the potential efficiency of MNA as a remediation alternative (USEPA, 1999). This step includes the gathering of site-specific data to quantify, with an acceptable level of confidence, the rate of the attenuation processes and to estimate the period of time required to achieve the defined remediation objectives. The data collected in this process is based on three independent but converging lines of evidence, which include (e.g., Wiedemeier at al., 1995, 1997; USDOE, 1998; USEPA, 1999; Pennington et al., 1999; USAirForce, 1999):

1. Historical groundwater and/or soil chemistry data that demonstrate a clear and meaningful trend of decreasing contaminant mass and/or concentration over time at appropriate monitoring points.

2. Hydrogeologic and geochemical data that illustrate that geochemical conditions are suitable for biodegradation and to indirectly demonstrate the type(s) and rates of the NA processes active at the site. This often includes (a) depletion of electron donors and acceptors; (b) increase in metabolic by-product concentrations; (c) decreasing parent compound concentrations; and (d) increase in daughter compound concentrations.

3. Data from field or microcosm studies, which directly demonstrate the occurrence of a particular NA process at the site and to verify the ability of in-situ contaminant degradation.

For achieving regulatory approval for MNA application it is generally necessary to provide both historical data (type 1 above) and data characterizing the nature and rates of NA processes active at the site (type 2 above). Where the latter is inadequate or inconclusive, data from microcosm studies (type 3 above) may also be required. In addition to these lines of evidence, analytical or numerical solute transport models can be used to examine the processes influencing the fate and transport of organic contaminants in groundwater (Wiedemeier et al., 1999). This approach was followed in this thesis. As further discussed in Chapter 8, a numerical transport model was applied to study the influence of sorption on the contaminant transport at the former manufactured gas plant site.

### 2.2.3 Limitations of NA documentation techniques

The problems associated with the site characterization and the NA documentation at heterogeneous field sites, as stressed by the National Research Council (NRC, 2000), is addressed in this study through the joint field scale application of a novel integral groundwater investigation method and a reactive transport modelling. The integral groundwater investigation method was applied at a heterogeneous sand and gravel aquifer (Chapter 4 and Chapter 5) as well as at a more homogeneous sand aquifer (Chapter 6). The applied methods can, in the scope of their specific objectives, together or individually be alternatives to conventional NA documentation approaches, which nearly all suffer from a variety of
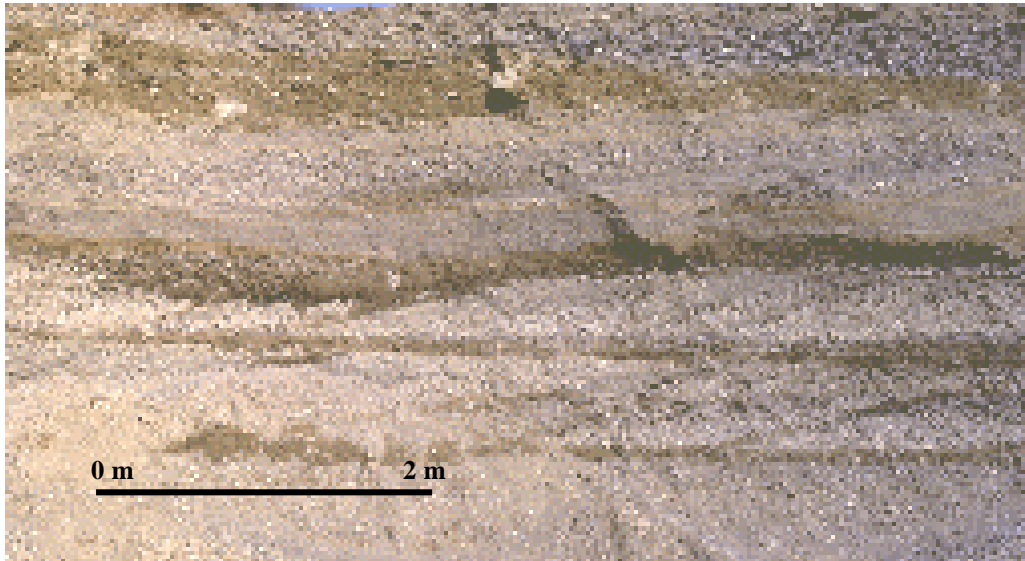
Figure 2.1.2: Outcrop of a heterogeneous alluvial sand and gravel aquifer (Klingbeil, 1998)

deficiencies and interpretational constrains.

For example, a widely used method for the documentation of natural attenuation is the use of historical point-scale concentration data from different monitoring points showing a decrease in contaminant concentrations with time (type 1 data above). However, in case of organic contaminants for example, decreasing concentrations with time at a specific monitoring point can simply be the result of plume migration and/or inappropriately placed monitoring wells (e.g., monitoring wells are located at the fringe or outside of the contaminant plume's extension).

In the presence of subsurface heterogeneities, the conduction of reliable site characterisations and field scale sampling campaigns can be a challenging task. From the small scale spatial variations in aquifer structure and facies shown in Figure 2.1.2 it is obvious that under heterogeneous conditions, small scale or "point scale" investigations and concentration measuring campaigns are only representative for a very small aquifer volume around the sampling location because aquifer properties like hydraulic conductivity and sorption capacity are highly variable in space. The

limitations of traditional site investigation techniques under heterogeneous conditions and an alternative integral groundwater investigation method, which was applied in this study, are further discussed in Chapters 4 and 5 of this thesis.

Another widely used approach for the determination of natural attenuation at a field site is to measure decreases in electron acceptors such as oxygen, nitrate, iron(III), and sulfate and increases in concentrations of products such as sulfide, carbon dioxide, or methane in contaminated aquifer regions, relative to background values (e.g., Baedecker et al., 1993; Schmitt et al., 1996; Anderson et al., 1998; Anderson and Lovley, 2000). Although these geochemical changes in the groundwater indicate in-situ responses to the groundwater contamination, they do not attest a reduction in contaminant mass in the affected aquifer (Gieg et al., 1999). Similarly, comparative measurements of specific types of microorganisms in contaminated and uncontaminated parts of an aquifer suggest a microbiological response to the contamination, but do not proof ongoing activity of the detected microorganisms nor their biodegradation capabilities with regard to the present groundwater contaminants

(NRC, 1993, Braddock and McCarthy, 1996; Grieg et al., 1999).

The measurement of the prevailing redox-conditions, for example obtained through the measurement of steady-state hydrogen concentrations, can be used to determine the predominant terminal electron accepting processes and thus the ongoing activity of in-situ microbial communities, but this does not verify that groundwater contaminants are biodegraded in this process (Grieg et al., 1999).

Alternatively, contaminant biodegradation can be studied through controlled microcosm studies and batch experiments in the laboratory (e.g., Nielsen and Christiansen, 1994; Nielsen et al., 1996), but these experiments only indicate that the groundwater contaminants are susceptible to biodegradation. They do not reliably proof that biodegradation also occurs in the field under field conditions (Höhener et al., 1998). In any case, considering the many factors influencing biodegradation of organic contaminants in groundwater, it seems likely, that reliable NA and biodegradation rate constants can be determined only in-situ (Madsen, 1991; NRC, 1993).

Acknowledging the need for in situ measurements, different studies (e.g., Nielsen et al., 1996; Godsy et al., 2000) used in-situ microcosms developed by Gillham et al. (1990a, 1990b) to measure point scale NA rates under fairly accurate field conditions. But the results of these studies are influenced by the placement of the microcosms as geochemical conditions can vary in space and time in a studied aquifer system. The results obtained through these studies therefore cannot represent true in-situ rates, but might be seen as fair approximations (Nielsen et al., 1996). Kao and Wang (2001) conclude that mass flux quantifications are more reliable and straightforward in NA efficiency evaluation than microcosm test, in-situ column studies and fate and transport model applications.

A promising new technique with the potential to provide a direct indication of biodegradation is the compound specific stable isotope analysis (CSIA) of stable isotope ratios like $\delta^2H$, $\delta^{13}C$, $\delta^{15}N$, $\delta^{18}O$, and $\delta^{37}Cl$. A detailed description of stable isotope geochemistry and CSIA is beyond the scope of this thesis and the interested reader is referred to standard textbooks, like Galimov (1985), Fritz and Fontes (1986) or Hoefs (1997). In the context of natural attenuation it is sufficient to say that elements like for example C and H, which make up the monoaromatic contaminants (BTEX), each occur in two stable isotopes, one light and one heavy in a characteristic ratio. Isotopic fractionation during the biodegradation of organic contaminants, which is estimated with the CSIA approach, is then a measure of the change in the ratio of heavy to light isotopes expressed as the $\delta$ value or ‰ difference relative to a defined standard. Due to different energetic requirements for chemical reactions with the different isotopes, microbial degradation of organic contaminants will result in a preferential degradation of the lighter isotope, resulting in a substrate that systematically becomes more enriched in heavy isotopes as biodegradation proceeds.

In general, compound-specific isotope ratios can be used to (i) distinguish between different contaminant sources, or events of contamination, if isotope ratios are conserved during transport in the groundwater, or (ii) demonstrate the occurrence of biodegradation, if biodegradation of the organic solute is accompanied by a characteristic isotopic fractionation. It has been shown that nondegradative processes such as sorption (Harrington et al., 1999), volatilisation (Slater et al., 1999; Huang et al.,

13

1999) and dissolution (Dempster et al., 1997; Slater et al., 1999) cause only very small isotope fractionations, which in many cases are smaller than the analytical uncertainty inherent to the CSIA approach. Significant changes in the isotope ratios can therefore often be attributed to microbial degradation processes.

Several studies have been published on the fractionation of carbon isotopes during the biotic and abiotic biodegradation of chlorinated solvents such as trichloroethane (TCE) and tetrachloroethene (PCE). Ertl et al. (1996) observed negligible carbon isotope fractionation, whereas Sherwood et al. (2001) observed a fractionation of –7.1‰ for the dechloronation of TCE to cis-DCE under sulfate reducing conditions. Hunkeler et al. (1999) studied the carbon isotope fractionation during the methanogenic dechloronation of PCE and reported enrichment factors between 2‰ and 26‰ for the different dechloronation steps. These results were later confirmed by Bloom et al. (2000) and Slater et al. (2001), who observed comparable fractionation factors of around 20‰.

The chloride ratio ($\delta^{37}Cl$) can also provide information on the microbial biodegradation activity as shown by Sturchio et al. (1998) for TCE and Heraty at al. (1999) for dichloromethane.

For chlorinated hydrocarbons, studies to date therefore indicate that a large and reproducible (carbon) isotope fractionation is associated with the biodegradation of these compounds and changes in the isotope ration can be used as an effective indicator to confirm intrinsic bioremediation of chlorinated solvents at field scale.

Several studies have focused on the $^{13}C/^{12}C$ fractionation during the biodegradation of monoaromatic hydrocarbons (BTEX) and petroleum hydrocarbons (e.g., Landmeyer et al., 1996;

Kelley et al., 1997; Meckenstock et al., 1999; Ahad et al., 2000) and crude oil (e.g., Jackson et al., 1996).

Aggarwal et al. (1997) combined measurements of $\delta^{13}C$ with $\delta^{18}O$ quantifications to investigate the effectiveness of intrinsic and enhanced biodegradation of diesel fuel.

For BTEX and other organic hydrocarbons, however, the evidence for applying stable isotope analysis in the same way as for the chlorinated hydrocarbons is less compelling. Changes in the isotopic ratio $\delta^{13}C$ during the anaerobic degradation of toluene under methanogenic and sulfate-reducing conditions, for example were seen to be very small (2.0‰ and 2.4‰, respectively, Ahad et al., 2000). In laboratory scale batch experiments, Meckenstock et al. (1999) reported values of around 6‰ enrichment in $^{13}C$ residual toluene under denitrifying, iron-reducing, and sulfate-reducing conditions. Stehmeier et al. (1999) documented only a 2‰ enrichment in $^{13}C$ in residual benzene in similar laboratory experiments.

For the biological degradation of the gasoline oxygenate Methyl *tert*-Butyl Ether (MTBE) Hunkeler et al. (2001) observed a more pronounced shift in the carbon isotope ratio of up to 6.9‰ after 97% of substrate degradation.

For aerobic environments, it is known that the degradation of organic contaminants is significantly faster then in anoxic environments. The degradation pathways of petroleum hydrocarbons are, however, not fully understood yet. Currently, it is therefore not possible to quantitatively estimate the amount of biodegradation in aerobic aquifer systems based on a CSIA because the fractionation factors needed for the analysis and associated to the degradation pathways cannot be assessed (Meckenstock et al., 2001).

In contrast to the generally small isotopic changes of the carbon isotopes, Ward et al. (2000) and Morasch et al. (2001) used the hydrogen ratio $\delta^2H$ for the assessment of biodegradation of toluene under anaerobic conditions and reported isotopic fractionations which are up to orders of magnitude larger compared to carbon isotope fractionations under similar conditions. However, quantitative evaluations of biological degradation activities at contaminated sites by the analysis of bacterial hydrogen isotope fractionation is currently difficult due to variations in the fractionation process between different bacterial strains (Morasch et al., 2001).

Moreover, the hydrogen isotope analyses currently suffers from a relatively high minimum contaminant concentration of around 2 mgl$^{-1}$ (Ward et al., 2000), which limits the field scale applicability of this approach as contaminant plumes often exhibit much smaller contaminant concentrations.

In summary, nearly all evidence suggests that for BTEX and other hydrocarbon contaminations, the expected carbon isotope fractionation during biodegradation is in the order of only a few ‰ and the change in the carbon isotope ratio is therefore a relatively insensitive parameter for the quantification of biodegradation. At field site with the possibility for different sources with different initial $\delta^{13}C$ values, the application of the CSIA approach will be a challenge because the small shifts in the $\delta^{13}C$ value could easily be masked by the isotopic differences of multiple contaminant sources or spills (e.g., Jackson et al., 1996).

On the other hand, if the apparent insensitive behaviour of stable carbon isotopes with respect to biodegradation by mixed consortia (Sherwood-Lollar et al., 1996; Meckenstock et al., 1999; Stehmeier et al., 1999; Ahad et al., 2000) is upheld, carbon isotope analysis could be used to investigate contaminant source zones or transport paths because aromatic hydrocarbons derived from different sources can have isotopically distinct $\delta^{13}C$ values (Dempster et al., 1997; Harrington et al., 1999) that apparently do not change significantly during contaminant transport.

For aromatic hydrocarbons, hydrogen isotope analysis could be an alternative for the quantification of biodegradation because the hydrogen ratio shows a stronger fractionation during the biotic degradation process (Ward et al., 2000). However, to date it is unknown if abiotic processes such as sorption, volatilisation, and dissolution can have an influence on the hydrogen isotope ratio.

In conclusion, traditional methods for the documentation of natural attenuation suffer from a number of interpretational constrains. A combination of several new methodologies could be an effective alternative for the documentation of NA at homogeneous and heterogeneous field sites. This novel approach could include (i) the integral mass flux quantification of target contaminants as shown in this study to investigate and document the reduction of mobile contaminant mass flux with travel distance, coupled with (ii) a carbon isotope analysis for the characterisation and identification of contaminant sources, and coupled with (iii) a hydrogen isotope analysis to derive the contribution of biodegradation on the measured mass flux reduction in flow direction.

Studies using contaminant mass flux estimations for the quantification of attenuation rate constants were published for example by Borden et al. (1997) and Kao and Wang (2001) for BTEX compounds, by Bockelmann et al. (2000a, 2000b; 2001a, 2001b) for BTEX and low molecular weight PAH compounds, by Semprini et al. (1995)

for chlorinated hydrocarbons, by King et al. (1999) for the attenuation of a coal tar creosote plume, and by Wilson et al. (2000) for the estimation of MTBE removal under methanogenic conditions. Most of these studies used point-scale flux estimation approaches and assumed that the measured mass flux reductions were solely a result of bio-degradation. Abiotic mass flux reducing processes such as sorption and volatili-sation were in these studies assumed to be insignificant, what could mostly not be proven.

Future natural attenuation studies could benefit from a combination of the integral investigation method with the carbon and hydrogen CSIA approach.

On the one hand, this could improve the natural attenuation documentation process by reducing the need of data interpolation through the integral mass flux estimation. On the other hand, an improved hydrogen isotope analysis could quantifying at field scale the relative contribution of biodegradation on the measured mass flux reduction, whereas the carbon isotope analysis could be used for the mapping of contaminant sources or spills.

This combined investigation method could be applied for contaminant sources, which consists of organic con-taminants, for which degradation path-ways and specific isotope fractionation factors have been described in the re-quired detail. Nowadays this informa-tion is available for BTEX and selected PAH compounds. However, the detec-tion limit of the hydrogen based CSIA has to be improved to be applicable not only close to the source, but also along the contaminant plume.

# 3 Transport and fate of organic solutes in groundwater

Numerous processes, some of which are induced by the hydrodynamic conditions in the aquifer, control the transport of solutes in porous media. The bulk movement of a solute is influenced by the effective porosity and the transmissivity of the surrounding aquifer material. However, the movement of a solute can be quite different to the bulk groundwater movement. A deviation of the solute's movement from the bulk groundwater movement can be caused by the concentration gradient and by interactions of the solute with the aquifer matrix (sorption) or by processes, which reduce the solute mass in the aquifer system, such as abiotic degradation and biodegradation in case of organic contaminants and radioactive decay in case of radioactive compounds.

The following chapter introduces the basic concepts that control the transport and fate of monoaromatic hydrocarbons (BTEX) and polycyclic aromatic hydrocarbons (PAH) in groundwater.

## 3.1 Advection

Advection is the main transport mechanism of bulk groundwater in an aquifer system. For solute transport, advection describes the portion of transport solely credited to the bulk motion of flowing groundwater. In a pure advective system, there is no exchange of solute mass between streamtubes and the direction of transport in a steady-state system is defined by the flow lines of the bulk groundwater. Because advection is the major trans-port mechanism, the knowledge of groundwater flow patterns is a key to the interpretation of solute migration in an aquifer.

Advective groundwater flow under laminar conditions can be described by *Darcy's Law* (in Freeze and Cherry, 1979) as:

$$\frac{Q}{A} = q = -K\frac{\partial h}{\partial l} \qquad (3.1)$$

with Q [$L^3T^{-1}$], A [$L^2$], q [$LT^{-1}$], K [$LT^{-1}$], h [L], and l [L] denoting the volumetric flow rate, the cross-sectional area, the volumetric flow rate per unit surface area or specific discharge, the hydraulic conductivity, the elevation of the hydraulic head and the distance between the head measurements, respectively. $\partial h/\partial l$ is also known as the hydraulic gradient.

In other words, *Darcy's Law* states that the velocity of the advective groundwater flow is proportional to the hydraulic gradient present in the aquifer system.

The specific discharge or Darcy velocity (q) is a macroscopic concept and differs from the actual groundwater or linear velocity (v), which does not use the whole cross-sectional area, but moves through the connected pore space of the aquifer only. This velocity can be derived from Equation 3.1 by introducing $n_e$ [-], the effective porosity, and $n_eA$ [$L^2$], the effective area of flow, into the equation, which leads to:

$$\frac{Q}{n_e A} = \frac{q}{n_e} = v = -\frac{K}{n_e}\frac{dh}{dl} \qquad (3.2)$$

## 3.2 Dispersion

Dispersion causes a spread of mass beyond the region it would normally occupy due to advection alone. Dispersion thereby reduces solute concentrations and induces solute into adjacent aquifer regions. Two different processes make up the hydrodynamic dispersion in porous media. First, mechanical dispersion due to mechanical mixing during fluid advection and, second, molecular dispersion caused by the random movement of molecules (*Brownian Motion*) due to their thermal-kinetic energy. The general concept of these two processes is shown in Figure 3.1.



**Mechanical dispersion**

**Molecular dispersion**
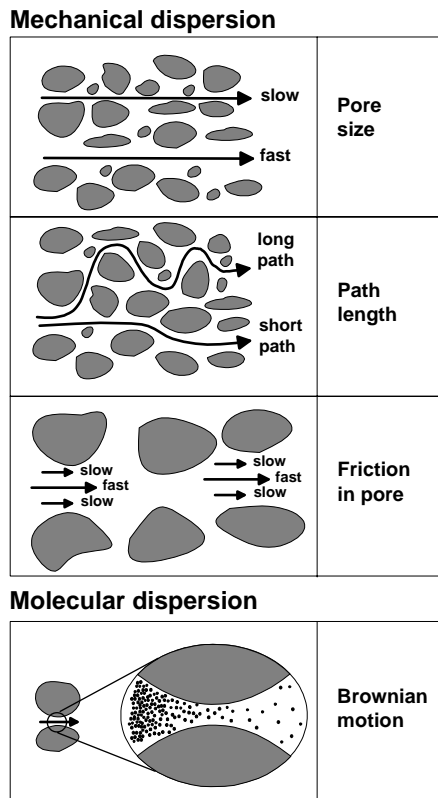
Figure 3.1: Processes of dispersion on a microscopic scale (after Freeze and Cherry, 1979).

Hydrodynamic dispersion is described by the dispersion coefficient, which can be expressed in terms of its two components:

$$D_l = \alpha_l v + D^*$$ (3.3)

where $\alpha_l$ [L], the longitudinal dispersivity, is a characteristic property of the porous media and v [$LT^{-1}$] is the linear groundwater velocity. The second component $D^*$ [$L^2T^{-1}$] represents the coefficient of molecular diffusion.

In areas with normal or high groundwater flow rates, molecular dispersion can be neglected (Davis et al., 1993). However, molecular dispersion (diffusion) plays an important role in the solute mass transfer between the main flow paths and low permeability zones, as well as for the contaminant transport into and out of aquifer particles.
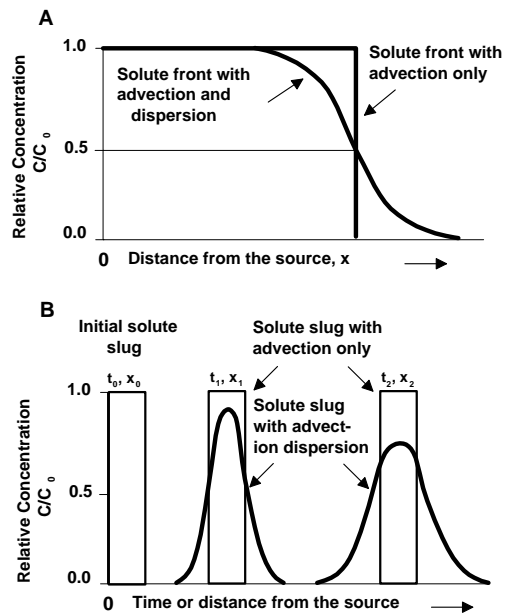


Figure 3.2: Breakthrough curves in one dimension showing the influence of advection and hydrodynamic dispersion. (A) continuous input, (B) slug input (after Wiedemeier et al, 1999).

Dispersion and dispersivity are scale dependent, but independent from solute properties. At pore scale, $\alpha$ incorporates pore scale processes such as the different velocities in matrix pores (Figure 3.1). At field scale it reflects aquifer heterogeneities. Hence $D_l$ generally increases with the transport or travel distance because more and more

18

aquifer heterogeneities are encountered. The influence of hydrodynamic dispersion on one dimensional solute transport in porous media is further illustrated in Figure 3.2 for continuous and temporal contaminant inputs. It can be seen that dispersion transforms sharp concentration fronts into gradual concentration profiles.

## 3.3 Diffusion

The transport of molecules in the direction of their concentration gradient is called diffusion. Diffusion only ceases to occur in the absence of a concentration gradient in the system. Apart from its concentration dependency, diffusion is also controlled by solute properties.

The mass of solute moving across a unit surface area due to diffusion is given by *Fick's first Law* (in Freeze and Cherry, 1979)

$$F = -D \frac{\partial C}{\partial l} \qquad (3.4)$$

where F [$ML^{-2}T^{-1}$], D [$L^2T^{-1}$], C [$ML^{-3}$], and l [L] denote the diffusive mass flux, the diffusion coefficient, the solute concentration and the distance, respectively.

For systems with a changing solute concentration with time, *Fick's second Law* must be applied. The one-dimensional form of *Fick's second Law* is (in Wiedemeier et al., 1999)

$$\frac{\partial C}{\partial t} = D \frac{\partial^2 C}{\partial l^2} \qquad (3.5)$$

where $\partial C/\partial t$ [$MT^{-1}$] is the change in concentration with time.

In porous media, the apparent diffusion coefficient $D_a$ is smaller than in a pure liquid system because of the longer transport paths caused by the tortuosity of the aquifer pores. The relationship between $D_a$ and D is given by

$$D_a = \omega\, D \qquad (3.6)$$

and $\omega$ [-] is an empirical coefficient. The value of $\omega$ is generally between 0.01 and 0.5 (Freeze and Cherry, 1979).

## 3.4 Sorption

Many solutes in groundwater do not behave conservatively, but can be removed from the dissolved phase by sorption onto the surfaces of the aquifer matrix (adsorption) or into porous matrix constituents (absorption). This process is often reversible and does therefore often only temporarily remove con-taminant mass from the dissolved phase. This temporal partitioning from the groundwater results in a slowing of the solute compared to the bulk groundwater movement. The slowing is referred to as the retardation of the solute.

Sorption of nonpolar compounds, in contrast to chemisorption, which changes the sorbed compound through a chemical reaction, is regarded to be due to weak intermolecular bonds between sorbate and sorbent. These bondings are generally reversible (Schwarzenbach et al., 1993), which implies that the sorption and desorption of nonpolar solutes follows similar processes.

If a solute pulse moves through an aquifer, a portion of the solute partitions from the groundwater onto the aquifer matrix. If the concentration in the groundwater declines again, for example due to plume migration or dilution, some portion of the sorbed solute will desorb and re-enter the solution due to the reversed concentration gradient. Sorption will therefore not necessarily remove solute mass from the

groundwater permanently, but will mainly retard its migration.

Solute sorption to the aquifer matrix comprises a number of different processes. Due to their nonpolar molecule structure, hydrocarbons mostly follow the process of hydrophobic bonding during sorption (Wiedemeier et al., 1999). As the surfaces of the aquifer matrix are often less polar than the water molecules, there is a strong affinity of the nonpolar groundwater contaminants to sorb to the aquifer matrix. In most aquifer systems, the amount of clay minerals and, most importantly, the organic carbon fraction of the aquifer matrix controls the degree of sorption of nonpolar organic contaminants.

In batch-experiments it is possible to predict the amount of sorption expected for a certain solute, if it interacts with a specific aquifer material under equilibrium conditions. With these experiments it is possible to visualize the solute distribution between solid and aqueous phase by plotting the solute concentration on solids versus the solute concentration in the aqueous phase at a constant temperature. These sorption isotherms generally exhibit one of three characteristic shapes, depending on the sorption mechanism. The three most important types of sorption isotherms are known as *Freundlich* isotherms, linear isotherms (a special case of the *Freundlich* isotherm), and *Langmuir* isotherms (Figure 3.3).

*Langmuir* isotherms describe sorption processes on surfaces with a limited amount of sorption sites. The isotherms therefore increase linearly for low concentrations, but asymptotically approach a maximum for higher concentrations as the availability of sorption sites decreases. For this type of isotherm, the equilibrium concentration on the solid phase $C_s$ [MM$^{-1}$] is calculated as (Domenico and Schwartz, 1990):

$$C_s = \frac{Q^0 K_L C_{aq}}{1 + K_L C_{aq}} \qquad (3.6)$$

with $Q^0$ [M], $K_L$ [MM$^{-1}$], and $C_{aq}$ [ML$^{-3}$] denoting the maximum sorptive capacity, the Langmuir equilibrium coefficient, and the dissolved contaminant concentration, respectively.
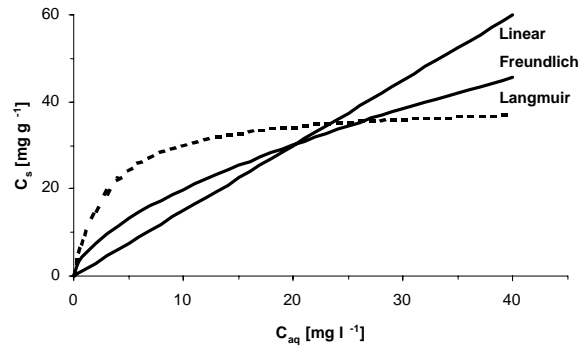


Figure 3.3: Characteristic sorption isotherm shapes

The *Freundlich* sorption model considers scenarios where the number of sorption sites relative to the number of solute molecules is very large (assumed unlimited). This is generally the case for dilute solutions, for example in contaminant plumes downgradient from a contaminant source. Mathematically, the *Freundlich* model is expressed as (Domenico and Schwartz, 1990):

$$C_s = K_{Fr} C_{aq}^{1/N} \qquad (3.7)$$

where $K_{Fr}$ [MM$^{-1}$] and $1/N$ [-] denote the Freundlich coefficient and the Freundlich exponent respectively. The value of $1/N$ controls the non-linearity of the *Freundlich* isotherm and is a compound specific quantity determined experimentally. Values of $1/N$ are typically between 0.6 and 1 (Kleineidam et al., 1999; Karapanagioti et al. 2000).

If $1/N$ is equal to 1, the simplest form of equilibrium isotherms occurs, e.g. the

linear sorption isotherm, which is a special case of the *Freundlich* isotherm. As an approximation, the linear isotherm can be used for solute concentrations of up to one-half of the solute's solubility (Lyman et al., 1992), which would for example be valid for BTEX compounds partitioning from fuel mixtures. The linear isotherm is expressed as (Fetter, 1993):

$$C_s = K_d C_{aq} \qquad (3.8)$$

where $K_d$ [-] denotes the equilibrium distribution coefficient.

The extent of the sorption process is directly correlated with the octanol-water partition coefficient $K_{ow}$ [-] of the solute and the percentage of organic carbon in the sediment $f_{oc}$ [-]. The distribution coefficient for a specific solute / aquifer material system can therefore be expressed as (Karickhoff et al., 1979):

$$K_d = K_{oc} f_{oc} \qquad (3.9)$$

As mentioned earlier, sorption slows the migration of a solute compared to the bulk groundwater movement. When the linear velocity of the bulk groundwater is greater than the average velocity of the solute, the solute is said to be retarded. This effect is described by the coefficient of retardation or the retardation factor R [-], defined as (Fetter, 1993):

$$R = \frac{v}{v_c} \qquad (3.10)$$

with v [LT$^{-1}$] and $v_c$ [LT$^{-1}$] denoting the linear groundwater velocity and the average solute velocity, respectively. If no sorption occurs, i.e. $K_d$ equals 0, the ratio $v/v_c$ and hence the retardation factor equals 1.

Assuming linear solute sorption and a fraction of organic carbon of less than 0.001, the retardation factor can be deduced from:

$$R = 1 + \frac{K_d \rho}{n_e} \qquad (3.11)$$

with $\rho$ [ML$^{-3}$] and $n_e$ [-] symbolizing the bulk density of the aquifer and the effective porosity of the aquifer, respectively.

The average solute velocity can subsequently be estimated by combining Equations 3.10 and 3.11 to

$$v_c = \frac{v}{1 + K_d \rho / n_e} \qquad (3.12)$$

Equilibrium sorption is the most commonly used model for sorption and natural attenuation studies (Wiedemeier et al., 1999). However, the use of the Local Equilibrium Assumption (LEA), which assumes instantaneous equilibrium between the solute and the aquifer solids (e.g., Bahr and Rubin, 1987) will for transport considerations lead to unrealistically high retardation factors (Merkel, 1996).

Recent studies demonstrated that solute sorption in groundwater systems is limited by low transfer rates to sorption sites, leading to highly non-linear sorption isotherms (Schüth, 1994; Grathwohl and Kleineidam, 1995; Grathwohl, 1998). The kinetic behaviour of the sorption and desorption processes is assumed to result from diffusion into and out of the intra-particle pore space of the porous aquifer constituents (Ball and Roberts, 1991; Grathwohl, 1998; Rügner et al. 1999). In this case the aquifer system needs a long time to reach equilibrium and this period of time cannot be neglected anymore. For transport studies of organic contaminants like BTEX or PAH, it is therefore important to include non-linear sorption isotherms due to diffu-

sion limited sorption into the transport calculations (Karapanagioti et al., 2001).

## 3.5 Volatilisation

Another attenuation process that can remove solute mass from the aqueous phase in saturated porous media is the volatilisation of the solute into soil gas. Controlling factors for the partitioning of a solute into soil gas are the mass transport coefficients for the solute in both water and soil gas, the sorption of the solute, the temperature, as well as the *Henry's Law* constant of the solute under study.

*Henry's Law* states that under equilibrium conditions and for non-reactive solutes, the concentration of a compound in the gaseous phase is directly proportional to the solute's concentration in the aqueous phase, and that the proportionality constant is a characteristic of the solute (Domenico and Schwartz, 1990). Stated mathematically, *Henry's Law* is given by:

$$C_a = HC_{aq} \qquad (3.13)$$

with $C_a$ [$ML^{-3}$], H [$PL^3M^{-1}$], and $C_{aq}$ [$ML^{-3}$] denoting the concentration in the soil gas, the *Henry's Law* constant, and the concentration in the aqueous phase, respectively.

For the organic groundwater contaminants included in this study, Henry's Law constants range from 5.8E-04 [atm $m^3mol^{-1}$] to 7.7E-03 [atm $m^3mol^{-1}$] for BTEX and from 2.1E-10 [atm $m^3mol^{-1}$] to 2.8E+00 [atm $m^3mol^{-1}$] for the PAH compounds (Wiedemeier et al., 1999). Because of the generally low Henry's Law constants of the BTEX and PAH compounds, as well as because of the small surface area of the groundwater exposed to soil gas, volatilisation of these compounds into soil gas is a rela-

tively slow process. Chiang et al. (1989) for example reported that less than 5% of the dissolved BTEX mass in a saturated porous medium was lost to volatilisation. In general, the impact of volatilisation on the reduction of organic solutes in groundwater can be assumed to be negligible (Wiedemeier et al., 1999).

However, for sample collection and analysis, volatilisation of solutes can be important. When samples are in contact with the atmosphere, the concentration of the solute can, with time, fall below detection limits (Domenico and Schwartz, 1990).

## 3.6 Dilution (Recharge)

The inflow of water from the unsaturated into the saturated zone is defined as groundwater recharge (e.g., Freeze and Cherry, 1979). The impact of groundwater recharge on the transport of organic solutes in groundwater is twofold.

First, the additional water entering the saturated zone will cause a dilution of a present contaminant plume in the subsurface. The mixing process between the recharge and the contaminated groundwater occurs mainly through mechanical and molecular dispersion at the fringe of the plume. Secondly, the inflow of potentially electron-acceptor rich water into the contaminated part of an aquifer can have an impact on the geochemical conditions in the aquifer and might enhance the biodegradation potential in the aquifer by supplying electron-acceptors.

Vroblesky and Chapelle (1994) for example studied the effect of a major rainfall event on a petroleum hydrocarbon-contaminated aquifer. They reported that the infiltrating rainwater

introduced oxygen into a formerly reducing groundwater, leading to the precipitation of iron(III) onto mineral grains. This iron(III) was subsequently available again for reduction by microorganisms causing a shift from methanogenesis to iron(III) reduction.

However, such shifts in the geochemistry of an aquifer due to rainfall events change the conditions in an aquifer only for a short time period before the geochemical conditions rebound back into their former state. Moreover, such a shift can also have adverse effects on the biodegradation potential, if the degradation of the groundwater contaminants is adversely affected by the changed geochemical conditions. This can for example be the case for degradation of chlorinated solvents in an anaerobic aquifer, which is recharged by aerobic precipitation water. The change to aerobic conditions would reduce the degradation

During the quantification of natural attenuation at field sites it is often difficult to distinguish between the effects that dilution, sorption, and biodegradation have on the solute concentration. It is therefore better to investigate the solute mass flux in an aquifer system compared to studying the decrease in concentration because the latter can be influenced by all described transport processes, whereas a mass flux investigation is primarily influenced by sorption and degradation only.

## 3.7 Biodegradation

The abiotic processes discussed above do not remove solute mass from the aquifer, but simply cause the transfer of solutes from one phase or location to another. Contrarily, biodegradation can be defined as the biologically catalysed reduction in complexity of chemicals (Alexander, 1999).

This results in a mass reduction of the complex chemical, which can for example be an organic groundwater contaminant. In case of organic contaminants like BTEX or PAH compounds, this process can lead to the conversion of complex organic compounds to inorganic products. A complete conversion from a complex organic compound to inorganic products like carbon dioxide ($CO_2$) and water ($H_2O$) is called mineralisation.

Microorganisms require a carbon source, electron acceptors and donors, water, and nutrients for microbial growth (Alexander, 1999). They gain energy from the breaking of chemical bonds and the transfer of electrons from the organic groundwater contaminant (the electron donor) to an electron recipient, which is generally called electron acceptor. This type of chemical reaction is termed oxidation-reduction reaction.

The ability of soil microorganisms to utilize aromatic hydrocarbons as sole carbon sources has been established since 1908, when a bacterium with the ability to grow aerobically on toluene and xylenes was isolated (Stormer, 1908; in Alvarez and Hunt, 1999). However, only in the last 20 years, evidence was obtained for the aerobic and anaerobic degradation of petroleum hydrocarbons and polycyclic aromatic hydrocarbons. The ubiquitous distribution of microorganisms capable of metabolising aromatic hydrocarbons was reported by Norris (1994) for example, who notes that viable petroleum-hydrocarbon-degrading consortia will be present at 99 per cent of sites. However, Weiner and Lovely (1998) documented a failure of benzene degrading bacteria to colonize a contaminated aquifer implying that BTEX degradation will not occur at all sites.

Table 3.1: Benzene degradation with various electron acceptors (adapted from Brady et al., 1998).

| Degradation | Electron donor | Reaction (without microbial growth) | Electron source |
|---|---|---|---|
| Aerobic | $O_2$ | $C_6H_6 + 7.5O_2 \rightarrow 6CO_2 + 3H_2O$ | Atmosphere |
| Denitrification | $NO_3^-$ | $C_6H_6 + 6NO_3^- + 6H^+ \rightarrow 6CO_2 + 3N_2 + 6H_2O$ | Agriculture, atmosphere |
| Iron(III) reduction | $Fe(OH)_3$ | $C_6H_6 + 60H^+ + 30Fe(OH)_3 \rightarrow 6CO_2 + 30Fe^{2+} + 78H_2O$ | Fe-(hydr)oxides |
| Sulfate reduction | $SO_4^{2-}$ | $C_6H_6 + 3.75\ SO_4^{2-} + 7.5H \rightarrow 6CO_2 + 3.75H_2S + 3H_2O$ | $CaSO_4$ |
| Methanogenesis | $CO_2$ | $C_6H_6 + 4.5H_2O \rightarrow 2.25CO_2 + 3.75CH_4$ | Atmosphere, minerals |

It is generally accepted that all BTEX compounds can be degraded aerobically (e.g., Alvarez and Vogel, 1991; Nielsen and Christensen, 1994). Under anaerobic conditions, the degradation of benzene, the most toxic and most difficult to degrade BTEX compound was reported for nitrate-reducing (Burland and Edwards, 1999), iron-reducing (e.g., Lovely et al., 1996; Rooney-Varga et al., 1999), sulfate-reducing (e.g., Edwards and Grbic-Galic, 1992; Phelps et al., 1998) and methanogenic conditions (e.g., Grbic-Galic and Vogel, 1987; Weiner and Lovley, 1998).

The biodegradation of petroleum hydrocarbons, especially BTEX compounds is therefore apparently limited primarily by electron acceptor availability and not by the redox conditions and generally continues until all readily available contaminants are oxidized (Wiedemeier et al., 1999).

Through the reduction of contaminant mass in an aquifer and the slowing of the migration rate of the contaminant front compared to the bulk groundwater, biodegradation can have a significant impact on contaminant transport in an aquifer.

In the United States, for example, different studies (e.g., Rice et al., 1995; Wiedemeier et al, 1995, Mace et al., 1997) have estimated that about 85 to 90 per cent or more of the dissolved petroleum-hydrocarbon plumes are at steady-state equilibrium or shrinking, mot likely due to biodegradation processes.

If a soil system is closed, i.e. the net import of electron acceptors is minimal, biodegradation of organic solutes in groundwater causes a predictable sequence of electron acceptor utilization which is illustrated in Figure 3.4. Through the sequential use of electron acceptors, biodegradation does change the geochemical conditions in a contaminated aquifer. The relevant reactions are shown in Table 3.1, using benzene, $C_6H_6$, as the exemplary organic contaminant and assuming a constant microbial population.
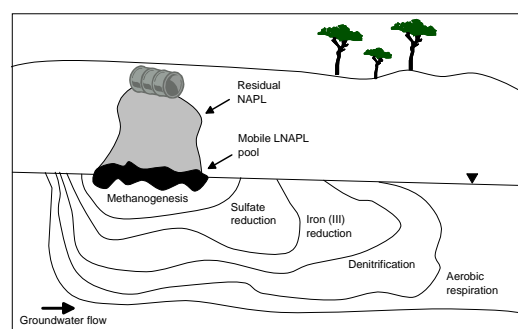


Figure 3.4: Conceptualisation of electron acceptor zones in an aquifer (adapted from Lovley et al., 1994).

The energetically preferred oxidation pathway of microorganisms in the subsurface is aerobic respiration, followed by nitrate-reducing, iron(III)-reducing, sulfate-reducing, and methanogenic res

piration. In some hydrologic environments manganese(IV) reduction can also occur, but this is generally a minor component of the electron acceptor flow compared to the other electron acceptors and was therefore omitted in this discussion.
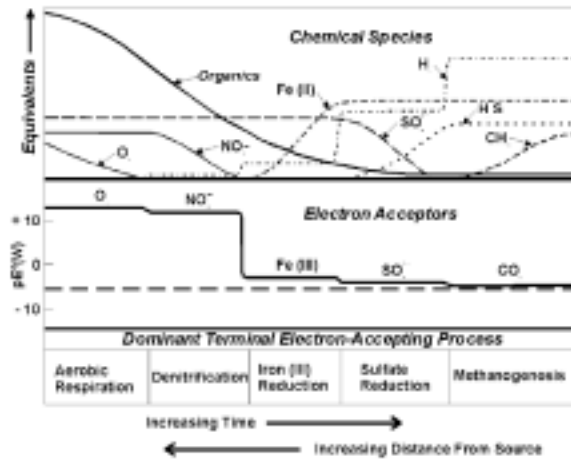


Figure 3.5: Geochemical evolution of groundwater contaminated with monoaromatic hydrocarbons (after Bouwer and McCarty, 1984).

The conceptual sequence of redox zones shown in Figure 3.4 can usually not be encountered in the field with similarly sharp redox fronts because under field conditions different redox zones usually overlap to a certain degree. The gradual change between redox conditions is shown in Figure 3.5. In this example an initially uncontaminated and aerobic groundwater is contaminated with organic contaminants, e.g. BTEX, leading to a sequential depletion of the different electron acceptor pools and a decrease in the oxidation potential of the groundwater with time.

Conceptually, Figure 3.6 illustrates the effects that the discussed abiotic and biotic processes have on the transport and fate of organic contaminants in groundwater. The purely advective transport results in a very sharp concentration front moving through the aquifer, which is generally distorted due to dispersive and diffusive processes. Sorption solely retards the migration of these distorted concentration fronts, whereas biodegradation removes contaminant mass from the aquifer and reduces the travel distance of the plume.
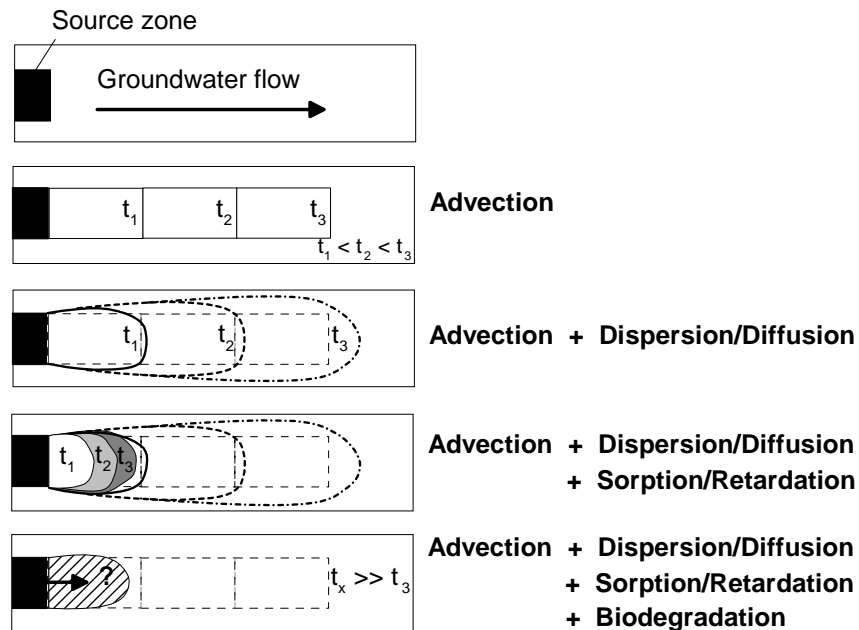


Figure 3.6: Development of contaminant plumes in groundwater with time ($t_1$-$t_3$ are points in time) (after Schiedek et al., 1997.)

# 4 The analytical quantification of field scale mass fluxes[2]

## 4.1 Abstract

A new integral groundwater investigation approach was used for the first time to quantify natural attenuation rates at field scale. In this approach, pumping wells positioned along two control planes were operated at distances of 140 m and 280 m downstream of a contaminant source zone at a former gasworks site polluted with BTEX- and PAH-compounds. Based on the quantified changes in total contaminant mass fluxes between the control planes, first-order natural attenuation rate constants could be estimated. For BTEX-compounds these ranged from $1.4E-02$ $d^{-1}$ to $1.3E-01$ $d^{-1}$, whereas for PAH-compounds natural attenuation rate constants of $3.7E-04$ $d^{-1}$ to $3.1E-02$ $d^{-1}$ were observed.

Microbial degradation activity at the site was indicated by an increase in dissolved iron mass flux and a reduction in sulphate mass flux between the two investigated control planes. In addition to information about total contaminant mass fluxes and average concentrations, an analysis of the concentration-time series measured at the control planes also allowed to semi-quantitatively delineate the aquifer regions most likely contaminated by the BTEX- and PAH-compounds.

## 4.2 Introduction

The processes of retardation and natural degradation significantly influence the migration of organic contaminants in groundwater (Borden et al., 1995; Wiedemeier et al. 1999). Natural attenuation of organic contaminants is based on these processes and can under ambient conditions be an alternative strategy for the remediation of contaminated sites (Chiang et al., 1989). As a remediation strategy, natural attenuation requires a careful monitoring and documentation program that comprises at least (i) the documentation of contaminant mass loss at field scale, (ii) the presentation of hydrogeochemical indicator trends, and (iii) the confirmation of microbial activity at the field site (Nyer and Duffin, 1997).

In this context, contaminant mass loss is the most critical factor to be documented because of its importance for risk assessment. For the documentation of contaminant mass loss at field scale, different investigation strategies have been used, such as monitoring of concentrations of contaminants and electron acceptors in space and time (e.g., Chiang et al., 1989; Gieg et al., 1999), field scale tracer experiments with isotopically labelled contaminants (e.g. Thierrin et al., 1995) or recalcitrant tracers (e.g., Wiedemeier et al., 1996), measurements of compound-specific stable isotope ratios in the field (e.g., Hunkeler et al., 1999), or the calculation of contaminant mass fluxes at control planes based on point scale measurements of contaminant concentrations

---

[2] Based on a publication in the Journal of Contaminant Hydrology

(e.g., King et al., 1999; Borden et al., 1997).

Inherent to these investigation approaches is the determination and subsequent interpolation of point scale measurements from boreholes. However, due to aquifer heterogeneity, the resulting plume delineation is strongly influenced by the positioning and the number of monitoring wells. In many cases the results are highly unreliable. In addition, contaminant source zones, specifically if a separate organic phase is present, exhibit a heterogeneous contaminant mass distribution in the subsurface leading to complex plume contours and variable downstream concentrations. It should be noted that a detected decrease of contaminant concentrations can hence be caused by the fact that a monitoring well system is mis-located at the fringe or even outside of the contaminant plume.

To overcome these difficulties, a new integral groundwater investigation method was developed (Teutsch et al., 2000; Ptak et al., 2000a), which is based on the in-situ quantification of contaminant mass fluxes across predefined control planes situated perpendicular to the mean groundwater flow direction. This method allows the simultaneous quantification of contaminant mass fluxes and average contaminant concentrations at control planes. In comparison with point scale measurements, it is based on a large sampling volume obtained by pumping.

This chapter presents the results and discussion of the first application of the new integral investigation approach for the quantification of effective natural attenuation rate constants at a former gasworks site. Attenuation rate constants were estimated based on mass flux changes of BTEX- (benzene, toluene, ethyl-benzene, o-, p-xylene) and selected PAH- (polycyclic aromatic hydro-

carbons) compounds across two control planes situated downgradient from a contaminant source zone at a former urban manufactured gas plant in SW-Germany. The mass fluxes across the control planes were calculated using an analytical solution derived by Schwarz (2001).

## 4.3 Integral groundwater investigation approach

In this method, one or more pumping wells are installed along a control plane perpendicular to the mean groundwater flow direction and operated simultaneously or sequentially downstream of a suspected pollutant source zone (Figure 4.1). Well positions, pumping rates, and pumping times are optimised to allow the well capture zones to cover the entire groundwater flow downstream of the contaminant site. During well operation, concentrations of target substances are measured as a function of time in the well discharge of each of the pumping wells. As a first step, these concentration-time series were interpreted using an analytical solution, which simplifies the problem to a steady-state situation and assumes that within the well capture zone (1) the flow towards the abstraction wells is radially symmetrical, i.e. the natural flow can be neglected during the pumping test; (2) the aquifer is homogeneous with regard to porosity, hydraulic conductivity and thickness, and (3) the concentration does not vary significantly or varies linearly along each of the streamtubes at the scale of the well capture zone, although it may vary from streamtube to streamtube. In other words, a possible concentration gradient (if not linear) in flow direction along a single streamline within the few tens of meters covered by the well capture zone is neglected.
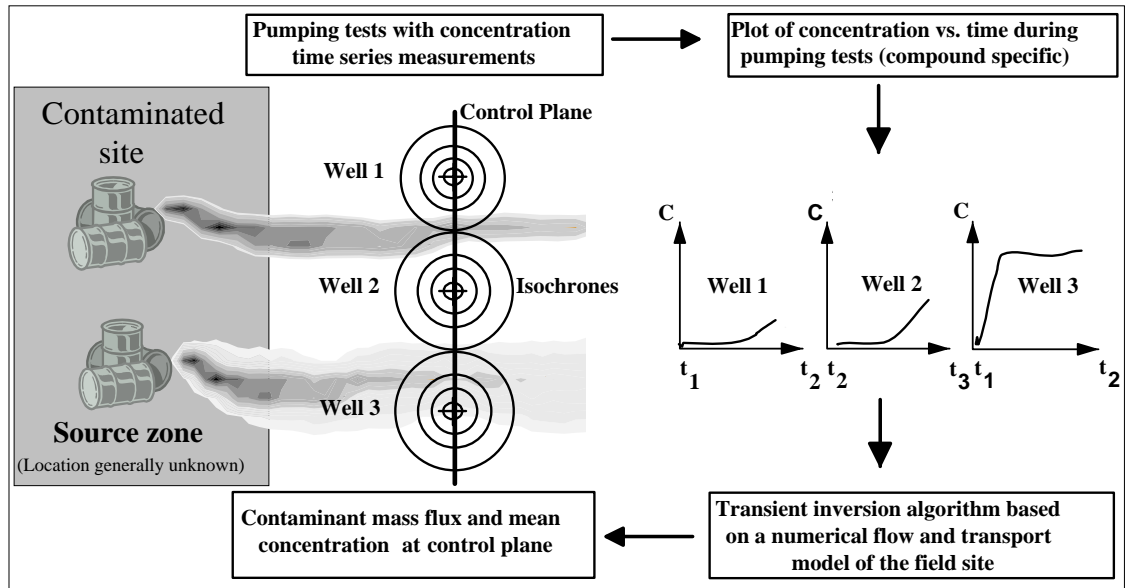
Figure 4.1: Illustration of the integral groundwater investigation method for the field scale quantification of contaminant mass fluxes

The introduction of concentration-time series obtained during pumping of a well into the analytical solution aims on the estimation of the mobile contaminant mass flux crossing a defined control plane. It does not focus on the quantification of the immobile contaminant mass trapped in low hydraulic conductivity zones of a heterogeneous aquifer within the well capture zone. The reason is that the mass flux of a target compound in the low permeability zones is generally considered to be relatively insignificant compared to the mass flux in the higher permeability preferential flow regions as seen in the following equation. The mass flux of a target compound can be estimated as:

$$MF = C_g \, Q \qquad (4.1)$$

with $C_g$ [$ML^{-3}$] and $Q$ [$L^3T^{-1}$] representing the contaminant concentration in the groundwater and the groundwater flow rate, respectively. If $Q$ approaches zero, so does the mobile mass flux in the respective aquifer region.

The first assumption of the analytical solution described above allows the treatment of a symmetrical problem around a pumping well. Based on the first two assumptions it is possible to describe the development of the isochrones around the pumping well and thus the well capture zone along the control plane, i.e. perpendicular to the groundwater flow direction, as a function of time:

$$r(t) = \sqrt{\frac{Q\,t}{\pi\,b\,n_e}} \qquad (4.2)$$

with $r(t)$, $Q$, $t$, $b$, $n_e$ symbolizing the radius [L] of the well capture zone at time $t$, the pumping rate [$L^3T^{-1}$], the time [T], the aquifer thickness [L] and the effective porosity [-], respectively. Based on the above said, a possible contaminant distribution in the groundwater prior to any pumping can be reconstructed using the measured concentration-time series at the pumping well.

For the reconstruction of a contaminant distribution prior to the pumping, the section of the control plane covered by the isochrones of a pumping well is separated into discrete streamtubes with

a characteristic and constant contaminant concentration (see assumption 3 above and Figure 4.2). The width of each streamtube is defined by the spatial increment $\Delta r$ [L] of the radius r [L] along the control plane between two consecutive sampling events as shown in Figure 4.2. Applying Equation 4.2, $\Delta r_i$ at time $t_i$ can be calculated as:

$$\Delta r_i = \sqrt{\frac{Q}{\pi\, n_e\, b}}(\sqrt{t_i} - \sqrt{t_{i-1}}) \quad (4.3)$$

The width of the streamtubes can therefore be controlled by the chosen time increment between two consecutive sampling events. The overall number of streamtubes at each well is then equal to twice the number of data points in the

concentration-time series because at each sampling time two streamtubes are crossing the control plane, one at each side of the well.

If the flow rate $Q_i$ [$L^3T^{-1}$] within a streamtube is given by:

$$Q_i = k|\nabla h|b\Delta r \quad (4.4)$$

where k [$LT^{-1}$], $|\nabla h|$ [-] and b [L] denote the hydraulic conductivity, hydraulic gradient and the aquifer thickness representative of a streamtube, all of which are all assumed to be constant for the analytical solution, then the total mass flux MF [$MT^{-1}$] of the target compound crossing the control plane at the section investigated by the pumping test can be estimated as:

$$MF = \sum_{i=1}^{2N} Q_i\, Cs_i \quad (4.5)$$
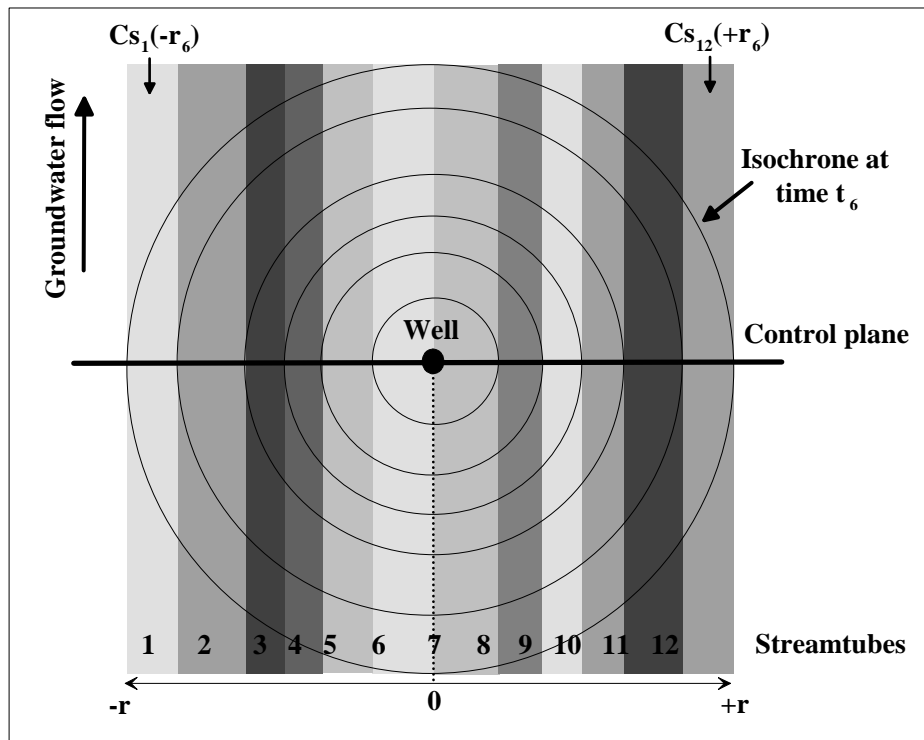


Figure 4.2: Pumping well with six sampling times and the corresponding isochrones and streamlines with Cs [$ML^{-3}$] and r [L] representing the concentration of the streamline and the radius, respectively (from Bockelmann et al., 2001a)

with N [-] and $Cs_i$ [ML$^{-3}$] representing the number of isochrones or data points in the concentration-time series and the concentration of the i-th streamtube crossing the control plane within the investigated well capture zone, respectively. Figure 4.2 illustrates the general approach for a pumping well with six sampling events. The total mass flux in this scenario would be the concentration $Cs_i$ of each streamtubeline multiplied by the natural groundwater flow within each streamtube (comp. Equation 4.5).

However, $Cs_i$ can not be measured in the field individually, as the well capture zone at a sampling time t [T] always intercepts streamtubes on both sides of the well, as seen from the control plane. For the flux quantification, we therefore define a theoretical concentration $Cx_i$, which is the average of the concentrations of the two streamtubes representative of time $t_i$ [T]:

$$Cx_i = \frac{Cs_i(-r_i) + Cs_i(+r_i)}{2} \qquad (4.6)$$

Combining Equation 4.5 and 4.6 yields:

$$MF = 2\sum_{i=1}^{N} Q_i Cx_i \qquad (4.7)$$

Schwarz (2001) presented a recursive formula for the calculation of $Cx_i$:

$$Cx_i = \frac{\pi\, Cp_i}{2\arccos\left(\frac{r(t_{i-1})}{r(t_i)}\right)} - $$

$$\frac{\sum_{k=1}^{i-1} Cx_k \left[\arccos\left(\frac{r(t_{k-1})}{r(t_i)}\right) - \arccos\left(\frac{r(t_k)}{r(t_i)}\right)\right]}{\arccos\left(\frac{r(t_{i-1})}{r(t_i)}\right)}$$

$$(4.8)$$

with $Cp_i$ [ML$^{-3}$] representing the concentration measured at the pumping

well at time $t_i$. For the first time step, $Cx_1$ equals $Cp_1$.

Subsequently, it is possible to calculate an average concentration $C_m$ [ML$^{-3}$] crossing the control plane as:

$$C_m = \frac{MF}{2\sum_{i=1}^{N} Q_i} \qquad (4.9)$$

with MF [M T$^{-1}$] and $Q_i$ [L$^3$ T$^{-1}$] denoting the total mass flux and the flow rate in the i-th streamtube, respectively. Retardation due to linear instantaneous sorption is not included in this study, but can be introduced into the analytical solution by transforming the time scale of concentration measurements, i.e. by dividing the time with a retardation factor R [-].

The mass flux determined with this method represents the total mass flux at the site, if the capture zone widths of the operated wells together are large enough to include the width of the entire potential source zone. It should be noted that total mass flux and average concentration can be simultaneously estimated for a number of target compounds. This may include not only the original contaminant, but also potential degradation products or electron acceptors, e.g. sulfate and nitrate, in case of a biodegradable contamination.

Deviations of the real aquifer conditions from the assumptions mentioned above would lead to an erroneous estimation of the control plane width in case of asymmetrical capture zones, as the extend of the well capture zones would not be adequately described with Equation (4.2). The analytical solution is also sensitive to errors concerning the parameters used for the computation of the isochrones and of the natural groundwater flow as seen from Equation (4.2) and Equation (4.4). As a

consequence, both an over- or under-estimation of the contaminant mass flux may result. A significant concentration gradient along the streamtubes would lead to an influence of higher concentrations from upgradient at the well and the concentrations measured during pumping would be relatively higher compared to a scenario without a significant gradient. Consequently, this would lead to an overestimation of the contaminant mass flux across the control plane.

In general, the analytical solution is a simplified estimation tool which can be applied to homogeneous or moderately heterogeneous field sites to estimate contaminant mass fluxes using a relatively small number of monitoring wells and without the need for a detailed groundwater flow and transport model. Like all analytical solutions, this method will suffer from the underlying simplifying assumptions if used in strongly heterogeneous conditions. If reliable assumptions about the groundwater flow and the shape of the well capture zone during pumping are available, a site specific decision can be made, whether an application of the analytical solution is satisfying or if a numerical solution (Ptak et al., 2000a) has to be employed. Using a numerical flow and transport model, it is possible to include spatially variable aquifer properties, asymmetrical well capture zones, retardation, specific boundary conditions and other site specific factors into the mass flux calculation.

The major drawback to the integral method is the cost of the pumping test required, respectively the costs for discharging the (potentially) contaminated groundwater during the pumping

test. Consequently, the pumping period should be reduced to the minimum possible.

## 4.4 Characteristic plume scenarios

Some typical scenarios can be described, where the concentration-time series obtained at a pumping well can be used to delineate various plume geometries and locations in the groundwater. To simplify the analysis, the plume concentration is assumed to be constant throughout the plume and the natural groundwater flow is ignored.

In Figure 4.3, four typical scenarios are displayed showing the concentration-time series at a pumping well and the interpreted subsurface plume location.

A type 1 scenario represents a site where the pumping well is located outside of a relatively narrow contaminant plume. At the beginning of the pumping, the well capture zone lies within the uncontaminated aquifer volume and the target compound concentrations in the well are below detection limit. As the well capture zone (isochrone) grows into the plume area, the contaminant concentrations in the well start to increase. At a later time, the well capture zone reaches the outer fringe of the plume and the contaminant concentrations in the well start to decrease again due to dilution. It is seen that the shape of the concentration-time series is controlled by the well location and the plume width.
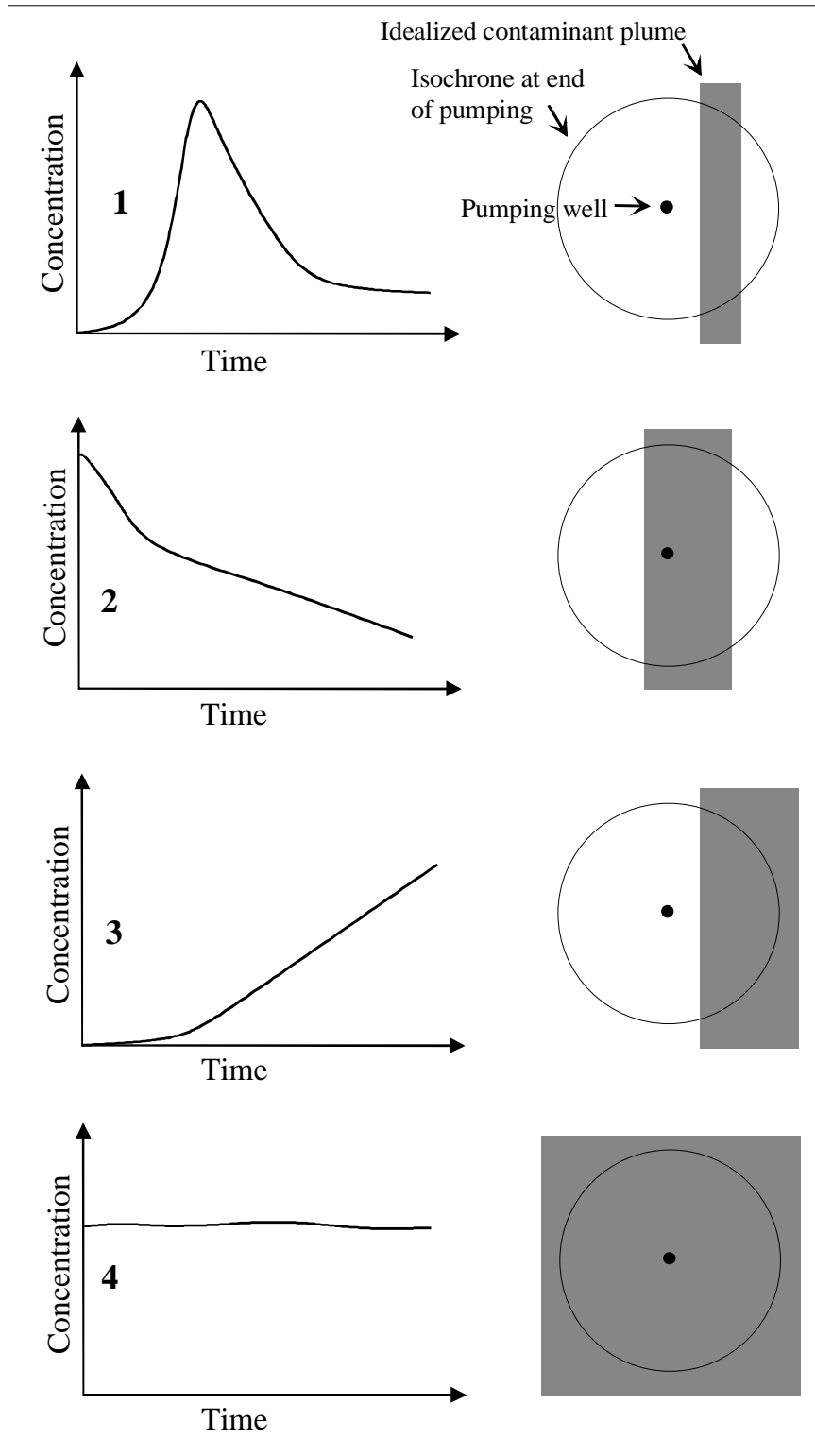
Figure 4.3: Four characteristic plume scenarios together with the expected concentration-time series (after Holder and Teutsch, 1999).

A type 2 scenario is observed in a pumping well, if the well is located within a contaminant plume, which itself is limited in width. In such a case, concentrations in the pumping well are high at the beginning of the pumping, but decrease as the size of the capture zone and hence the dilution increases with time.

A type 3 scenario is observed, if the pumping well is located outside of the contaminant plume and the plume width reaches beyond the maximum extent of the well capture zone. In such a case, the overall width of the contaminant plume cannot be assessed because the plume fringe is not reached by the well isochrone.

Finally, a type 4 scenario is characterized by a more or less constant contaminant concentration within the operated well. This indicates that the well is located within a wide plume with a insignificantly varying contaminant concentration. It should be noted that only under this specific condition, the contaminant concentrations measured in the well actually represents the real concentration in the plume.

The introduced scenarios will be used for the delineation of possible plume positions at the studied field site based on measured concentration-time series at the pumped wells.

## 4.5 Using mass fluxes to estimate natural attenuation rate constants

In the study presented, the integral groundwater investigation approach as illustrated in Figure 4.1 is extended such as to directly determine at field scale the change of mass fluxes in flow direction due to natural attenuation. This is implemented by using two or more control planes (CP) downgradient from a pollutant source zone (Figure 4.4).

If the compound-specific total mass fluxes MF [$MT^{-1}$] and the average non-retarded groundwater travel time $\Delta t$ [T] between two control planes are known, it is possible to quantify the compound-specific effective first-order natural attenuation rate constants as:

$$MF_{,CP(II)} = MF_{,CP(I)}e^{-\lambda R \Delta t} \quad (4.9)$$
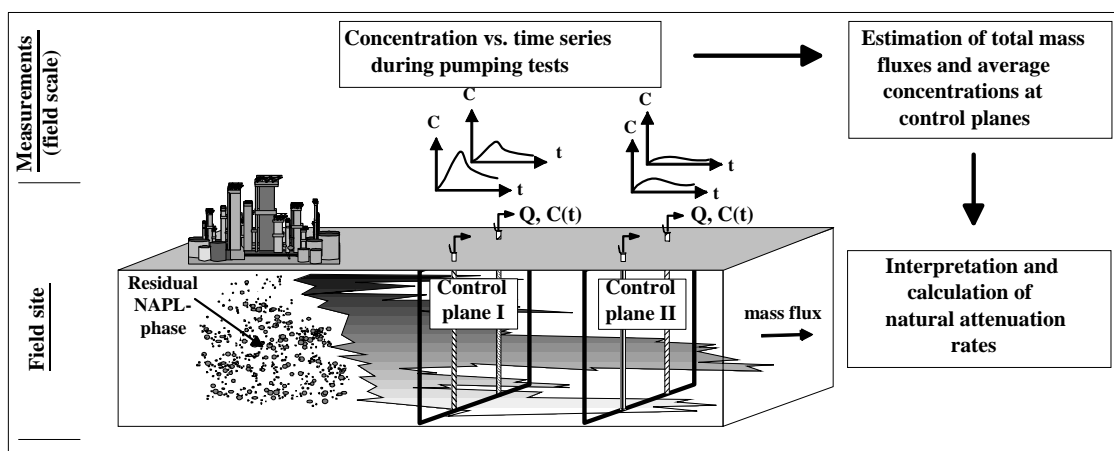


Figure 4.4: Concept of a two control plane approach for the quantification of natural attenuation rate constants at field scale (from Bockelmann et al., 2001a)

leading to

$$\lambda = -\ln\left(\frac{MF_{CP(II)}}{MF_{CP(I)}}\right)\frac{1}{R\,\Delta t} \qquad (4.10)$$

with $\lambda$ [T$^{-1}$], MF$_{CP(I)}$, MF$_{CP(II)}$ [MT$^{-1}$] and R [-] representing the effective natural attenuation rate constant, the measured compound specific mass fluxes at CP 1 and CP 2 and the retardation factor, respectively.

If organic compounds are subject to kinetic sorption as a consequence of diffusion into *intra*-particle pores of the aquifer minerals (Rügner et al., 1999), with a negligible contribution of sorption on the outer surface of the mineral grains, then the retardation factor may be omitted respectively set to one. The reason is that biodegradation of organic compounds can occur only outside of the *intra*-particle pores of the aquifer material present at the studied site. Rügner et al. (1999) showed that the typical pore radius of this material is generally < 100 nm, preventing the migration of microbes into the *intra*-particle pores. In this case, the time relevant for degradation is the time the contaminants spend within the inter-particle pore space, i.e. the time when the contaminant molecules are not absorbed by the minerals. This study therefore assumes a retardation factor equal to one for the computation of the natural attenuation rate constants for kinetically sorbing solutes.

It should be noted, that the differences in compound-specific mass fluxes between any two control planes can be due to degradation, sorption, and volatilization of the target compound. With the method presented here, it is not possible to differentiate between these different processes and therefore the natural attenuation rate constant ($\lambda$) calculated incorporates all these mass flux reducing factors yielding a total or effective value. However, dilution (e.g. due to recharge) and dispersion do not affect the results obtained by the integral investigation approach.

## 4.6 Application at a former urban gasworks site

### 4.6.1 Site description

A former urban gasworks in the Neckar valley near Stuttgart, Germany, was chosen as an experimental site to apply the new groundwater investigation approach in the field. The setting has an overall length of approximately 800 m, a width between 160 m and 400 m, and is bounded by a valley boundary in the west and the Neckar river in the east (Figure 4.5). During the experiments, the test site was equipped with 67 fully penetrating and fully screened sampling and monitoring wells. To allow for simultaneous multilevel sampling, 12 wells were equipped with a multilevel packer system (Schirmer et al., 1995, Ptak et al., 2000b).

The gasworks site was in operation from 1875 to 1970. Subsurface pollution at the site was recognised during construction activities in 1970. Until then, various types of coal processing products were handled at many different locations at the site and may have contributed to its pollution. It is assumed that most of the spillage occurred as a result of the destruction during World War II between 1943 and 1944, leading to the formation of a contaminant pool in the subsurface. The main source, which still continuously feeds the contaminant plumes at the site, has hence an age of close to 60 years.

Today, non-aqueous phase liquids (NAPLs) are present in both the unsatu
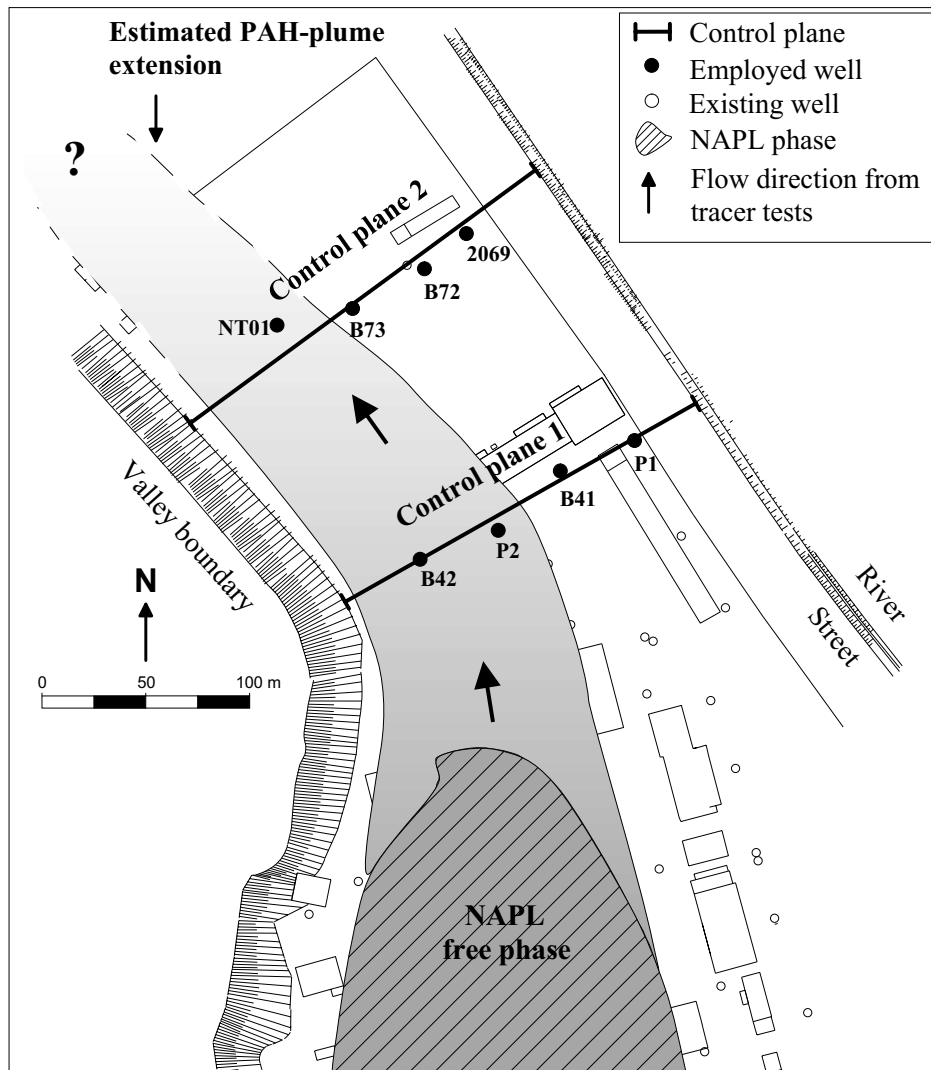
Figure 4.5: Overview of the field site with the location of the source zone and the monitoring and sampling wells

rated and saturated zones. Dissolution from the free NAPL phase still feeds the contaminant plume (Zamfirescu and Grathwohl, 1998). The historic development of the site suggests that a variety of contaminant point sources make up the zone of NAPL phase shown in Figure 4.5. This zone of free NAPL (= source zone), covers a total area of approximately 20,000 m$^2$ (Herfort, 2000). In the source zone, total BTEX concentrations in groundwater range up to 12 mgl$^{-1}$ and PAH concentrations are up to 3.2 mgl$^{-1}$ (Zamfirescu and Grathwohl, 1998). The resulting contaminant plume has an approximate width of 120 m and low molecular weight PAH-compounds were detected at a distance of 280 m downstream of the source zone, at concentrations of up to 190 µgl$^{-1}$ (acenaphtene). The overall length of the PAH-plume at the site is unknown yet as no monitoring wells are available downstream of control plane (CP) 2 (see Figure 4.5). For BTEX-compounds, the overall length of the plume is thought to be less than 280 m, as only p-xylene showed concentrations exceeding 0.2 µgl$^{-1}$ at CP 2 (see Figure 4.5).

It should be mentioned that for this site, it is known that volatilization of organic contaminants is not significant (Eiswirth et al., 1998). Thus, sorption and degradation can be regarded as the dominating mass flux reducing processes at the site, with chemical and biological degradation being the only processes that actually reduce the contaminant mass itself.

## 4.7    Geology and hydrogeology

The contaminated aquifer is composed of shallow Quaternary gravels with locally embedded sand, silt and loamy clay. Based on pumping tests, the average hydraulic conductivity at the site was estimated as 3.3E-03 $ms^{-1}$ (Herfort, 2000). The thickness of the aquifer varies spatially between 0 m and 5.5 m, due to a structured base and a partial replacement by anthropogenic fills at the top. The artificial fills originate from excavation works and the removal of World War II rubble. They locally replace both the natural aquifer material and the confining overbank deposits. The latter unit represents the naturally occurring confining layer at the site, and has a varying thickness of 1 m to 2 m. It consists of muddy, fine grained sediments with a high content of organic matter.

Figure 4.6 and Figure 4.7 illustrates the changes in the major geological features of the site with geological cross sections of CP 1 and CP 2.

Hydraulic heads at the site were monitored over a 3-year period with no indi-cation of significant seasonal changes or temporally variable groundwater flow directions (Herfort, 2000). The steady state of the local groundwater flow regime is due to the artificial regulation of the water level of the river that runs parallel to the eastern border of the field site (Figure 4.5). Tracer tests conducted at the site revealed a groundwater flow direction following the shape of the valley boundary (N-NW, see Figure 4.5). Average groundwater flow velocities within the aquifer were estimated from tracer tests as 2.0 $md^{-1}$ (Bösel *et al.*, 2000). Hydrogeochemically, the uncontaminated aquifer upstream of the gasworks site is characterized by an average dissolved oxygen concentration of less than 1.0 $mgl^{-1}$, a pH-value of about 7, non-detectable concentrations of BTEX and PAH, and dissolved iron concentrations of 70 $\mu gl^{-1}$.

## 4.8    Design of pumping campaigns for the integral groundwater investigation approach

A total of eight pumping wells, positioned along two control planes (CP) located 140 m (CP 1) and 280 m (CP 2) downstream of the source zone, were operated in two consecutive campaigns with four active wells each, to obtain a complete coverage of the aquifer width at both control planes (Figure 4.5).

The two pumping campaigns lasted 29 days and 33 days at CP 1 and CP 2 respectively. Within the pumping
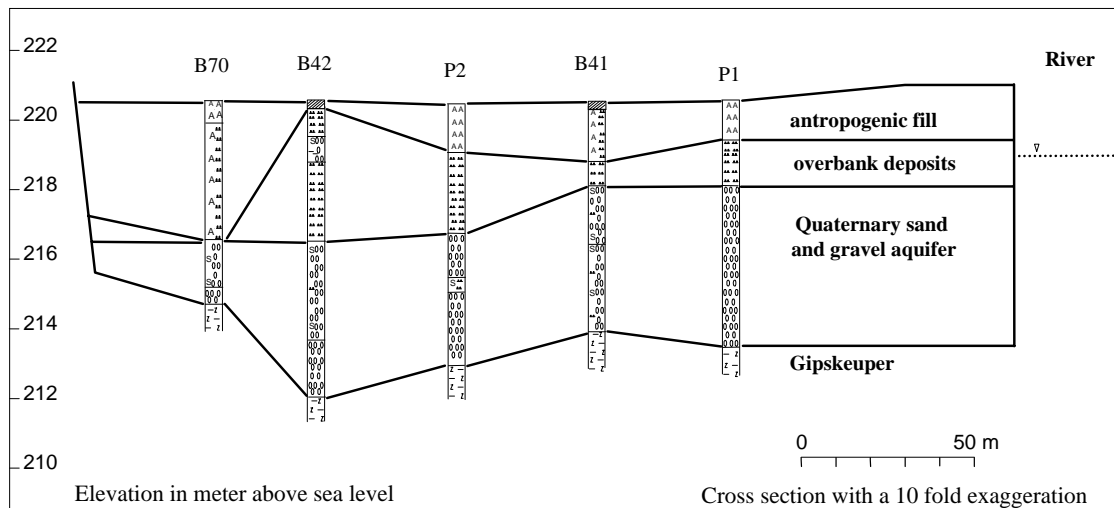
Figure 4.6: Geological cross section at control plane 1
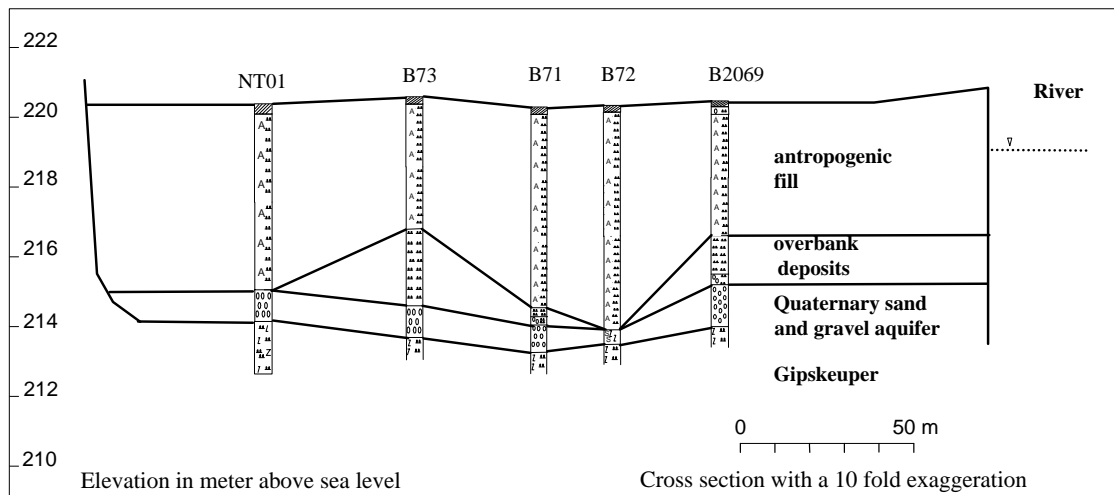


Figure 4.7: Geological cross section at control plane 2

campaigns, all the wells situated at a control plane were pumped sequentially allowing the groundwater table to recover to natural levels before the subsequent pumping test was started.

At CP 2 well NT01 has been operated for 62 hours at the beginning and for 120 hours at the end of the pumping campaign 24 days later. The duration of the individual pumping tests, as well as the input parameters used for solving analytically the inversion problem, are presented in Table 4.1. Target substances were BTEX- and PAH-compounds.

In addition to the organic target compounds, time series of temperature, electrical conductivity, pH, redox potential and dissolved oxygen were also measured during both pumping campaigns using standard probes placed within a flow-through cell to prevent gaseous exchange with the atmosphere. Groundwater samples were taken in sample bottles equipped with Teflon septums. The samples were stored at $4^{o}C$ to minimize microbial activity in the samples. Within 24 hours, BTEX samples were concentrated by purge and

Table 4.1: Hydraulic input parameters for the analytical mass flux quantification

| Well | Aquifer thickness [m] | Transmissivity [m²s⁻¹] | Hydraulic gradient [c] [-] | Pumping rate [m³s⁻¹] | Duration [h] | Max. radius [m] | Data points [d] |
|---|---|---|---|---|---|---|---|
| Control plane I | | | | | | | |
| B42 | 4.0 | 7.8E-03 | 0.002 | 4.08E-03 | 144 | 33.5 | 21 |
| P2 | 3.8 | 3.2E-03 | 0.0012 | 1.44E-03 | 96 | 16.7 | 11 |
| B41 | 2.96 | 3.1E-02 | 0.0015 | 4.16E-03 | 96 | 32.1 | 19 |
| P1 | 3.35 | 2.8E-02 | 0.0013 | 4.85E-03 | 96 | 32.6 | 19 |
| Control plane II | | | | | | | |
| NT01 [a] | 0.9 | 5.2E-03 | 0.0013 | 2.95E-03 | 62 | 39.4 | 34 |
| NT01 [b] | 0.9 | 5.2E-03 | 0.0013 | 3.46E-03 | 120 | 59.4 | 33 |
| B73 | 0.8 | 4.0E-03 | 0.0016 | 2.33E-03 | 73 | 40.2 | 34 |
| B72 | 0.3 | 6.0E-03 | 0.00065 | 1.03E-04 | 49 | 11.3 | 11 |
| 2069 | 1.5 | 2.1E-02 | 0.0036 | 2.52E-03 | 120 | 39.2 | 32 |

(a) First campaign at well NT01  (b) Second campaign at well NT01 24 days later
(c) Derived from hydraulic potential differences between upgradient monitoring well and abstraction well
(d) Number of data points in the concentration-time series measured at the well

Table 4.2 :Mass fluxes at the control planes 1 and 2

| Control Plane 1 [gd⁻¹] | B42 | P2 | B41 | P1 | Total |
|---|---|---|---|---|---|
| Acenapthene | 24.4 | 3.5 | 2.7 | 9.2 E-03 | 30.6 |
| PAH$_{tot}$ | 25.0 | 3.7 | 2.8 | 1.7 E-01 | 31.7 |
| Benzene | 1.6 | 0.2 | n.d. | n.d. | 1.8 |
| BTEX$_{tot}$ | 1.8 | 0.2 | n.d. | n.d. | 2.0 |
| SO$_4$ | 34,500 | 5,100 | 109,500 | 68,300 | 217,400 |
| NO$_3$ | n.d. | n.d. | n.d. | 240 | 240 |
| Fe(II) | 450 | 100 | 1,020 | 540 | 2110 |
| Mn(II) | 40 | 5 | 490 | 160 | 695 |
| Cl | 12,300 | 1910 | 62,130 | 30,050 | 106,390 |

| Control Plane 2 [gd⁻¹] | NT01 | B73 | B72 | 2069 | Total |
|---|---|---|---|---|---|
| Acenapthene | 11.8 | 5.6 E-01 | 6.7 E-03 | 3.9 E-01 | 12.8 |
| PAH$_{tot}$ | 12.2 | 6.0 E-01 | 1.5 E-02 | 6.2 E-01 | 13.4 |
| Benzene | n.d. | 1.6 E-04 | 2.0 E-05 | 1.0 E-01 | 9.4 E-02 |
| BTEX$_{tot}$ | 0.02 | 2.7 E-03 | 7.9 E-04 | 1.0 E-01 | 0.1 |
| SO$_4$ | 29,000 | 20,000 | 440 | 162,800 | 212,240 |
| NO$_3$ | 60 | n.d. | n.d. | 690 | 750 |
| Fe(II) | 740 | 500 | 40 | 1850 | 3,130 |
| Mn(II) | 50 | 70 | 2 | 320 | 442 |
| Cl | 11,220 | 10,470 | 300 | 80,990 | 102,980 |

n.d. = not detectable

trap and analysed on a HP 6890 GC-MS. PAH samples were extracted with cyclohexane (liquid-liquid extraction) and analysed on a HP 5890 GC-MS. Additional time series of inorganic nutrients ($SO_4^{2-}$, $PO_4^{2-}$, $NO_3^-$) and other inorganic constituents ($Cl^-$, $Fe^{2+}$, $Mn^{2+}$) were measured by ion chromatography and atomic adsorption spectrometry using standard methods. The obtained concentration-time series of the organic compounds are shown in Figure 4.8 to Figure 4.10.

## 4.9 Results and discussion

Table 4.2 summarises the compound-specific mass fluxes obtained from the two pumping campaigns at the field site, employing the analytical inversion solution of the integral groundwater investigation approach. To our knowledge, this is the first field scale study, where an integral investigation approach for the simultaneous quantification of mass fluxes of both organic contaminants and inorganic hydrogeochemical parameters was applied.

### 4.9.1 Chloride mass flux

The chloride mass flux at the field site was estimated as approximately 106,000 $gd^{-1}$ and 103,000 $gd^{-1}$ at CP 1 and CP 2 respectively (Table 4.2). Assuming (1) that chloride behaves conservatively during transport and (2) that there is no additional chloride source between the two control planes, the small difference (~ 3%) suggests that basically the same groundwater transport paths were captured at both control planes.

### 4.9.2 Mass flux of electron acceptors

To study mass flux changes of possible electron acceptors used for microbial degradation of organic contaminants, sulphate ($SO_4^{2-}$), nitrate ($NO_3^-$),

40

dissolved iron ($Fe^{2+}$), and dissolved manganese ($Mn^{2+}$) were included in the integral site investigation. Compared to CP 1, CP 2 showed an increase of about 1,000 $gd^{-1}$ (~ 50 %) in dissolved iron mass flux indicating ongoing iron reduction at the site. The sulphate flux crossing the two control planes appeared to decrease by around 5,000 $gd^{-1}$ (~ 2%), is hence comparable to the change in chloride flux between the control planes and could be due to different capture widths or uncertainties in the input parameters used for the flux quantification. However, the overall sulphate flux at the site is very high and microbial sulphate reduction may account for only a relatively small decrease of the total flux. Consequently, such a minor reduction might not be measurable at sites with a very high total sulphate flux. However, anaerobic sulphate reduction at the site is further indicated by $H_2S$ concentrations of up to 1.8 ppm in the gaseous phase in the abstraction wells along CP 2. Ongoing sulphate reduction is therefore likely to occur, although flux estimations remained inconclusive.

Due to the presence of sulphide in the system, precipitation of sulphide compounds is possible. This might cause an underestimation of iron and manganese reduction in the system as only the mass flux of dissolved species was quantified. Precipitation of manganese is also the likely reason for the observed reduction in dissolved manganese mass flux between the two control planes.

Nitrate was mostly found in samples with negligible contaminant concentrations (wells B41 and P1 at CP 1 and well 2069 at CP 2). As nitrate is present in the groundwater in uncontaminated areas, it is possible to conclude that anaerobic microbial degradation activity utilizing nitrate as an electron acceptor occurred between the source and CP 1,

leading to a nitrate depletion in the contaminated aquifer regions at the control plane. At CP 1 nitrate could only be found at well P1, located outside of the main contaminant plumes. However, nitrate could be found in some of the samples taken at well NT01 at CP 2. This might indicate an inflow of nitrate containing water from the slopes into the valley between the two control planes. Even so, the apparent increase in total nitrate mass flux between the two CPs was credited to well 2069 situated outside of the main contaminant plume, where about 90% of the nitrate mass flux across CP 2 was found (see Table 4.2). At this well, nitrate concentrations decreased from about 6 $mgl^{-1}$ to below detection limit within two days of pumping. This suggests a relatively small nitrate plume at the well, which was diluted with time to concentrations below detection limit (see scenario 2, Figure 4.3). The origin of the nitrate is uncertain, as concentrations upstream at well P1 did not significantly exceed 1 $mgl^{-1}$.

### 4.9.3   Mass flux of PAH-compounds

During the following discussions frequent reference will be made to characteristic concentration-time series scenarios as described in Figure 4.3. The illustrated scenarios shown in Figure 4.3 will be referenced by their individual scenario number only.

With regard to organic contaminants, polycyclic aromatic hydrocarbons (PAHs) dominate the contaminant mass flux at the two control planes. Overall PAH mass fluxes of about 32 $gd^{-1}$ and 13 $gd^{-1}$ at CP 1 and CP 2, respectively, were an order of magnitude higher compared to BTEX mass fluxes (comp. Table 4.2). Of the PAH-compounds, acenaphthene (*Ace*) displayed the highest individual contribution to the total PAH mass flux with approximately 31 $gd^{-1}$ at CP 1 and about 13 $gd^{-1}$ at the downgradient control plane.

Compared to other PAH-compounds, *Ace* has a relatively high water solubility of about 30 $mgl^{-1}$ (Mackay and Shiu, 1977), and a relatively low $logK_{ow}$ of around 4 (Yalkowsky and Valvani, 1979), and is therefore one of the PAH-compounds with a relatively high mobility. The highest PAH mass fluxes at the site were obtained at wells B41 and P2 at CP 1 and at well NT01 at CP 2 (Table 4.2). Nearly all of the *Ace* mass flux across CP 2 was found at well NT01, whereas all other wells at that control plane showed total PAH mass fluxes of less than 1 $gd^{-1}$.

Figure 4.8 illustrates the PAH concentration-time series obtained at the two control planes during the pumping campaigns. It can be seen that the *Ace* concentration-time series of well B42 relatively quickly reached a concentration plateau of about 250 $\mu gl^{-1}$ and remained constant for about 4 days of continuous pumping. From the concentration-time series it can be assumed that well B42 is located within a PAH plume and that the plume itself is relatively homogeneous with regard to the *Ace* mass distribution in the subsurface (see scenario 4).
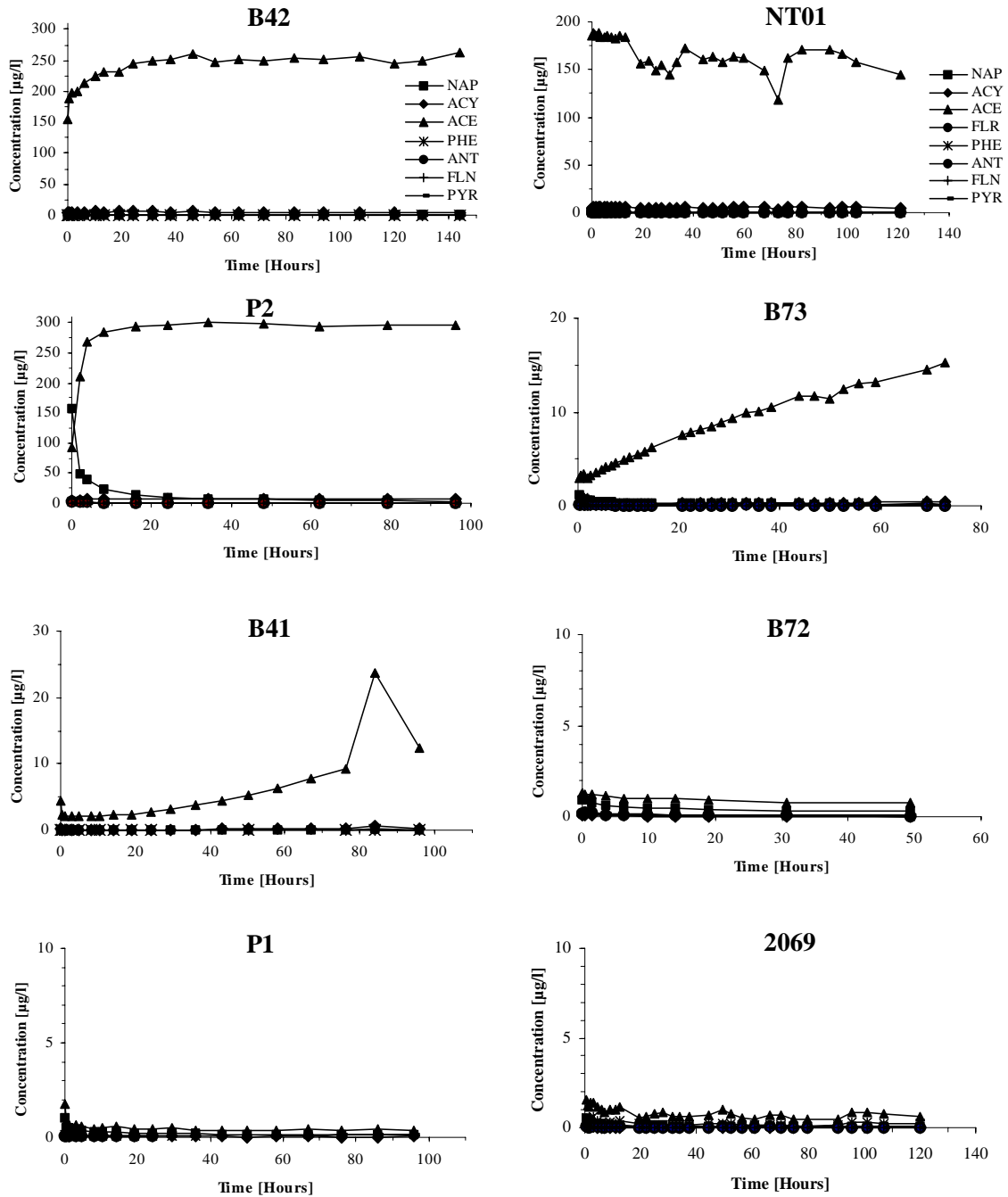
Figure 4.8: Concentration-time series of PAH compounds measured at the wells at control plane 1, shown on the left, and at control plane 2, shown on the right. Abbreviations: NAP-Naphthalene, ANY-Acenaphthylene, ACE-Acenaphthene, FLR-Fluorene, PHE-Phenanthrene, ANT-Anthracene, FLN-Fluoranthene, PYR-Pyrene.

As the *Ace* concentration did not decline during the entire pumping period, it can be concluded that the spatial extend of the PAH plume perpendicular to the groundwater flow direction at CP 1 is larger than the well capture zone of well B42 at the end of the pumping. The

slightly lower *Ace* concentrations at the beginning of the pumping test might be due to reduced *Ace* concentrations in the well itself and/or to lower *Ace* concentrations in the close vicinity of the well.

The *Ace* concentration-time series at well P2 at CP 1 (see Figure 4.8) can

also be characterized as a type 4 concentration-time series (compare scenario 4 in Figure 4.3). Again, the contaminant concentrations increased quickly at the beginning of the pumping, after which the concentration measured stayed at approximately 300 µgl$^{-1}$ for close to three days of constant pumping. This data illustrates the presence of a PAH plume in the surrounding area of the well, which was not completely covered by the expanding well capture zone. This plume also showed to be relatively homogeneous with regard to *Ace* concentrations in the subsurface.

The increase of the *Ace* concentration in well P2 correlated with a decrease in naphthalene (*Nap*) concentrations from about 150 µgl$^{-1}$ to about 3 µgl$^{-1}$ during the first 6 hours of pumping. The decrease in *Nap* is likely caused by anaerobic degradation by sulphate reducing micro-organisms, as described, for example, by Meckenstock et al. (2000).

The reason for the simultaneous increase of Ace concentrations remains uncertain, but might be a results of local heterogeneities in the contaminant distribution in the groundwater. At all other operated wells at the two control planes, *Nap* concentrations were generally below 1 µgl$^{-1}$. At well P2, after the decline of *Nap* concentrations, *Ace* concentrations measured were consistently about 50 µgl$^{-1}$ higher compared to concentrations measured at well B42. As multiple point sources of NAPL contamination exist at the site under study (Zamfirescu and Grathwohl, 2001) the observed concentration difference might be caused by PAH plumes originating from different point sources. However, an analysis of the overall PAH plume compositions at the two wells did not show significant differences suggesting a similar contaminant source.

At well B41 at CP 1 (Figure 4.5), the *Ace* concentration-time series followed a type 3 scenario (see Figure 4.3). The

concentrations continuously increased during pumping, suggesting that with time, the increasing well capture zone covered an increasing part of the PAH plumes outer fringe, causing the concentration readings to increase with time. At the end of the pumping test, the measured *Ace* concentrations were about an order of magnitude lower compared to *Ace* concentrations measured at the wells B42 and P2 to the west of well B41 (Figure 4.5).

This supports the conclusion that well B41 is located within a relatively clean part of the aquifer, and that the contaminant plume was partly drawn towards the well during well operation. At the eastern end of CP 1 at well P1, only background concentrations of PAH-compounds could be found during pumping, supporting the conclusion that the PAH contamination of the aquifer at the field site is limited to the western section of CP 1.

At CP 2, over 90 % of the total PAH mass flux was found at well NT01 located at the western end of the control plane (Figure 4.5 and Table 4.2). The *Ace* concentration-time series measured at this well (Figure 4.8) indicates that the well is located within the contaminant plume and that during well operation the well capture zone did not reach the outer fringe of the encountered plume (scenario 4), as the concentrations in the well would then have declined again (scenario 2).

Of the other wells at CP 2, only B73 showed elevated *Ace* concentrations (Figure 4.8) that increased continuously during pumping (scenario 3), indicating that with time and with a growing well capture zone, more contaminated water was pulled from the area around well NT01 towards B73.

In conclusion, it is proposed that the main PAH mass flux crosses CP 1 between the valley boundary to the west and well B41 to the east. At CP 2, the

PAH plume is most likely located between the valley boundary to the west and well B73 to the east. Figure 4.5 illustrates the proposed PAH-plume position in relation to the positioning of the abstraction wells and control planes.

### 4.9.4 Mass flux of BTEX-compounds

At CP 1, BTEX concentrations above background values were found only at wells B42 and P2. At both wells, total BTEX mass flux was dominated by benzene, showing an increase in benzene concentrations with time during the pumping tests (Figure 4.9). At well B42, benzene concentrations increased steadily during pumping from below detection limit to about 25 ugl$^{-1}$ after five day of pumping. Towards the end of the pumping test, ethylbenzene also began to increase with time. The characteristic form of the benzene concentration-time series (scenario 3 in Figure 4.3) and the absence of measurable benzene concentrations at the beginning of the pumping indicate that in contrast to the PAH contamination, well B42 is likely to be located outside of the BTEX plume crossing CP 1. From well P2, similar BTEX concentration-time series were obtained, leading to the same conclusion with regard to the location of the BTEX plume crossing CP 1.

A noticeable difference between data from B42 and P2,were elevated BTEX concentrations in the first sample taken from P2, which were most likely caused by a contamination of the well from surface runoff. Apart from this artefact, benzene concentrations increased steadily in the well during four days of pumping following a scenario 3 development. In both wells, a similar BTEX plume composition, dominated by benzene was found, and both wells displayed comparable BTEX concentrations during well operation, leading to the conclusion that it is likely that the same BTEX plume was encountered during the pumping tests at B42 and P2. In addition, no BTEX-compounds were found above detection limits during the operation of wells B41 and P1 at CP 1, supporting the presence of a single BTEX-plume, which crosses the control plane between the wells B42 and P2.

Theoretically, the measured benzene concentration-time series could also be the result of two distinct BTEX-plumes crossing CP 1, one situated to the west of B42 and one located within the surrounding area of well P2. As no additional mass flux information is yet available for the area between the valley boundary to the west and well B42 to the east, this alternative interpretation cannot be falsified.
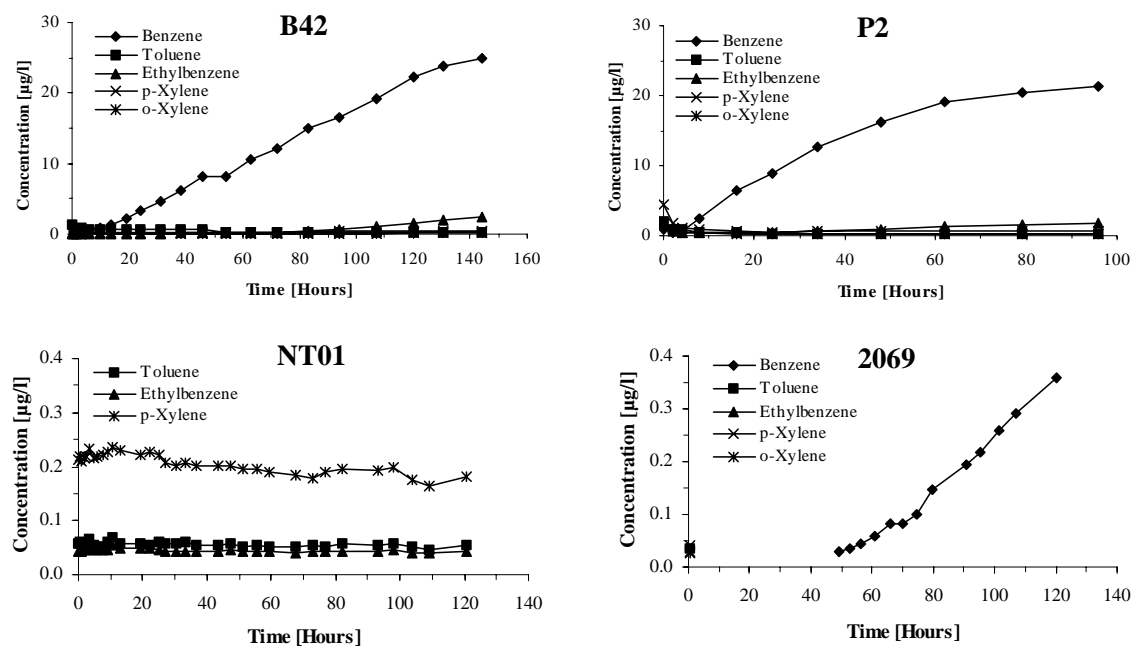
Figure 4.9: Concentration-time series of BTEX compounds measured at the wells at control plane I1 shown above, and at control plane 2, shown below.

At CP 2, approximately 280 m downstream of the source zone and about 140 m downstream of control plane 1, BTEX concentrations significantly above the analytical detection limit of 0.05 $\mu gl^{-1}$ were obtained from wells NT01 and 2069 only (Figure 4.9).

At well NT01, BTEX concentrations stayed more or less constant during well operation at about 0.2 $\mu gl^{-1}$ for p-xylene and at less than 0.1 $\mu gl^{-1}$ for ethylbenzene and toluene. Benzene, which dominated the total BTEX mass flux at CP 1, could not be detected at any well at CP 2, apart from well 2069. This was surprising, as no BTEX-compounds were detected 140 m upstream from well 2069 at the wells B41 and P1 (Figure 4.5 and Table 4.2).

In addition, only benzene could be detected at well 2069, whereas all other BTEX-compounds stayed below detection limits. Moreover, apart from the first sample taken during the pumping, only late time data at well 2069 showed measurable benzene concentrations, which stayed below detection limit for the first 2 days of pumping and sub-

sequently increased from there to about 0.35 $\mu gl^{-1}$ towards the end of the pumping test. The first sample from the well, taken after about 500 seconds of pumping showed BTEX concentrations close to detection limit, which was most likely due to contamination of the well from surface runoff and not due to a contamination of the aquifer itself. The origin of the benzene contamination encountered later by the capture zone of well 2069 can be allocated to an area either between the two control planes or further downstream from well 2069, but within the area covered by the capture zone of the well.

Due to the most likely presence of an additional source encountered during operation of well 2069, mass fluxes estimated at this well were not incorporated into the estimation of first-order natural attenuation rate constants shown in Table 4.3.

### 4.9.5 Well positioning and reproducibility

Figure 4.5 illustrates the estimated PAH-plume position and the location of the abstraction wells used for the integral groundwater investigation. It is seen that at CP 2 only a single well was located within the area affected by the PAH contamination.

At the beginning of the site investigations, a groundwater flow direction to the north was assumed and the monitoring network installed accordingly. Despite this non-optimal monitoring, total contaminant mass flux and mean concentration were determined by adapting the pumping rate and pumping duration for the wells available to achieve a complete coverage of the downstream aquifer.

During well operation, a situation may occur, where a contaminant plume is pulled towards a pumping well, passing through previously uncontaminated aquifer material. To check for the reproducibility of the results from the application of the investigation approach, pumping of well NT01 at CP 2 was repeated 24 days after the first pumping campaign. A comparison of the measured concentration-time series in the well discharge is presented in

Figure 4.10 for toluene, p-xylene and acenaphthene. It can be seen that the concentration-time series for toluene and p-xylene are almost identical during both campaigns, with both compounds starting at a slightly higher initial concentration during the first pumping period. After approximately 8 hours of well operation, the two experiments yield effectively similar results.

For acenaphthene, some discrepancy between the two campaigns can be seen, with a lower concentration measured during the second pumping campaign. However, as the observed discrepancy is only about 10%, it is inconclusive whether the effect is an indication for a transient situation remnant from the previous pumping or caused by other factors such as sampling and analytical errors. Due to the difference in the concentration-time series, the second pumping campaign would yield a 10% smaller acenaphthene flux compared to the first data set. It can be concluded that at this site, the effects of repeated pumping are smaller than the uncertainties in input parameters like porosity or hydraulic conductivity.
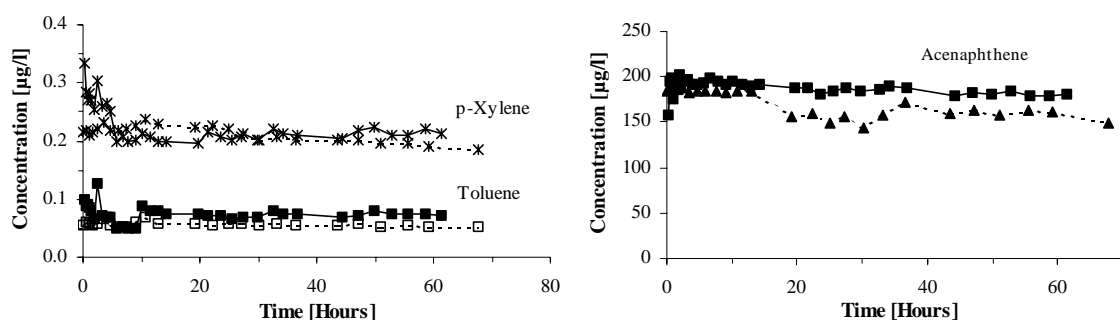


Figure 4.10: Concentration-time series of p-xylene, toluene and acenaphthene at well NT01. Continuous line: Initial pumping campaign. Dotted line: Second pumping campaign 24 days later.

### 4.9.6 Effective natural attenuation rate constants

Based on contaminant mass fluxes at the two investigated control planes, compound specific effective natural attenuation rate constants have been estimated using Equation 4.10.

Table 4.3: First-order natural attenuation rate constants of the organic contaminants for the transport between the two investigated control planes

| Compound | Natural attenuation rate constant [$d^{-1}$] |
|---|---|
| Benzene | 1.3E-01 |
| Toluene | 3.1E-02 |
| Ethylbenzene | 5.1E-02 |
| o-Xylene | 1.4E-02 |
| p-Xylene | 3.8E-02 |
| Naphthalene | 2.9E-02 |
| Acenaphthylene | 6.9E-03 |
| Acenaphtene | 1.3E-02 |
| Fluorene | 1.2E-02 |
| Anthracene | 1.8E-02 |
| Fluoranthene | 3.7E-03 |
| Pyrene | 3.1E-02 |

The input parameters for the analytical mass flux quantification are shown in Table 4.1. Aquifer thicknesses were extracted from drilling logs, transmissivity values were estimated from pumping test data and hydraulic gradients were derived from differences in hydraulic potential between upgradient monitoring wells and abstraction wells prior to any pumping. An average groundwater velocity of 2 $md^{-1}$ was assumed based on tracer test analyses (Bösel et al., 2000), yielding an average travel time of 70 days between the two control planes. Effective natural attenuation rate constants were only estimated for compounds that were detected at both control planes. Higher molecular weight PAH-compounds with concentration < 0.05 $\mu gl^{-1}$ (analytical detection limit) at CP 2, approximately 280 m downgradient of the contaminant source zone and were not included in the calculation of effective natural attenuation rates.

For benzene, a relatively high effective natural attenuation rate of 1.3E-01 $d^{-1}$ has been estimated in this study, which is about an order of magnitude higher compared to attenuation rate constants proposed in the literature (e.g. Wiedemeier et al., 1999). In comparison, estimated $\lambda$-values for toluene, ethylbenzene and o-,p-xylene were in the range of 1.4E-02 $d^{-1}$ to 5.1E-02 $d^{-1}$ and agree well with attenuation rates published for other sites (e.g. Aronson and Howard, 1997). Based on the mass flux analyses of potential electron acceptors between the control planes, the relatively high attenuation rates for BTEX are likely to be a result of microbial degradation processes, utilizing predominantly iron and sulphate as electron acceptors. With concentrations of up to 500 $mgl^{-1}$ sulphate should be readily available for microbial organisms. Consequently, the supply of electron acceptor is not a limiting factor at the site.

For PAH-compounds, estimated $\lambda$-values for the transport distance between the two control planes ranged from 3.7E-03 $d^{-1}$ to 3.1E-02 $d^{-1}$. These values are based on a retardation factor equal to one and agree well with attenuation rates published by Mackay et al. (1992) and Howard et al. (1991). However, pyrene and naphthalene both showed similar and therefore unexpectedly high $\lambda$-values of about 3.0E-02 $d^{-1}$. Comparing these two PAH-compounds, it is very likely that different reactive transport processes dominated the attenuation of the individual compounds.

For the more mobile, more easily biodegradable naphthalene, it may be assumed that biodegradation is the predominant attenuation process. However, it is possible that for PAHs like pyrene, with a relatively low water solubility and a relatively high log $K_{oc}$ value, a significant diffusive uptake into aquifer mineral grains, acting as a contaminant mass sink, still occurs at the site. Using a retardation factor > 1 in Equation 4.10 would yield the expected smaller attenuation rate constant

compared to the value for naphthalene. But as effective natural attenuation rates are obtained from the two-control-plane-approach, it is impossible to quantify the relative contributions of the two processes of degradation and sorption, respectively. This separation requires sophisticated reactive transport modelling studies.

Therefore, in the next step, the integral groundwater investigation approach will be combined with a tool to evaluate the effect of sorption on the contaminant mass flux reduction between the control planes. Subsequently, the contribution of biodegradation to the reduction of the mass flux will be directly quantified at field scale.

## 4.10 Conclusion

An integral groundwater investigation approach for the quantification of total contaminant mass fluxes and first-order effective natural attenuation rate constants was developed and applied to a former urban gasworks site. At the site, BTEX- and PAH-compounds are continuously released from an area of free phase NAPL (Zamfirescu and Grathwohl, 2001) feeding contaminant plumes migrating downgradient from the source zone.

Two control planes, consisting of four monitoring wells each, were installed more or less perpendicular to the mean groundwater flow direction at distances of 140 m and 280 m downgradient from the contaminant source. At the control planes, compound-specific mass fluxes were measured

and used for the estimation of effective first-order natural attenuation rates. It was concluded that the encountered BTEX- and PAH-plumes are biodegraded under anaerobic conditions utilizing mainly sulphate and iron reduction in the process.

Evidence for intrinsic biodegradation is given by the reduction of contaminant mass with transport distance from the source, which occurred together with a an increase of dissolved iron ($Fe^{2+}$) mass flux. Effective natural attenuation rate constants at the site were estimated as $1.6E\text{-}02$ $d^{-1}$ to $1.3E\text{-}01$ $d^{-1}$ for BTEX- and $4.1E\text{-}03$ $d^{-1}$ and $3.3E\text{-}02$ $d^{-1}$ for PAH-compounds.

The interpretation of the concentration-time series measured at the abstraction wells furthermore allowed to delineate aquifer regions most likely contaminated by BTEX- and PAH-compounds. It was demonstrated that the aquifer contamination at the site is limited to the western section of the control planes. To derive the relative contribution of contaminant degradation and sorption on mass flux reduction between the control planes, the integral groundwater investigation will be coupled to a numerical reactive transport model, which explicitly simulates the sorption kinetics of organic compounds.

For site assessments, the applied integral investigation approach reduces the number of monitoring wells needed and significantly increases the level of certainty of the results. The mass fluxes obtained can be used for risk assessment purposes, as well as for the design of effective remediation strategies.

# 5 Field scale quantification of mass fluxes and natural attenuation using a limited monitoring network[3]

## 5.1 Abstract

At many "real world" field sites the number of available monitoring wells is limited, due to economic or geological reasons. Under such restricted conditions it is difficult to perform a reliable field investigation and to quantify primary lines of evidence for natural attenuation, like the documentation of a decrease of contaminant mass flux in flow direction. This study reports the results of a groundwater investigation at a former manufactured gas plant situated in a Quaternary river valley in south-west Germany. The location, infrastructure and aquifer setting is typical of many industrial sites in Germany. Due to difficult drilling conditions (coarse glaciofluvial gravel deposits and an anthropogenic fill above the aquifer) only 12 monitoring wells were available for the investigation and localisation of the contaminant plume. These wells were situated along three control planes downgradient from the contaminant source, with four wells along each plane. Based on the sparse set of monitoring wells, field scale mass fluxes and first-order natural attenuation rate constants of benzene, toluene, ethylbenzene, o,p-xylene (BTEX) and low molecular weight polycyclic aromatic hydrocarbons (PAH) were estimated utilizing different point scale and also a new integral investigation method.

The results show that even at a heterogeneous site with a sparse monitoring network point scale investigation methods can provide reliable information on field scale natural attenuation rates, if a dependable flow model or tracer test data is available. If this information is not available, only the new integral investigation method presented can yield adequate results for the quantification of contaminant mass fluxes under sparse monitoring conditions.

## 5.2 Introduction

Widespread sources of organic contaminants in shallow aquifer systems are leaking underground storage tanks and pipelines, petrol stations and manufactured gas plant sites. At such locations, groundwater contaminants generally include benzene, toluene, ethylbenzene and xylenes (BTEX) and/or polycyclic aromatic hydrocarbons (e.g. 16-EPA-PAH). The application of traditional remediation approaches like pump and treat can lead to very high remediation costs because of the time needed for site clean up (Barker et al., 1995) and often these approaches do not accomplish the required remediation targets (Travis and Doty, 1990).

During the last decades, the potential for natural biodegradation of organic contaminants in groundwater under various redox conditions has been extensively studied and documented for both BTEX (e.g. ,Gibson et al. 1968; Major et al., 1988; Edwards et al., 1992; Vogel and Grbic-Galic, 1986) and PAH (e.g., Cerniglia, 1992; McNally et al., 1998; Coates et al., 1997; Genthner et al., 1997) compounds. These laboratory studies have been accompanied by reports from several field and research sites (e.g., Barker et al., 1987; Chiang et al., 1989; King et al., 1999),

---

which demonstrated that contaminant distribution and migration in aquifer systems is influenced by processes such as biotic and abiotic degradation, sorption, volatilisation and dispersion. This led to the development of the concept of natural attenuation, which acknowledges the potential for a contaminant mass flux reduction in an aquifer system without human interference and which was implemented in different regulatory guidelines as an alternative remediation strategy under favourable field conditions (e.g., USEPA, 1999).

The application of natural attenuation as a remediation strategy is based on a detailed monitoring and documentation procedure (Nyer and Duffin, 1997; Gieg et al. 1999). This documentation is often difficult to accomplish at field scale, as the required lines of evidence, for example the reliable documentation of a reduction of contaminant concentrations or mass fluxes in flow direction, is hard to be achieved. Recently, it has been shown by Kao and Wang (2001) that the field scale estimation of contaminant mass fluxes at contaminated sites is a valuable approach for the evaluation of natural attenuation. Einarson and Mackay (2001) demonstrated that the estimation of contaminant mass fluxes is a powerful and economic way to characterize the relative significance of a contaminant release, which can help to prioritise site remediation.

Due to the importance of mass flux and natural attenuation estimations for both risk assessments and remediation projects, additional work is needed to evaluate the applicability of different field methods under various aquifer conditions, for different contaminant plume geometries, as well as under different configurations of the monitoring network. Einarson and Mackay (2001) concluded that considerable insight can be gained by modelling, but comparisons of different approaches at real sites would be extremely valuable. During the last few years, different studies

have estimated field scale contaminant mass fluxes using point scale approaches mostly based on an extensive multilevel sampling monitoring network (e.g., King et al., 1999; Einarson et al., 2000; Kao and Wang, 2001). However, at many non-research field sites the available number of monitoring wells is limited, making a reliable point scale site investigation difficult. Recently, an alternative integral groundwater investigation method (IGIM) has been proposed by Teutsch et al. (2000), which reduces the number of monitoring wells needed for the site investigation by increasing the sample volume at each well through pumping. However, the reliability of both mass flux estimation approaches (point scale-based and integral) is controlled by the estimation of the groundwater discharge or velocity at the investigated field site and the spatial variability thereof, which is generally difficult to predict.

This chapter presents a case study of a typical "real world" industrial site in southwest Germany where due to the geological setting and the unavailability of appropriate drilling technologies only a limited number of monitoring wells are available for the site investigation and where the objective was to reliably quantify contaminant mass fluxes and field scale natural attenuation rate constants. To achieve this goal, both point scale and integral investigation methods were utilized at three control planes which are assumed to be situated orthogonal to the mean groundwater flow direction at increasing distances from the source. This study reports on the possibilities and limitations of different point scale and integral groundwater investigation methods under conditions which are typical for many sparsely monitored industrial sites.
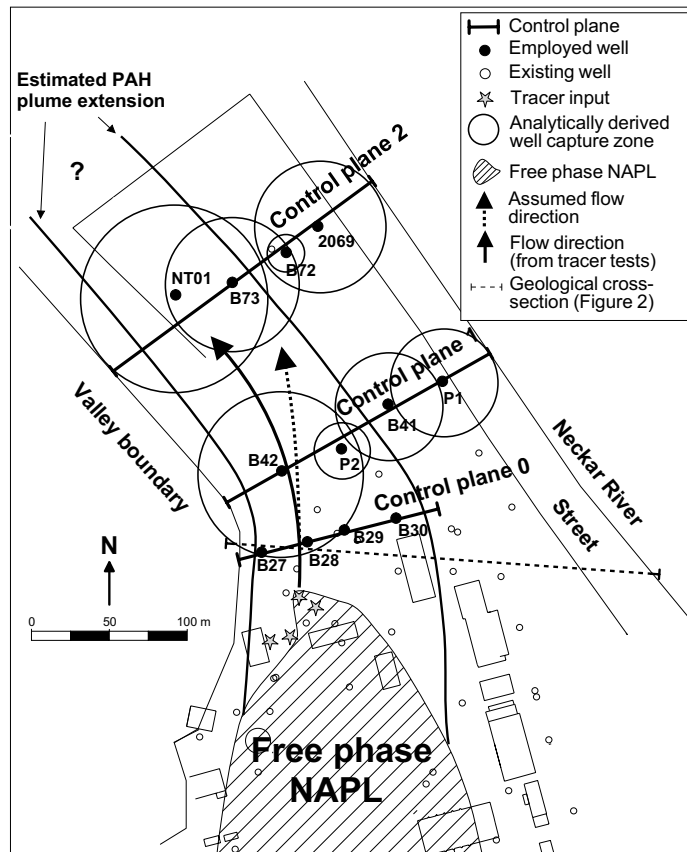
Figure 5.1: Site overview with the location of the employed wells and control planes. Labelled wells denote wells used in this study. Point scale concentrations were measured at all control planes shown. Integral investigations were conducted at control planes 1 and 2 only. Tracer injection locations are marked with a star. Tracer breakthrough curves have been monitored in all downgradient wells up to well NT01 (Bösel et al., 2000). A transport path including wells B28, B42, and NT01 was identified and confirmed by stable concentrations of a few heterocyclic compounds (Zamfirescu, 2000).

## 5.3    The field site

The study site is a former manufactured gas plant site situated in a Quaternary river valley in south-west Germany (Figure 1). The gas plant was in operation between 1870 and 1974. During this time the local groundwater was contaminated through contaminant input from tar pits, accidental spills, leaking storage tanks and pipelines,and a nearly complete site destruction during 1944. The age of the groundwater contamination is between 60 years and 130 years. Nowadays, an extended pool of free phase non-aqueous phase liquids (NAPL) forms a contaminant source at the site that covers an area of approximately 20,000 square metres. In the source zone, maximum BTEX

concentrations in the groundwater are around 12 mgl$^{-1}$. Maximum dissolved PAH concentrations in the groundwater in the source area are around 3.2 mgl$^{-1}$ (Zamfirescu and Grathwohl, 1998). The free phase NAPL is a continuous source for the dissolution of organic contaminants into the groundwater.

The average time scale for the complete dissolution of BTEX and PAH compounds from such a free phase NAPL pool lies in the order of decades to centuries for BTEX and centuries or more for PAH compounds (Grathwohl, 2000), which leads to the conclusion that a constant source term can be assumed at this site. Due to the age of the groundwater contamination and because the groundwater flowfield at the site has been observed for three years without showing significant seasonal changes or temporally variable groundwater flow di-

rections (Herfort, 2000), it can be assumed that the temporal variability in the dissolved contaminant concentration in the source is negligible.

The contaminated shallow aquifer is a Quaternary sand and gravel aquifer of glaciofluvial origin. The major aquifer 33m. A geological cross-section is shown in Figure 5.2.
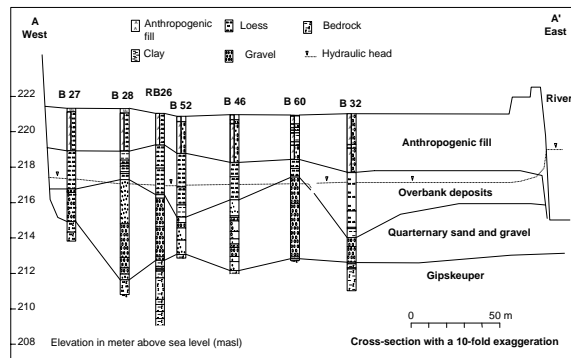


Figure 5.2: Geological cross-section of the field site (after Herfort et al., 1998). For the location of the cross-section refer to Figure 5.1.

The top of the mainly confined aquifer is bounded by clay-rich overbank deposits, overlain by an anthropogenic fill, which consists of building rubble and varies in thickness from 0.5m to 5.7m, with a mean of 2.9m. Based on 36 pumping tests, the arithmetic average of the hydraulic conductivity at the site was estimated as $3.3*10^{-3}$ $ms^{-1}$, with a variance in $ln(k_f)$ of 1.55 (Herfort, 2000).
Transport parameters and especially the flow direction downgradient from the main source area have been determined in the field during a large scale natural gradient multitracer test using fluoresceine, eosine, sodium naphthionate and sodium bromide as tracers. The tracer input occurred in four wells along the northern end of the source area (Figure 5.1) and tracer breakthrough curves were examined in all monitoring wells downgradient from the source up to a transport distance of about 280m. From this test the effective field scale porosity and average groundwater flow velocity were estimated as 0.13 and $2.0md^{-1}$ respectively (Bösel et al., 2000). The anoxic groundwater at the site ($<0.5$ $mgl^{-1}$ $O_2$)

52

facies are a unimodal gravel, a bimodal gravel with a sandy matrix and a pure sand facies, comprising about 59%, 34%, and 7% respectively of the deposit. The respective long ranges of the facies structures in a spherical variogram are 56m, 51m, and

shows evidence of sulphate reduction and ongoing iron reduction with concentrations of around 12 $mgl^{-1}$ of dissolved iron at control plane 2 (Figure 5.1) and background sulphate concentration of 300 $mgl^{-1}$ to 400 $mgl^{-1}$, which are influenced by local recharge of highly mineralised groundwater from a deeper aquifer. The relatively high sulphate content in the shallow aquifer originates from recharge from a highly mineralised deeper aquifer, which occurs at different locations within the river valley. At the investigated field site, a negligible recharge of approximately 0.6 l/s occurs upgradient from control plane 1 shown in Figure 5.1.

## 5.4    Methodology and data sets

The methods used in this study are standard point scale methods for the quantification of contaminant mass fluxes and natural attenuation rates  and a new integral mass flux quantification method.

Based on point scale concentration measurements, at least three different approaches exist for the analysis of the natural attenuation (NA) of a contaminant plume: (1) the determination of effective NA rate constants based on the reduction in contaminant concentrations along a transport path ("Centreline" method), (2) the quantification of contaminant mass fluxes at groundwater fences or control planes situated orthogonal to the mean groundwater flow direction ("Groundwater fence" method), and (3) the interpretation of the contaminant plume's spatial moments estimated from plume snapshots taken at different times ("Plume mapping"). The latter was not applied at the field site because the dissolved contami-

nant concentration migrating from the source was not a function of time but can be assumed to show only minor temporal variations due to the nature and extent of the source zone and the relatively stable groundwater flow field at the site. At other locations, such as those with pulse inputs of contaminants or those with highly soluble groundwater contaminants, one can encounter variable source strengths with time. For MTBE contaminations, for example, dissolved contaminant concentrations often show a time dependency with initially high dissolved concentrations which then decline with time. This is caused by the relatively high water solubility of the contaminant which can result in a preferential dissolution from a NAPL source (Einarson and Mackay, 2001).

The three field methods used in this study were the standard point scale "Centreline" (e.g., Buscheck and Alcantar, 1995; Zamfirescu, 2000) and "Groundwater Fence" method (e.g. Borden et al., 1997; King et al., 1999; Kao and Wang, 2001), as well as a new integral groundwater investigation method (Teutsch et al., 2000; Bockelmann et al., 2001). These three methods are discussed hereafter.

### 5.4.1 "Centreline" method

This method is based on the assumption that the plume has reached a dynamic equilibrium between the contaminant mass input into the plume and the contaminant mass loss due to biotic and abiotic processes, i.e. the spatial contaminant distribution in the groundwater is not a function of time. It furthermore requires the localisation of a representative contaminant transport path from the source in the direction of flow. This can, for example, be achieved with a detailed site investigation or by employing a reliable flow and transport model or good tracer test data.

The assumed stability of the contaminant distribution in the groundwater may occur if the investigated contaminant source, e.g. a NAPL pool, has been in place for a long time (years to decades for

BTEX and decades to centuries for PAH) and does not show a time variant dissolution rate, so that the partitioning of the mobile and sorbed contaminant mass, including diffusive contaminant exchanges between aquifer regions with different hydraulic conductivities, has approached equilibrium within the area of the investigated transport path.

Many "real world" sites show complex source zones with the possibility of different contaminant plumes migrating downgradient from the source. This can distort the concentration gradients in the direction of flow. At such sites, the application of the centreline method may prove to be very difficult due to problems associated with the localisation of a representative transport path, i.e. the "centreline" of the contaminant flux migrating downgradient from the source. Under such conditions each plume needs to be investigated separately, which in most cases is practically impossible. Nevertheless, this method is proposed as a field method for the investigation of apparent natural attenuation rate constants in some regulatory guidelines (e.g. New Hampshire Department of Environmental Services (NHDES, 1999) and can under the favourable conditions stated above yield information on the apparent natural attenuation potential at a field site.

Assuming that the contaminant fate along this transport path is representative of the overall contaminant fate at the studied site, this method yields apparent field scale natural attenuation rates based on the determination of a reduction of contaminant concentrations along the identified transport path. Under idealised conditions, with a single, well defined contaminant plume in a homogeneous aquifer, monitoring wells used for this approach should be placed along the longitudinal axis or "centreline" of the contaminant plume. The problem is then reduced to identifying the flow direction downgradient from the source. Assuming that the observed concentration decrease in the plume follows a first-order reaction, the

overall attenuation rate constants $k$ [T$^{-1}$] can be estimated by fitting measured concentrations to an one-dimensional analytical solution (Buscheck and Alcantar, 1995):

$$c(x) = c_0 \exp\left(-k\frac{x}{v_x}\right) \qquad (5.1)$$

with $c(x)$, $c_0$, $x$, $t$ and $v_x$ representing the concentration as a function of distance [ML$^{-3}$] from the source, the concentration at the source [ML$^{-3}$], the distance travelled [L], the time [T] and the linear horizontal groundwater velocity [LT$^{-1}$], respectively.

### 5.4.2   Mass flux estimation from point concentrations

Especially in North America, different field sites have been investigated using a mass flux estimation method based on the determination of point scale contaminant concentrations at "well screens" or "groundwater fences" (e.g., Semprini et al., 1995; Borden et al., 1997; King et al. 1999; Barker et al., 2000). These screens or fences commonly comprise closely-spaced monitoring wells situated orthogonal to the mean groundwater flow direction at increasing distances from the contaminant source. The investigated aquifer cross-sections or control planes can be straight lines in a uniform flowfield or curvilinear in a non-uniform one.

Target compound concentrations are determined at each sampling port of the multilevel wells. To ensure a complete capture of the investigated plume, both the vertical and horizontal extent of the plume should be bounded by sampling ports yielding non-detects of the target compounds at the plume fringes. This can result in a relatively large number of monitoring wells, if they are closely-spaced and the contaminant plume shows a significant width. At some sites the geological setting allows for the application of modern direct push sampling technologies which enable a cost effective installation of the required

monitoring network. However, this is not always the case, especially for coarse gravely sediments.

To quantify the total mass discharge ($M_d$) [M T$^{-1}$] at the investigated control planes, the concentration point measurements at each sampling port i is representative for an area $A_i$, which is the area of the respective polygon that extends to half the distance to the adjacent sampling ports. For all i sampling ports at a control plane, the areas $A_i$ yield together a plane of connected rectangles or polygons (i.e. the groundwater fence).

The mass flux $M_{di}$ [MT$^{-1}$] related to an individual sampling port located within a groundwater fence is then defined as (Borden et al., 1997):

$$M_{di} = C_i q_i A_i \qquad (5.2)$$

with $C_i$ [ML$^{-3}$] representing the concentration measured at the sampling location and $q_i$ [LT$^{-1}$] the specific discharge perpendicular to the groundwater fence. The total mass discharge $M_d$ [MT$^{-1}$] crossing a groundwater fence with $n$ sampling ports can subsequently be calculated as

$$M_d = \sum_i^n M_{di} \qquad (5.3)$$

In this study, the mass flux approach based on point scale concentration measurements was applied at the three control planes shown in Figure 5.1.

Because the specific discharge $q_i$ and the target compound concentration $C_i$ are assumed to be constant over the total area $A_i$ associated to each sampling port, the estimated total mass flux $M_d$ across the investigated control plane is subject to uncertainty which increases with the distance between the sampling ports and with the temporal and spatial variability of both the target compound concentrations and the hydraulic aquifer properties.

### 5.4.3 Mass flux estimation from integral concentration data

Spatially integrated mass fluxes and average contaminant concentrations can be estimated by placing one or more pumping wells along a control plane positioned perpendicular to the mean groundwater flow direction downgradient of a suspected pollutant source zone. These wells are then simultaneously or sequentially pumped to investigate the complete groundwater discharge from a suspected source zone, as illustrated for a two-well scenario in Figure 5.3.

During pumping, concentrations of the target substances are determined as a function of time (concentration-time series, CT-series). Since each concentration value within the measured CT-series is associated with a distinct aquifer region covered by the well capture zone, information on the spatial distribution of both concentrations and mass fluxes can be obtained from this method. In this study, an analytical interpretation (Teutsch et al., 2000; Ptak and Teutsch, 2000; Bockelmann et al., 2001a) of the CT-series has been employed. This simplified method is based on the following assumptions: (1) It assumes that within the well capture zone the flow towards the abstraction well is radially symmetrical, i.e. the influence of a natural groundwater gradient is negligible, (2) the aquifer within the each well capture zone is homogeneous with regard to porosity, hydraulic conductivity and thickness, i.e. the groundwater flow across the control plane in the area investigated by the respective well can be approximated with an uniform flowfield, which is described by Darcy's Law, and (3) the contaminant concentration gradient within the well capture zone is either negligible or linear along each of the captured streamtubes. The contaminant concentrations may vary from streamtube to streamtube.
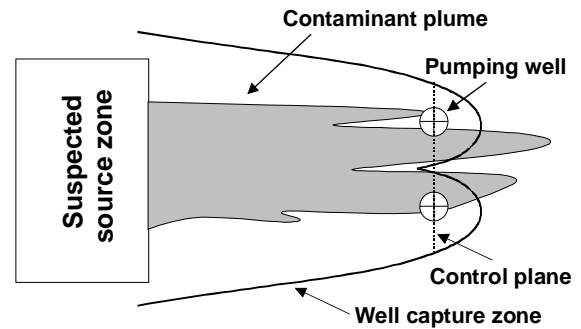


Figure 5.3: Principle of the integral groundwater investigation. The total mass discharge from a suspected source zone can be investigated by capturing the complete groundwater discharge downgradient from the source at defined control planes using one or multiple pumping wells. The contaminant concentrations are determined as a function of time in the discharge of the wells during pumping. Using a simplified analytical solution or a numerical algorithm based on a numerical flow and transport model, the mass discharge [$MT^{-1}$] at the control plane can be quantified. By increasing the sample volume through pumping, the mass quantification is possible without regionalization of point scale data.

The development of the well capture zone with time can then be described as:

$$r(t) = \sqrt{\frac{Q\,t}{\pi\,h\,n_e}} \qquad (5.4)$$

with $r(t)$, $Q$, $t$, $h$, $n_e$ symbolizing the radius [L] of the well capture zone at time $t$, the pumping rate [$L^3T^{-1}$], the time [T], the aquifer thickness [L] and the effective porosity [-], respectively. A probable contaminant distribution in the groundwater prior to any pumping can then be reconstructed analytically based on the measured CT-series at the pumping well. For this reconstruction, the section of the control plane covered by the isochrones of a pumping well is separated into discrete streamtubes with a different contaminant concentrations. The width of each streamtube is defined by the spatial increment $\Delta r$ [L] of the radius r [L] along the control plane between two consecutive sampling events. Applying Equation 5.4, the increment $\Delta r_i$ between sampling times $t_{i-1}$ and $t_i$ can be calculated as:

$$\Delta r_i = \sqrt{\frac{Q}{\pi\, n_e\, b}}\left(\sqrt{t_i} - \sqrt{t_{i-1}}\right) \qquad (5.5)$$

The width of the streamtubes can therefore be controlled by the chosen time increment between two consecutive sampling events. The overall number of streamtubes at each well is equal to twice the number of data points in the CT-series because at each sampling time two streamlines crossing the control plane, one at each side of the well, are intercepted. As the concentration measured at a pumping well is always a mixture of the concentrations of the two intercepted streamtubes, the total mass discharge $M_d$ [MT$^{-1}$] crossing the control plane investigated by the pumping well can be defined as:

$$M_d = 2\sum_{i=1}^{D} Q_i Cx_i \qquad (5.6)$$

with $D$ [-], $Q_i$ [L$^3$T$^{-1}$], and $Cx_i$ [ML$^{-3}$] denoting the number of sampling events in the CT-series, the groundwater flow rate within the $i$-th streamtube, and a theoretical concentration, which is the average of the concentrations of the two intercepted streamtubes at pumping time $t_i$ [T]. Schwarz (2001) developed a recursive formula for the calculation of $Cx_i$:

$$Cx_i = \frac{\pi\, Cp_i}{2\arccos\left(\dfrac{r(t_{i-1})}{r(t_i)}\right)} - \frac{\displaystyle\sum_{k=1}^{i-1} Cx_k\left[\arccos\left(\dfrac{r(t_{k-1})}{r(t_i)}\right) - \arccos\left(\dfrac{r(t_k)}{r(t_i)}\right)\right]}{\arccos\left(\dfrac{r(t_{i-1})}{r(t_i)}\right)}$$

$$(5.7)$$

with $Cp_i$ [ML$^{-3}$] representing the concentration measured at the pumping well at time $t_i$. For the first sampling event of the CT-series, $Cx_1$ equals $Cp_1$. A more detailed development of the analytical inversion of measured CT-series is given elsewhere (Ptak and Teutsch, 2000; Bockelmann et al., 2001a; Schwarz, 2001).

Based on the CT-series measured during the integral groundwater investigation, a possible contaminant distribution in the subsurface prior to pumping can be reproduced. Limiting factors for the application of the spatially integral investigation are the transmissivity at the site, which controls the width of the well capture zone that can be achieved in reasonable pumping times, and the possible treatment costs for the pumped contaminated groundwater.

For the reliable quantification of the contaminant mass fluxes, it has to be assured that the well capture zones of the employed wells cover the complete groundwater discharge of the suspected contaminant source zone to intercept all possible contaminant plumes in the groundwater. It is obvious that an incomplete capture of the contaminant plumes results in an underestimation of the mass discharge at the investigated site.

For homogeneous conditions or conditions where the investigation scale is much larger than the scale of local heterogeneities, the size of the well capture zones can be calculated with analytical formulae (e.g. Equation 5.4). For heterogeneities of significant extent compared to the scale of integration, the exact quantification of the width of the well capture zones is more challenging and may require field measurements of hydraulic heads during pumping in order to define the well capture zones or a dependable flow model which adequately represents the different zones hydraulic conductivity in the heterogeneous aquifer.

Alternatively, the individual well could also be "overpumped" to ensure complete plume capture, i.e. the investigated control plane is then larger than the assumed width of the source zone or of the width of a located contaminant plume (Figure 5.3). A possible dilution of the target compound

concentrations due to in-well mixing with uncontaminated groundwater does not influence the mass flux estimation as long as the dilution does not decrease the contaminant concentrations below analytical detection limits. Nowadays detection limits are usually far below regulatory limits. A possible in-well dilution should, under most conditions, not influence the mass flux estimation. Total mass fluxes and average concentrations can be simultaneously estimated for a number of targets at each abstraction well. This may include not only the original contaminant, but also potential degradation products or geochemical indicators, e.g. pH, EC, sulphate, nitrate or dissolved iron.

The integral approach applied in this study is a simplified analytical tool. As with all analytical approximations, it experiences growing uncertainties in the results with an increasing level of heterogeneity in the system. Well capture zones could for example develop asymmetrically around the well, leading to uncertain control plane widths, or preferential flow-paths across the control plane could be over- or underestimated by the use of an average groundwater flux at the scale of the individual well capture zone. If a relatively large number of monitoring wells and detailed information on the spatial distribution of the hydraulic conductivity in the aquifer are available, a numerical inversion of the CT-series can be applied, which can account for aquifer heterogeneities and asymmetrical well capture zones by employing a numerical flow and transport model (Ptak et al., 2000a; Schwarz, 2001).

### 5.4.4 Quantification of natural attenuation rates using mass flux measurements

If compound-specific total mass fluxes $M_d$ [MT$^{-1}$] have been quantified at different distances from a contaminant source zone using either point scale or integral investigation approaches and if the average travel time $\Delta t$ [T] between the two existing

control planes is known, it is possible to quantify the compound-specific effective first order natural attenuation (NA) rate constant [T$^{-1}$]:

$$Md_{CP(2)} = Md_{CP(1)}e^{-\lambda \Delta t} \qquad (5.8)$$

leading to

$$\lambda = -\ln\left(\frac{Md_{CP(2)}}{Md_{CP(1)}}\right)\frac{1}{\Delta t} \qquad (5.9)$$

with $\lambda$ [T$^{-1}$], $Md_{CP(1)}$ and $Md_{CP(2)}$ representing the effective natural attenuation rate constants and the measured compound-specific mass fluxes at control plane 1 and 2, respectively.

It should be noted that the differences in mass fluxes between any two control planes can be due to degradation, sorption, and volatilization of the target compound. In general, the application of Equation 5.9 does not enable differentiation between these processes. NA rate constants estimated in this way consequently incorporate all mass flux reducing factors. It is furthermore assumed that the dissolution from the source is not a function of time, so that the observed mass flux reductions are mainly due to NA processes and not caused by time variant dissolution rates from the source, which might occur at some sites.

Dilution (e.g. due to recharge) and dispersion do not affect the results because of the spatial integration inherent to the mass flux estimation using the IGIM. McAllister and Chiang (1994) reported that volatilization of the more volatile BTEX-compounds generally accounts for only 5 to 10 percent of mass reduction at most sites. Eiswirth et al. (1998) demonstrated that for the field site studied here, volatilization of organic contaminants is not significant.

Because the contaminant plume at the field site is between 60 and 130 years old, we assume equilibrium conditions with regard to sorption for the target compounds in this study. Degradation of the target

compounds is therefore regarded as the dominating mass flux reducing process.

### 5.4.5 Concentration data

For the application of the different point scale and integral investigation approaches used in this study, three distinctive data sets have been used.

**Data set 1** shown in row (a) in Table 5.1 and Table 5.2 consist of conventional point scale concentrations measurements from all wells situated at the three control planes (CP) shown in Figure 1, apart from wells B72 and B73 situated at CP 2. These wells were installed only after the completion of the first sampling campaign, which was conducted 8 months prior to the subsequent integral site investigation. The estimation of natural attenuation rates based on the "centreline" method (Equation 5.1) used data set 1.

**Data set 2** shown in row (b) in Table 5.1 and Table 5.2 includes point concentration measurements taken simultaneously with the integral site investigation at CP 1 and CP 2. Measurements were determined during the pumping for the integral groundwater investigation after approximately three borehole volumes were purged. Data sets 1 and 2 thus represent point concentration measurement snapshots of the site at different times. For all point scale mass flux estimation at CP 2,data from data set 2 was used for the wells B72 and B73. This follows the assumption of a relatively constant contaminant discharge from the source.

**Data set 3** consists of the complete concentration-time series recorded during the two to six day pumping test periods at CP 1 and CP 2. More details about the integral site investigation and the documentation of the concentration-time series is given by Bockelmann et al. (2001a).

Table 5.1: Point scale concentration measurements of BTEX and other hydrocarbon compounds during two sampling campaigns.

| $[\mu gl^{-1}]$ | | Benz | Tol | E-Benz | p-Xyl | o-Xyl | Iso-PB | PB | 1,3,5-TMB | 1,2,4-TMB | 1,2,3-TMB | Indane | Indene |
|---|---|---|---|---|---|---|---|---|---|---|---|---|---|
| B27 | *a)* | 74.2 | 0.24 | 35.3 | 1.46 | 0.87 | 8.83 | 1.04 | 0.06 | 0.20 | 0.41 | n.d. | 6.18 |
| B28 | *a)* | 214.3 | 0.54 | 50.7 | 1.31 | 0.52 | 10.4 | 2.35 | 0.12 | 0.30 | 0.48 | 0.04 | 12.1 |
| B29 | *a)* | n.d. | 0.11 | 0.15 | 0.34 | n.d. | 0.42 | 0.13 | 0.12 | 0.18 | 0.08 | n.d. | 0.27 |
| B30 | *a)* | n.d. | 0.12 | 0.17 | 0.38 | n.d. | 0.53 | 0.10 | 0.10 | 0.17 | 0.07 | n.d. | 0.29 |
| B42 | *a)* | 26.7 | 0.34 | 3.77 | 0.63 | 0.05 | 3.86 | 0.72 | 0.06 | 0.15 | 0.06 | n.d. | 1.35 |
| | *b)* | n.d. | 1.42 | 0.08 | 0.22 | n.d. | 0.45 | 0.14 | 0.04 | 0.03 | n.d. | n.d. | 0.52 |
| P2 | *a)* | n.d. | n.d. | 0.09 | 0.11 | n.d. | 0.12 | n.d. | 0.03 | 0.07 | 0.03 | n.d. | 0.10 |
| | *b)* | 0.85 | 2.07 | 1.75 | 4.34 | 1.73 | 0.59 | 0.24 | 1.92 | 3.12 | 0.97 | 5.89 | 16.5 |
| B41 | *a)* | n.d. | 0.07 | 0.13 | 0.12 | n.d. | n.d. | n.d. | 0.02 | 0.05 | n.d. | n.d. | n.d. |
| P1 | *a)* | n.d. | 0.16 | 0.10 | 0.10 | n.d. | n.d. | n.d. | n.d. | n.d. | n.d. | 1.05 | n.d. |
| NT01 | *a)* | 0.14 | 0.14 | 0.22 | 0.33 | 0.07 | 0.56 | 0.05 | 0.07 | 0.17 | 0.06 | 0.15 | 0.24 |
| | *b)* | n.d. | 0.06 | 0.04 | 0.21 | n.d. | 0.52 | 0.08 | 0.08 | 0.07 | 0.03 | n.d. | 0.10 |
| B73 | *b)* | n.d. | n.d. | n.d. | 0.02 | n.d. | 0.02 | n.d. | n.d. | n.d. | n.d. | n.d. | 0.03 |
| B72 | *b)* | 0.03 | 0.15 | 0.06 | 0.17 | 0.08 | n.d. | n.d. | 0.01 | n.d. | n.d. | n.d. | 0.02 |
| 2069 | *a)* | n.d. | n.d. | 0.09 | 0.07 | n.d. | n.d. | n.d. | n.d. | 0.03 | n.d. | 0.04 | n.d. |
| | *b)* | n.d. | 0.03 | n.d. | 0.04 | 0.03 | n.d. | n.d. | n.d. | n.d. | n.d. | n.d. | n.d. |

Benzene (Benz), Toluene (Tol), Ethylbenzene (E-Benz), p-Xylene (p-xyl), o-Xylene (o-xyl), Isopropylbenzene (Iso-PB), Propylbenzene (PB),
Trimethylbenzenes (TMB)
*a)* Point measurements (conventional sampling), data set 1
*b)* Early time data during pumping, data set2
n.d. = not detectable

Table 5.2: Point scale concentration measurements of low molecular weight PAH during two sampling campaigns

| [µgl⁻¹] | | Nap | Acy | Ace | Flr | Phe | Ant | Fln |
|---|---|---|---|---|---|---|---|---|
| B27 | *a)* | 0.72 | 4.31 | 99.4 | 3.65 | 0.14 | 0.15 | n.d. |
| B28 | *a)* | 0.72 | 5.34 | 210.2 | 1.16 | 0.32 | 0.35 | 0.13 |
| B29 | *a)* | 0.53 | 8.63 | 324.4 | 0.23 | 0.24 | 0.26 | 0.12 |
| B30 | *a)* | 0.52 | 4.05 | 207.6 | 0.11 | n.d. | n.d. | n.d. |
| B42 | *a)* | 0.38 | 3.77 | 158.2 | 0.20 | 0.19 | 0.21 | n.d. |
| | *b)* | 0.46 | 3.93 | 154.6 | n.d. | 0.06 | 0.33 | 0.11 |
| P2 | *a)* | 0.41 | 1.59 | 62.2 | n.d. | n.d. | n.d. | n.d. |
| | *b)* | 156.6 | 4.24 | 92.6 | 2.70 | 2.29 | 0.52 | 0.36 |
| B41 | *a)* | 0.50 | n.d. | 0.10 | n.d. | n.d. | n.d. | n.d. |
| | *b)* | 0.03 | 0.12 | 4.46 | n.d. | 0.09 | 0.03 | 0.12 |
| P1 | *a)* | 0.47 | n.d. | 0.15 | n.d. | n.d. | n.d. | n.d. |
| | *b)* | 1.06 | 0.18 | 1.74 | 0.06 | 0.13 | 0.02 | n.d. |
| NT01 | *a)* | 0.38 | 3.66 | 182.6 | 0.14 | n.d. | 0.11 | n.d. |
| | *b)* | 0.30 | 5.06 | 184.8 | 0.19 | 0.37 | 0.30 | 0.11 |
| B73 | *b)* | 1.11 | 0.09 | 2.91 | 0.19 | 0.38 | n.d. | 0.04 |
| B72 | *b)* | 0.94 | 0.08 | 1.30 | 0.16 | 0.74 | n.d. | 0.24 |
| 2069 | *a)* | 0.38 | n.d. | 0.15 | n.d. | n.d. | n.d. | n.d. |
| | *b)* | 0.52 | 0.08 | 1.58 | 0.09 | 0.51 | n.d. | 0.07 |

Naphthalene (Nap), Acenaphthylene (Acy), Acenaphthene (Ace), Fluorine (Flr), Phenanthrene (Phe), Anthracene (Ant), Fluoranthene (Fln)
*a)* Point measurements (conventional sampling), data set 1
*b)* Early time data during pumping, data set 2
n.d. = not detectable

## 5.5 Results and Discussion

### 5.5.1 Mass fluxes derived from conventional point scale sampling

The concentration data sets 1 and 2 were used for the quantification of contaminant mass fluxes based on Equations 5.2 to 5.4 and using the hydraulic parameters shown in Table 5.3. The results illustrate that the main contaminant plume migrates approximately parallel to the valley boundary. At CP 1 and CP 2 the main contaminant plume was therefore only intercepted by two of the four wells along the control planes. Obviously, this information became available only after the installation and sampling of the monitoring wells. Mass flux estimations for CP 0, where all four wells are located within the main contaminant plume are therefore comparably reliable, whereas the results for the other two control planes can be interpreted as

Table 5.3: Input parameters for point scale mass flux calculations

| Well | Aquifer thickness [m] | Hydraulic conductivity [ms⁻¹] | Hydraulic gradient* [-] |
|---|---|---|---|
| B27 | 1.85 | 0.00053 | 0.00078 |
| B28 | 5.70 | 0.00142 | 0.0067 |
| B29 | 3.85 | 0.0026 | 0.0056 |
| B30 | 2.50 | 0.00068 | 0.0027 |
| B42 | 4.00 | 0.0020 | 0.0020 |
| P2 | 3.80 | 0.0008 | 0.0012 |
| B41 | 2.96 | 0.0105 | 0.0015 |
| P1 | 3.35 | 0.0084 | 0.0013 |
| NT01 | 0.90 | 0.0058 | 0.0013 |
| B73 | 0.80 | 0.0050 | 0.0016 |
| B72 | 0.30 | 0.0200 | 0.0006 |
| 2069 | 1.50 | 0.0100 | 0.0036 |

* Derived from hydraulic head differences between adjacent monitoring wells.
Width of the groundwater fence section at each well at control plane 0 equal to 30 m.
Width of the groundwater fence section at each well at control plane 1 and 2 equal to 40 m.

Table 5.4: Estimated compound-specific mass fluxes across the control planes (CP) shown in Figure 5.1. Mass fluxes for data sets 1 and 2 (point scale data) were estimated with Equation 5.3, for data set 3 (integral data) Equation 5.7 was employed for the mass flux quantification.

| | Data set 1 | | | Data set 2 | | Data set 3 | |
| | CP 0 | CP 1 | CP 2 | CP 1 | CP 2 | CP 1 | CP 2 |
| | Mass flux $[gd^{-1}]$ | Mass flux $[gd^{-1}]$ | Mass flux $[gd^{-1}]$ | Mass flux $[gd^{-1}]$ | Mass flux $[gd^{-1}]$ | Mass flux $[gd^{-1}]$ | Mass flux $[gd^{-1}]$ |
|---|---|---|---|---|---|---|---|
| **Benzene** | 30.289 | 1.438 | 0.004 | 0.011 | 0.000 | 1.815 | 0.000 |
| **Toluene** | 0.094 | 0.050 | 0.005 | 0.104 | 0.012 | 0.040 | 0.004 |
| **Ethylbenzene** | 7.220 | 0.238 | 0.030 | 0.028 | 0.002 | 0.130 | 0.004 |
| **p-Xylene** | 0.241 | 0.067 | 0.029 | 0.069 | 0.019 | 0.045 | 0.016 |
| **o-Xylene** | 0.076 | 0.003 | 0.021 | 0.023 | 0.008 | 0.012 | 0.001 |
| **Isopropylbenzene** | 1.539 | 0.210 | 0.014 | 0.032 | 0.013 | 0.336 | 0.042 |
| **Propylbenzene** | 0.353 | 0.039 | 0.001 | 0.011 | 0.002 | 0.043 | 0.005 |
| **1,3,5-Trimethylbenze** | 0.036 | 0.007 | 0.002 | 0.028 | 0.002 | 0.013 | 0.006 |
| **1,2,4-Trimethylbenze** | 0.071 | 0.017 | 0.012 | 0.043 | 0.002 | 0.011 | 0.005 |
| **1,3,5-Trimethylbenze** | 0.081 | 0.004 | 0.001 | 0.013 | 0.001 | 0.004 | 0.002 |
| **Indane** | 0.006 | 0.132 | 0.014 | 0.078 | n.d. | 0.015 | 0.000 |
| **Indene** | 1.756 | 0.074 | 0.007 | 0.247 | 0.003 | 0.048 | 0.006 |
| **Naphthalene** | 0.186 | 0.165 | 0.145 | 2.242 | 0.179 | 0.185 | 0.024 |
| **Acenaphthylene** | 2.061 | 0.224 | 0.089 | 0.310 | 0.141 | 0.653 | 0.402 |
| **Acenaphthene** | 79.310 | 9.389 | 4.404 | 10.497 | 4.830 | 30.658 | 12.337 |
| **Fluorene** | 0.205 | 0.011 | 0.010 | 0.043 | 0.034 | 0.013 | 0.005 |
| **Phenanthrene** | 0.080 | 0.010 | 0.018 | 0.064 | 0.160 | 0.027 | 0.027 |
| **Anthracene** | 0.087 | 0.011 | 0.003 | 0.032 | 0.007 | 0.049 | 0.014 |
| **Fluoranthene** | 0.036 | n.d. | 0.004 | 0.030 | 0.024 | 0.008 | 0.006 |

n.d. = not detectable

relatively rough estimates due to the large uncertainty inherent to the regionalization of the point concentration data.

Nevertheless, based on data set 1 nearly all target compounds showed a reduction in mass flux in flow direction. Of the BTEX and hydrocarbon compounds only o-xylene and indane displayed an apparent increase in flux between the control planes (Table 5.4), which is evidence for the high uncertainty of the point concentration based mass flux estimations using the sparse monitoring network at the site.

The estimation of PAH mass fluxes based on data set 1 showed unexpected results for naphthalene, phenanthrene and fluoranthene (Table 5.4). Although naphthalene is generally assumed to be one of the more biodegradable PAHs (under aerobic conditions), naphthalene mass flux was approximately constant at all investigated control planes at around 1 gd⁻¹.

For phenanthrene, estimated mass fluxes apparently increased from CP 1 to CP 2 and fluoranthene was only detected at CP 0 and CP 3. Consequently, NA rate constants for these compounds could not be computed from data set 1.

Due to well positioning at CP 1, the area $A_i$ associated with each monitoring well (Equation 5.2) had a width of 40 m. The regionalization of the point scale con centration data hence resulted in homogeneous 40 m wide contaminant stripes or streamtubes crossing the control plane, which introduces large uncertainties into the results.

Focusing on the main contaminants at the site, i.e. benzene and acenaphthene for BTEX and PAH, respectively, possible effects of the regionalization can be investigated. Although the benzene flux at CP 1 agrees well with the result from the

integral method, the respective acenaphthene flux was underestimated by a factor of 3 compared to integral mass flux results. On average, the mass fluxes based on data set 1 deviated from the integral mass fluxes by approximately 97% ± 108% at CP 1 and by 143% ± 132% at CP 2.

Such regionalization effects are a function of the well positioning with regard to the contaminant plume and the distance between two neighbouring monitoring wells. The impact can be reduced by installing additional monitoring wells along the control plane and thereby reducing the scale of the point scale data regionalization. It is generally difficult to assess how many monitoring wells are needed for a reliable flux estimation under heterogeneous conditions because the exact plume geometry is generally unknown (Barker et al., 2000). A sufficient level of certainty can often be achieved by installing detailed groundwater fences as described above, if economically feasible and applicable under the site specific geological conditions.

Mass flux results based on data set 2 illustrate the problem of plume detection by point scale investigations with few monitoring wells. The possibility of missing a contaminant plume in the groundwater increases with the width of the suspected source zone for any given number of monitoring wells. The indane plume at CP 2 (Table 5.4), was not detected during the sampling for data set 2. In addition, similar to the estimations based on data set 1, phenanthrene showed an apparent increase in mass flux between CP 1 and CP 2, primarily due to the discussed regionalization effects. Compared to the integral mass fluxes the results based on data set 2 showed an average deviation of about 22% ± 18% at CP 1 and 63% ± 48% at CP 2, again highlighting the high uncertainty in the results introduced by the sparse monitoring network.
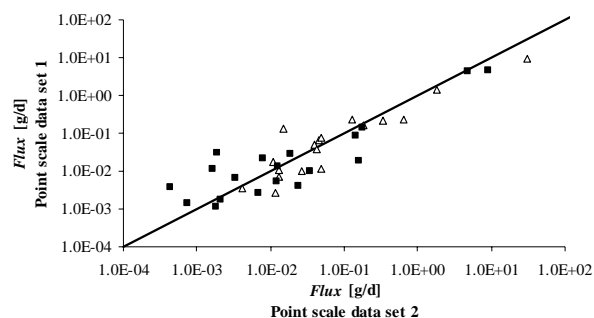


Figure 5.4: Correlation between mass fluxes derived from different point scale data at control planes 1 and 2. Triangles and boxes represent control plane 1 and 2, respectively.

Mass fluxes estimated with data set 2 were not systematically biased compared to results from data set 1. The comparison of the two point data mass fluxes (Figure 5.4) appears to show a smaller spread for mass fluxes at CP 2. This should be noted with care, however, as both data sets use the same concentration measurements at CP 2 at the wells B72 and B73. Although the main flux at CP 2 is located around well NT01, i.e. this well shows the highest point scale concentrations at CP 2 (Table 5.1 and Table 5.2), the use of the same concentration data at well B73 increases the relationship between the point data flux estimations at CP 2.

One possible reason for the different flux estimations at CP 1 based on the two point scale data sets could be a shift in the plume position at CP 1 leading to different contaminant concentration distributions at the monitoring wells. However, such a significant change in the flow conditions seems unlikely, as Herfort (2000) reported no significant changes in the groundwater flowfield at the site over a three year period. Alternatively, the observed discrepancies in contaminant fluxes at CP 1 could originate from different sampling times during well operation leading to different well capture zones and sampling volumes. With heterogeneous contaminant distributions in the subsurface this can significantly influence concentration measurements. During the sampling for data set 1, pumping rates of 0.6 – 0.7 ls$^{-1}$ were

applied, whereas pumping rates during the sampling for data set 2 at CP 1 were mainly around 4 l s$^{-1}$ because the data was obtained during the pumping for the integral site investigation. Mass flux differences between the two point scale data sets could be a result of a spatially heterogeneous contaminant distribution in the subsurface.

### 5.5.2 Mass fluxes derived from the integral investigation method

The general principle of the integral groundwater investigation method and a comparison with standard point scale sampling is discussed hereafter. Figure 5.5 schematically illustrates concentration-time series typically observed during an integral site investigation based on different contaminant distributions in the subsurface indicated by the simplified plumes. Marked on the time axis in Figure 6 is also the typical sampling time for point scale concentration measurements, after which the pump is usually switched off. It is obvious from the concentration-time series shown in scenarios 1 and 3 (Figure 5.5) that in this example the use of point scale or early time data for flux estimations (point scale approach) would lead to an underestimation of contaminant mass flux as the average contaminant concentration is underestimated by early time pumping data, whereas early time data from scenario 2 would lead to an overestimation of the respective flux. If regionalized to a larger control plane width, point scale measurements yield reliable results only for homogeneous concentration distributions in the groundwater (compare scenario 4). If heterogeneous conditions prevail (scenarios 1 to 3), it is not possible to predict whether the point scale approach will over- or underestimate the mass flux. This is due to the fact that the real contaminant distribution is usually unknown prior to site investigation.
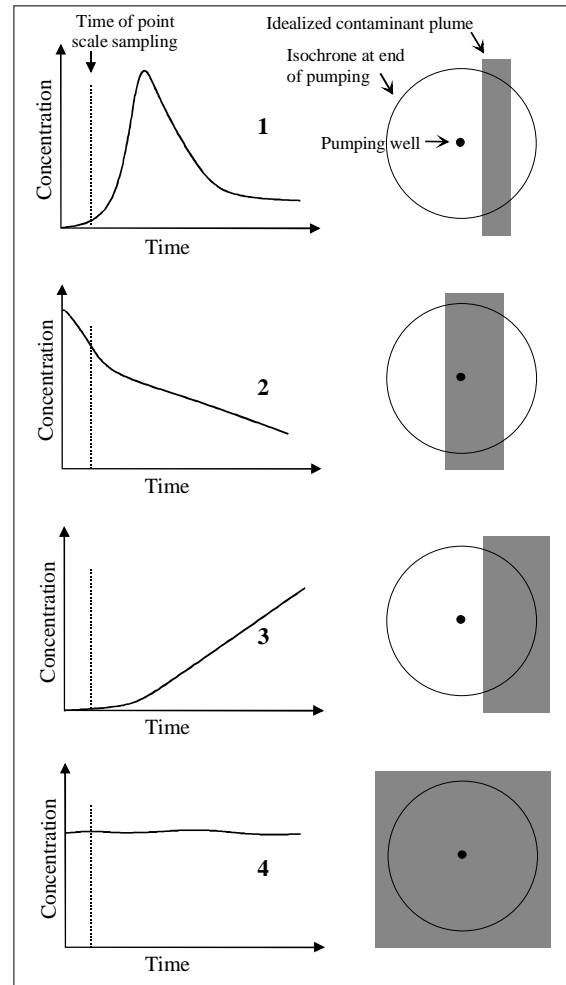


Figure 5.5: Scheme of concentration-time series typically recorded in the discharge of pumping wells during an integral site investigation. Scenarios 1 to 3 illustrate different heterogeneous contaminant distributions in the subsurface, scenario 4 represents a homogenous case (after Bockelmann et al., 2001a).

For the integral mass flux quantification at the study site, an analytical approach (Bockelmann et al., 2001a) was utilized (Equations 5.5-5.8). The concentration-time series determined during the pumping tests at CP 1 and CP 2 were used for the compound-specific contaminant mass flux estimations. The theoretical well capture zones at the end of the pumping tests derived from Equation 5.5 are illustrated in Figure 5.1. Pumping rates at the wells were based on the maximum yield, illustrating a variability in the aquifer thickness (Figure 5.2) and transmissivity distribution at the site. The hydraulic parameters derived

from the pumping test analysis were used as effective values for the scope of the respective well capture zone in the analytical approximation of the groundwater flow. At CP 1, pumping rates were 1.4 ls⁻¹ at well P2 and between 4.1 ls⁻¹ to 4.8 ls⁻¹ at the other wells. At CP 2, well B72 was pumped at only 0.1 ls⁻¹, all other wells at 2.3 ls⁻¹ to 3.5 ls⁻¹. The low pumping rate at well B72 was due to an aquifer thickness of only 0.3 m at this location. Due to the absence of a reliable flow model for the numerical delineation of the well capture zones, the wells were "overpumped" (pumped for a longer time period) to increase the width of the investigated control planes at each well and to increase the probability of a complete capture of the mass discharge from the NAPL pool at the field site (Figure 5.1).

The reliability of the analytically derived mass fluxes depends mainly on an adequate estimation of the investigated control plane width and on a good approximation of the groundwater flow within each well capture zone. A significant deviation from the theoretical width of the well capture zones at the well B42 (CP 1) and well NT01 (CP 2), could have caused an incomplete capture of the main contaminant plume, i.e. an underestimation of the total mass discharge across the control planes, if some part of the mass flux is migrating close to the valley boundary (Figure 5.1) although there is an inflow of groundwater from the valley slopes into the shallow valley aquifer. Without a detailed delineation of the well capture zones and the contaminant distribution in the groundwater, this uncertainty has to be acknowledged but cannot be quantified.

Due to the greater sampling volume employed by the integral site investigation at the field site, the probability of detecting the contaminant plumes in the groundwater is increased, leading to mass flux estimations at a higher level of certainty than through a small number of point scale investigations. The results of the IGIM are therefore used in this paper as the reference in the comparison with the other

investigation methods. During the integral investigation all target compounds were detected at both CPs and in contrast to the point scale investigation no compound showed an apparent flux increase in flow direction. Only phenanthrene exhibited an apparently conservative, i.e. non-degrading, transport between CP 1 and CP 2 (Table 5.4). Benzene and acenaphthene could be identified as the major contaminants at the site, with the BTEX flux being nearly completely attenuated during the transport between CP 1 and CP 2, whereas the PAH compounds still exhibited a total mass flux exceeding 30 gd⁻¹ at CP 2.
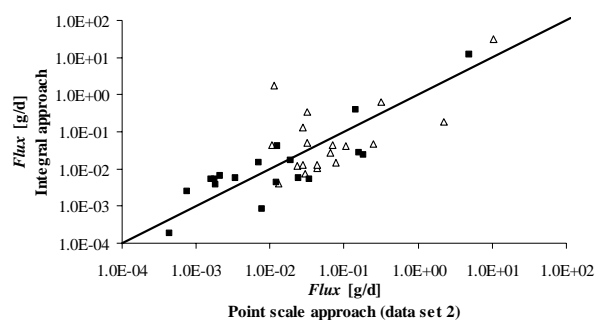


Figure 5.6: Correlation between mass fluxes derived from integral (data set 3) and point scale data (data set 2) at control planes 1 and 2. Triangles and boxes represent control plane 1 and 2, respectively.

A comparison based on data set 2 and the integral data (set 3) illustrates that the point scale approaches both over- and underestimated the compound-specific contaminant fluxes (compared to the integral reference) at the two CPs (Figure 5.1), which is primarily a result of the sparse monitoring network at the two CPs.

From the discussed results, it can be concluded that the limited monitoring, the level of heterogeneity of the geology, source zone, and contaminant distribution in the groundwater encountered at the field site prevented the reliable application of a point scale mass flux approach. Only with an increased number of monitoring wells along the main contaminant plume should the point scale mass flux method be

applied at this field site. Assuming an average distance of 1 m (e.g. Barker et al., 1987) to 3 m (e.g. Einarson et al., 2000, in Einarson and Mackay, 2001) between the multilevel sampling wells along a closely-spaced groundwater fence, 34 to 100 multilevel wells would be needed for a single control plane along a contaminant plume of around 100m width as encountered at this site. For smaller contaminant plumes such an installation can be economically feasible, but for larger plumes this might often not be the case, especially if heavy drilling equipment is required for each sampling well as at our field site. The distance between the sampling wells could be increased, but this will lead to increased uncertainties in the results if the site shows higher levels of heterogeneity as commonly encountered in coarse grained fluvial sediments. It should be noted however that the integral investigation method will not provide direct and detailed information concerning the spatial distribution of the contaminant concentrations within the well capture zone.

### 5.5.3 Natural attenuation rate constants based on mass flux data

For the reliable quantification of natural attenuation (NA) rate constants at field scale, a complete capture of the contaminant plume at all investigated control planes has to be achieved and the mass discharge from the source has to be assumed constant through time. It can then be concluded that observed mass flux reductions between two control planes are primarily caused by NA processes. Due to the age of the contamination (Grathwohl, 2000), the stability of the groundwater flowfield (Herfort, 2000), and the minor influence of mass losses due to volatilisation (Eiswirth et al., 1998), the estimated NA rate constants at the study site were interpreted as indicators of the biodegradation potential at the study site.
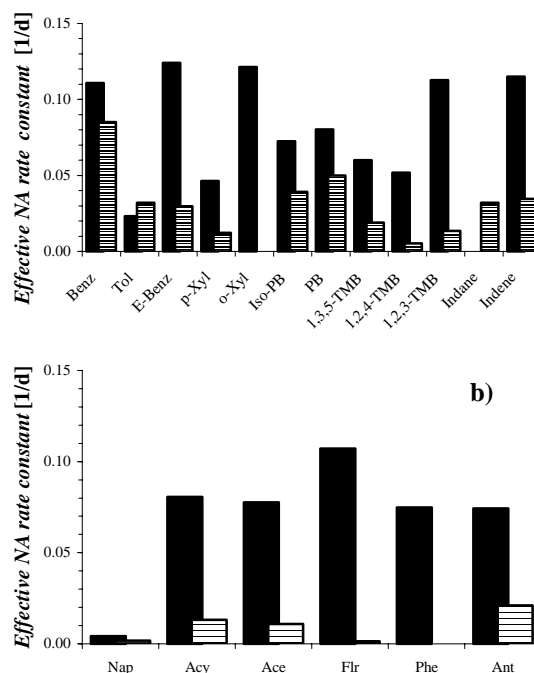


Figure 5.7: Effective natural attenuation rate constants derived for the transport between control planes 0 and 1 (solid bar) and control planes 1 and 2 (patterned bar) based on conventional point measurements (data set 1). a) BTEX and additional hydrocarbons, b) low molecular weight PAH.

Effective natural attenuation (NA) rates calculated for the contaminant transport between CP 0 and CP 1 and between CP 1 and CP 2 based on data set 1 are shown in Figure 5.7. Although the estimated mass fluxes for CP 1 and CP 2 are uncertain, it can be deduced that the attenuation of the targeted organic compounds is faster closer to the source and slower further downgradient. Only toluene displays an inverse behavior. This could indicate that for some compounds the anaerobic degradation rate is concentration dependent or dependent on the dominant redox conditions which change with distance from the contaminant source.

A comparison between the estimated NA rate constants from data set 2 and the integral data (data set 3) shows that apart from benzene and the trimethylbenzenes, the results agree reasonably well (Figure 5.8).
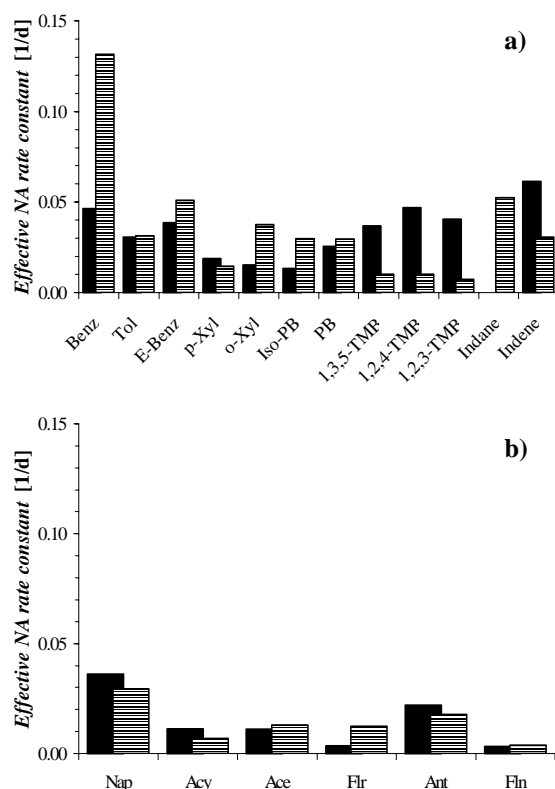
Figure 5.8: Effective natural attenuation rate constants derived for the transport between control planes 1 and 2 based on point scale (data set 2, solid bar) and integral (data set 3, patterned bar) measurements. a) BTEX and additional hydrocarbons, b) low molecular weight PAH.

The difference in the benzene NA rate is due to an underestimation of the benzene flux at CP 1 and a respective overestimation at CP 2 by the point scale approach. At CP 1 this is due to the spatial location of wells B42 and P 2, which are both situated at the fringe of the BTEX plume crossing CP 1. Point data obtained at these wells consequently lead to an underestimation of the respective contaminant flux as the benzene concentration-time series in these wells followed a type 3 scenario (Figure 5.5). The difference in the NA rates derived from the point scale and the integral approach is generally lower than the respective difference in mass flux because the estimation of NA rates is based on the relative change in flux in flow direction and not on the absolute mass flux values.

## 5.5.4 Natural attenuation rates based on a centreline approach

Tracer breakthrough curves from a natural gradient multitracer experiment (Bösel et al., 2000) were used to localise a single transport path between CP 0 and CP 2. The identified transport path incorporated the wells B28, B42 and NT01 situated at CP 0, 1, and 2, respectively (Figure 5.1). This is corroborated by the fact that some heterocyclic compounds behaved conservatively in the plume along this flowpath based on point concentration measurements. Dimethyl-benzofuran for example showed approximately constant concentrations of about 3.5 µg l$^{-1}$ along this flowpath (Zamfirescu, 2000).

Due to the location of the transport path in relation to known contaminant sources at the site, it was assumed that the transport path was situated at or close to the centres of the PAH and BTEX plumes, which do not entirely overlap due to the different locations of the former tar pits and benzene distilleries at the site. With the "Centreline" method previously discussed, point scale concentration measurements from the three wells along this transport path were used to calculate effective natural attenuation rates for multiple organic contaminants using Equation 5.1.

Figure 5.9 shows the calculated effective NA rates in comparison to results from the integral groundwater investigation. It can be seen that the results agree well with an average deviation of only 41% ± 35%. The largest differences were recorded for benzene and toluene. As mentioned before, it was seen after drilling and sampling that that well B42 is not situated in the centre, but at the periphery of the main BTEX plume crossing CP 1. This may explain that the benzene and toluene mass fluxes were underestimated during this point scale based approach and, consequently, estimated NA rates based on this data are lower than the corresponding values from the integral approach. The PAH plume on

65

the other hand was seen to have a greater width so that well B42 at CP 1 was located closer to the centre of the plume and point scale sampling techniques produced more representative PAH concentrations, resulting in a smaller deviation in the respective NA rate constants compared to the integral results.
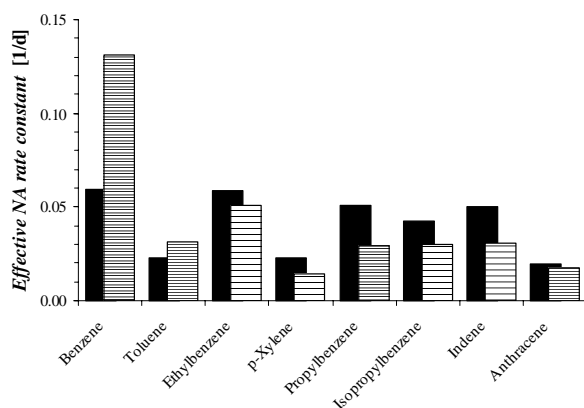


Figure 5.9: Effective natural attenuation rates of selected compounds derived from the point scale centerline approach (solid bar) and from the integral investigation (patterned bar). Point scale results based on Zamfirescu, 2000.

Both methods yielded effectively similar results with regard to field scale NA rates at the studied field site. For the successful application of the point scale "Centreline" method, a detailed site investigation including a tracer test was necessary to identify and localise the investigated transport path because the transport direction changed with the distance from the source (Figure 5.1). Having identified the transport path, the estimation of NA rates is easier and faster to conduct compared to the integral groundwater investigation method. However, the latter has the advantage of estimating the mass discharge ($M_d$) at different distances from the source which can help in the development of remediation strategies and in conducting environmental risk assessments.

## 5.6    Conclusions

For our site, and for similar sites with a limited number of monitoring wells, it can be concluded that mass flux estimations based on sparse point scale data can be highly unreliable and that the results should be carefully interpreted as they can be subject to a large degree of uncertainty. If additional wells cannot be installed due to economic, geological, or other limitations, an integral site investigation can be an alternative for the field scale quantification of both contaminant mass fluxes and natural attenuation rates.

For the study site it was shown that the integral site investigation yielded more dependable mass flux results and also allowed for the estimation of compound-specific apparent natural attenuation rates, which agreed well with attenuation rates estimated using the "Centreline" point scale approach which required a long-term tracer test for the delineation of a contaminant transport path.

For the integral mass flux quantification a simple analytical solution was used, which assumes homogeneous conditions in the aquifer at the scale of the well capture zones, which may lead to considerable uncertainties if applied to the heterogeneous conditions encountered at our site.

Besides this and other "real world" field applications, more research is needed under controlled experimental conditions to better understand the possibilities and limitations of the individual field methods under various geological and contaminant source configurations. Presently, a field scale comparison is being conducted at a field site in Borden, Canada, which includes a densely spaced groundwater fence and which will allow for a detailed comparison of the point scale and integral mass flux quantification.

# 6 Comparison of two mass flux estimation approaches at an UST site [4]

## 6.1 Abstract

Contaminant mass discharge has been used to assess contaminant mass loss in order to demonstrate the occurrence of natural attenuation at field sites. In this study, the commonly used approach to estimate contaminant mass discharge, the monitoring of multilevel wells, is compared to a more recent approach, the integral groundwater investigation approach that makes use of the concentration-time series obtained from pumping wells.

The two approaches were applied at a control plane located approximately 40m downgradient of the source zone at former site P-52 of Canadian Forces Base Borden, Ontario, Canada. This hydrocarbon plume shows evidence of natural bioattenuation. The methods provided similar estimates of the mass discharging across the control plane. The sources of uncertainties in the mass discharge estimates inherent in each approach were evaluated and the maximum uncertainty of either method was estimated to be about 40% for this specific situation.

This uncertainty suggests that sources of uncertainty should be examined and minimised and that resulting values of contaminant mass discharge should be used cautiously. The choice of mass discharge estimation approach will often depend on the specific site geology, on specific objectives and on potential remedial actions anticipated for the actual field situation. For this plume in a shallow, rather homogeneous sandy aquifer, the multilevel well approach appeared more viable as it was cheaper and more easily and rapidly implemented.

## 6.2 Introduction

Natural attenuation has emerged as the approach of choice for remediating groundwater at many contaminated sites (Wiedemeier et al., 1999). The use of natural attenuation as a remedial option is referred to as monitored natural attenuation (MNA) by the U.S. Environmental Protection Agency (U.S. EPA). Demonstrating that sufficient mass loss is occurring in a plume is critical for implementing MNA. To evaluate the efficiency of natural attenuation, several authors (Semprini et al., 1995; Borden et al., 1997; King et al., 1999; Wilson et al., 2000; Kao and Wang, 2001) used the contaminant mass discharge approach to estimate contaminant mass loss.

Basically the mass discharge approach compares the mass discharge of the selected chemical across plane(s) perpendicular to groundwater flow and interprets differences in terms of potential mass loss mechanisms. Semprini et al. (1995) assessed the anaerobic transformation of chlorinated aliphatic hydrocarbons in groundwater. Borden et al. (1997) estimated the effective first-order decay coefficients for MTBE and BTEX in a groundwater plume. Wilson et al. (2000) estimated the rate of removal of MTBE under methanogenic conditions near a subsurface source. King et al. (1999) quantified the mass loss in a coal tar creosote plume generated in the Borden aquifer. Kao and Wang (2001) used the mass discharge approach to calcu-

---

[4] Based on a manuscript submitted to the Journal of Contaminant Hydrology

late the apparent biodegradation rates of BTEX in groundwater plumes. They concluded that mass discharge and *in situ* tracer tests were more reliable and straightforward in evaluating natural attenuation and intrinsic biodegradation than microcosm tests, *in situ* column studies and fate and transport modeling.

The most common method to establish contaminant mass discharge is to monitor a set of multilevel wells positioned on a control plane perpendicular to the plume, at different distances from the source and/or over time (Kao and Wang, 2001, Borden et al., 1997, Semprini et al., 1995, King et al., 1999 and, Wilson et al., 2000). Polygons are drawn around a sampling point that typically extend half the distance to the adjacent sampling points. For each polygon, a value of mass discharge is derived based on the measured aqueous concentration and on the local Darcy flux. The total contaminant mass discharge for a control plane is then the sum of all individual polygon discharges. Because point-scale concentration and hydraulic conductivity measurements as well as the hydraulic gradient are assumed constant over the size of a polygon, the multilevel well approach is subject to a certain degree of uncertainty. The larger the spatial and temporal variations in the aquifer properties and in the contaminant distributions, the greater the uncertainty in the discharge estimate may be for any given monitoring grid.

To overcome the difficulties associated with the interpolation of a point-scale measurement, an integral groundwater approach (Teutsch et al., 2000; Ptak et al., 2000a) has been used by Bockelmann et al. (2001a) to estimate contaminant mass discharge. With this approach, the mass discharge is obtained by sampling the discharge of one or more pumping wells placed along a control plane perpendicular to the mean groundwater flow direction. The premise is that the concentrations measured at a pumping well are representative of the contaminant distribution

within the increasing capture zone of the well. The undisturbed concentration distribution is reconstructed with the use of an analytical solution (Schwarz, 2001) based on a time-dependant calculation of isochrones and mass balances for the increasing capture zones. In general, the analytical solution is a simplified estimation tool which can be applied to homogeneous or moderately heterogeneous aquifers to estimate contaminant mass discharges using a relatively small number of monitoring wells and without the need for a detailed groundwater flow and transport model (Bockelmann et al., 2001a).

Both the multilevel well and the integral groundwater investigation approaches were applied in an unconfined sand aquifer contaminated with hydrocarbons and showing evidence of natural attenuation. The objective of this study was to compare the two groundwater investigation approaches and to investigate the uncertainty associated with their mass discharge estimates.

## 6.3    Site characterisation

The unconfined, shallow aquifer at the P-52 site at Canadian Forces Base Borden, Ontario, Canada was contaminated by leaded gasoline leaking from underground storage tanks (USTs). The spill and/or leaks most probably occurred between 1964 and 1985. The minimum volume was estimated to be 7500 L. As of 1999, the zone containing residual hydrocarbon phase and the hydrocarbon plume were estimated to extend 60m and 250m downgradient of the old USTs respectively.

Table 6.1 presents the aquifer characteristics.

The dissolved hydrocarbons migrated in the well-characterised, unconfined Borden aquifer composed of fine to medium sand. At the site, the aquifer overlies a discontinuous sandy silty-clay aquitard. The aquifer thickness varies from 4.0m to 9.1m over

Table 6.1: Unconfined aquifer characteristics

| Parameter | Value | Reference |
|---|---|---|
| Radial hydraulic conductivity | 6E-6 to 2E-4 $ms^{-1}$ | Sudicky (1986); Béland-Pelletier (2001b) |
| Hydraulic gradient | -0.015 to -0.010 | Béland-Pelletier (2001b) |
| Porosity | 0.33 | Mackay et al. (1986) |
| Aquifer thickness | 4 to >15m | Béland-Pelletier (2001b) |
| Depth to water table | 2 to 4m | Béland-Pelletier (2001b) |
| Saturated thickness in vicinity of mass discharge experiments | 2.8m | Béland-Pelletier (2001b) |
| Specific yield | 0.1 | Béland-Pelletier (2001b) |
| Specific storage | $0.005m^{-1}$ | Béland-Pelletier (2001b) |
| Organic carbon content | 0.02% | Mackay et al. (1986) |

the first 200m of the P-52 plume. Beyond 200m, the aquifer thickness increases to more than 15m as no aquitard material was intersected to that depth. The groundwater flow appears to be focused towards the discontinuity of the aquitard. The first portion of the plume, where the mass discharge approaches were tested, is under the influence of a northward groundwater flow direction. Figure 6.1 presents the vertically averaged concentration of total BTEX obtained from multilevel wells sampled on August 1999 along with the water table elevation surveyed on October 1999.

Béland-Pelletier (2001b) provided evidence that natural attenuation of BTEX was occurring at this site. The BTEX distributions were much more restricted than predicted without allowing their biotransformation. The BTEX plume is generally anaerobic and electron acceptor utilisation is evident. Concentrations of dissolved oxygen (DO), nitrate ($NO_3^-$) and sulphate ($SO_4^{2-}$) are lower and concentrations of ferrous iron ($Fe^{2+}$) and methane ($CH_4$) are higher in the plume than in background groundwater.
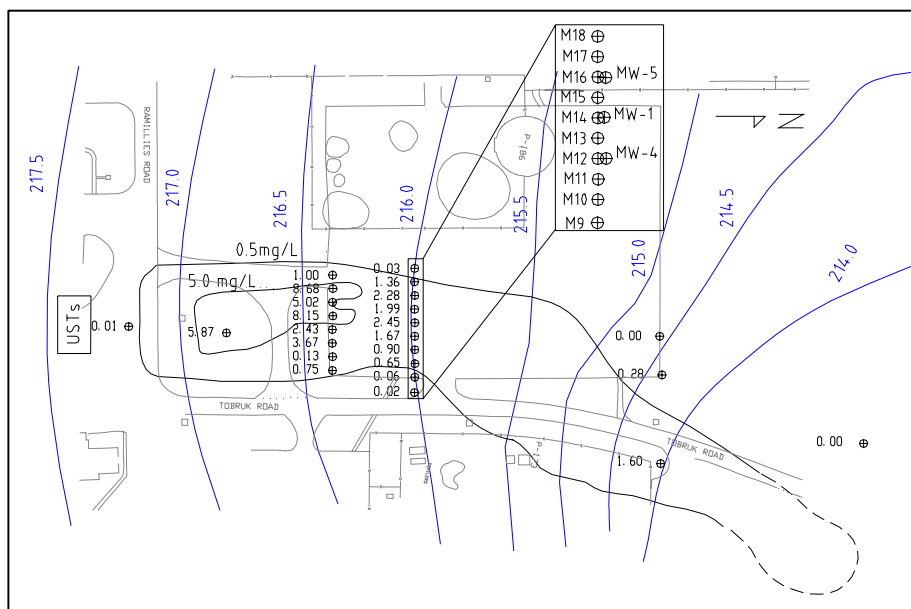


Figure 6.1: The BTEX plume originating from leaking USTs at the P-52 site. Contours are of using vertically averaged total BTEX concentrations ($mgl^{-1}$). Water table elevation (masl) in October, 1999 is based on measurements in about 20 wells, but only the location of multilevel and pumping wells (blown up area) used in this comparison are shown.

## 6.4 Integral groundwater investigation method

### 6.4.1 Approach

The integral groundwater investigation approach is designed to estimate the mobile mass discharge of a contaminant plume at a specific transect or control plane located perpendicular to the groundwater flow direction, downstream of a source zone (Teutsch et al., 2000; Ptak et al., 2000a). The mass discharge is obtained from sampling contaminant concentrations over time in one or more pumping wells placed along the control plane. The concentration-time series measured in groundwater from the pumping wells under transient pumping conditions are interpreted in this study using an analytical solution presented by Schwarz (2001) (Equation 6.1a). The solution provides values of concentrations $Cx_i$ for each section of the capture zone defined by the spatial increment dr of the radius r along the control plane between two consecutive sampling events (see Figure 6.2).
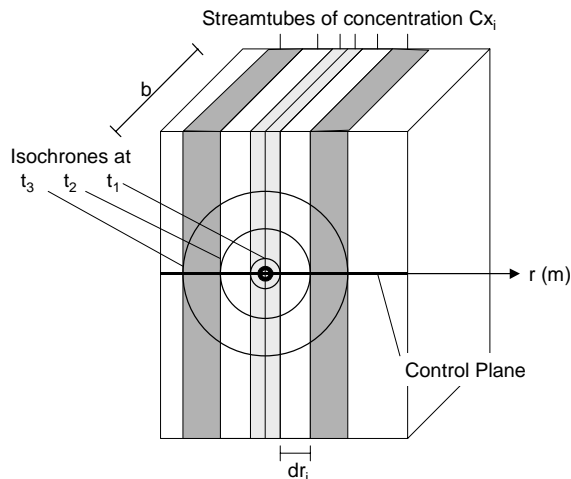


Figure 6.2: Spatial distribution of concentrations derived from the analytical solution (symmetrical concentration distribution shown)

These sections are referred to as streamtubes. The concentration $C_{pi}$ measured in the well for all sampling events except the

first is always the average concentration of the intercepted streamtubes. The analytical solution therefore provides a symmetrical reconstruction of the concentration distribution i.e. assigns the average (theoretical) concentration, $C_{xi}$ to the two streamtubes corresponding to any sampling event as shown on Figure 6.2.

$$Cx_i = \frac{\pi \, Cp_i}{2 \arccos\left(\frac{r(t_{i-1})}{r(t_i)}\right)} - \frac{\sum_{k=1}^{i-1} Cx_k \left[ \arccos\left(\frac{r(t_{k-1})}{r(t_i)}\right) - \arccos\left(\frac{r(t_k)}{r(t_i)}\right) \right]}{\arccos\left(\frac{r(t_{i-1})}{r(t_i)}\right)}$$

(6.1a)

with:

$$r(t) = \sqrt{\frac{Q_p t}{\pi b n_e}} \qquad (6.1b)$$

where $Cx_i$ [ML$^{-3}$] represents the average (theoretical) concentration of the two streamtubes crossing the control plane within the investigated well capture zone, corresponding to the i-th sampling event. For the first sampling event, $C_{xi}$ equals $C_{p1}$. $Cp_i$ [ML$^{-3}$] stands for the concentration measured at the pumping well at time $t_i$ and $r(t_i)$ [L] is the radius of the well capture zone at time $t_i$. $Q_p$ [L$^{-3}$T] represents the pumping rate and t [T], k [-], b [L], and $n_e$ symbolize the time, the number of the concentration measurement, the aquifer thickness, and the effective porosity, respectively.

The analytical solution assumes that within the well capture zone: (1) the flow towards the pumping well is radially symmetrical, i.e. the natural flow can be neglected during the pumping test; (2) the aquifer is homogeneous with regard to porosity, hydraulic conductivity and thickness; and (3) the concentration may vary from streamtube to streamtube but does not vary significantly or varies linearly along

each of the streamtubes at the scale of the well capture zone (Bockelmann et al., 2001a).

The groundwater discharge $Q_i$ at the control plane for each streamtube is given by:

$$Q_i = K \; i \; b \; dr_i \qquad (6.2)$$

where K, i and b represent the hydraulic conductivity, the hydraulic gradient and the aquifer thickness representative of a streamtube, all of which are assumed to be constant over all streamtubes for the analytical solution. $dr_i$ is the width of a streamtube. As the reconstructed concentration distribution, based on the analytical solution, is symmetrical around the well and $Q_i$ is assumed the same in both streamtubes at sampling time $t_i$, the integral mass discharge, $I_t$, is then equal to twice the sum of the streamtube concentrations ($Cx_i$) to one side of the well times the specific streamtube discharge ($Q_i$) of these streamtubes as shown in Figure 6.2. That is:

$$I_t = 2\sum_{i=1}^{k} Q_i Cx_i \qquad (6.3)$$

where k represents the number of isochrones or data points in the concentration time series and is then equal to half the number of streamtubes.

## 6.5    Field test at the P-52 site

A five-day pumping test was run in November, 1999. Three pumping wells positioned approximately 40m downgradient of the source zone were used for the test. The pumping wells, MW1, MW4 and MW5 (Figure 6.1), were standard 0.05m ID (2in) monitoring wells screened over the entire saturated thickness. MW1 was located in the centre of the plume and MW4 and MW5 were located 10m east and west of MW1 respectively.

The initial pumping rate was 10Lmin$^{-1}$ for all three wells. The wells were sampled for each anticipated increase of 0.15m in the idealised cylindrical capture zone radius (r) as given by Equation 6.1b. The sampling intervals ranged from every 30 minutes in the beginning to 6 hours near the end of the test.

For every sampling round, drawdown was measured in 17 observation wells distributed around the pumping wells. The three wells were pumped at an average discharge of 10Lmin$^{-1}$ during the entire test except for MW4 whose pumping rate was reduced to 5Lmin$^{-1}$ halfway through the test to avoid excessive drawdown. The presence of a clay lens, identified in the core of M12 located less than 1.5m from MW4, might have contributed to the inefficiency of MW4.

The concentration-time series measured at the pumping wells during the test are presented in Figure 6.3. The analytes were benzene, toluene, ethylbenzene, p,m-xylene, o-xylene, the trimethylbenzene isomers (TMBs) and naphthalene. Overall, MW1 presents the highest concentrations for all compounds followed by MW5 and MW4. This is consistent with the location of the pumping wells with regard to the plume position. During the first 200 to 300min the concentrations at all three wells show an abrupt rise followed by a drop. It is believed that these high variations at early pumping times are due to the complex flow in the saturated and unsaturated zone that developed in response to the pumping of the unconfined aquifer. The concentrations at MW1 slowly increased after approximately 2000min. Because MW1 is located near the centre of the plume, its capture zone might have extended towards an area of the plume with relatively higher contaminant concentration.

Contaminant mass discharges were derived for each pumping well. The change in pumping rate at MW4 was
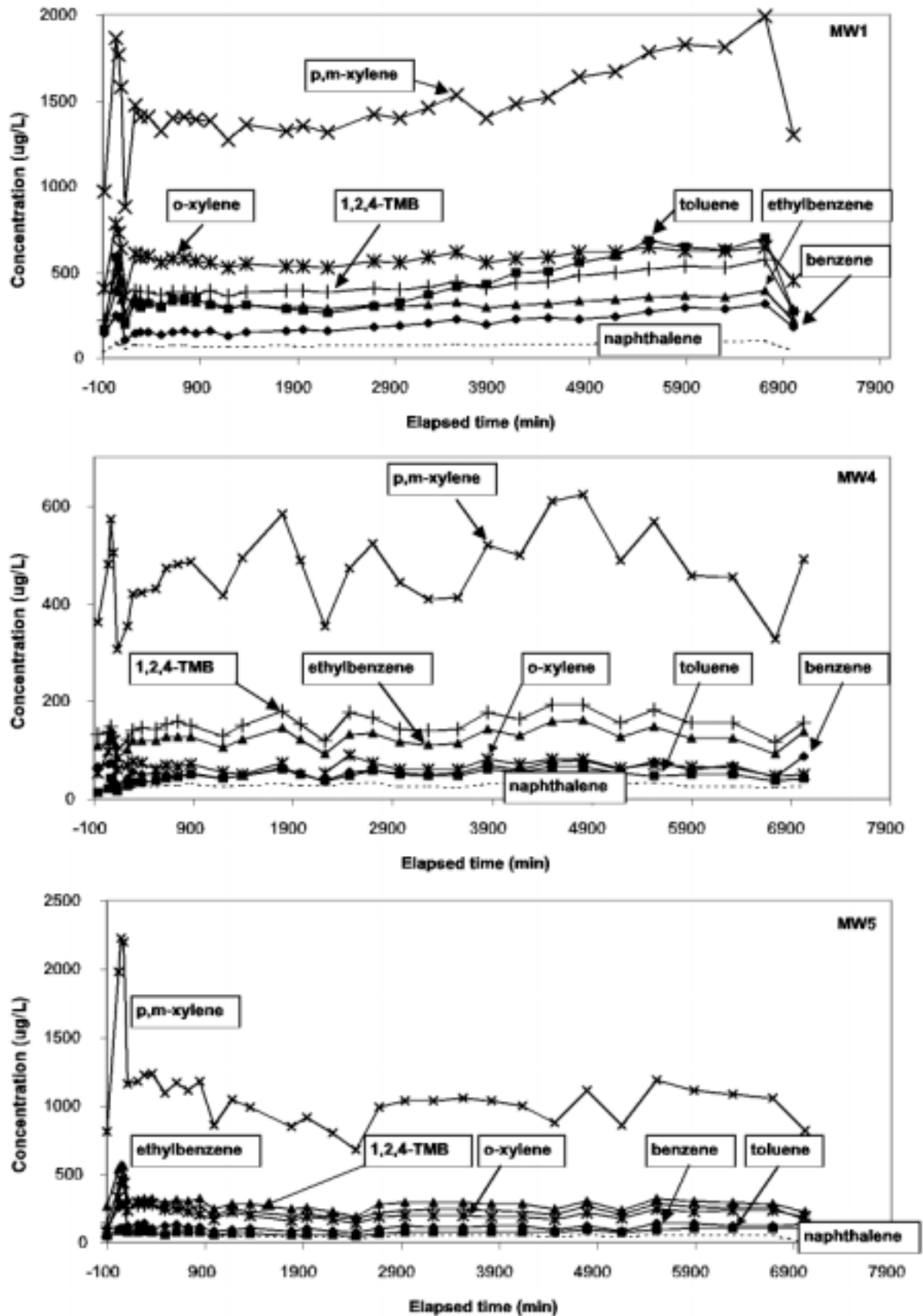
Figure 6.3: The concentration-time series for selected analytes from the three pumping wells. Series have been censored to remove very occasional outliers

Table 6.2: Mass discharges (gd⁻¹) from the multilevel well monitoring method ("Wells") and the integral groundwater investigation method ("Integral") and their estimated relative uncertainties

| Compound | Calculated Comparative Mass Discharge (gd⁻¹) | | Uncertainty in Physical Measurement (%) | | | Uncertainty in Assumptions and Procedures (%) | | Total Uncertainty (%) | |
|---|---|---|---|---|---|---|---|---|---|
| | Wells | Integral | Analytical Error | | Other Physical Measure-ments | Assumptions and Procedures | | Total Uncertainty | |
| | | | Wells | Integral | | Wells | Integral | Wells | Integral |
| benzene | 0.45 | 0.49 | 20 | 10 | 7 | 32 | 38 | 38 | 40 |
| toluene | 0.81 | 0.75 | 10 | 10 | 7 | 32 | 38 | 34 | 40 |
| ethylbenz. | 0.59 | 0.86 | 10 | 10 | 7 | 32 | 38 | 34 | 40 |
| p,m-xylene | 2.05 | 3.61 | 10 | 10 | 7 | 32 | 38 | 34 | 40 |
| o-xylene | 0.61 | 1.01 | 10 | 10 | 7 | 32 | 38 | 34 | 40 |
| 1,3,5-TMB | 0.17 | 0.23 | 10 | 10 | 7 | 32 | 38 | 34 | 40 |
| 1,2,4-TMB | 0.63 | 1 | 10 | 10 | 7 | 32 | 38 | 34 | 40 |
| 1,2,3-TMB | 0.23 | 0.39 | 10 | 10 | 7 | 32 | 38 | 34 | 40 |
| naphthalene | 0.11 | 0.19 | 20 | 15 | 7 | 32 | 38 | 38 | 41 |

treated as two different stress periods. The hydraulic input parameters used by the analytical solution were n = 0.33, i = -0.012, Kx = Ky = 4.00E-05 ms⁻¹, and b = 2.8m. Table 6.2 shows the integral mass discharge for the control plane cover by all three wells for each compound.

## 6.6 Multilevel well method

### 6.6.1 Approach

For the mass discharge quantification based on a multilevel well approach, the point-scale concentration measurement ($C_i$) obtained from the sampling port of a multilevel well is extrapolated over an area ($A_i$) of the polygon that extends to half the distance to the adjacent sampling ports. During the multilevel well installation, soil samples are collected and analysed for hydraulic conductivity ($K_i$). The irregularly distributed $K_i$ values are interpolated onto a grid with dimensions equal to those of the sampling port network to obtained a interpolated hydraulic conductivity value $K_i$ for each polygon. A hydraulic gradient (i) is calculated from observation points located up and downgradient of the multi-level wells control plane. A uniform gradient across the control plane was assumed. The groundwater discharge for each polygon is then: $Q_i = K_i' * i * A_I = q_i * A_i$. The total mass discharge (F) is the sum of all the individual mass discharges ($F_i$) going through each polygon (Equation 6.4).

$$F = \sum_{i=1}^{n} F_i = \sum_{i=1}^{n} C_i q_i A_i \qquad (6.4)$$

To obtain a meaningful estimate of mass discharge from the multilevel well all the contaminant plume should be captured by the monitoring network. Extrapolation of the instantaneous mass discharge in time may need to make assumptions about temporal variability of source strength or flow velocity and flow direction. Note also that the total mass discharge is obtained using either the multilevel well or the integral groundwater investigation method. The dispersive mass discharge is usually small relative to the advective discharge and so can be neglected. Further, the sorption between the aquifer solids and the aqueous phase is assumed to be at equilibrium so no change in mass discharge is attributed to sorption processes.

### 6.6.2 Multilevel well installation and measurements

Ten (10) multilevel wells were installed perpendicular to the flow direction (labelled M9 to M18 in Figure 6.1), 1.5m upgradient of the pumping wells MW1, MW4 and MW5. The multilevel wells were 5.0m apart and had eight 0.0016m ID (1/16in) Teflon tubing sampling ports staggered 0.40m along a 0.013m ID (½in) PVC centre stock. This generated a sampling grid of 8 sampling ports by 10 multilevel wells. The multilevel wells were sampled in August 1999. At that time, the hydraulic gradient measured between two fully screened piezometers located less than 40m from the multilevel wells control plane was –0.013. The soil samples collected during the installation of the multilevel wells were analysed by falling head permeameter for hydraulic conductivity. The 52 hydraulic conductivity values obtained from the permeameter test were interpolated on the 8 by 10 sampling grid using linear Kriging with no drift. This interpolation technique was found to give the most realistic distribution of hydraulic conductivity with a variance and a mean close to the range observed for the Borden sand aquifer on site and about 200m upgradient (Sudicky, 1986).

The drawdown in the pumping wells of the shallow unconfined aquifer limited the pumping rate to 10L/min and, even with three wells operating for 5 days, the total cross-sectional area covered by the pumping wells was less than the one covered by the multilevel wells. Hence, for the comparison of the two approaches, it was necessary to modify the cross-sectional area covered by the multilevel wells to assure that both approaches represented the same aquifer control plane. The limits of the 5-day capture zone of the pumping wells were obtained from MODPATH particle tracking and were projected onto the multilevel wells sampling grid. In this way, only the polygons that lay within the limits of the capture zone were used to

calculate the multilevel well mass discharge. The polygons were truncated when necessary. The "corrected" multilevel well mass discharge obtained for each individual compound is presented on Table 6.2.

## 6.7 Uncertainty in mass discharge estimates

### 6.7.1 Uncertainty in multilevel well mass discharge estimate

The uncertainty in the multilevel well mass discharge estimate is generated by the uncertainties in the input parameters for Equation 6.4: hydraulic conductivity, hydraulic gradient, concentration measurements and area of interpolation. These uncertainties were of two types: first, the uncertainties in the physical measurements of the input parameters and second, the uncertainties inherent to the underlying assumptions and procedures. The relative uncertainty values were propagated to the multilevel well mass discharge estimate using Equation 6.5, adapted from Bevington and Robinson (1992), assuming a Gaussian data distribution. According to this equation, the uncertainty in the mass discharge estimate (E) is equal to:

$$E = \sqrt{\sum_{i=1}^{n} E_i^2} \qquad (6.5)$$

where $E_i$ is the individual relative uncertainty.

This procedure for summing the relative uncertainty is statistically correct for the relative uncertainties in the physical measurements which are multiplied in the multilevel well mass discharge equation (Equation 6.4). However, the second category of uncertainties, the relative uncertainties inherent to the approach and to the underlying assumptions, are not part of a single equation and are therefore difficult

to evaluate using conventional statistics. In this study the uncertainty in the mass discharge estimate inherent to the approach and to the underlying assumptions was evaluated by comparison between a set of reasonable scenarios for the resolution of the mass discharge estimate and the chosen scenario (see details below). The second category uncertainties were then expressed as a relative difference between the mass discharge estimates of the tested scenarios and the chosen mass discharge estimate value. Because more weight should be attributed to the higher uncertainties and to keep the same procedure throughout the analysis, Equation 6.5 was also used to propagate the second category relative uncertainties to the multilevel well mass discharge estimate.

The relative uncertainty in the analytical measurement of concentration was up to 20% for benzene and naphthalene and up to 10% for the remaining compounds (toluene, ethylbenzene, xylenes and TMBs). The total relative uncertainty in the physical measurements of length, time and elevation used to derive the individual K, i and A values summed to 7% according to Equation 6.5. The uncertainty in the mass discharge estimate attributed to the physical measurement uncertainties was, accordingly, mostly a function of the uncertainty of the concentration measurements and was estimated to be up to 21% for benzene and naphthalene and 12% for the remaining compounds (toluene, ethylbenzene, xylenes and TMBs) by Equation 6.5.

The true mass discharge for one given control plane is defined as being the mass discharge obtained when an infinite number of concentration sampling points and associated groundwater fluxes are available. Since such a distribution is impossible to obtain, the true mass discharge has to be approximated, with the multilevel well approach, from point-scale measurements that are interpolated over a certain area (polygon). In this study, it was assumed that the sampling grid density of approximately 0.7 sampling points per m$^2$ adequately captured the spatial variability of the contaminant distribution of the studied control plane. In other words, it was assumed that the point-scale concentration and hydraulic properties measurements were representative of the respective polygon area ($A_i$) to which they were assigned and that the sampling grid density provided a good estimate of the true mass discharge at the control plane. To test this assumption, a sampling grid density analysis was performed on a higher density sampling grid, fence 7A of King et al (1999), located in the same Borden aquifer but about 300m further upgradient and the results were applied to the P-52 sampling grid.

King et al. (1999) used a set of multi-level well fences in the Borden sand pit research area to monitor a dissolved coal tar creosote plume including naphthalene. One of the fences used, fence 7A, had a sampling grid density of 4.2 sampling points per m$^2$ (7 multilevel wells about 1.5m apart, each with 14 points spaced 20cm apart). The density of fence 7A being 6 times higher than the P-52 one, it was assumed that the discretization of fence 7A was small enough to provide a close estimate of the true discharge of the creosote plume. It was then decided to assess the impact of a less extensive monitoring network on the naphthalene mass discharge of fence 7A. To do that, it was assumed that the concentration of any given point within the limit of fence 7A could be obtained by performing a bilinear interpolation on the four closest measured points or "real points". Several mass discharges were computed using 98 different grid configurations corresponding to a range of sampling grid density between 0.1 and 4.2 sampling points/m$^2$. To be consistent with common practices, the horizontal and vertical spacing of the sampling points within one grid were kept constant. Also, the groundwater discharge was assumed constant throughout the fence area to
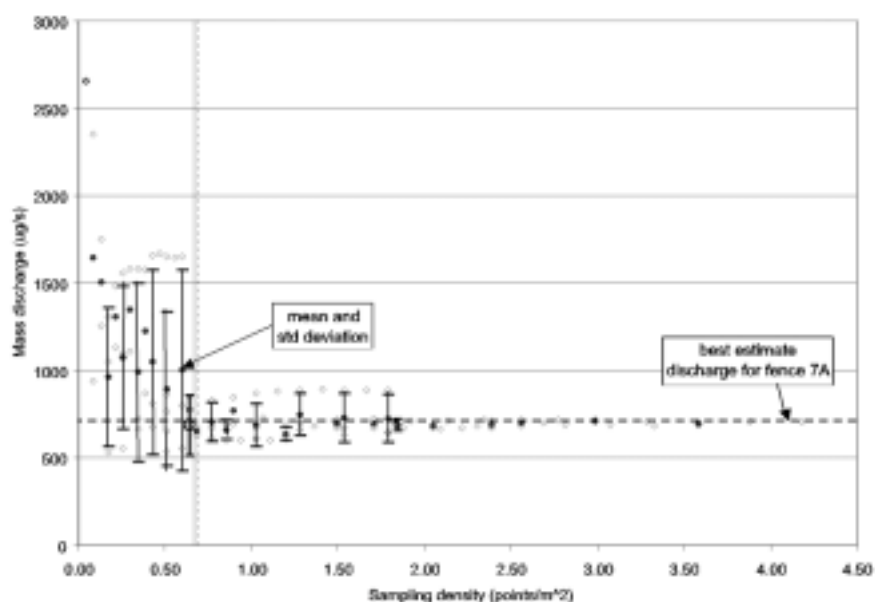
Figure 6.4: Variation of mass flux of naphthalene ($\mu gs^{-1}$) versus monitoring fence density using fence 7A from King et al. (1999)

simplify the analysis. This was reasonable given the homogeneity of the Borden aquifer.

The mass discharge estimates were plotted against their respective densities (Figure 6.4). The results illustrated the uncertainty in the mass discharge estimate generated by the grid density. The lower the density, the larger the difference between the range of mass discharge estimates and the true mass discharge value. From Figure 6.4, it can be deduced that, using a sampling density of 0.7 sampling points/$m^2$ (F1 and F2 fences at the P-52 site), the mass discharge calculated at site P-52 could differ from the true mass discharge by up to 25%. The sampling grid density of 0.7 sampling points/$m^2$ hence generated a relative uncertainty in the mass discharge estimate of up to 25%.

The nature of the contamination and the aquifer properties at both the P-52 and the King et al. (1999) sites are sufficiently similar to support this inference about the uncertainties due to sampling grid density. Both plumes consisted of LNAPL

contaminant; both plumes migrated in the unconfined Borden sand aquifer; both plumes were generated by source zones that presented a relatively uniform contaminant distribution; and both plumes present a similar degree of contaminant distribution heterogeneity as illustrated by the similarity of their cross-sectional shape (Figure 6.5).

The multilevel well mass discharge estimation involved the interpolation of point-scale hydraulic conductivity measurements onto the 8 x 10 sampling grid by Kriging. This interpolation technique was found to best match the observed hydraulic conductivity distribution. Because the interpolated hydraulic conductivity distribution remains an estimate of the true distribution, the sensitivity of the mass discharge estimate to the chosen interpolated distribution was tested. In order to do so, the mass discharge was derived for four different distributions. Three distribution were generated by different interpolation techniques: linear Kriging, Inverse Distance to a Power, and quadratic surface Polynomial Regression, and one distribution by the use of a uniform hydraulic

conductivity value for the entire grid corresponding to the geometric mean of the observed hydraulic conductivity measurements. The difference in mass discharge estimates between all four distributions was expressed relatively to



Figure 6.5: Cross sectional views of the naphthalene plume at fence 7A of King et al. (1999) above and of the benzene plume from fence 1 at the P-52 site below. Concentrations are shown in mgl$^{-1}$

the mass discharge estimate derived from the Kriging distribution. The difference between the Kriging distribution and geometric mean distribution was the highest at 14%. This was assumed to be the relative uncertainty in the mass discharge estimate generated by the choice of the interpolation technique. This uncertainty is relatively low compared to other sources of uncertainty and is likely the results of the homogeneity of the Borden aquifer.

In this procedure a uniform hydraulic gradient was assigned to the control plane. The hydraulic gradient was observed to fluctuate over time. Since the results from this approach need to be extrapolated to the time of the pumping test to allow comparison of the two approaches, a relative uncertainty needs to be assigned to this temporally variable hydraulic gradient. Within one month of the multilevel sampling round, the gradient was observed to fluctuate between –0.012 and –0.013. Since the gradient is assumed constant over the control plane, the difference in hydraulic gradient attributed to temporal variation, 8%, corresponds to the uncertainty in the mass discharge estimate generated by the chosen magnitude of the hydraulic gradient.

Finally, as mentioned before, the capture zone limits had to be approximated in order to sub-sample the multilevel well sampling grid to provide a similar control plane for the comparison between the two mass discharge approaches. The capture zone was approximated by applying the MODPATH particle tracking option of the MODFLOW groundwater flow model. The model, with a normalised Root Mean Squared error (RMS) below 7% for the entire simulation time, was well calibrated to the hydraulic head surveyed during the 5-day pumping test. Certain limitations of MODFLOW, especially the assumption of strictly saturated flow and the need to turn nodes above the water table inactive in the pumping wells, generated an uncertainty in the delineation of the upper limits of the
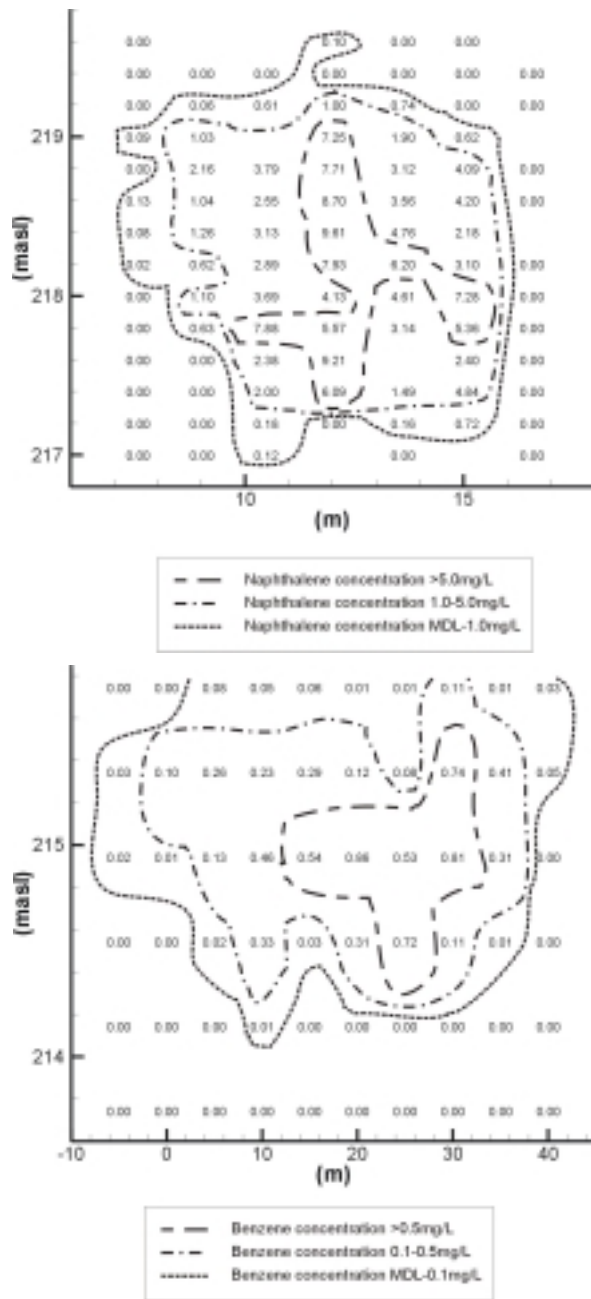
capture zone. These two aspects accentuated the influence of the vertical gradient in the upper part of the aquifer causing the capture zone radius to be narrower at the top (Figure 6.6). However, the delineation of the capture zone in the lower part of the aquifer is thought to be a good approximation because the model was calibrated with hydraulic heads measured in that portion. Hence, the best approximation of the capture zone extent is thought to be between the one provided by MODFLOW (Figure 6.6) and one that would have a constant radius over the whole thickness equal to the one calculated by MODFLOW for the lower portion of the aquifer. These two capture zone extent scenarios generated mass discharge estimates that differed by 11% and therefore the relative uncertainty in the mass discharge estimate attributed to the capture zone delineation was estimated to be 11%.
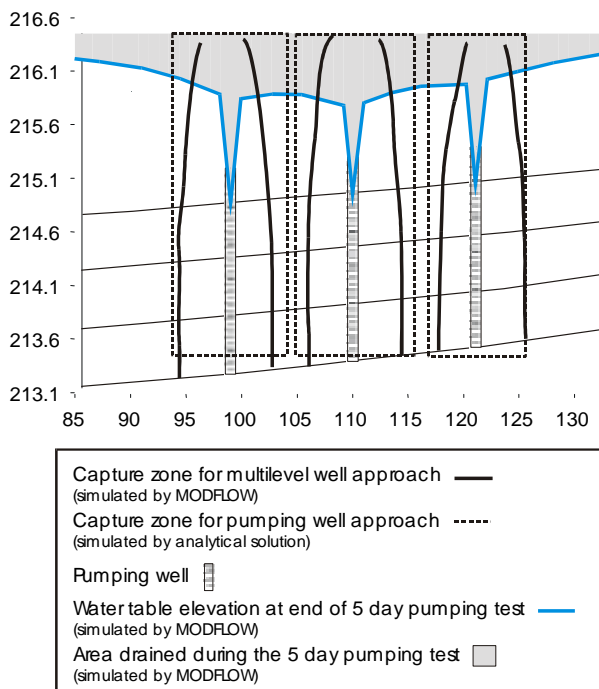


Figure 6.6: Modelled capture zones at the end of the 5-day pumping test. Capture zones for pumping wells were simulated with MODFLOW and MODPATH.

It was shown that the relative uncertainty in the multilevel well mass discharge estimate generated by the

78

uncertainties in the physical measurements was up to 21%. The different K distribution, the temporal fluctuations in the hydraulic gradient and the adequacy of the sampling grid density generated a relative uncertainty in the mass discharge estimate of up to 14%, 8% and 25%, respectively. The overall relative uncertainty in the multilevel well mass discharge estimate is then 37% according to Equation 6.5.

## 6.8    Uncertainty in the integral approach mass discharge estimate

As it was the case for the multilevel well mass discharge estimate, an uncertainty is attributed to the physical measurements of the terms of the integral approach mass discharge equations. The measurements are: the pumping rate ($Q_p$), the pump discharge concentration ($C_p$), the hydraulic conductivity (K), the hydraulic gradient (i), the saturated thickness (b), the porosity (n) and the time (t). It was seen that, except for the analytical error in the concentration measurements, all physical measurements involved in the multilevel well approach generated an uncertainty of 7% in the mass discharge estimate. This turned out to be negligible when compared to the other sources of uncertainties. Because of that, it was decided not to recalculate the physical measurement uncertainties of the integral approach, except for the analytical error. Rather, the relative uncertainty in these aspects was assumed to be similar to the estimated total uncertainty of the physical measurements of the multilevel well approach - 7%. This was further supported by the common use of some of the physical measurements by both techniques. Also the uncertainties attributed to the underlying assumptions described below were expected to be significantly higher than the uncertainty in the physical measurements and therefore it appeared logical to focus on the

uncertainties in the underlying assumptions.

The relative error for the analysis of the pumping test samples was up to 15% for naphthalene and up to 10% for the remaining compounds (benzene, toluene, ethylbenzene, xylenes and TMBs). This analytical error was summed with the 7% uncertainty in $Q_p$, K, i, b, n and t using Equation 6.5 and a relative uncertainty in the integral approach mass discharge estimate of up to 17% for naphthalene and up to 12% for the remaining compounds.

The integral approach also carries uncertainties generated by its underlying assumptions. The presence of a groundwater gradient at the site induced a deviation from the first assumption of radially symmetrical flow to the pumping wells. As a result, the control plane used by the integral groundwater investigation method was larger than the one used for the multilevel well mass discharge estimation as shown in Figure 6.6. The control plane for the integral groundwater investigation method was given by the pumping rate and the total duration of the test according to the cylindrical capture zone model (Equation 6.1b). The control plane for the multilevel well approach was obtained by modelling the response of the aquifer to the pumping wells and was based on the observed head distribution over the duration of the test. Hence, the control plane and accordingly the groundwater discharge used for the integral groundwater investigation method is approximately 37% larger than the one used for the multilevel well approach. Hence, the relative uncertainty in the integral approach control plane area is up to 37%.

The second assumption of a homogeneous aquifer with regard to porosity, hydraulic conductivity and thickness was considered valid at the site. The homogeneous aquifer properties were supported by previous research in the Borden aquifer

(e.g., Sudicky, 1986), by hydrogeologic characterization of site P-52 and by the radially symmetrical drawdown cone measured during the pumping test. A numerical simulation was done to derive the hydraulic parameter values for the integral approach mass discharge calculation. The model simulated the flow in response to pumping in a homogeneous aquifer. The model was considered well calibrated when the normalised Root Mean Squared error (RMS), which represents the difference between the simulated and observed hydraulic head expressed as a percentage of total head loss, stayed below 7% for the entire simulation time. Although a RMS below 7% is considered a good fit, the difference between the observed and simulated head of 7% might indicate a problem with the conceptual model of the site. Two factors linked to the homogeneous aquifer assumption could be responsible for the 7% difference between the observed and simulated head. First, the hydraulic property values used in the model are inexact and, second, the aquifer is not perfectly homogeneous. In any case the calibration criterion, RMS of 7%, can be used as an estimate of the uncertainty associated to the homogeneous aquifer assumption.

Because evidence of natural attenuation was found at the site, a certain concentration gradient exists along the flow direction at all scales. Consequently, the third assumption of negligible or linearly changing concentrations along the flow direction may not be entirely fulfilled. The concentration gradient within the well capture zones was not quantified during this study. However, the relatively constant concentration-time series suggest a fairly uniform concentration distribution within the well capture zones and the possible deviation from the third assumption was assumed to be minor.

For the integral approach the propagation of the uncertainties inherent in the physical measurements and in the under-

lying assumptions presented a challenge. The uncertainties generated by the underlying assumptions affected the integral mass discharge solution at different levels. For example, the uncertainty in the capture zone delineation could affect both the discharge through the control plane and the reconstruction of the contaminant distribution within the well capture zones. For that reason it was difficult to know what these uncertainties represented statistically and what propagation error equation to apply. Furthermore, the uncertainties were expressed relatively to different measurements: to the physical measurement (17%), to the control plane area (37%) and to the head loss in the domain (7%). Because the uncertainty in the integral approach mass discharge estimate is needed in order to compare that estimate to the multilevel well mass discharge estimate, it was decided to follow the error propagation procedure established for the multilevel well mass discharge estimate. In order to do so, the above uncertainties were assumed to represent a relative uncertainty in the integral approach mass discharge estimate. These uncertainties were then summed using Equation 6.5. The total relative uncertainty in the integral mass discharge estimate using the simplified analytical solution is hence 41% at this site.

## 6.9 Comparison of the results of the two methods

The calculated mass discharges at fence F2 are shown in Table 6.3. The mass discharges calculated from the integral groundwater investigation method using three pumping wells are shown in Table 6.2. For most analytes, the integral approach produced lower estimates of mass discharge. When the total analyte mass discharge is summed for both methods, the integral method total analyte mass discharge of 8.5 $gd^{-1}$ is only about 5% less than the summed mass discharge of 8.9 $gd^{-1}$ via the multilevel well method. As pointed out above, the control plan for the integral method did not extend across the whole plume width and so the multilevel well control plane was recalculated to include a similar coverage.

Figure 6.6 shows the compound specific mass discharges derived from the two investigation approaches with the multilevel well approach "corrected" as discussed previously. In general, the integral groundwater investigation approach yielded larger mass discharges.

Table 6.3: Mass discharge for aromatic compounds at upgradient fence F1 and downgradient fence F2 in the dissolved plume at the P-52 site, CFB Borden, ON. Differences in mass discharge greater than the uncertainty in estimation are in bold

| Compound | Discharge ($gd^{-1}$) | | Uncertainty in discharge (%) | Charge in discharge (%) |
| --- | --- | --- | --- | --- |
| | F1 | F2 | | |
| benzene | 0.72 | 0.69 | 37 | - 4 |
| toluene | 3.47 | 1.23 | 32 | **- 65** |
| ethylbenzene | 0.75 | 0.94 | 32 | + 25 |
| p-, m-xylene | 2.99 | 3.23 | 32 | + 8 |
| o-xylene | 1.39 | 1.03 | 32 | - 26 |
| 1,3,5-TMB | 0.48 | 0.24 | 32 | **- 50** |
| 1,2,4-TMB | 1.1 | 0.98 | 32 | - 11 |
| 1,2,3-TMB | 0.42 | 0.36 | 32 | - 14 |
| naphthalene | 0.20 | 0.16 | 37 | - 20 |
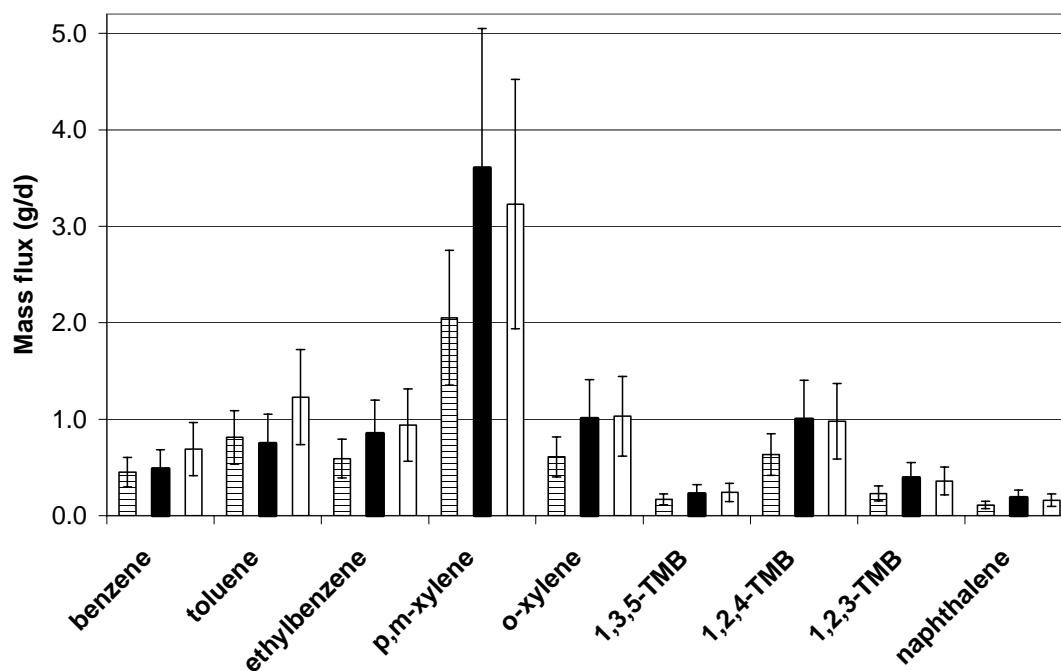
Figure 6.7: Mass discharge estimated by the integral groundwater investigation method (black bar) and by the multilevel well method using the "corrected" control plane (structured bar) and for the whole control plane or fence (white bar). Error bars reflect total uncertainty from Table 6.2.

The total analyte mass discharges obtained from the integral and the multilevel well approaches were 8.5 gd$^{-1}$ and 5.7 gd$^{-1}$ respectively. The total analyte mass discharge from the "corrected" multilevel well approach is hence 33% higher than the discharge derived from the integral groundwater investigation approach. Since the difference in ground-water discharges between the two approaches was estimated to be 37%, it appears that the deviation from the cylin-drical assumption could be mainly respon-sible for the relatively higher integral groundwater investigation mass dis-charges.

The 33% difference is not observed for all compounds. During the analysis, a correlation between the difference in mass discharges from the two approaches and the smoothness of the concentration time series measured was observed for some compounds. For example, Figure 6.3 shows a relatively large variation of p-,m-

xylene concentrations at MW1 and MW4 and the integral (1.85 gd$^{-1}$ at MW1 and 0.62 gd$^{-1}$ at MW4) and multilevel (0.75gd$^{-1}$ at MW1 and 0.27 gd$^{-1}$ at MW4) approach discharges for those compounds at those wells differed by more than 120%. This suggested that when the concentration distribution is uniform, the assumption of a negligible concentration gradient inherent in both approaches is more likely to be fulfilled and the mass discharge estimates from each technique will be more similar. However, the observed correlation does not provide information regarding which of the two techniques, or if both, fail to meet the assumption.

The relative uncertainty in the integral approach was estimated to be between 40%-41% and the uncertainty in the multilevel well was estimated to be between 34%-38% depending on the compound. Figure 6.7 shows the mass discharge estimate along with their relative uncertainty. The figure demonstrates that

the range of discharge values overlap for all compounds. Overall, this suggests that both approaches provided similar estimates of the contaminant mass discharge at the control plane.

## 6.10  Discussion

It should be noted that the two approaches did not sample exactly the same aquifer thickness. The multilevel well sampling ports were all positioned below the water table whereas the pumping wells captured water from both below and above the water table (capillary fringe zone). Although the capillary fringe was captured by the pumping wells, the analytical solution used in the interpretation of the integral approach did not account for that groundwater flow. Hence, both techniques neglected the mass discharge of the capillary fringe. For the control plane studied here there was no evidence of contaminant mass in the capillary fringe and it was likely that the contaminant mass discharge at the capillary fringe was indeed negligible (see Figure 6.5). Nonetheless, before implementing these mass discharge approaches, the contaminant distribution in the capillary fringe should be investigated and taken into account if judge potentially significant.

The overall research cost including the planning, installation of wells, execution, laboratory analysis and interpretation was estimated as $7500 for the multilevel well approach and $14200 for the integral approach. Both techniques required the definition of the plume width at the control plane which was provided by the site characterization work. Both techniques also required an estimate of the Darcy flux; that is, an estimate of the hydraulic gradient and of the hydraulic conductivity at the control plane. The hydraulic gradient was obtained from the observation wells installed during the initial site charac-

terization. The multilevel well approach made used of the soil retrieved during the installation of the multilevel well to obtain material from which a detailed hydraulic conductivity distribution was derived from falling head permeameter tests performed on 51 soil samples. The integral approach required a unique value of hydraulic conductivity representative of the control plane. That value was obtained from calibrating a groundwater flow model to the time-drawdown curves of 17 observation wells monitored during the pumping test. In this shallow unconfined aquifer the pumping test included a well efficiency test to plan the number of wells and pumping rates and duration needed to cover the studied control plane. The cost for estimating the hydraulic conductivity for the integral approach ($1500) was approximately 1.5 times the cost for the multilevel well approach ($900) at this site. Alternatively, an effective K value can be obtained from the drawdown data recorded during the long-term pumping test or from the recovery phase of the pumping test.

The concentration distribution at the control plane for the multilevel well approach was obtained from 60 water samples. To represent the same control plane, the integral approach used 99 concentration measurements. The cost for sampling and analyses were estimated as $3800 for the multilevel well approach and $7500 for the integral approach. At other sites (e.g., Ptak et al., 2000a; Bockelmann et al., 2001a) larger dr increments were found to yield reliable mass discharge estimates and the smoothness of the concentration-time series suggest, in hindsight, fewer samples could have been collected at this site.

A total of 18 days was needed to complete the interpretation of the multilevel well mass discharge and 26 days were needed to calculate the integral approach mass discharge.

Because the volume of water purged was significant during the pumping test, a strategy for the disposal of the effluent water had to be defined prior to the start of the test. This was not necessary for the multilevel well approach since the volume of water purged was minimal during the sampling of the multilevel wells. Because permission to infiltrate the effluent water over the source zone was obtained, the disposal of the contaminated effluent water at the site turned out to be simple and cheap. In other circumstances however, the disposal of the contaminated water from the integral approach might induce an important stress on the budget. For example, the likely cost of treating the contaminated water on site with activated carbon was estimated to be $10 000.

Because no single factor could explain the difference between the mass discharge estimates derived from the two approaches, it is not possible to confirm which approach provided the best accuracy. However, since the range of mass discharge estimates by both approaches overlaps, it is believed that the two approaches similarly represented the contaminant mass discharge of the studied control plane. For this aquifer and contaminant plume conditions, it was shown that the multilevel well approach was cheaper and faster than the integral approach. The above analysis of the density of sampling points required for the multilevel well approach suggested that savings that could have been obtained by using fewer wells or points would have been gained at a cost in quality of the mass discharge estimate. However, because of the relatively smooth concentration-time series distributions observed at the pumping wells, it would be possible to optimise a subsequent pumping test at the site by decreasing the sampling frequency. In this way, fewer samples would be collected and the cost of the integral approach would decrease.

The choice of mass discharge estimation approach is not generally obvious and so should be specific for each situation. For example, if inexpensive multilevel wells or groundwater concentration profiling (e.g., Wilson et al., 2000) cannot be used, the high cost of multilevel wells could easily leave the integral groundwater investigation much less expensive. Also, as the heterogeneity of the aquifer increases, the accuracy of the interpolation of the point-scale concentration measurements decreases and with it the accuracy of the multilevel well mass discharge. Because the increase in heterogeneity would likely induce a deviation from the cylindrical capture zone assumption, the accuracy of the integral method mass discharge as derived by the analytical solution will also decrease with an increase in heterogeneity. However, a numerical solution for the integral groundwater investigation method is available (Schwarz, 2001) and has been successfully applied at a landfill site in Southern Germany (Ptak et al., 2000a). Through the utilization of a numerical model, the numerical solution of the integral groundwater investigation method approach accounts for aquifer heterogeneities and asymmetrical well capture zones and might be a better investigation approach for heterogeneous aquifer conditions provided the heterogeneities are adequately characterized.

In addition, the questions to be answered or the remediation technique to be implemented at a should be taken into consideration when choosing between the two approaches. For instance, because the multilevel well approach provides a spatial distribution of concentration and aquifer properties it is better suited for the design of some permeable reactive barriers in which mixing of influent water is minimised (e.g., Morkin et al., 2000). However, when a spatial integration of the mass discharge is needed such as for the design of a pump-and-treat system, many reactive barriers or for the estimation of the contaminant mass discharge to enter the capture zone of a water supply well, the integral

groundwater investigation method is more appropriate.

The uncertainty of about 40% inherent in each mass discharge estimation indicate that values of contaminant mass discharge should be used cautiously. Mass discharge estimates should be presented with their associated uncertainties and conclusions based on the mass loss of contaminant should only be drawn if the decrease in mass is higher than the uncertainty in the result. For example, Table 6.3 shows the mass discharge calculated for the upgradient (F1) and downgradient (F2) fences placed downgradient of the apparent source zone at the P-52 site. For some analytes (e.g., p-,m-xylene) the mass discharges apparently increases at the downgradient fence. Note, however, that these changes in mass discharge are less than the estimated uncertainty. Only for toluene and 1,3,5-TMB is the upgradient versus downgradient difference in mass discharge greater than the estimated uncertainty of about 40%. For both analytes, mass discharge is reduced at the downgradient fence, supporting natural attenuation for at least toluene and 1,3,5-TMB in this plume.

# 7 The integral groundwater investigation method (IGIM): Comparison of analytical and numerical results[5]

## 7.1 Abstract

Compound-specific mass fluxes and attenuation rate constants for benzene, toluene, ethylbenzene, and xylenes (BTEX), as well as for selected low molecular weight polyaromatic hydrocarbon (PAH) compounds were estimated at a former manufactured gas plant using an integral groundwater investigation method (IGIM). This method utilizes long term pumping tests at control planes situated perpendicular to the mean groundwater flow direction to estimate contaminant mass fluxes and contaminant distribution in the groundwater at the control planes. For this reason contaminant concentrations at each pumping well are measured as a function of time. These concentration-time series (CT-series) can be assessed using a simplified analytical procedure assuming homogeneous aquifer properties at the scale of the respective well capture zone, or by employing a numerical flow and transport model.

This study compares the results of the analytical and numerical inversion of the CT-series data at a heterogeneous field site. Both inversion methods allowed to identify the major contaminants at the site. Although the transmissivity in the aquifer varied by orders of magnitude, the differences between the analytically and numerically derived mass fluxes were only 20% ± 12% for BTEX and 74% ± 60% for PAH compounds. The faster and easier analytical inversion of the integral CT-series data can therefore be an alternative method for the field scale quantification of contaminant mass fluxes, if the site is effectively homogeneous or if in a first step of the site investigation a simplified analytical mass flux estimation is sufficient.

## 7.2 Introduction

The literature is abundant with reports demonstrating the possibility of in-situ or intrinsic bioremediation and natural attenuation of benzene, toluene, ethylbenzene, and the xylenes (BTEX) (e.g., Barker et al., 1987; Edwards and Grbic-Galic, 1994; Burland and Edwards, 1999; Anderson and Lovley, 2000) and polyaromatic hydrocarbons (PAH) compounds (e.g., McNally et al., 1998; Rockne and Strand, 1998; Meckenstock et al., 2000) in contaminated groundwater under various hydrogeochemical conditions. Key processes controlling the efficiency of natural attenuation are diffusion, sorption and biodegradation (Karapanagioti et al., 2001). Volatilization of organic contaminants has typically only a minor to negligible influence on the overall contaminant attenuation (Chiang et al., 1989; Wiedemeier et al., 1999).

For the demonstration and documentation of natural attenuation at field sites and for the assessment of groundwater contamination hazards, the development of reliable methods for the quantification of contaminant mass fluxes in groundwater is critical (Eggleston and Rojstaczer, 2000).

---

[5] Based on a manuscript for Groundwater and on Bockelmann et al., 2001b.

The most common method to establish contaminant mass flux in groundwater is to monitor a set of multilevel wells positioned at a control plane or groundwater fence perpendicular to the plume, at different distances and/or times from the source (e.g. Semprini et al., 1995, Borden et al., 1997, King et al., 1999, Wilson et al., 2000, Kao and Wang, 2001; Einarson and Mackay, 2001). In this method polygons around each sampling location are defined, which generally extend half the distance to the adjacent sampling point. The mass flux in each polygon is calculated based on the measured contaminant concentration and on the local Darcy flux. The total contaminant mass flux at the control plane is then equal to the sum over all individual polygon mass fluxes. As the aquifer properties within each polygon are assumed constant, this approach is subject to a methological uncertainty, which increases for any given monitoring grid with the spatial and temporal variations in the aquifer properties.

Although modern direct push technologies have significantly reduced the installation costs for a detailed monitoring grid, such an installation is sometimes not feasible due to buildings, roads or other infrastructures, which limit the accessibility of the aquifer or because of the local geology. Coarse fluvial gravel sediments can lead to difficult drilling conditions and prevent the use of direct-push sampling technology. It is therefore important to develop alternative investigation methods, which can investigate inaccessible aquifer locations, and which require only a small number of monitoring wells for a complete site investigation. Moreover, these new investigation methods should be less susceptible to interpretation errors due to the uncertainty inherent to the regionalisation of point-scale data.

This study reports about the application of a new Integral Groundwater Investigation Method (IGIM), which was applied to two control planes situated 140 m and 280 m downgradient from a contaminant source zone at a former manufactured gas plant (MGP) site in south-west Germany. The IGIM is based on the evaluation of concentration-time series (CT-series) measured at pumping wells located at control planes, which are situated orthogonal to the mean groundwater flow direction, to reconstruct the undisturbed concentration distribution in the groundwater prior to the pumping, and to estimate compound-specific contaminant mass fluxes crossing the control planes. Due to the increased sampling volume this method is not subject to the limitations of data regionalization and aquifer inaccessibility.

In a first step, the measured CT-series can be interpreted using a simplified analytical procedure assuming ideal, homogeneous aquifer conditions and a negligible groundwater gradient at the scale of the individual well capture zones. In a second step, the CT-series can be interpreted using a numerical procedure, which is based on a site-specific flow and transport model and can hence account for spatial variability in the hydraulic aquifer parameters, if this information is available. In addition, the use of a numerical flow model allows to take a non-stationary development of well capture zones into account.

This study presents the results of the integral site investigation at the MGP site and compares the analytically and numerically derived compound-specific mass fluxes and natural attenuation rates of the targeted BTEX and PAH compounds.

## 7.3    Site characterization

The field site is a former manufactured gas plant (MGP) located in the Neckar River valley in SW Germany (Figure 7.1). The local aquifer is situated 3m to 4m below land surface and mainly consists of unconsolidated quaternary sand and gravel. The aquifer thickness varies spatially and has an average thickness of about 3m.

Based on pumping tests, the arithmetic average of the hydraulic conductivity at the site was estimated as $3.3*10^{-3}$ ms$^{-1}$ (Herfort, 2000).
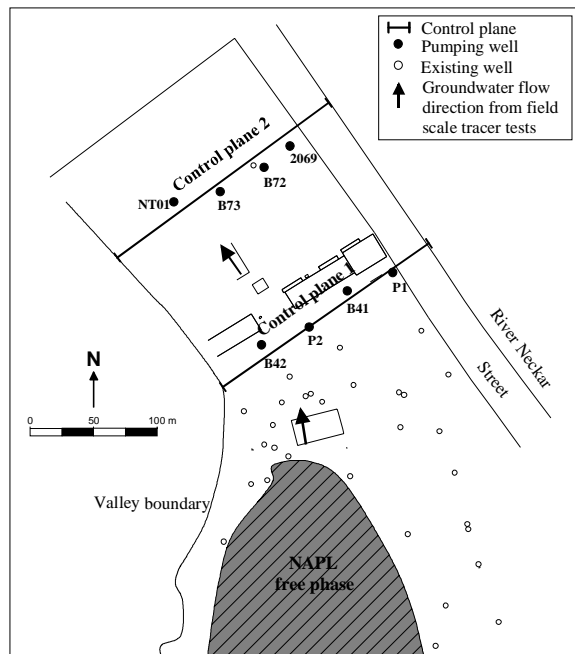


Figure 7.1: Field site overview

Hydraulic heads at the site were monitored over a 3-year period with no indication of significant seasonal changes or temporally variable groundwater flow directions (Herfort, 2000). The steady-state of the local groundwater flow field is due to the artificial regulation of the water level of the river that runs parallel to the eastern border of the field site. Transport parameters have been determined in the field during a large scale natural gradient multitracer test using fluoresceine, eosine, sodium naphthionate and sodium bromide as tracers (Bösel et al., 2000). From this test average effective porosity and average groundwater flow velocity were estimated as 0.13 and 2.0 md$^{-1}$, respectively.

The contaminant source zone shown in Figure 7.1 comprises different point sources in which total BTEX concentrations in the groundwater range up to 12 mgl$^{-1}$. PAH concentrations in the source zone are up to 3.2 mgl$^{-1}$ (Zamfirescu, 2000). Of the investigated PAHs, only acenaphthene shows high concentrations of

190 µgl$^{-1}$ at distances of about 280 m downgradient from the source zone at well NT01 (Figure 7.1). Of the BTEX contaminants, only p-xylene showed concentrations exceeding 0.2 µg/l at control plane 2 (well B73, Figure 7.1). The age of the groundwater contamination at the site is between 60 and 100 years (Herfort, 2000; Zamfirescu, 2000).
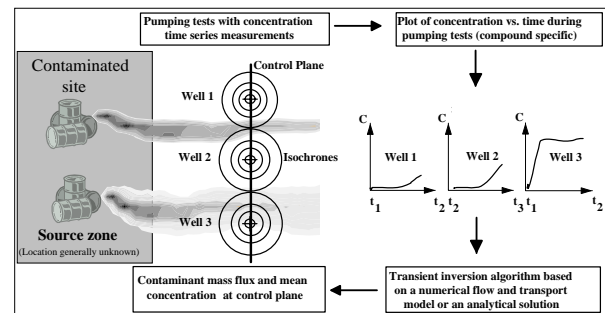


Figure 7.2: Concept of the Integral Groundwater Investigation Method (IGIM)

## 7.4 Integral Groundwater Investigation Method (IGIM)

The concept of the IGIM is illustrated in Figure 7.2. In this method, one or more pumping wells are placed along a control plane perpendicular to the mean groundwater flow direction and operated simultaneously, or in subsequent pumping campaigns, downgradient of a suspected pollutant source zone. The well positions, pumping rates and pumping times are chosen to allow the well capture zones to cover the overall width of the contaminated site or of the suspected contaminant source. During pumping, as the well capture zones increase, concentrations of groundwater contaminants are measured as a function of time (CT-series) at each of the pumping wells. Since each concentration value within the measured CT-series is associated with a distinct aquifer region covered by the well capture zone, information on the spatial distribution of both concentrations and mass fluxes can be obtained from this method, in addition to

information on the total mass fluxes of the investigated compounds.

As a first step, the determined CT-series were interpreted using an analytical solution (Schwarz, 2001; Teutsch et al., 2000; Bockelmann et al., 2001a), which simplifies the problem to a steady-state situation and assumes that within the individual well capture zone (1) the flow towards the abstraction wells is radially symmetrical, i.e. the natural groundwater flow can be neglected during the pumping test; (2) at this scale the aquifer is homogeneous with regard to porosity, hydraulic conductivity and thickness, and (3) prior to the pumping the concentration gradient in the well capture zone is linear or not existent along each of the intercepted streamtubes although it may vary from streamtube to streamtube (Figure 7.3a).

The first assumption of the analytical solution allows to deal with a symmetrical problem around the respective pumping well. Together with the second assumptions, it is possible to describe the development of the isochrones around the pumping well and thus the well capture zone along the control plane, i.e. perpendicular to the groundwater flow direction, as a function of time:

$$r(t) = \sqrt{\frac{Q\,t}{\pi\,b\,n_e}} \qquad (7.1)$$

with $r(t)$, $Q$, $t$, $b$, $n_e$ symbolizing the radius [L] of the well capture zone at time $t$, the pumping rate [$L^3T^{-1}$], the time [T], the aquifer thickness [L] and the effective porosity [-], respectively.

A probable contaminant distribution in the groundwater prior to any pumping can then be reconstructed analytically based on the measured CT-series at the pumping well. For this reconstruction, the section of the control plane covered by the isochrones of a pumping well is separated into discrete streamtubes. Based on the third assumption a distinct contaminant concen-

tration is allocated to each streamtube (Figure 7.3a). The width of each stream-tube is defined by the spatial increment $\Delta r$ [L] of the radius r [L] along the control plane between two consecutive sampling events as shown in Figure 7.3a. Applying Equation 7.1, the increment $\Delta r_i$ between sampling times $t_{i-1}$ and $t_i$, respectively the width of the intercepted streamtubes, can be calculated as:

$$\Delta r_i = \sqrt{\frac{Q}{\pi\,n_e\,b}}(\sqrt{t_i} - \sqrt{t_{i-1}}) \qquad (7.2)$$
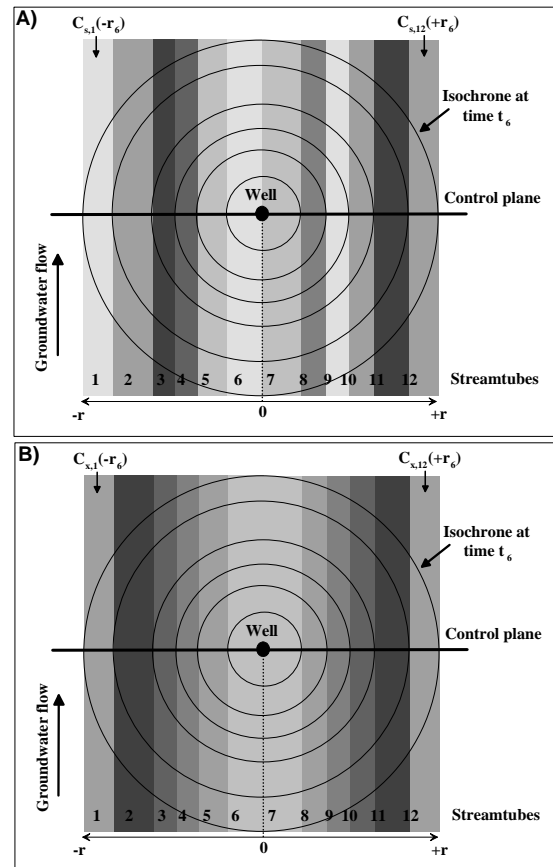


Figure 7.3: Concept of the delineation of the well capture zone into different streamtubes with constant contaminant concentrations at the well capture zone scale. At every additional sampling event, two new streamtubes are intercepted by the increasing well capture zone, one at each side of the pumping well. Shown is the situation for a pumping well with six sampling events for A) the individual concentrations $C_{s,i}$ of the respective streamtubes and B) for the theoretical average concentration $C_{x,i}$

The width of the streamtubes and the level of detail of the integral investigation can therefore be controlled by the chosen time increment between two consecutive sampling events.

The total number of streamtubes at each well is equal to twice the number of data points in the CT-series because at each sampling time two streamtubes crossing the control plane, one at each side of the well, are intercepted.

The total mass flux MF $[MT^{-1}]$ of a target compound crossing the control plane at the section investigated by the pumping test can be estimated as:

$$MF = \sum_{i=1}^{2D} Q_i\, C_{s,i} \qquad (7.3)$$

with D [-], $Q_i$ $[L^3T^{-1}]$, and $C_{s,i}$ $[ML^{-3}]$ representing the number of isochrones or data points in the CT-series, the groundwater flux within the i-th streamtube, and the concentration of the i-th streamtube crossing the control plane, respectively. The groundwater flux $Q_i$ is given by:

$$Q_i = k|\nabla h|b\Delta r_i \qquad (7.4)$$

where k $[LT^{-1}]$, $|\nabla h|$ [-] and b [L] denote the hydraulic conductivity, hydraulic gradient and the aquifer thickness, all of which are assumed to be constant for the analytical solution.

Figure 7.3 illustrates the general approach for a pumping well with six sampling events. The total mass flux in this scenario would be the concentration $C_{s,i}$ of each streamtube (Figure 7.3a) multiplied by the natural groundwater flux $Q_i$ within each streamtube (see Equation 7.3). In the analytical solution $Q_i$, the specific groundwater flux per unit width of the control plane, is assumed constant. $C_{s,i}$ can not be measured in the field individually, as the well capture zone at a sampling time $t_i$ [T] always intercepts streamtubes on both sides of the well, as seen from the

control plane. For the flux quantification, we therefore define a theoretical concentration $C_{x,i}$ $[ML^{-3}]$ (Figure 7.3b), which is the average of the concentrations of the two streamtubes representative of time $t_i$ [T]:

$$C_{x,i} = \frac{C_{s,i}(-r_i) + C_{s,i}(+r_i)}{2} \qquad (7.5)$$

Combining Equation 7.3 and 7.5 yields:

$$MF = \sum_{i=1}^{2D} Q_i C_{x,i} \qquad (7.6)$$

Schwarz (2001) presented a recursive formula for the calculation of $C_{x,i}$:

$$Cx_i = \frac{\dfrac{\pi\, Cp_i}{2\arccos\left(\dfrac{r(t_{i-1})}{r(t_i)}\right)} - \displaystyle\sum_{k=1}^{i-1} Cx_k\left[\arccos\left(\dfrac{r(t_{k-1})}{r(t_i)}\right) - \arccos\left(\dfrac{r(t_k)}{r(t_i)}\right)\right]}{\arccos\left(\dfrac{r(t_{i-1})}{r(t_i)}\right)}$$

$$(7.7)$$

with $C_{p,i}$ $[ML^{-3}]$ representing the concentration measured at the pumping well at time $t_i$. For the first time step, $C_{x,1}$ equals $C_{p,1}$.

Subsequently, it is possible to calculate an average concentration $C_m$ $[ML^{-3}]$ of solutes crossing the control plane as:

$$C_m = \frac{MF}{2\displaystyle\sum_{i=1}^{D} Q_i} \qquad (7.8)$$

with MF $[MT^{-1}]$ and $Q_i$ $[L^3T^{-1}]$ representing the total mass flux and the flow rate in the i-th streamtube, respectively. Retardation of the contaminants during the pumping tests is not included in this study. Retardation due to linear instantaneous sorption can be introduced into the

analytical solution by transforming the time scale of the concentration measurements, i.e. by dividing the time with a retardation factor R [-] (Bockelmann et al., 2001a).

In the numerical solution (Schwarz, 2001; Ptak et al., 2000a) used in a second step of the evaluation, we utilized a groundwater flow (MODFLOW-96, Harbaugh and McDonald, 1996) and a transport model (MODPATH, Zheng, 1990) to numerically simulate the temporal and spatial development of the isochrones around the operated abstraction wells and to compute the spatially variable groundwater flow across the investigated control planes. It was hence possible to include spatially variable aquifer properties and asymmetrical well capture zones into the numerical mass flux calculation. Asymmetrically well capture zones can occur due to a heterogeneous distribution of the aquifer properties around the abstraction well and/or because of the influence of a significant groundwater gradient at a study site. The comparison of the analytical and numerical mass flux results for the study site illustrates the possibilities and limitations of the analytical mass flux estimation at heterogeneous field sites.

The mass flux determined with the IGIM represents the total mass flux at the site, if the capture zone widths of the operated wells together are large enough to capture the total groundwater flow through the contaminant source. This is usually the case when the well capture zone is located downstream of the contaminant source and the capture zone width exceeds the width of the contaminant source.

It should be noted that total mass flux and average concentration can be simultaneously estimated for a number of target compounds. This may include not only the original contaminant, but also potential degradation products or electron acceptors, e.g. sulfate and nitrate, in case of a biodegradable contamination.

The major points of concern of this method are the possible treatment costs of the extracted groundwater and the transmissivity at the study site because the latter limits the size of the well capture zones that can be achieved during acceptable pumping times. In addition, for the numerical solution of the IGIM a defendable flow and transport model is required, which requires a detailed knowledge of the spatial distribution of the hydraulic parameters at the studied field site.

## 7.5 Groundwater flow model

The groundwater flow model used for the numerical inversion of the measured CT-series is based on a regional groundwater flow model, which is described elsewhere in more detail (Holder and Teutsch, 2000).
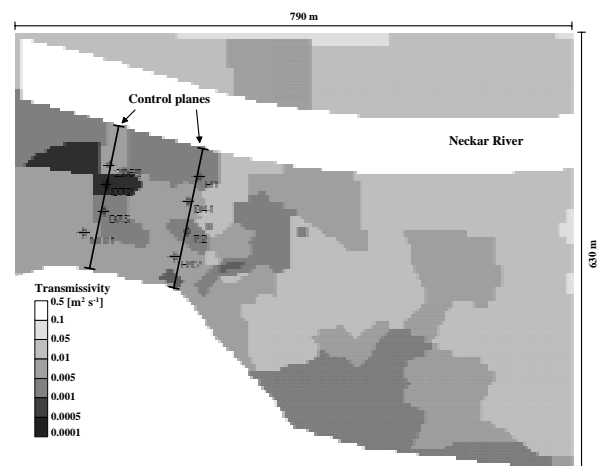


Figure 7.4: Transmissivity distribution in the groundwater flow model with the location of the pumping wells operated for the integral groundwater investigation method

The 2-D groundwater flow model domain at the MGP site was 790 m x 630 m in x- and y-dimension (Figure 7.4), with a spatial increment of 5 m x 5 m, which was refined to 1 m x 1 m in the area affected by the pumping tests. The heterogeneous aquifer thickness (z-dimension) was obtained from over 60 borehole logs from the study site (Gaißer, 1998). The transmissivity distribution in the model was derived from more than 50

pumping test and 25 slug tests. In the flow model, the transmissivity values observed in the field were evenly distributed around the location of each tested borehole leading to the heterogeneous transmissivity distribution shown in Figure 7.4. Based on data from a natural gradient field scale tracer test (Bösel et al. 2000) a uniform effective porosity of 0.13 was assumed for the site. For the transient simulation of the pumping tests, a uniform specific storage of $10^{-4}$ m$^{-1}$ was used in the simulation, which corresponds to the average value found in the River Neckar valley (Holder and Teutsch, 2000).

## 7.6 Estimation of attenuation rate constants

The mass fluxes measured with the IGIM at the two control planes shown in Figure 1, were used to estimate first-order attenuation rate constants based on the decrease in mass flux between the two control planes. If the compound-specific total mass fluxes MF [MT$^{-1}$] across two control planes (CP) and the average non-retarded groundwater travel time $\Delta t$ [T] between the CPs are known, it is possible to quantify compound-specific first-order attenuation rate constants as:

$$MF_{CP(2)} = MF_{CP(1)}e^{-\lambda R\Delta t} \qquad (7.9)$$

leading to

$$\lambda = -\ln\left(\frac{MF_{CP(2)}}{MF_{CP(1)}}\right)\frac{1}{R\,\Delta t} \qquad (7.10)$$

with $\lambda$ [T$^{-1}$], $MF_{CP(1)}$ [MT$^{-1}$], $MF_{CP(2)}$ [MT$^{-1}$], and R [-] representing the effective (natural) attenuation rate constant, the measured compound specific mass fluxes at CP 1 and CP 2, and the retardation factor, respectively. If organic compounds are subject to kinetic sorption as a consequence of diffusion into intraparticle

pores of the aquifer minerals (e.g., Rügner et al., 1999), with a negligible contribution of sorption on the outer surface of the mineral grains, then the retardation factor may be omitted respectively set to one. The reason is that biodegradation of organic compounds can only occur outside of the intraparticle pores of the aquifer material if the pore radius is very small.

For our MGP site, Rügner et al. (1999) showed that the typical pore radius of the aquifer material is generally < 100 nm, preventing the migration of microbes into the intraparticle pores. In this case, the time relevant for degradation is the time the contaminants spend within the interparticle pore space, i.e. the time during which the contaminant molecules are not absorbed by the minerals. Assuming a diffusion limited sorption process into the intraparticle pores of the aquifer material for all target compounds, this study therefore assumes a retardation factor equal to one for the computation of the natural attenuation rate constants.

## 7.7 Results and Discussion

The comparison of the analytically and numerically derived mass fluxes and the corresponding attenuation rate constants of the target compounds for the transport between the operated control planes are shown in Table 7.1 and Figure 7.5.
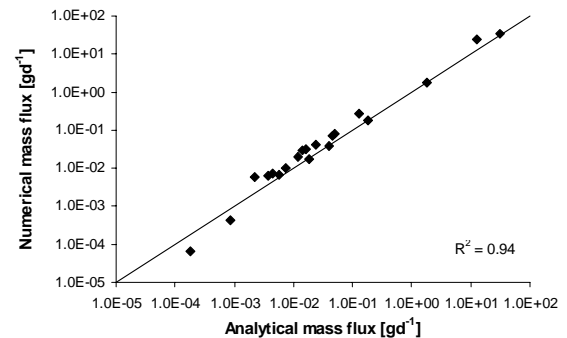


Figure 7.5: Scatter plot of the numerically and analytically derived mass fluxes of the organic contaminants at the study site. Straight line denotes the main diagonal

Table 7.1: Contaminant mass fluxes and first-order attenuation rate constants ($\lambda$) across control planes 1 and 2 employing an analytical and a numerical inversion during the integral groundwater investigation method.

| | Analytical solution | | | Numerical solution | | |
|---|---|---|---|---|---|---|
| | Control plane 1 | Control plane 2 | | Control plane 1 | Control plane 2 | |
| | Integral flux | Integral flux | $\lambda^1$ | Integral flux | Integral flux | $\lambda^1$ |
| Compound | [gd$^{-1}$] | [gd$^{-1}$] | [d$^{-1}$] | [gd$^{-1}$] | [gd$^{-1}$] | [d$^{-1}$] |
| Benzene | 1.82E+00 | 1.84E-04 | 1.31E-01 | 1.77E+00 | 6.41E-05 | 1.46E-01 |
| Ethylbenzene | 1.30E-01 | 3.67E-03 | 5.10E-02 | 2.63E-01 | 6.25E-03 | 5.34E-02 |
| Toluene | 3.97E-02 | 4.43E-03 | 3.13E-02 | 3.94E-02 | 7.03E-03 | 2.46E-02 |
| o-Xylene | 1.18E-02 | 8.48E-04 | 3.76E-02 | 1.98E-02 | 4.32E-04 | 5.46E-02 |
| p-Xylene | 4.51E-02 | 1.64E-02 | 1.44E-02 | 6.86E-02 | 3.12E-02 | 1.13E-02 |
| Naphthalene | 1.85E-01 | 2.36E-02 | 2.94E-02 | 1.76E-01 | 4.02E-02 | 2.11E-02 |
| Acenaphtene | 3.07E+01 | 1.23E+01 | 1.30E-02 | 3.38E+01 | 2.40E+01 | 4.92E-03 |
| Anthracene | 4.94E-02 | 1.43E-02 | 1.77E-02 | 7.88E-02 | 2.96E-02 | 1.40E-02 |
| Fluoranthene | 7.52E-03 | 5.78E-03 | 3.77E-03 | 1.02E-02 | 6.90E-03 | 5.53E-03 |
| Pyrene | 1.88E-02 | 2.17E-03 | 3.08E-02 | 1.67E-02 | 5.87E-03 | 1.50E-02 |

[1] For the transport between the two control planes.

The main contaminants at the site are acenaphthene for the PAH and benzene for the BTEX compounds with mass fluxes of approximately 33.8 gd$^{-1}$ and 1.8 gd$^{-1}$ across control plane 1 (Figure 7.1).

It can be seen from Figure 7.5 that the analytically derived mass fluxes tend to be smaller with an average deviation of 42% ± 41% with the two extremes of around 1% for toluene at control plane 1 and 186% for benzene at control plane 2. Compared to for example uncertainties attributed to hydraulic conductivity estimations at field sites, which can easily incorporate an order of magnitude, the deviation of roughly a factor of 2 between the two inversion methods seems acceptable.

The differences between the respective mass flux results were mainly caused by the assumption of a homogeneous aquifer and a spatially constant groundwater flux across the control planes for the application of the analytical inversion of the CT-series data. Preferential flow paths and spatially changing groundwater flow rates across the control planes could only be incorporated into the contaminant mass flux quantification by employing the numerical flow and transport model.

Another reason for the differences in the mass flux results were the differences in the representation of the well isochrones at the pumping wells in the analytical and

numerical solution. In the numerical solution, the well isochrones were described using a particle backtracking algorithm using MODPATH (Zheng, 1990). Although the numerically simulated isochrones at the wells developed radially at the beginning of the pumping tests, they became asymmetrical towards the end of the pumping as shown in Figure 7.6. This effect is partly artificial and depends on the model resolution.
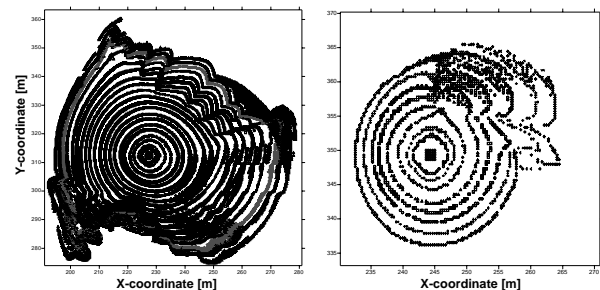


Figure 7.6: Exemplary overviews of the particle backtracking utilized at well B42 (left) and well P2 (right) for the spatial delineation of the well isochrones used for the numerical inversion of the concentration-time series. The close resemblance to radial conditions minimizes the differences between the numerical and analytical mass flux quantification

The asymmetrical capture zone development caused a deviation in the width of the intercepted streamtubes between the analy-

tical and the numerical solution and increased the differences between the two solutions for late time pumping data. The radial development of the isochrones in the numerical solution can be attributed to the fact that the spatial heterogeneity of the aquifer was, to a certain degree, averaged out during the development of the underlying flow model. The transmissivity values derived from the hydraulic tests conducted at the site (over 50 pumping and 25 slug tests) were represented in the model by a homogeneous transmissivity field around the respective well or borehole forming a heterogeneous pattern of transmissivity only at a large scale. In the presence of a small natural groundwater gradient, and for pumping times where the well capture zones did not extend further than the homogeneous transmissivity areas around the pumping wells, the isochrones developed roughly symmetrical. For later times, however, aquifer regions with different transmissivities increasingly influenced the pumping well. This caused a deformation of the isochrone shapes as seen in Figure 7.6. The major distinguishing factors between the analytical and numerical inversion of the CT-series were hence the spatial distribution of the groundwater flow across the control planes and the spatial extend as well as the form of the well capture zones, especially for late time pumping data.

The differences in the attenuation rate constants based on the analytical and numerical mass flux results were on average 20% ± 12% for BTEX and 74% ± 60% for the PAH compounds. The relatively high difference for the PAH compounds was caused by an underestimation of the total PAH mass flux by a factor of two at the second control plane by the analytical solution. This underestimation was a combined result of the discussed differences in the well capture zones and of the difference in the analytically and numerically estimated groundwater flow within the respective well capture zones. As seen from Equations 7.3 and 7.4, uncertainties

in one of the physical properties of the aquifer have a linear effect on the resulting mass flux estimation.

If a defendable groundwater flow and transport model exists, aquifer heterogeneities can be accounted for, but it is important to check for the quality of the numerical inversion of the CT-series data. A first estimation of the quality of the numerical inversion of the concentration data can be obtained by comparing the measured concentration-time series with the concentration-time series obtained from the contaminant concentration distribution in the groundwater as derived from the numerical inversion. In other words, does a pumping test simulated in the numerically derived contaminant distribution in the groundwater result in a CT-series similar to the CT-series measured in the field?
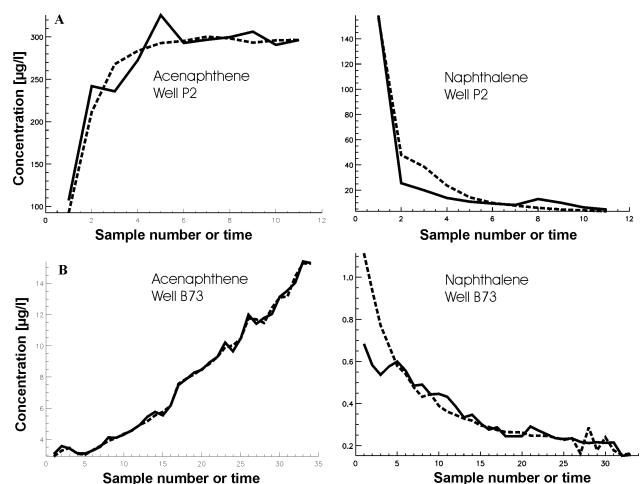


Figure 7.7: Comparison between measured acenaphthene (left) and naphthalene (right) concentration-time series (dotted line) with the corresponding concentration-time series obtained from the numerical inversion of the concentration-time series (solid line). Examples shown for well P2 at control plane 1 and for well B73 at control plane 2.

For this study, Figure 7.7 presents a comparison between the acenaphthene and naphthalene concentration-time series measured in the field and the corresponding concentration-time series based on the numerical inversion of the

concentration data. It can be seen that the numerical inversion generally shows a good agreement with the measured data and that the numerical inversion yields acceptable results for different forms of measured concentration-time series.

Although the transmissivity values in the flow model (Figure 7.4) varied significantly, the assumption of aquifer homogeneity at the scale of the respective well capture zone, as used by the analytical procedure, allowed for reasonable contaminant mass flux results compared to the numerically derived mass flux estimations. If this level of certainty is acceptable, for example during a first screening of multiple sites to develop a priority list for further investigations and/or actions, the application of the faster and easier analytical procedure is appropriate. Obviously, the analytical solution of the IGIM is recommended for homogeneous sites and for sites were not enough data is available to develop a defendable groundwater flow and transport model. The results of the analytical solution, however, should be interpreted with care and the uncertainty in the input parameters and hence in the results should be accounted for. The same care is also recommended for the numerical approach as uncertainties in the underlying groundwater model influence the numerical mass flux estimation.

## 7.8 Conclusions

We have documented the field scale application of an integral groundwater investigation method (IGIM) at a former manufactured gas plant site utilizing two control planes situated at increasing distances from the contaminant source. It was shown that the analytical solution of the IGIM is a simple and quick alternative for homogeneous or moderately hetero-

geneous field sites and can be used without a detailed groundwater flow and transport model. Like all analytical solutions, this method will suffer from the underlying simplifying assumptions if used in strongly heterogeneous conditions. If reliable assumptions about the natural groundwater flow and the shape of the well capture zone during pumping are available, a site specific decision can be made, whether an application of the analytical solution is satisfying or if a numerical solution has to be employed. The latter can incorporate aquifer heterogeneities into the determination of contaminant mass fluxes by employing a site-specific groundwater flow and transport model for the delineation of well capture zones with time and for the computation of spatially variable groundwater flow across the control planes.

The determined contaminant mass flux reductions in flow direction can be used for the field scale quantification of compound-specific natural attenuation rate constants. At our site, benzene exhibited the fastest and acenaphthene showed the slowest attenuation rate for the transport between the two investigated control planes.

Future work is needed to incorporate contaminant retardation into the IGIM. More field work is also needed to compare IGIM with other field scale methods under controlled conditions. This would help to better understand the applicability and limitations of IGIM under various geological settings and source zone geometries. Moreover, as the IGIM only quantifies total mass flux reductions without distinguishing between the individual mass flux reducing processes, the combination of the field scale integral investigation with field scale reactive transport modelling using integral input data would be valuable.

# 8 Reactive transport modelling at a former MGP site[6]

## 8.1 Abstract

Contaminant mass flow rates can be quantified at field scale by using point-scale or integral groundwater investigation methods. In the context of risk assessment or natural attenuation studies, the observed mass flow data are often difficult to interpret because field scale mass flow measurements document the total effect of all natural mass flow reducing processes like degradation, sorption, volatilization, and dilution.

At a former manufactured gas plant (MGP) site contaminated with poly-aromatic hydrocarbons (PAH) and volatile organic hydrocarbons (BTEX), we combine an integral groundwater investigation of contaminant mass flow rates with a reactive contaminant transport model that accounts for diffusion-limited sorption and desorption ("sorption kinetics") of the organic contaminants. The objectives are to (1) quantify the relative importance of diffusion-limited sorption and degradation on the observed reduction of mass flows in flow direction, and (2) to use the site as an example for investigating numerically to which extent the results of the integral groundwater investigation method (IGIM) are influenced by contaminant plume displacements during pumping, i.e. to quantify the impact of the reactive contaminant transport towards the pumping well on the integral mass flow estimations.

Modeling results using acenaphthene, the dominating contaminant at the field site as the model compound, illustrate that the measured mass flow reductions between the investigated control planes are indications for ongoing intrinsic biodegradation at the site. The transport simulations furthermore show that diffusion-limited sorption and desorption of organic contaminants during the contaminant transport towards a pumping well can influence the integral mass flow quantification if the studied aquifer has a high organic carbon content and the target compound is relatively strongly hydrophobic. In the simulated scenarios, contaminant plume displacement influenced the integral mass flux quantifications by up to 60%. This influence decreases with the age of the contamination and increases with the distance of the well from the main contaminant plume.

## 8.2 Introduction

During the last few years, the investigation of the natural attenuation of organic contaminants in groundwater has been a topic of high importance in the environmental sciences. Numerous studies have focused on the documentation of contaminant degradation at both laboratory and field scale (e.g. Barker et al., 1987; Rockne and Strand, 1998; Burland and Edwards, 1999).

Different methods have been developed for the measurement of the change in contaminant mass flow along a transport path. The most common method is to install a set of multilevel wells perpendicular to the groundwater flow direction and to measure the target compound concentrations at each of the sampling ports as a function of time or distance from the source (e.g. Borden et al., 1997; Kao and Wang, 2001; Einarson and Mackay, 2001).

The total contaminant mass flow estimated with this method is defined as the sum of the mass flow rates quantified for polygons centered around each of the installed sampling ports. These polygons usually extend to half the distance to the adjacent sampling port. As the contaminant concentration and the physical aquifer parameters within each polygon are

---

[6] Based on Bockelmann et al., 2001c and on Bockelmann et. al, 2002.

assumed to be constant or homogeneous, this method is subject to a level of uncertainty that increases with the size of the individual polygons, i.e. with the distance between the different sampling ports and with the change of aquifer properties and contaminant concentrations in the groundwater both in space and time.

To reduce this uncertainty, the distance between monitoring wells should be minimized. However, for large contaminant plumes or under difficult geological conditions, the installation of a detailed multilevel monitoring network can be difficult due to economical constraints.

A more recent alternative for the field scale mass flux estimation is the integral groundwater investigation method (IGIM) (Teutsch et al., 2000; Ptak et al., 2000; Schwarz, 2002; Bockelmann et al., 2001). In this method, one or more pumping wells are operated in parallel or subsequently at control planes situated downgradient from the contaminant source so that the combined well capture zones cover the complete width of the suspected source zone or plume. During pumping, contaminant concentrations are measured as a function of time (concentration-time series, CT series) at each of the pumping wells.

The obtained information is then used for the quantification of total contaminant mass flow rates and average contaminant concentrations crossing the investigated control plane(s) using an analytical or numerical solution of the inversion problem.

The advantage of the IGIM is the increased sampling volume, which reduces the number of monitoring wells required for site investigation. In addition, due to the larger sampling volume, regionalization of point-scale data is unnecessary and the level of certainty in the results is increased (Bockelmann et. al, in press).

The major points of concern are the possible treatment costs for the extracted groundwater and the difficulties in the exact delineation of the width of the well capture zones. The expenses associated with the IGIM are affected by the transmissivity and effective porosity of the field site, as the transmissivity and effective porosity control the capture zone width that can be achieved within reasonable pumping rates and pumping times.

Both of the discussed mass flow estimation methods can only measure the combined effects of all mass flow reducing processes occurring at an investigated field site. However, especially in the context of risk assessment and natural attenuation studies it is important to differentiate between processes such as sorption and degradation because apart from volatilization, which has typically only a minor to negligible influence on the overall contaminant attenuation (Chiang et al., 1989; Wiedemeier et al., 1999), degradation is the only process that effectively removes contaminant mass from the groundwater.

In an accompanying study (Bockelmann et al., 2001, Chapter 4), we reported about the application of the IGIM at two control planes situated downgradient from a contaminant source at a former MGP site in south west Germany. The results of the IGIM study are used in the present paper as input for (1) the simulation of the reactive contaminant transport between the investigated control planes and (2) for the numerical investigation of the impact of plume displacement, as it occurs during application of the IGIM, on the results of the IGIM.

The objectives of this study are to quantify the relative importance of diffusion-limited sorption and degradation on the measured mass flow reduction and hence to obtain an indication of ongoing biodegradation of the organic contaminants at the field site, and, secondly, to investigate the sensitivity of the IGIM on the placement of the pumping wells with regard to the position of the contaminant plume in the groundwater.

To this aim, a Monte Carlo type modeling approach is applied and the contaminant transport between the two

investigated control planes is simulated using acenaphthene, the dominating groundwater contaminant at the site, as a model compound. The characteristic aquifer realizations and contaminant plume modeling results are subsequently used for the numerical simulation of 5-day IGIM pumping tests at two monitoring wells situated 90 m downgradient from the source and 30 m apart from each other.

## 8.3 Transport modeling approach

### 8.3.1 Site characterization and model setup

The field site is a former manufactured gas plant (MGP) located in the Neckar River valley in south-west Germany (Figure 8.1). The local aquifer is situated 3 to 4 m below land surface and consists mainly of unconsolidated Quaternary sand and coarse gravel deposits. The aquifer thickness varies spatially with an average of about 3 m. Based on pumping tests, the arithmetic average of the hydraulic conductivity at the site was estimated as $3.3*10^{-3}$ m/s (Herfort et al., 1998; Herfort, 2000). Hydraulic heads at the site were monitored over a 3-year period with no indication of significant seasonal changes or temporally variable groundwater flow directions (Herfort, 2000). The average effective porosity and average groundwater flow velocity were estimated during a field scale tracer test as 0.13 and 2.0 m/d, respectively (Bösel, 1998; Bösel et al., 2000).

The site is predominantly contaminated with acenaphthene and benzene. An integral mass flow quantification at two control planes (Bockelmann et al., 2001) (Figure 8.1) yielded at control plane 1 an acenaphthene flux of about 34 g/d, which decreased to about 24 g/d at control plane 2. The acenaphthene flow rate at control plane 1 was used as the input flow rate for

the transport modeling conducted in this study. The age of the groundwater contamination at the site lies between 60 and more than 100 years (Herfort, 2000; Zamfirescu, 2000). A more detailed site description is given elsewhere (Herfort et al., 1998, Bockelmann et al., 2001).
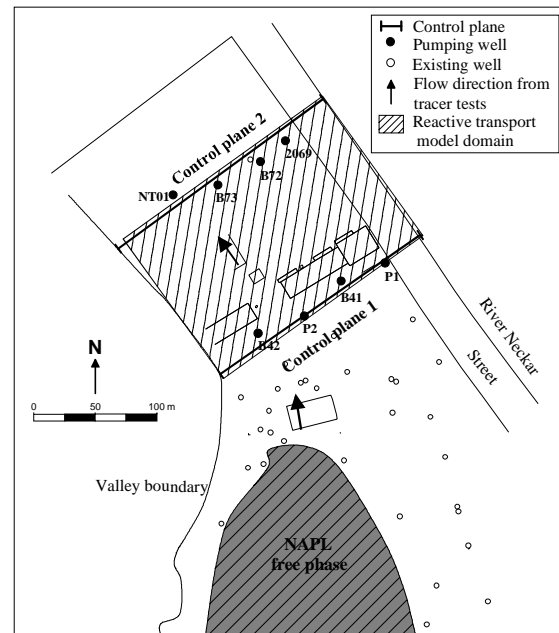


Figure 8.1: Site overview with the location of the control planes and the corresponding pumping wells, as well as the geometry and location of the model domain (Figure 8.2) used for reactive transport modelling

The transport model domain shown in Figure 8.1 comprises the local aquifer between the two operated control planes, which is represented in the model as a 3-D heterogeneous 140 m long, 200 m wide and 3 m thick confined aquifer with cell increments of 1 m in the x- and z-dimension and 2 m in the y-dimension yielding 43200 model cells.

The hydraulic heads observed in the field are used as the initial hydraulic heads in the model, with a downgradient constant head boundary and an upgradient general head boundary. The remaining two boundaries match no-flow conditions.

Contaminant plume development is simulated under steady-state flow condi-
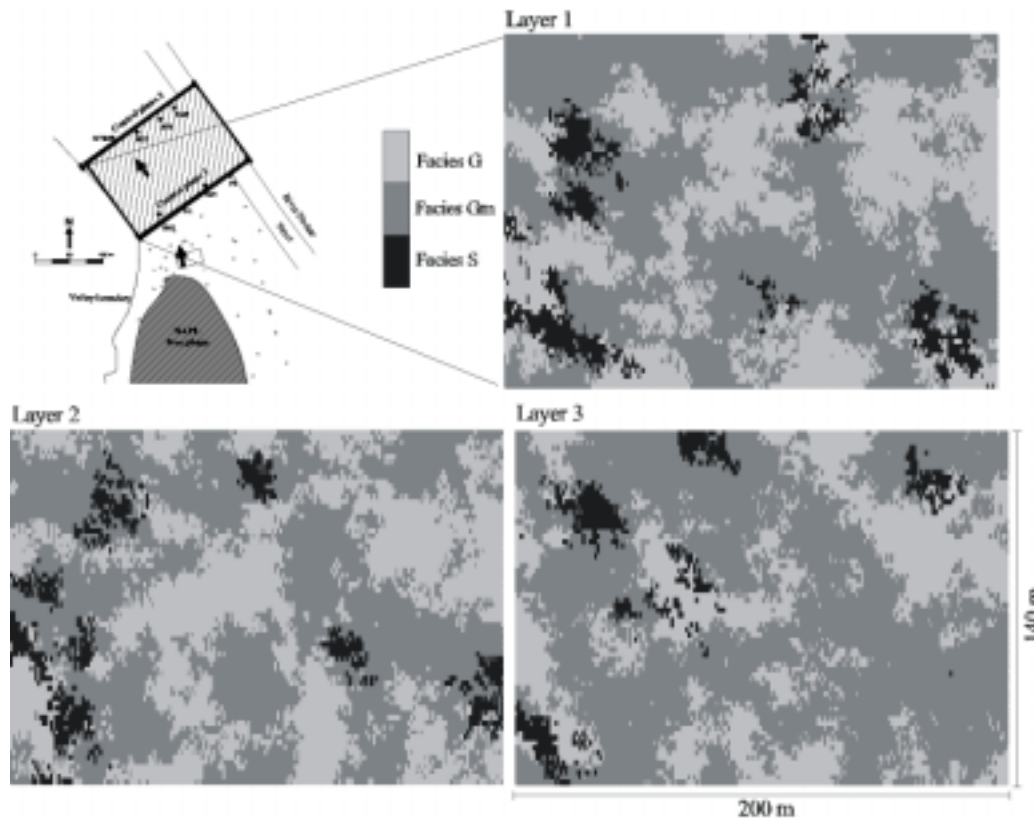
Figure 8.2: Typical facies distribution in the geostatistical aquifer realizations. Layer 1 denotes the top and Layer 3 the bottom of the aquifer.

tions. Pumping tests are simulated under transient flow conditions. Due to its dominating mass flow at the study site (Bockelmann et al., 2001), acenaphthene is chosen as the model contaminant.

Table 8.1: Observed aquifer facies and their lithological composition

| Facies | Share [%] | Lithological composition | | |
| | | G_eff[1] [%] | Limestone [%] | Quarz [%] |
| --- | --- | --- | --- | --- |
| G | 33.7 | 100 | - | - |
| Gm | 59.0 | - | 67.4 | 32.6 |
| S | 7.3 | - | 14.7 | 85.3 |

[1] G-eff is the artificial description of the facies G with a reduced number of effective grain sizes as described by Herfort (2000)

At the MGP site three distinctive geological facies were identified (Herfort et al., 1998; Herfort, 2000) (Table 8.1): a unimodal gravel without matrix (G, mass share of 33.7%), a bimodal gravel with a sandy matrix (Gm, mass share of 59.0%), and a pure sand facies (S, mass share of

7.3%). A typical distribution of the individual facies in the three transport model layers is shown in Figure 8.2.

The identified geological facies are correlated with hydraulic and physico-chemical properties, thus pursuing a statistical facies modeling approach as described by Ptak (1997). The relevant input parameters for each facies, as used by the MT3D-IPD transport model described below, were obtained through sieve analyses (Herfort et al., 1998; Herfort, 2000) and sorption batch experiments (Grathwohl and Kleineidam, 1995; Kleineidam et al., 1999a, b; Schüth and Grathwohl, 1994; Rügner et al., 1999). Acenaphthene sorption parameters for the different facies are shown in Table 8.2.

Hydraulic conductivities of the individual geological facies at the site were estimated by Herfort (2000) using Beyer's (1964) empirical relationship between hydraulic conductivity and grain size distribution:

Table 8.2: Physical and chemical parameters of the lithological components used in the transport simulations. Freundlich parameters are given for acenaphthene.

| Lithology | $\varepsilon$ [-] | $\tau_f$ [-] | $\rho$ [gcm$^{-3}$] | $K_{Fr}$ [l kg$^{-1}$] | 1/N [-] | Retardation factor[4] [-] |
|---|---|---|---|---|---|---|
| G_eff[1] | 0.013 | 61.8 | 2.72 | 19.00 | 0.83 | 42.8 |
| Limestone[2] | 0.012 | 59.0 | 2.73 | 10.86 | 0.83 | 16.6 |
| Quartz[3] | 0.0005 | 9.0 | 2.65 | 0.07 | 1.00 | 3.9 |

$\varepsilon$: intraparticle porosity, $\tau$: tortuosity; $\rho$: bulk density; $K_{Fr}$: Freundlich coefficient, determined for concentrations in ug/l; 1/N: Freundlich exponent. Physical data from: [1] Herfort (2000); [2] Rügner et al. 1997; [3] Grathwohl and Kleineidam, 1995
[4] For acenaphthene under equilibrium conditions as derived from Equation 8.7.

$$K = c(u) \, d^2_{10} \qquad (8.1)$$

where c(u) is an empirical constant defined as $d_{60}/d_{10}$ and $d_{10}$ and $d_{60}$ are the diameters of the grains, where 90% respective 40% of the sample mass are retained in a sieve analysis.

### 8.3.2 Quantification of mass flow reduction

Contaminant mass flow reduction between the two control planes is mainly due to retardation and degradation. The simultaneous impact of both attenuation processes is reflected by the mass flow rates reported above in Section 8.3.1. In the present modeling study, mass flow reduction due to retardation is quantified by employing a process-oriented approach accounting for non-equilibrium physico-chemical interactions between organic contaminants and the aquifer material. The impact of degradation is decoupled and can be derived from the differences between measured and simulated mass flow rates.

A growing number of studies have shown that non-equilibrium physico-chemical interactions of organic contami-nants with aquifer material (sorption kinetics) is caused by the release and uptake of contaminants by intra-particle pores through a diffusive process. In addition, equilibrium sorption is found to be active within the intra-particle pores (e.g. Luthy et al. 1997; Grathwohl, 1998; Rügner et al., 1999; Karapanagioti et al., 2001). This intra-particle sorption process follows an isotherm, which can be highly non-linear (Rügner et al., 1997; Klein-eidam et al., 1999).

In this study, the combined process is termed diffusion-limited sorption. It is incorporated through the use of the MT3D-IPD transport model package (Liedl and Ptak, in review). This transport model package utilizes the conventional MT3D code (Zheng, 1990) and a newly added IPD code (Jaeger and Liedl, 2000), which accounts for intra-particle diffusion and intra-particle equilibrium sorption. In MT3D-IPD, contaminant uptake by or release from the aquifer material is therefore modeled at the grain scale.

The apparent diffusion coefficient $D_a$ [L$^2$T$^{-1}$], which accounts for the non-linearly retarded diffusive transport of contaminants inside the grains, is reduced as compared to the aqueous diffusion coefficient, due to the size and shape of intra-particle pores, and due to the equilibrium sorption of solutes within intra-particle pores. Employing a Freund-lich isotherm, to quantify non-linear equilibrium sorption within the intra-particle pores, $D_a$ is defined as (Rügner et al., 1999):

$$D_a = \frac{D_{aq}\varepsilon}{(\varepsilon + K_{Fr}C^{\frac{1}{n_{Fr}}-1}\frac{\rho}{n_{Fr}})\tau_f} \qquad (8.2)$$

where $(\varepsilon + K_{Fr} C^{\frac{1}{n_{Fr}}-1} \frac{\rho}{n_{Fr}})$ denotes the capacity factor $\alpha$. $\rho$, $\varepsilon$, $\tau_f$ and $D_{aq}$ are the bulk density of the mineral grains [ML$^{-3}$], the intra-particle porosity [-], the tortuosity factor [-] and the aqueous diffusion coefficient [L$^2$T$^{-1}$], respectively.

$K_{Fr}$ [(L³M$^{-1}$)$^{1/n_{Fr}}$] and $1/n_{Fr}$ [-] are the parameters of the Freundlich sorption isotherm. $C$ [ML$^{-3}$] denotes intra-particle solute concentration, which depends on time and radial distance from the center of the grains. $C$ is determined within the MT3D-IPD simulations.

In Equation 8.2, $\tau_f$ is the only parameter, which cannot be directly measured. However, due to the similarities between electrical conductivity and aqueous diffusion in porous media, a relationship similar to Archie's law can predict the tortousity $\tau_f$ based on the intra-particle porosity $\varepsilon$ alone (Rügner et al., 1999):

$$\tau_f = \varepsilon^{1-m} \qquad (8.3)$$

with m representing an empirical exponent which is around 2 in sedimentary rocks (Wakao and Smith, 1962; Grathwohl, 1998).

It is therefore possible to rely only on measurable input parameters for the reactive transport model, avoiding fitting parameters like rate coefficients of first-order kinetics for example.

Recent studies have also shown that different source rocks and different grain sizes of the aquifer material influence the interaction of reactive compounds with the aquifer material (Grathwohl and Klein-eidam, 1995; Grathwohl, 1998; Klein-eidam et al., 1999b, Rügner et al., 1998).

The MT3D-IPD package therefore allows to consider physico-chemical aquifer heterogeneities caused by different intra-particle sorption and diffusion parameters of different lithological components of the aquifer facies. Aquifer facies, like gravel or sand for example, can be separated into different grain size fractions,

100

which can consist of different lithological components like limestone, sandstone or quartz, each associated with an individual set of physico-chemical parameters, e.g. sorption capacity, intra-particle porosity, tortousity, and sorption isotherms among others.

The quantification of the relative importance of diffusion-limited sorption and biodegradation to the observed contaminant mass flow reduction between the two investigated control planes is based on a mass balance approach.

Assuming that biodegradation and diffusion-limited sorption of the organic contaminants are the major attenuation processes at the site and simplifying in a first step the problem by decoupling these two processes, it is possible to determine the importance of biodegradation by modeling the reactive transport of a contaminant accounting for diffusion-limited sorption only.

The reduction in contaminant mass flux, $\Delta MF$ [MT$^{-1}$] between two investigated control planes using the IGIM, can then be described as:

$$\Delta MF = \Delta MF_s + \Delta MF_b \qquad (8.4)$$

leading to:

$$\Delta MF_b = \Delta MF - \Delta MF_s \qquad (8.5)$$

with $\Delta MF_s$ [MT$^{-1}$] denoting the reduction in contaminant mass flow due to diffusion-limited sorption, and $\Delta MF_b$ [MT$^{-1}$] representing the biodegraded contaminant mass flow.

At sites with old contaminant sources, $\Delta MF_s$ is often very small because physico-chemical equilibrium between the immobile and the mobile contaminant phase is approached. Under such conditions, and if other mass flow reducing processes like volatilization are not significantly contributing to the measured mass flow reduction, the measured reduction in conta-

minant mass flows can directly indicate the intrinsic biodegradation potential at the studied site.

To be able to quantify this potential at our site, the reactive transport modeling between the two investigated control planes aims at the quantification of $\Delta MF_s$. Neglecting degradation processes, the model simulations therefore allow to identify the minimum timeframe, in which the diffusion-limited contaminant sorption is significantly contributing to the attenuation process for the contaminant transport between the control planes.

This is investigated by evaluating the modeled integral mass flow for the downgradient control plane 2. From the transport model, the integral mass flow across the control plane can be calculated according to

$$F_{plane} = \sum_{i=1}^{k} Q_{ff,i}\, C_{w,i} \qquad (8.6)$$

where $F_{plane}$ [$MT^{-1}$], k, $Q_{ff,i}$ [$L^3 T^{-1}$], and $C_{w,i}$ [$ML^{-3}$] denote the total mass flow across the control plane, the number of cells along the control plane, the volumetric groundwater flux across the front face of the i-th model cell, and the solute concentration in the i-th cell, respectively.

At the beginning of the conducted transport simulations, the aquifer material is assumed to be uncontaminated and a time-invariant input flux of acenaphthene is used as a boundary condition. The input flux and its spatial distribution across the upgradient boundary is given by the acenaphthene flux measured at control plane 1 (compare Section 8.3.1).

### 8.3.3 Ranking of aquifer realizations

The plume development within the model domain is mainly controlled by the spatial distribution of the physico-chemical aquifer properties, i.e. by the spatial distribution of the geological facies. As the true facies distribution within the model

domain is known only at the location of the individual monitoring wells, a simplified Monte Carlo approach, based on the application of a replacement transfer function (RTF), as suggested by Journel (1989) and applied by Teutsch (1990), is employed to account for different equiprobable facies distributions.

In this approach, the generated aquifer realizations (parameter fields) are ranked, followed by the utilization of only a reduced number of aquifer realizations for the time intensive numerical reactive transport modeling. The ranking process thereby reduces the total computational effort. The type of RTF employed for the ranking and the subset chosen from the ranked aquifer realizations closely depend on the investigated hypothesis.

In our case, the RTF is obtained by reactive particle tracking because the objective in this study is to provide insights into the possible extremes of the mass flow breakthrough at the down-gradient control plane 2 (Figure 8.1), being correlated with preferential flowpaths in which contaminant mass is quickly transported towards the downgradient control plane.

The individual aquifer realizations are generated using SISIMPDF, a sequential indicator simulation code from the GSLIB program library (Deutsch and Journel, 1992). The geostatistical parameters of the experimental and theoretical variograms shown in Table 8.3 are based on a geostatistical site characterization, which employed 1420 data points from drilling logs and 120 sieve analyses of aquifer material (Peter, 2002).

The different realizations are spatially conditioned based on the facies distribution encountered during the drilling of the monitoring network at the control planes. Because the hydraulic conductivity distribution varies with the spatial facies distribution in each aquifer realization, using effective porosities from Bösel et al. (2000), facies specific hydraulic

Table 8.3: Parameters of the experimental and theoretical variograms for each lithofacies. (ldis: lag distance; ltol: lag tolerance; n: nugget; s: sill; r: range) (Peter, 2001).

| Direction[1] | Lithofacies G | | | | | Lithofacies Gm | | | | | Lithofacies S | | | | |
|---|---|---|---|---|---|---|---|---|---|---|---|---|---|---|---|
| | Exp. Vario. | | Theor. Vario. | | | Exp. Vario. | | Theor. Vario. | | | Exp. Vario. | | Theor. Vario. | | |
| | ldis | ltol | n | s | r | ldis | ltol | n | s | r | ldis | ltol | n | s | r |
| 1 | 25 | 12.5 | 0.06 | 0.22 | 58 | 20 | 10 | 0.05 | 0.26 | 45 | 20 | 10 | 0.006 | 0.046 | 60 |
| 2 | 25 | 12.5 | " | " | 48 | 20 | 10 | " | " | 38 | 20 | 10 | " | " | 40 |
| 3 | 0.2 | 0.1 | " | " | 5 | 0.2 | 0.1 | " | " | 5 | 0.2 | 0.1 | " | " | 2 |

[1] Investigated directions are (1) 112.5° east from north, (2) 22.5° east from north and (3) vertical direction

conductivities are calibrated in each realization to match the observed average field scale groundwater velocity of 2 m/d. Calibration is done by multiplying all $K_f$ values from an individual realization with an appropriate factor. Its average value is 0.37±0.12.

Due to the spatial conditioning of the aquifer realizations and the relatively small model domain, only 30 out of 200 generated aquifer realizations show less than 10 percent deviation between the facies mass shares in the respective realization compared to the input values (Table 8.1). To minimize the possible error induced by large deviations from the input facies shares, only these 30 aquifer realizations are used for the RTF ranking. The average differences between the input mass shares of the respective facies and the mass shares in the 30 remaining aquifer realizations are 5.7% ± 3.4% for facies G, 3.2% ± 1.6% for facies Gm, and 5.9% ± 2.8% for facies S.

The RTF ranks the 30 aquifer realizations based on the median of the reactive particle travel times assuming equilibrium sorption. For the RTF procedure, the travel time of a conservative particle moving through a model cell is multiplied by the equilibrium retardation factor of the facies located in the specific model cell to yield the travel time of a reactive particle undergoing equilibrium sorption. The effective retardation factor

for each facies (Table 8.1) is calculated as (e.g. Freeze and Cherry, 1979):

$$R = 1 + \frac{\rho_b}{n} K_d \qquad (8.7)$$

with $\rho_b$ [$ML^{-3}$], n [-], and $K_d$ [$L^3M^{-1}$] denoting the bulk mass density of the aquifer material, porosity and the distribution coefficient, respectively.

The distribution coefficient of a single facies is assumed to be the (mass share) weighted sum of the distribution coefficients of its individual lithological components. The distribution coefficient of each component under equilibrium conditions can be calculated using the Freundlich model as (e.g. Domenico and Schwartz, 1990):

$$K_d = K_{Fr} C_w^{\frac{1}{n_{Fr}}-1} \qquad (8.8)$$

with $C_w$ [$ML^{-3}$] representing the concentration of solute in bulk solution.

As the physico-chemical parameters are correlated to the facies, the resulting retardation factor distribution matches the (heterogeneous) facies distribution in each realization.

## 8.4 Transport modeling results and discussion

### 8.4.1 Implications for natural attenuation at the MGP site

As explained before, field scale mass flow rates of acenaphthene measured at the upgradient control plane 1 are used as time-invariant input for the reactive transport modeling to estimate the influence of diffusion-limited sorption on the contaminant attenuation with time. To better understand the combined impact of diffusion-limited sorption of the facies distribution found at the test site, model simulations for individual facies (physico-chemically homogeneous aquifer) with the same hydraulic transport properties as at the studied site are conducted first.
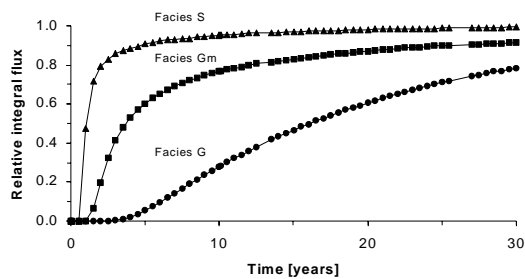


Figure 8.3: Relative integral flux of acenaphthene at control plane 2 for three single-facies aquifer realizations. Constant contaminant input of 0.3 [gl$^{-1}$] occurred in a homogeneous 50m wide source zone in all three model layers at control plane 1. Sorption parameters for the different facies are shown in Table 8.2.

Breakthrough curves for individual facies are shown in Figure 8.3. The pure sand aquifer exhibits the fastest break-through at control plane 2 caused by the very small Freundlich coefficient of the controlling lithocomponent quartz (Table 8.1 and Table 8.2).

The small Freundlich coefficient indicates a small sorption capacity and a fast approach to equilibrium conditions (large apparent diffusion coefficient). Compared to the other two facies, the influence of diffusion-limited sorption on long-term mass flow reductions can be

expected to be the smallest for a pure sand aquifer. For the measurements of CT series in pumped wells within short time intervals (e.g., in the order of days), however, the sand facies is highly important due to the fast sorptive uptake and release of contaminants.

The homogeneous gravel aquifer, on the other hand, attenuates about two thirds of the input flow after 10 years of time-invariant flow input at control plane 1 (Figure 8.3). This is due to the high limestone content of the gravel facies (Herfort, 2000) and its high sorption capacity for acenaphthene denoted by a Freundlich coefficient of 19 l/kg (Table 8.2). The bimodal gravel facies is a mixture of the other two facies and therefore exhibits intermediate sorption characteristics.

For the reactive particle tracking of the 30 equiprobable facies distributions (aquifer realizations) it is assumed that the distribution and transport of the con-taminant flux in groundwater is correlated to the groundwater flux in the aquifer in a way that most of the mass is transported in the preferential flow paths. Each cell and flow path is therefore represented in the particle tracking based on its share of the overall groundwater flow.

The average of the median of the reactive particle travel times over all realizations is 1385 days ± 425 days. Table 8.4 presents the two fastest (F4 and F20) and the two slowest (F1 and F18) realizations that are chosen for the transport modeling and the pumping test simulations. By using these two groups of realizations, the spread in the transport times of all 30 realizations is represented in the modeling approach.

The normalized breakthroughs with time of the acenaphthene mass flows at control plane 2 in the four aquifer realizations F1, F4, F18, and F20 are shown in Figure 4. In all realisations, the diffusion-limited sorption of acenaphthene

103

Table 8.4: Transport times of the reactive particles in the four aquifer realizations utilized for transport modelling

| Realisation | Peak arrival time [d] | Number of particles | Recovery rate [%] | Median arrival time [d] |
|---|---|---|---|---|
| Number of particles per cell proportional to the groundwater flow in the cell | | | | |
| F1 | 1215 | 5136 | 100 | 2843 |
| F4 | 335 | 9726 | 100 | 1157 |
| F18 | 705 | 8614 | 100 | 1788 |
| F20 | 645 | 8424 | 100 | 1035 |

is a key attenuation process during the first 10 to 20 years of the contamination, assuming a time-invariant contaminant input at control plane 1 and a decoupling of diffusion-limited sorption and degradation. The latter is not included in the simulation.

For later times the importance of diffusion-limited sorption decreases. Only F1, the slowest realization according to the flux-weighted reactive particle tracking, shows a relative integral mass flow of less than 90% of the input flow at control plane 2 after 30 years of simulated plume development. All other realizations demonstrate a relative integral flow of over 90% after 30 years of plume development (Figure 8.4). It can therefore be concluded that nowadays, after up to 100 years of contamination at the MGP site, diffusion-limited sorption is not significantly attenuating the contaminant flow. Snapshots of the dissolved acenaphthene concentrations after 10 and 30 years of plume development are provided in Figure 8.5 for the four aquifer realizations considered in this study.

For the assessment of natural attenuation, it is important to point out that the transport model assumes a time-invariant contaminant input, which is based on the assumption of a constant contaminant dissolution from the source and a steady-state groundwater flow field. The 30 years timeframe in which sorption losses have to be accounted for at this site has to be interpreted as a minimum timeframe because biodegradation is not included in the simulation. Biodegradation of the contaminants might lead to an extension of the timeframe in which sorption is an important attenuation process because it extends the time needed for the aquifer material to approach equilibrium with the dissolved contaminant concentration phase by reducing the dissolved contaminant mass in the system. This slows down the migration of the contaminant plume front.
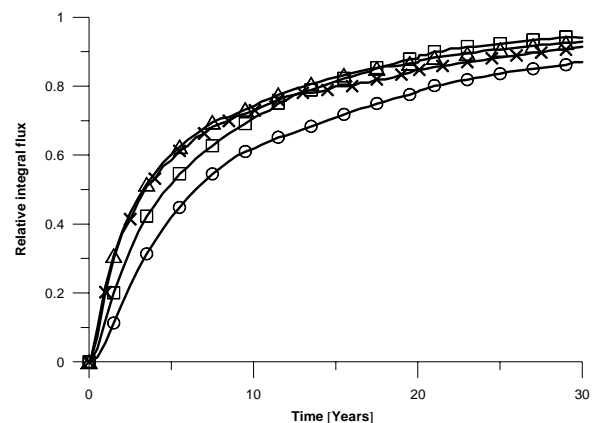


Figure 8.4: Modelled relative integral mass flux of acenaphthene at control plane 2 situated 140m downgradient from the modelled source at control plane 1. Simulation started with an uncontaminated aquifer and accounted for intra-particle diffusion and non-linear sorption of acenaphthene. The differences between the realizations F1 (circles), F4 (triangles), F18 (squares), and F20 (crosses) decline with time as the partitioning of acenaphthene approaches equilibrium.
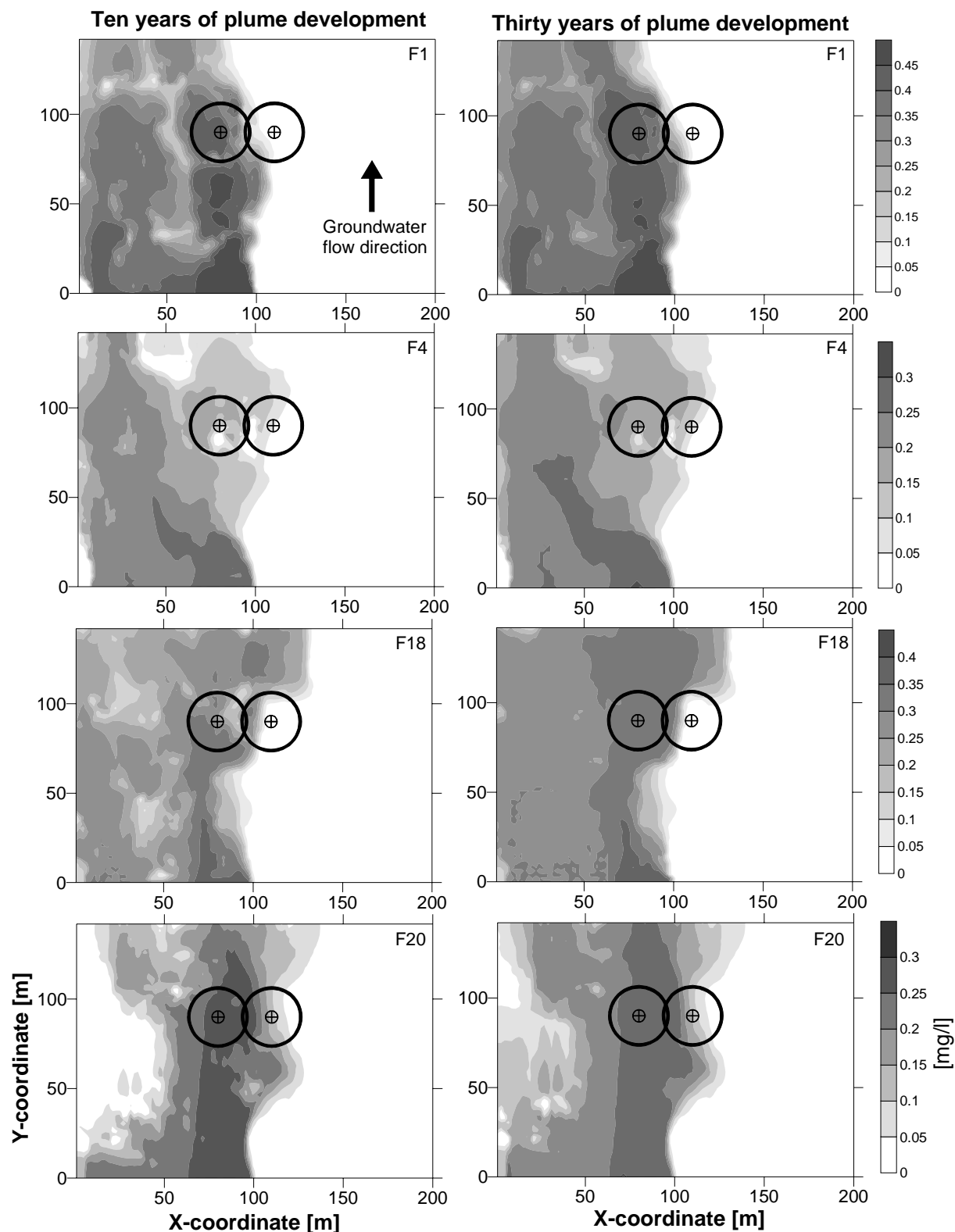
Figure 8.5: Snapshots of the aqueous phase acenaphthene distribution in the first model layer of aquifer realizations F1, F4, F18, and F20 after 10 years (left column) and 30 years (right column) of constant contaminant input at the downgradient boundary. The different contaminant plumes were used for the simulation of independent pumping tests at the two well locations indicated in the figures. Circles delineate the last (analytically derived) isochrone of the pumping tests. Acenaphthene concentrations shown in [mgl$^{-1}$]. The distribution of the constant input concentrations at the upgradient boundary were calibrated to represent the mass flux measured at the study site across control plane 1 (Figure 8.1).

Although biodegradation is not accounted for, the transport simulation results suggest that nowadays $\Delta MF_s$, the reduction of contaminant mass flow due to diffusion-limited sorption, is very small for the transport between the investigated control planes taking into account the 60 to more than 100 years of continuous contaminant dissolution from the NAPL pool at the site.

This implies that the observed reduction in mass flow at the site is primarily a result of biodegradation of the contaminants (assuming a complete capture of the contaminant plume at both control planes). Other mass flux reducing processes, which, according to the present state of knowledge, are assumed to be insignificant at our site. The potential for microbial contaminant degradation of most of the groundwater contaminants at the site has recently been shown by microcosm studies conducted with contaminated aquifer material (Althoff et al., 2001).

The implications for the other groundwater contaminants at the site depend on their physico-chemical properties. With a water solubility of around 3.5 mg/l (Mackay and Shiu, 1977) and a $\log K_{ow}$ of around 4 (Yalkowsky and Valvani, 1979; Miller et al., 1985) acenaphthene has a much higher sorption affinity to the aquifer material than, for example, volatile organic compounds like benzene, toluene, ethylbenzene, and xylenes (BTEX). For BTEX, water solubilities range from 170 $mgl^{-1}$ to 1780 $mgl^{-1}$, and $\log K_{ow}$ values are between 2.1 to 3.2 (Verschueren, 1983) illustrating a greater mobility in groundwater. The timeframe, in which BTEX compounds are attenuated through kinetic sorption is therefore significantly smaller compared to acenaphthene. It is concluded that intrinsic biodegradation is nowadays the key attenuation process responsible for the decrease in BTEX fluxes between the two investigated control planes.

For PAH compounds with a strongly hydrophobic character, however, sorption can still be significantly contributing to the

determined mass flow reduction. The relative importance of sorption to the reduction in mass flow should thereby increase with the $\log K_{ow}$ of the target compound. For pyrene, for example, with a $\log K_{ow}$ of around 5.2 (Yalkowsky and Valvani, 1979), diffusion-limited sorption is likely to be a key attenuation process in the field despite the age of the groundwater contamination.

### 8.4.2 Sensitivity of the IGIM to reactive transport processes

As mentioned before, the application of the IGIM results in a displacement of the contaminant plume in the subsurface. During the extended pumping test of the IGIM, a distant contaminant plume may be pulled towards the pumping well into a formerly uncontaminated aquifer region, giving rise to diffusion-limited uptake of contaminants by the previously uncontaminated aquifer material and the dissolved contaminant phase.

On the other hand, a narrow contaminant plume centered around the pumping well is quickly and completely captured by the increasing well capture zone. Continued pumping will then pull groundwater from less contaminated aquifer regions through the contaminated aquifer regions towards the pumping well. This may initiate a diffusion-limited release of contaminants from the aquifer material into the dissolved phase, thus effectively increasing the total dissolved contaminant flow.

Both effects (uptake and release) influence the measurement of CT series in a pumping well and impact the IGIM. Because the exact contaminant distribution in the dissolved and sorbed phase is generally unknown, it is only possible to numerically investigate the impact of diffusion-limited sorption/desorption processes on the IGIM in different plume scenarios.

For the investigation of these effects, the acenaphthene plume scenarios after 10

years and 30 years of plume development, that were generated during the plume development modeling, are used as initial contaminant distribution. The pumping wells in each scenario are situated 30 m apart and 90 m downgradient from the source. At these wells independent 5-day pumping tests are simulated. The well locations and the size of the well capture zones at the end of the pumping in the different realizations are shown in Figure 8.5. It can be seen that in all plume scenarios the easterly well is always outside of the main contaminant plume, whereas the westerly well is mostly located in the main contaminant plume.

To study the influence of diffusion-limited sorption on the measurement of CT series in the pumping wells two pumping tests are simulated at each pumping well for every aquifer/plume age realization. Both simulations use the same starting conditions, but deviate from each other in the transport characteristics of the contaminant. In particular, the mass flow rates are identical.

In a first step, pumping tests are simulated assuming non-reactive contaminant transport towards the pumping well for each scenario (case 1). In a second step, the pumping test simulations are repeated assuming diffusion-limited reactive contaminant transport towards the pumping well as is expected under field conditions (case 2). This case accounts for changes in the mobile contaminant mass flow within the well capture zone due to diffusion-limited uptake / release processes and will therefore result in CT series being different from the CT series obtained by the non-reactive simulations.

Mass flows at the investigated wells are back-calculated for all CT series by applying the analytical transient inversion algorithm developed by Schwarz (2002) and used by Bockelmann et al. (2001). It has to be noted that this algorithm does not account for physico-chemical reactions, i.e. perfect estimates of mass flow rates can at best be expected for case 1. Mass

flow deviations encountered for case 2, therefore, provide a measure for the impact of diffusion-limited sorption / desorption on the IGIM.

The results of the pumping test simulations for all plume scenarios shown in Figure 8.5 are summarized in Table 8.5. Contaminant mass flow rates are calculated using the analytical solution of the IGIM (Schwarz, 2002; Bockelmann et al., 2001). As expected, the influence of reactive contaminant transport towards a pumping well is smallest for a well located within the main contaminant plume. Apart from realization F1, all plume scenarios show a mass flow deviation between 0% and 8% due to sorption / desorption. This deviation declines with the age of the contaminant plume as the contaminant partitioning within the well capture zone approaches equilibrium with time. In realization F1, the westerly well is close to the plume fringe, and a more hetero-geneous spatial contaminant distribution is encountered around the well compared to other aquifer realizations, which increases the difference between the non-reactive and reactive mass flow to around 23%.

If the pumping well is located outside of the main contaminant plume the reactive contaminant transport induces a higher difference in the mass flow results compared to the results from the non-reactive scenarios of around 0% to 59% depending on the aquifer realization.

The differences between the aquifer realizations are caused by the different spatial facies distributions, which control the hydraulic parameter distribution on the one hand, i.e. the plume location, and the spatial distribution of the sorption parameters on the other hand, i.e. the sorption capacities and diffusive uptake / release rates. In realization F1 for example (Figure 8.5), the easterly well is located within a sand lens with fast sorption kinetics (Figure 8.4 and Table 8.2) which leads to a significant reduction in the

Table 8.5: Mass flux results based on simulated concentration-time series recorded during 5-day pumping tests in different aquifer realizations. For each well and plume scenario, the contaminant transport towards the pumping well was modelled for non-reactive and reactive (kinetic sorption / desorption) conditions. Mass fluxes are shown for 10 years and 30 years of plume development prior to the pumping. Model contaminant was acenaphthene. Reactive transport conditions assumed a kinetic sorption by intraparticle diffusion with a non-linear Freundlich sorption isotherm. Sorption parameters are listed in **Error! Reference source not found.**. Well locations in relation to the acenaphthene plumes prior to the pumping are shown in Figure 8.5.

| Realization | Age of plume | Non-reactive transport during pumping Mass flux [gd$^{-1}$] | Reactive transport during pumping Mass flux [ d$^{-1}$] | Difference[1] [%] |
|---|---|---|---|---|
| | | Well located in the plume | | |
| F1 | 10 years | 7.91 | 9.69 | 22.5 ± 0.6 |
| | 30 years | 8.32 | 10.34 | 24.3 ± 2.3 |
| F4 | 10 years | 2.99 | 3.23 | 8.0 ± 0.12 |
| | 30 years | 4.89 | 4.61 | 5.7 ± 1.5 |
| F18 | 10 years | 8.12 | 8.26 | 1.7 ± 3.0 |
| | 30 years | 8.59 | 8.69 | 1.2 ± 3.1 |
| F20 | 10 years | 7.09 | 7.00 | 1.3 ± 0.1 |
| | 30 years | 7.60 | 7.61 | <0.0 ± 1.9 |
| | | Well located outside of the plume | | |
| F1 | 10 years | 2.03 | 0.86 | 57.6 ± 6.4 |
| | 30 years | 2.15 | 0.88 | 59.1 ± 2.6 |
| F4 | 10 years | 2.34 | 1.64 | 29.9 ± 0.1 |
| | 30 years | 2.74 | 2.49 | 9.1 ± 1.7 |
| F18 | 10 years | 7.37 | 3.92 | 46.8 ± 0.2 |
| | 30 years | 7.56 | 4.19 | 44.6 ± 3.5 |
| F20 | 10 years | 3.52 | 3.46 | 1.7 ± <0.0 |
| | 30 years | 3.87 | 3.76 | 2.9 ± 1.9 |

[1] Uncertainty represents the mass balance error of the kinetic transport model

dissolved contaminant mass during the transport towards the pumping well. As the plume is pulled through the sand lens, the formerly uncontaminated sand matrix is quickly sorbing a significant fraction of the dissolved contaminant mass. This induces the relatively high difference of about 59% between the mass flow results from the non-reactive transport and the reactive transport scenario.

Compared to other uncertainties encountered at "real-world" field sites, for example uncertainties associated with the distribution of hydraulic conductivity and porosity in the aquifer, the observed discrepancies appear small in comparison but should not be totally neglected. It is noteworthy that this discrepancy is highly dependent on the physico-chemical proper-ties of the studied aquifer and the target contaminant. As seen from Figure 8.3, a

sand aquifer generally has a very low organic carbon content and a small sorp-tion capacity, but often shows fast sorptive uptake. The displacement of a contaminant plume into a formerly uncontaminated sand lens can therefore significantly influence the mass flow results of the IGIM.

This effect would be less pronounced in a gravel aquifer consisting mainly of lime-stone with a higher organic carbon content and a higher sorption capacity, but gener-ally much slower uptake rates. Obviously the importance of diffusion-limited sorp-tion during plume displacement would decrease with increasing slowness of sorp-tion kinetics in the investigated aquifer.

It is noteworthy, that the difference in the mass flow results of the IGIM can be two-sided. If sorption processes prevail, the mass flow might be underestimated,

whereas desorption processes would lead to an overestimation of the contaminant mass flow. The latter can, for example, occur, if a pumping well is located in the center of a narrow plume and clean groundwater is pulled through the contaminated aquifer region towards the pumping well (realization F18 in Table 8.5).

The transport results discussed here are all based on acenaphthene as the model contaminant. BTEX compounds would show a much smaller deviation in the flow quantifications because of their less hydrophobic nature, i.e. smaller $K_{ow}$ values compared to acenaphthene. For high molecular weight PAH compounds, however, the situation is opposite to that of the BTEX compounds and the influence of sorption on the mass flow estimations could be more pronounced compared to acenaphthene.

## 8.5    Conclusions

In this study we expand a novel integral groundwater investigation approach by integrating a reactive transport model into the site investigation. The measured contaminant mass flow rates can be used as input parameters for the transport model simulating the contaminant transport at the study site. For our site it is shown that the observed mass flow reduction of the BTEX compounds is associated with intrinsic biodegradation of the contaminants, whereas for higher molecular weight PAH compounds the attenuation rate constants are still influenced by sorption of the contaminants during transport.

The simulation of pumping tests under different contaminant plume conditions demonstrate that at the study site the influence of kinetic contaminant sorption / desorption on the measurement of concentration-time series in a pumping well is negligibly small, if the well is located in the main contaminant plume. If the pumping well is located at the edge or outside of the main contaminated aquifer region, the influence decreases with the age of the plume and with decreasing sorptive uptake rates of the investigated aquifer.

However, for aquifers with a higher organic carbon content, which is associated with larger uptake rates, the diffusion-limited sorption / desorption of strongly hydrophobic contaminants can introduce significant errors into the pumping test based integral mass flow quantification. Nevertheless, for acenaphthene at our site, the largest uncertainty caused by diffusion-limited sorption / desorption processes was around 60%. This effect is small compared to the average uncertainty attributed to the determination of relevant hydraulic parameters at a field site.

Future work is needed to include biodegradation and compound interactions like preferential sorption / degradation into the transport model simulation and to combine the mass flow results of the integral groundwater investigation method with Langrangian transport model tools like SMART (Finkel et al., 1999). These models are also based on an integral control plane approach and can directly incorporate integral mass flow rates into the transport model simulation. Moreover, additional simulations with various geological situations and contaminants would be valuable to assess the possible uncertainties of integral mass flow quantification methods under different field conditions.

# 9 Conclusion

This thesis focused on the field scale quantification and modelling of contaminant mass fluxes in porous media. Compound-specific contaminant mass fluxes were quantified at two field sites using integral and point-scale investigation approaches. At one field site, the integral site investigation was coupled to the field scale modelling of acenaphthene as the model contaminant.

**Integral groundwater investigation.** At a former MGP site, the integral groundwater investigation method (IGIM) was extended by investigating two control planes located at increasing distances from the contaminant source. Measured concentration-time series (CT-series) were interpreted using an analytical and numerical approach.

Without the need for a detailed flow and transport model, the simplified analytical interpretation of the CT-series allowed for a fast and easy quantification of contaminant mass fluxes at the field site. With the simplified analytical approach, it was possible to identify acenaphthene and benzene as the main contaminants at the site, as well as localise the aquifer areas most likely located within the contaminant plumes.

The numerical mass flux estimation required a site specific flow and transport model for the inversion of the CT-series. To be able to reliably simulate pumping test, the flow model had to be able to simulate transient flow conditions. With the numerical approach it was possible to incorporate aquifer heterogeneities and asymmetrical well capture zones into the mass flux estimation process.

Assuming that the numerical approach quantified the "true" contaminant mass flux at the MGP site, the analytical approach was seen to be a fair approximation.

The analytically derived contaminant mass fluxes displayed an average deviation of 42% ± 41% to the numerical mass flux results. The total spread in the contaminant mass flux results was between 1% and 186%.

Looking at the relative change in mass flux of individual contaminants between the two control planes, a relatively good agreement in the results of the two inversion approaches was found. The average discrepancy between the analytical and numerical mass flux approach in this context was only 23% ± 31%.

In the absence of a reliable flow model, which usually requires a detailed knowledge of the aquifer heterogeneities at a field site, it was shown in this thesis that at the former MGP site, the simplified analytical inversion of the CT-series allowed for the identification of the main contaminants, and for the localisation of the contaminated aquifer regions. Applied at two control planes situated at increasing distances downgradient from the contaminant source, it also allowed for the quantification of the relative reduction in contaminant mass flux in flow direction with an acceptable degree of certainty.

If the higher level of certainty provided by the numerical solution is not required or if not enough data on aquifer heterogeneities is available for the development of a dependable flow model, it is concluded that the analytical inversion approach is an easy to use tool for the integral estimation of contaminant mass fluxes at field scale, if the inherent assumptions of circular isochrones during the pumping, non-existent or linear concentration gradients within the well capture zones, and effective aquifer homogeneity at the scale

of the well capture zones are met at the respective field site.

The overall advantages of the integral groundwater investigation method include the possibility of a complete site investigation with only a limited number of monitoring wells, the ability to investigate inaccessible aquifer regions, e.g. below buildings, the mass flux estimation without the need for data regionalization, and the opportunity for quantifying natural attenuation rate constants directly at field scale. The latter requires the investigation at two or more control planes located at different distances from the contaminant source in the groundwater flow direction. Especially at sites with difficult drilling conditions, where modern direct push technologies like Geoprobe™ cannot be applied, or at sites with very wide contaminant plumes, the IGIM is the appropriate field scale mass flux estimation method.

The major disadvantages and limitations of the IGIM are the potentially high treatment costs for the pumped contaminated groundwater, the dependency on the local aquifer transmissivity and porosity for acceptable capture zone widths in reasonable pumping times, the inherent problem, especially under heterogeneous aquifer conditions, to define the exact extend of individual well capture zones, the loss of detailed information on the vertical contaminant distribution in the investigated aquifer, and the neglect of the contaminant retardation in the inversion of the CT-series. Moreover, in aquifer settings with a large natural groundwater flow, the technical limitations on the pumping rate can limit the applicability of the approach.

By neglecting the contaminant retardation during the inversion process, the reconstructed contaminant concentration field prior to the pumping can be incorrect. For the mass flux estimation, the derived concentration field, i.e. the concentrations in the streamtubes, is multiplied with the groundwater flow in each streamtube. As

the respective streamtube concentration might be erroneous and might not represent the true situation prior to the pumping, the resulting mass flux estimation can be incorrect, too.

This effect most likely decreases with the age of the contaminant plume because the effects of retardation (i.e. sorption) decreases in importance with time as the sorbed and dissolved contaminant phase in an aquifer approach equilibrium.

Nevertheless, this effect increases with the distance of the well location from the main contaminant plume because of reactive transport processes during the transport of the dissolved contaminant mass towards the pumping well.

The further investigation of this effect and the implementation of the contaminant retardation into the inversion algorithm could be an important objective for future work. It would help to compute reliable spatial contaminant distributions which could be used for the estimation of the environmental hazard, as well as for the estimation of contaminant mass fluxes.

**Natural attenuation (NA) rate constants.** The utilization of the IGIM at two control planes located at increasing distances from the contaminant source enabled the direct field scale quantification of contaminant natural attenuation rate constants. These attenuation rate constants, however, incorporate the effects of all mass flux reducing processes occurring at the field site and have to be interpreted accordingly.

The quantification of NA rate constants at the MGP site illustrated a high attenuation of BTEX compounds and a less pronounced attenuation of PAH compounds between the two control planes. The reduction in contaminant mass flux occurred simultaneously with an increase in reduced electron acceptors (e.g., dissolved $Fe(II)$), indicating ongoing anaerobic biodegradation.

A comparison of the results with NA rate quantifications using other field investigation approaches showed a good agreement in the different results, demonstrating the applicability of the integral NA rate constant approach.

**High detail method comparison.** At a benzene contaminated homogeneous field site in Borden, Canada, the IGIM was compared with a conventional multilevel sampling screen or groundwater fence approach using a high detail sampling procedure and an intensive infrastructure. For the IGIM, samples frequencies were in accordance with theoretical streamtube widths of 0.15m. Multilevel sampling slots were placed 0.4m apart along 10 multilevel wells situated 5m apart, yielding a 8x10 sampling grid.

The analytically derived integral mass flux estimates were effectively similar to the mass fluxes quantified through the multilevel point-scale approach. The close fit in the results highlights the applicability of the analytical IGIM approach under homogeneous field conditions. However, for thin plumes and homogeneous, easy to drill aquifers, the multilevel point-scale approach can be cheaper than the IGIM.

**Reactive transport modelling.** At the former MGP site, the integral site investigation was extended by a reactive modelling of the contaminant transport between the two control planes. For this objective a new transport modelling code was used that incorporates the diffusion limited intra-particle sorption of the target compounds into the transport modelling process.

Based on a geostatistical description of the field site, equiprobable aquifer realisations were generated. To reduce the computational effort, these realisations were ranked with a fast replacement transfer function (RTF). It was seen that the median of the travel times of reactive particles in the aquifer realisations can be

used as a ranking parameter to describe the long term sorption characteristics of the aquifer realisations.

The transport modelling results demonstrated that the simulated acenaphthene plumes, approached equilibrium in the modelled aquifer region after approximately 30 years of constant contaminant input. The input flux was chosen to represent the measured acenaphthene flux quantified at the upgradient control plane during the field investigation.

As a consequence it could be concluded for the MGP site that the quantified mass flux reductions of BTEX and low molecular weight PAH compounds are mainly a result of microbial degradation processes. For high molecular weight PAH compounds however, sorption might still be an important attenuation factor even after up to 100 years of plume development. One reason for this is the high limestone and organic carbon content of the local aquifer sediments, which provides effective sorption sites for these compounds. The effective retardation factors of these compounds is hence orders of magnitude higher compared to compound classes with a higher water solubility, like BTEX for example.

The simulated plume scenarios were subsequently used for the simulation of long-term pumping tests to investigate the sensitivity of the IGIM on reactive transport processes during the pumping of monitoring wells.

The results of multiple plume and aquifer scenarios suggest that the IGIM is influenced by the reactive contaminant transport towards a pumping well because sorption / desorption processes can change the mobile contaminant phase that is transported towards a pumping well. The maximum effect observed in the simulations was around 60% change in mass flux due to reactive transport processes.

It was also seen from the simulations that these effects decrease in importance with the age of the contaminant plume and increase with the distance of the pumping well from the main contaminated aquifer region, i.e. with the distance from the contaminant plume.

**Future work.** As this thesis documented the first field scale implementation of the IGIM in the context of a natural attenuation study, more data from other field sites would be valuable to confirm the applicability of the approach for different aquifer and contaminant plume conditions.

As the neglect of the contaminant retardation was seen to adversely effect the integral mass flux quantification under certain conditions, future work should implement reactive contaminant transport and retardation into the inversion algorithms.

It would also be valuable to get information on the vertical contaminant distribution during the integral site investigation. In a first step, this could be achieved by a multilevel pumping in the monitoring wells, followed by the individual interpretation of the concentration-time series obtained at different aquifer depths. However, the numerical simulation of the hydraulic interchanges between aquifer layers during pumping might be challenging.

The simulation of the contaminant transport using a discrete transport model was seen to be very time intensive at the field scale. The coupling of the integral field scale mass flux quantification with "integral", control plane based, Lagrangian transport models should be an objective of future work to develop a tool box that allows the integral site investigation and the identification of mass flux reducing processes by numerical modelling of the contaminant transport. Using a control plane based modelling approach, the measured contaminant mass fluxes would not be required to be discretized again, but could be used as direct input parameters for the transport simulation.

In the scope of this thesis, the analytical IGIM was compared with a traditional groundwater fence approach at a relatively homogeneous field site. Future work should include the comparison of the numerical IGIM both at homogeneous and heterogeneous field site to investigate the relative advantages and limitations of different field investigation approaches under various conditions.

Finally, the further investigation of the sensitivity of the IGIM on the reactive contaminant transport towards an abstaction well could yield valuable insights into the possible uncertainty in field scale mass flux estimations. In this thesis, the investigation was limited to the encountered aquifer and facies conditions and only one model compound was investigated. Further modelling work including multiple compounds and aquifer settings would therefore be very valuable.

# 10 References

**Aggarwal P. K., Fuller M. E., Gurgas M. M., Manning J. F., and Dillon M. A.** (1997) Use of stable oxygen and carbon isotope analysis for monitoring the pathways and rates of intrinsic and enhanced in situ biodegradation. *Environmental Science and Technology* 31, 590-596.

**Ahad J. M. E., Sherwood-Lollar B., Edwards E. A., Slater G. F., and Sleep B. E.** (2000) Carbon isotope fractionation during anaerobic biodegradation of toluene: Implications for intrinsic bioremediation. *Environmental Science and Technology* 34, 892-896.

**Alexander M.** (1999) *Biodegradation and Bioremediation*. Academic Press.

**Althoff K., Mundt M., Eisenträger A., Dott W., and Hollender J.** (2001) Microcosm-experiments to assess the potential for natural attenuation of contaminated groundwater. *Water Research* 35(3), 720-728.

**Alvarez P. J. J. and Vogel T. M.** (1991) Substrate interactions of benzene, toluene, and para-xylene during microbial degradation by pure cultures and mixed culture slurries. *Applied and Environmental Microbiology* 57, 2981-2985.

**Alvarez P. J. J. and Hunt C. S.** (1999) Health and environmental assessment of the use of ethanol as a fuel oxygenate - Volume 3: The effects of ethanol on BTEX biodegradation and natural attenuation, pp. 39. Lawrence Livermore National Laboratory.

**Anderson R. T., Rooney-Varga J. N., Gaw C. V., and Lovley D. R.** (1998) Anaerobic benzene oxidation in the Fe(III) reduction zone of petroleum-contaminated aquifers. *Environmental Science and Technology* 32, 1222-1229.

**Anderson R. T. and Lovley D. R.** (2000) Anaerobic bioremediation of benzene under sulfate-reducing conditions in a petroleum-contaminated aquifer. *Environmental Science and Technology* 34, 2261-2266.

**API** (1997) Methods for measuring indicators of intrinsic bioremediation: Guidance manual. American Petroleum Institute.

**Aronson D. and Howard P. H.** (1997) Anaerobic degradation of organic chemicals in groundwater: A summary of field and laboratory studies. American Petroleum Institute.

**ASTM** (1997) Standard guide for remediation of groundwater by natural attenuation at petroleum release sites. American Society for Testing and materials.

**Baedecker M. J., Cozzarelli I. M., Eganhouse R. P., Siegel D. I., and Bennett P. C.** (1993) Crude oil in a shallow sand and gravel aquifer: III. Biogeochemical reactions and mass balance modelling in anoxic groundwater. *Applied Geochemistry* 8, 569-586.

**Bahr J. M. and Rubin J.** (1987) Direct comparison of kinetic and local equilibrium formulations for solute transport affected by surface reactions. *Water Resources Research* 32(3), 438-452.

**Ball W. P. and Roberts P. V.** (1991) Long-term sorption of halogenated organic chemicals by aquifer material. 2. Intraparticle diffusion. *Environmental Sciences and Technology* 25, 1237-1249.

**Barker J. F., Patrick G. C., and Major D.** (1987) Natural attenuation of aromatic hydrocarbons in a shallow sand aquifer. *Groundwater Monitoring and Review* Winter, 64-71.

**Barker G. W., Raterman K. T., Fisher J. B., Corgan J. M., Trent G. L., Brown D. R., and Sublette K. L.** (1995) Assessment of natural hydrocarbon bioremediation at two gas condensate production sites. In *Intrinsic bioremediation* (ed. R. E. Hinchee, J. T. Wilson, and D. C. Downey), pp. 181-188. Battelle.

**Barker J. F., Beland-Pelletier C., Blaine F., Devlin J. F., King M. W. G., and Schirmer M.** (2000) Monitored natural attenuation - can mass fluxes through monitoring fences document mass loss in groundwater plumes? *Groundwater 2000*, 311-312.

**Beland-Pelletier C., Barker J. F., Bockelmann A., and Ptak T.** (2001a) Evaluation of two techniques to estimate the mass flux of contaminants in groundwater. *2nd Joint IAH-CNC/CGS Groundwater Specialty Conference*, in print.

**Beland-Pelletier, C.** (2001b) The use of contaminant mass discharge estimates in natural attenuation assessment: a comparison of two approaches. M.Sc. Thesis, University of Waterloo.

**Bevington P. R. and Robinson D. K.** (1992) *Data reduction and error analysis for the physical science*. McGraw-Hill, Inc.

**Beyer W.** (1964) Beschreibung d Wasserdurchlässigkeit von Kiesen und Sanden. *Zeitschrift für Wasserwirtschaft-Wassertechnik* 14, 165-168.

**Bloom Y., Arvena R., Hunkeler D., Edwards E., and Frape S. K.** (2000) Carbon isotope fractionation during microbial dechlorination of trichloroethene, cis-1,2-dichloroethene, and vinyl chloride: Implications for assessment of natural attenuation. *Environmental Science and Technology* 34(2768-2772), 2768-2772.

**Bockelmann A., Peter A., Ptak T., R. L., and Teutsch G.** (2000a) Investigation of natural attenuation rates at field scale. *7th international FZK/TNO Conference on Contaminated Soil (ConSoil 2000)*, 478-481.

**Bockelmann A., Ptak T., and Teutsch G.** (2000b) Field scale quantification of contaminant mass fluxes and natural attenuation rates using an integral investigation approach. *Groundwater 2000*, 309-310.

**Bockelmann A., Ptak T., and Teutsch G.** (2001a) An analytical quantification of mass fluxes and natural attenuation rate constants at a former gasworks site. *Journal of Contaminant Hydrology* 53 (3-4), 429-453.

**Bockelmann A., Ptak T., and Teutsch G.** (2001b) Quantifizierung des natürlichen Rückhalte- und Abbaupotentials im Feldmaßstab am Beispiel des Testfelds Süd. *2. Symposium "Natural Attenuation - Neue Erkenntnisse, Konflikte Anwendungen*, 121-128.

**Bockelmann A., Ptak T., Liedl R., and Teutsch G.** (2001c) Mass flux, transport and natural attenuation of selected organic contaminants at a former urban gasworks site. *Prospects and limits of natural attenuation at tar oil contaminated sites*, (Ed. Wiesner, J.), Dresden, Dechema, pp. 325-336.

**Bockelmann, A., Zamfirescu, D., Ptak, T., Grathwohl, P., Teutsch, G.** (2002) Quantification of mass fluxes and natural attenuation rates at an industrial site with a limited monitoring network: A case study. *Journal of Contaminant Hydrology*, in print.

**Borden R. C., Gomez C. A., and Becker M. T.** (1995) Geochemical indicators of intrinsic bioremediation. *Ground Water* 33(2), 180-189.

**Borden R. C., Daniel R. A., LeBrun IV L. E., and Davis C. W.** (1997) Intrinsic biodegradation of MTBE and BTEX in a gasoline-contaminated aquifer. *Water Resources Research* 33(5), 1105-1115.

**Bösel, D.**, 1998. Entwicklung eines hydrogeologischen Modells für das Testfeld Süd (Neckartal bei Stuttgart): Durchführung von Tracerversuchen und sedimentgeologische Tiefenkartierung. Diplomarbeit, Institut für Geologie und Paläontologie, Universität Tübingen.

**Bösel D., Herfort M., Ptak T., and Teutsch, G.** (2000) Design, performance, evaluation and modelling of a natural gradient multitracer transport experiment in a contaminated heterogeneous porous aquifer. *Tracers and Modelling in Hydrogeology*, 45-51.

**Bouwer E. J. and McCarty P. L.** (1984) Modelling of trace organics biotransformation in the subsurface. *Ground Water* 22(4), 433-440.

**Braddock J. F. and McCarthy K. A.** (1996) Hydrologic and microbiological factors affecting persistence and migration of petroleum hydrocarbons spilled in a continuous-permafrost region. *Environmental Science and Technology* 30(2626-2633).

**Brady P. V., Brady M. V., and Borns D. J.** (1998) *Natural Attenuation - CERCLA, RBCA's, and the Future of Environmental Remediation.* Lewis Publishers.

**Burland S. M. and Edwards E. A.** (1999) Anaerobic benzene degradation linked to nitrate reduction. *Applied and Environmental Microbiology* 65(2), 529-533.

**Burr D. T. and Sudicky E. A.** (1994) Nonreactive and reactive solute transport in three-dimensional heterogeneous porous media: Mean displacement, plume spreading, and uncertainty. *Water Resources Research* 30(3), 791-815.

**Buscheck T. E., Kirk P. E., O'Reilly T., and Nelson S. N.** (1993) Evaluation of intrinsic bioremediation at field sites. *Ground water management* 17, 367-381.

**Buscheck T. and O'Reilly K.** (1995) Protocol for monitoring intrinsic bioremediation in groundwater. Chevron Research and Technology Company.

**Buscheck T. and O'Reilly K.** (1997) Protocol for monitoring natural attenuation of chlorinated solvents in groundwater. Chevron Research and Technology Company.

**Buschek S. M. and Alcantar C. M.** (1995) Regression techniques and analytical solutions demonstrating intrinsic bioremediation. In *Intrinsic bioremediation* (ed. R. E. Hinchee, T. J. Wilson, and D. Downey), pp. 106-116. Batelle Press.

**Caldwell K. R., Tarbox D. L., Barr K. D., Fioenza S., Dunlap L. E., and Thomas S. B.** (1992) Assessment of natural bioremediation as an alternative to traditional active remediation at selected Amoco Oil Company sites, Florida. *Petroleum hydrocarbons and organic chemicals in ground water: Prevention, detection, and restoration*, 509-525.

**Carey M. A., Finnamore J. R., Morrey M. J., and Marsland P. A.** (2000) Guidance on the assessment and monitoring of natural attenuation of contaminants in Groundwater. Environment Agency R & D Dissemination Centre.

**Cerniglia C. E.** (1992) Biodegradation of polycyclic aromatic hydrocarbons. *Biodegradation* 3, 351-368.

**Chiang C. Y., Salanitro J. P., Chai E. Y., Colhart J. D., and Klein C. L.** (1989) Aerobic biodegradation of benzene, toluene, and xylene in a sandy aquifer - data analysis and computer modeling. *Ground Water* 27(6), 823-834.

**Coates J. D., Woodward J., Allen J., Philip P., and Lovley D. R.** (1997) Anaerobic degradation of polycyclic aromatic hydrocarbons and alkanes in petroleum-contaminated marine harbor sediments. *Applied and Environmental Microbiology* 63(9), 3589-3593.

**Dahlstohm K.** (1999) NATO/CCMS pilot study - Evaluation of demonstration and emerging technologies for the treatment of contaminated land and groundwater (Phase III). *Tour de Table presentation NATO-CCMS meeting*.

**Davis R. K., Pederson D. T., Blum D. A., and Carr J. D.** (1993) Atrazine in a stream-aquifer sytem: estimation of aquifer properties from atrazine concentration profiles. *Ground Water Monitoring and Remediation* Spring, 134-141.

**Dempster H. S., Scherwood-Lollar B., and Feenstra S.** (1997) Tracing organic contaminants in groundwater: A new methodology using compound-specific isotopic analysis. *Environmental Science and Technology* 31, 3193-3197.

**Deutsch C. V. and Journel A. G.** (1992) *GSLIB Geostatistical software library and user's guide*. Oxford University Press.

**Domenico P. A. and Schwartz F. W.** (1990) *Physical and chemical hydrogeology*, pp. 824, Wiley.

**Edwards E. A. and Grbic-Galic.** (1992) Complete mineralization of benzene by aquifer microorganisms under strictly anaerobic conditions. *Applied and Environmental Microbiology* 58(8), 2663-2666.

**Edwards E. A., Wills L. E., Reinhard M., and Grbic-Galic D.** (1992) Anaerobic degradation of toluene and xylene by aquifer microorganisms under sulfate-reducing conditions. Applied and Environmental Microbiology *58(3)*, 794-800.

**Edwards E. A. and Grbic-Galic D.** (1994) Anaerobic degradation of toluene and o-xylene by a methanogenic consortium. *Applied Environmental Microbiology* 60, 313-320.

**Eggleston J. R. and Rojstaczer S. A.** (2000) Can we predict subsurface mass transport. *Environmental Science and Technology* 34, 4010-4017.

**Einarson M. D., Langdon R. L., and Barker J. F.** (2000) Hydraulic performance of a funnel-and-gate groundwater treatment system in a shallow tidally-affected aquifer. Project report to Naval Facilities Engineering Command.

**Einarson M. D. and Mackay D. M.** (2001) Predicting impacts of groundwater contamination. *Environmental Science and Technology* 35(3), 66A-73A.

**Eiswirth M., Hötzl H., Reichert B., and Weber K.** (1998) Grundwasser- und Bodenluftuntersuchungen im Testfeld Süd. *Grundwasser* 3(4), 151-158.

**Ertl S., Seibel F., Eichinger L., Frimmel F. H., and Kettrup A.** (1996) Determination of the 13C/ 12C Isotope Ratio of Organic Compounds for the Biological Degradation of Tetrachloroethene (PCE) and Trichloroethene (TCE). *Acta Hydrochemica et Hydrobiologica* 24, 16-21.

**FDER** (1990) No further action and monitoring only guidelines for petroleum contaminated soil. Florida Department of Natural Resources.

**Feenstra S., Mackay D. M., and Cherry J. A.** (1991) A method for assessing residual NAPL based on organic chemical concentrations in soil samples. *Groundwater Monitoring and Review* 11(2), 128-136.

**Fetter C. W.** (1993) *Contaminant hydrogeology*. Macmillan Publishing Company.

**Finkel M., Liedl R., and Teutsch G.** (1999) Modelling surfactant-enhanced remediation of polycyclic aromatic hydrocarbons. *Environmental Modelling & Software* 14, 203-211.

**Fischer C. L. J., Schmitter R. D., and ONeil Lane E.** (1999) Manufactured Gas Plants: The Environmental Legacy. Georgia Institute of Technology.

**Freeze R. A. and Cherry J. A.** (1979) *Groundwater*. Prentice Hall.

**Fritz P. and Fontes J. C.** (1986) Handbook of environmental isotope geochemistry, Vol. 2, pp. 557. Elsevier.

**Gaißer J.** (1998) GIS-gestützte Modellierung der Geometrie des Neckarkiesaquifers im Bereich der Neckartalaue Stuttgart und Forced Gradient Tracer Tests zur Bestimmung der Bandbreite der Transportparameter. MSc Thesis, Eberhard-Karls-Universität Tübingen.

**Galimov E. M.** (1985) *The biological fractionation of isotopes*. Academic Press.

**Genthner R. B. S., Townsend G. T., Lantz S. E., and Mueller J. G.** (1997) Persistence of polycyclic aromatic hydrocarbon components of creosote under anaerobic enrichment conditions. *Archives of Environmental Contamination and Toxicology* 32, 99-105.

**Gibson D. T., Koch J. R., and Kallio R. E.** (1968) Oxidative degradation of aromatic hydrocarbons by microorganisms - I. Enzymatic formation of catechol from benzene. *Biochemistry* 7, 2653-2662.

**Gieg L. M., Kolhatkar R. V., McInerney M. J., Tanner R. S., Harris S. H. J., Sublette K. L., and Suflita J. M.** (1999) Intrinsic bioremediation of petroleum hydrocarbons in a gas condensate-contaminated aquifer. *Environmental Science and Technology* 33(15), 2550-2560.

**Gillham R. W., Robin M. L., and Ptacek C. J.** (1990) A device for in situ determination of geochemical transport parameters 1. Retardation. *Ground Water* 28(6), 666-672.

**Gillham R. W., Starr R. C., and Miller D. J.** (1990) A device for in situ determination of geochemical transport parameters 2. Biochemical reactions. *Ground Water* 28(6), 858-862.

**Godsy M., Warren E., Cozzarelli I. M., Bekins B. A., and Eganhouse R. P.** (2000) Determining BTEX biodegradation rates using in site microcosms at the Bemidji site, Minnesota: Trials and tribulations, pp. 9. U.S. Geological Survey.

**Grathwohl P. and Kleineidam S.** (1995) Impact of heterogeneous aquifer materials on sorption capacities and sorption dynamics of organic contaminants. *Groundwater Quality: Remediation and Protection*, 79-86.

**Grathwohl P.** (1998) *Diffusion in natural porous media: Contaminant transport, sorption/ desorption and dissolution kinetics*. Kluwer.

**Grathwohl P.** (2000) Time scales of remediation of complex source zones. *Contaminated Site Remediation: From source zones to ecosystems*, 635-650.

**Grathwohl P., Eberhardt C., Klenk I., Rügner H., and Maier U.** (2000) Transverse vertical dispersivity in aquifer materials: Implications on mass transfer across the capillary fringe and the length of steady state plumes. *Groundwater 2000*, 19-20.

**Grbic-Galic D. and Vogel T. M.** (1987) Transformation of toluene and benzene by mixed methanogenic cultures. *Applied and Environmental Microbiology* 53, 254-260.

**Grifoll M., Selifonov S. A., and Chapman P. J.** (1994) Evidence for a novel pathway in the degradation of Fluorene by *Pseudomonas* sp. strain F274. *Applied and Environmental Microbiology* 60, 2438-2449.

**Harbaugh A. W. and McDonald M. G.** (1996) User's documentation for MODFLOW-96, an update to the U.S. Geological Survey modular finite-difference ground-water flow model, pp. 63. U.S. Geological Survey.

**Harrington R. R., Poulson S. R., Drever J. I., Colberg P. J. S., and Kelly E. F.** (1999) Carbon isotope systematics of monoaromatic hydrocarbons: Vaporization and adsorption experiments. *Organic Geochemistry* 30(8a), 765-775.

**Heraty L. J., Fuller M. E., Huang L., Abrajano T., and Sturchio N. C.** (1999) Isotopic fractionation of carbon and chloride by microbial degradation of dichloromethane. *Organic Geochemistry* 30, 793-799.

**Herfort M., Ptak T., Hümmer O., Teutsch G., and Dahmke A.** (1998) Testfeld Süd: Einrichtung der Testfeldinfrastruktur und Erkundung hydraulisch-hydrogeochemischer Parameter des Grundwasserleiters. *Grundwasser* 3(4), 159-166.

**Herfort M.** (2000) Reactive transport of organic compounds within a heterogeneous porous aquifer. Ph. D., Universität Tübingen.

**Hoefs J**. (1997) *Stable isotope geochemistry.* Springer Verlag.

**Höhener P., Hunkeler D., Hess A., Bregnyrd T., and Zeyer J.** (1998) Methodology for the evaluation of engineered in situ bioremediation: Lessons from a case study. *Journal of Microbiological Methods* 32(2), 179-192.

**Holder T. and Teutsch G.** (1999) Bestimmung der Schadstoffimmission im Grundwasser – Verfahrensprinzip, Messung und Modellierung, pp. 31-65. Schriftenreihe des Amtes für Umweltschutz.

**Holder T. and Teutsch G.** (2000) Standortmodell für das Gelände des ehemaligen Gaswerks, Talstr. 117, Stuttgart-Ost, pp. 19. University of Tübingen.

**Howard P. H., Boethling R. S., Jarvis W. F., Meylan W. M., and Michalenki E. M.** (1991) *Handbook of environmental degradation rates.* Lewis Publishers.

**Huang L., Sturchio N. C., Abrajano T., Heraty L. J., and Holt B. D.** (1999) Carbon and chlorine isotope fractionation of chlorinated aliphatic hydrocarbons by evaporation. *Organic Geochemistry* 30(8a), 777-785.

**Hunkeler D., Aravena R., and Butler B. J.** (1999) Monitoring microbial dechlorination of tetrachloroethene (PCE) in groundwater using compound-specific stable carbon isotope ratios: Microcosm and field studies. *Environmental Science and Technology* 33, 2733-2738.

**Hunkeler D., Butler B. J., Aravena R., and Barker J. F.** (2001) Monitoring biodegradation of Methyl tert-Butyl Ether (MTBE) using compound-specific carbon isotope analysis. *Environmental Science and Technology* 35, 676-681.

**Jackson A. W., Pardue J. H., and Araujo R.** (1996) Monitoring crude oil mineralization in salt marches: Use of stable carbon isotope ratios. *Environmental Science and Technology* 30, 1139-1144.

**Jäger R. and Liedl R.** (2000) Prognose dr Sorptionskinetik organischer Schadstoffe in heterogenem Aquifermaterial. *Grundwasser* 5(2), 57-66.

**Journel A. J.** (1989) *Fundamentals of geostatistics in five lessons.* AGU.

**Kao C. M. and Wang Y. S**. (2001) Field investigation of natural attenuation and intrinsic biodegradation rates at an underground storage tank site. *Environmental Geology* 40(4-5), 622-631.

**Karapanagioti H. K., Kleineidam S., Sabatini D. A., Grathwohl P., and Ligouis B.** (2000) Impacts of heterogeneous organic matter on phenanthrene sorption: Equilibrium and kinetic studies with aquifer material. *Environmental Science and Technology* 34, 406-414.

**Karapanagioti H. K., Gossard C. M., Strevett K. A., Kolar R. L., and Sabatini D. A.** (2001) Model coupling intraparticle diffusion / sorption, nonlinear sorption, and biodegradation processes. *Journal of Contaminant Hydrology* 48, 1-21.

**Karickhoff S. W., Brown D. S., and Scott T. A.** (1979) Sorption of hydrophobic pollutants on natural sediments. *Water Resources Research* 13(241-248).

**Keely J. F.** (1989) Performance evaluation of pump-and-treat remediations. R.S. Kerr Environmental Research Laboratory.

**Kelley M., Magar V., Brauning S., Shahan J., and Wickramanayake G. B.** (1996) Intrinsic bioremediation of petroleum hydrocarbons, pp. 53. Naval Facilities Engineering Service Center.

**Kelley C. A., Hammer B. T., and Coffin R. B**. (1997) Concentrations and stable isotope values of BTEX in gasoline-contaminated groundwater. *Environmental Science and Technology* 31(9), 2469-2472.

118

**King M. W. G., Barker J. F., and Hamilton K. A.** (1995) Natural attenuation of coal tar organics in groundwater. In *Intrinsic bioremediation* (ed. R. E. Hinchee, J. T. Wilson, and D. C. Downey), pp. 171-180. Battelle.

**King M. W. G., Barker J. F., Devlin J. T., and Butler B. J.** (1999) Migration and natural fate of a coal tar creosote plume 2. Mass balance and biodegradation indicators. *Journal of Contaminant Hydrology* 39, 281-307.

**Kleineidam S., Rügner H., and Grathwohl P.** (1999a) Impact of grain scale heterogeneity on slow sorption kinetics. *Environmental Toxicology and chemistry* 18(8), 1673-1678.

**Kleineidam S., Rügner H., Ligouis B., and Grathwohl P.** (1999b) Organic matter facies and equilibrium sorption of phenanthrene. *Environmental Science and Technology* 33(10), 1637-1644.

**Köhne M. and Piotrowski J. A.** (1995) Geostatistische Regionalisierung von Durchlässigkeitsbeiwerten (kf) im testfeld Belau, Schleswig-Holstein: 2D-, 3D- und Indikator-Kriging. *Zeitschrift der deutschen geologischen Gesellschaft* 146, 399-414.

**Landmeyer J. E., Vroblesky D. A., and Chapelle F. H.** (1996) Stable carbon isotope evidence of biodegradation zonation in a shallow jet-fuel contaminated aquifer. *Environmental Science and Technology* 30(4), 1120-1128.

**Liedl, R. und Ptak, T.,** 2002. Modelling of diffusion-limited retardation of contaminants in hydraulically and lithologically non-uniform aquifers. *Journal of Contaminant Hydrology*, in review.

**Lovley D. R., Chapelle F. H., and Woodward J. C.** (1994) Use of dissolved $H_2$ concentrations to determine distribution of microbially catalyzed redox reactions in anoxic groundwater. *Environmental Science and Technology* 28(7), 1205-1210.

**Lovley D. R., Woodward J. C., and Chapelle F. H.** (1996) Rapid anaerobic benzene oxidation with a variety of chelated Fe(III) forms. *Applied and Environmental Microbiology* 62, 288-291.

**Luthy R. G., Aiken G. R., Brusseau M. L., Cunningham S. D., Gschwend S. D., Pignatello J. J., Reinhard M., Traina S. J., Weber W. J. J., and Westall J. C.** (1997) Sequestration of hydrophobic organic contaminants by geosorbents. *Environmental Science and Technology* 31(12), 3341-3347.

**Lyman W. J., Reidy P. J., and Levy B.** (1992) *Mobility and degradation of organic contaminants in subsurface environments*. C.K. Smoley.

**Mace R. E., Fisher R. S., Welch D. M., and Parra S. P.** (1997) Extend, mass, and duration of hydrocarbon plumes from leaking petroleum storage tank sites in Texas. Bureau of Economic Geology, University of Texas at Austin.

**Mackay D. and Shiu W. J.** (1977) Aqueous solubility of polynuclear hydrocarbons. *Journal of Chemical Engeneering Data* 22(4), 399-402.

**Mackay D. M., Freyberg D. L., Roberts P. V., and Cherry J. A.** (1986) A natural gradient experiment on solute transport in a sand aquifer, 1. Approach and overview of plume movement. *Water Resources Research* 22(13), 2017-1029.

**Mackay D. M. and Cherry J. A.** (1989) Groundwater contamination: Pump-and-treat remediation. *Environmental Science and Technology* 23(6), 630-636.

**Mackay D., Shiu W. Y., and Ma K. C.** (1992) *Illustrated handbook of physical-chemical properties and environmental fate for organic chemicals*. Lewis.

**Madsen E. L.** (1991) Determining in situ biodegradation: facts and challenges. *Environmental Science and Technology* 25(10), 1663-1673.

**Major D. W., Mayfield C. I., and Barker J. F.** (1988) Biotransformation of benzene by denitrification in aquifer sand. *Ground Water* 26, 8-14.

**Martin H.** (1997) Entwicklung von Dosimetern zur Beprobung von Schadstoffen im Grundwasser. Diplomarbeit, Eberhard-Karls-Universität Tübingen.

**McAllister P. M. and Chiang C. Y.** (1994) A practical approach to evaluating natural attenuation of contaminants in ground water. *Ground Water Monitoring and Remediation*, 161-173.

**McNally D. L., Mihelcic J. R., and Lueking D. R.** (1998) Biodegradation of three- and four-ring polycyclic aromatic hydrocarbons under aerobic and denitrifying conditions. *Environmental Science and Technology* 32, 2633-2639.

**Meckenstock R. U., Morasch B., Warthmann R., Schink B., Annweiler E., Michaelis W., and Richnow H. H.** (1999) 13C/12C isotope fractionation of aromatic hydrocarbons during microbial degradation. *Journal of Environmental Microbiology* 1, 409-414.

**Meckenstock R. U., Annweiler E., Michaelis W., Richnow H. H., and Schink B.** (2000) Anaerobic naphtalene degradation by a sulfate-reducing enrichment culture. *Applied and Environmental Microbiology* 66(7), 2743-2747.

**Meckenstock R. U., Morasch B., Kästner M., Vieth A., and Richnow H. H.** (2001) Assessment of bacterial degradation activities in the environment by analysis of stable carbon isotope fractionation. *Environmental Microbiology* submitted.

**Merkel P**. (1996) *Desorption and release of polycyclic aromatic hydrocarbons (PAH) from contaminated aquifer material*. Universität Tübingen.

**Miller M. M., Wasik S., Huang G.-L., Shiu W.-Y., and MacKay D. M.** (1985) Relationship between octanol-water partition coefficient and aqueous solubility. *Environmental Science and Technology* 19(6), 522-529.

**MOC.** (1995) A practical approach to evaluating intrinsic bioremediation of petroleum hydrocarbons in groundwater, pp. variously paginated. Mobil Business Resources Corporation, Remediation Support: Groundwater Technology Group, Environmental Health and Safety Department and the Environmental Health Risk Assessment Group.

**Morasch B., Richnow H. H., Schink B., and Meckenstock R. U.** (2001) Stable hydrogen and carbon isotope fractionation during microbial toluene degradation: Mechanistic and environmental aspects. *Environmental Microbiology* submitted.

**Morkin M., Devlin J. F., and Barker J. F.** (2000) In situ treatment of a mixed contaminant plume. *Journal of Contaminant Hydrology* 45, 283-302.

**MPCA.** (1997) Draft guidelines: Natural attenuation of chlorinated solvents in groundwater. Minnesota Pollution Control Agency.

**Murarka I. P.** (1995) Site management trends and research directories in the United States of America. *Land Contamination and Reclamation* 3(4), 1995.

**NCDWM.** (2000) Guidance on developing a monitored natural attenuation remediation proposal for chlorinated organics in ground water, pp. 18. North Carolina Division of Waste Management.

**NHDES.** (1999) Guidelines for selection of natural attenuation for groundwater restoration, pp. 17. New Hampshire Department of Environmental Services: Waste Management Devision.

**Nielsen P. H. and Christiansen T. H.** (1994) Variability of biological degadation of aromatic hydrocarbons in an aerobic aquifer determined by laboratory batch experiments. *Journal of Contaminant Hydrology* 15, 305-320.

**Nielsen P. H., Bierge P. L., Nielsen P., Smith P., and Christensen T. H.** (1996) In situ and laboratory determined first-order degradation rate constants of specific organic compounds in an aerobic aquifer. *Environmental Science and Technology* 30, 31-37.

**NJDEP.** (1995) Technical requirements for site remediation, and classification exception areas. New Jersey Department of Environmental Protection.

**NRC.** (1993) *In situ bioremediation: When does it work?* National Academy Press.

**NRC.** (1994) *Alternatives for groundwater cleanup*. National Academy Press.

**NRC.** (2000) *Natural attenuation for groundwater remediation*. National Academic Press.

**Nyer E. K. and Duffin M. E.** (1997) The state of the art of bioremediation. *Ground Water Monitoring and Remediation* Spring, 64-69.

**Pennington J. C., Zakikhani M., and Harrelson D. W.** (1999) Monitored natural attenuation of Explosives in groundwater - Environmental Security technology certification program completion report, pp. 234. U.S. Army Corps of Engineer Waterways Experiment Station.

**Peter A.** (2001) Assessing natural attenuation at field scale by stochastic reactive transport modelling. Ph.D., University of Tübingen.

**Phelps C. D., Kerkhof L. J., and Young L. Y**. (1998) Molecular characterization of a sulfate-reducing consortium which mineralizes benzene. *FEMS Microbiological Ecology* 27, 269-279.

**Ptak T.** (1997) Evaluation of reactive transport processes in a heterogeneous porous aquifer within a non-parametric numerical stochastic transport modelling framework based on sequential indicator simulation of categorical variables. In *geoENV I - Geostatistics for Environmental Applications* (ed. A. Soares), pp. 153-164. Kluwer Academic Publishers.

**Ptak T., Schwarz R., Holder T., and Teutsch G.** (2000a) Ein neues integrales Verfahren zur Quantifizierung der Grundwasserimmission, Teil II: Numerische Lösung und Anwendung in Eppelheim. *Grundwasser* 4(5), 176-183.

**Ptak T., Schirmer M., and Teutsch G.** (2000b) Development and performance of a new multilevel groundwater sampling system. In *Risk, regulatory and monitoring considerations: Remediation of chlorinated and recalcitrant compounds* (ed. G. B. Wickramanayake, A. R. Gavaskar, M. E. Kelley, and K. W. Nehring), pp. 95-102. Batelle Press.

**Ptak T. and Teutsch G.** (2000) Development and application of an integral investigation method for the characterization of groundwater contamination. *Contaminated Soil (ConSoil) 2000*, 198-205.

**Rice D. W., Grose R. D., Michaelsen J. C., Dooher B. P., MacQueen D. H., Cullen S. J., Kastenberg W. E., Everett L. G., and Marino M. A.** (1995) California leaking underground fuel tank (LUFT) historical case analyses. California State Water Resources Control Board.

**Rieß J.** (1998) Beprobung gaswerksspezifischer Schadstoffe im Abstrom des "Testfeld Süd". Diplomarbeit, Eberhard-Kalrs-Universität Tübingen.

**Rockne K. J. and Strand S. E.** (1998) Biodegradation of Bicyclic and Polycyclic Aromatic Hydrocarbons in Anaerobic Enrichments. *Environmental Science and Technology* 32, 3962-3967.

Rooney-Varga J. N., Anderson R. T., Fraga J. L., Ringelberg D., and Lovley D. R. (1999) Microbial communities associated with anaerobic benzene degradation in a petroleum-contaminated aquifer. *Applied and Environmental Microbiology* 65(7), 3056-3063.

Rügner H., Kleineidam S., and Grathwohl P. (1997) Sorptionsverhalten organischer Schadstoffe in heterogenem Aquifermaterial am Beispiel des Phenanthrens. *Grundwasser*(3), 133-138.

Rügner H., Kleineidam S., and Grathwohl P. (1999) Long term sorption kinetics of phenanthrene in aquifer materials. *Environmental Science and Technology* 33(10), 1645-1651.

Schettler I. (1998) Tiefenhorizontierte Schadstoffverteilung im Grundwasser eines Gaswerkstandorts ("Testfeld Süd"): Felderprobung von Multilevelpackersystemen und Laborversuche zur Eignung von Probenahmeschläuchen. Diplomarbeit, Eberhard-Karls-Universität Tübingen.

Schiedek T., Teutsch G., and Grathwohl P. (1997) Literaturstudie zum natürlichen Rückhalt / Abbau von Schadstoffen im Grundwasser. Landesanstalt für Umweltschutz Baden Würtemberg.

Schirmer M., Jones I., Teutsch G., and Lerner D. N. (1995) Development and testing of multiport sock samplers for groundwater. *Journal of Hydrology* 171, 239-257.

Schmitt R., Langguth H.-R., Püttmann W., Rohns H. P., Eckert P., and Schubert J. (1996) Biodegradation of aromatic hydrocarbons under anoxic conditions in a shallow sand and gravel aquifer of the Lower Rhine Valley, Germany. *Organic Geochemistry* 25(1/2), 41-50.

Schüth C. (1994) *Sorptionskinetik und Transportverhalten von polyzyklischen aromatischen Kohlenwasserstoffen (PAK) im Grundwasser – Laborversuche.* Eberhard-Karls-Universität Tübingen.

Schwarz R. (2001) Grundwasser-Gefährdungsabschätzung durch Emmissions- und Immissionsmessungen an Deponien und Altlasten. Ph.D. Thesis, Universität Tübingen.

Schwarzenbach R. P., Gschwend P. M., and Imboden D. M. (1993) *Environmental organic chemistry*. John Wiley & Sons.

Semprini L., Kitanidis P. K., Kampell D. H., and Wilson J. T. (1995) Anaerobic transformation of chlorinated aliphatic hydrocarbons in a sand aquifer based on spatial chemical distribution. *Water Resources Research* 31(4), 1051-1062.

Sherwood-Lollar B., Slater G. F., Sleep B., Witt M., Klecka G. M., Harkness M., and Spivack J. (2001) Stable carbon isotope evidence for intrinsic bioremediation of tetrachloroethene and trichloroethene at Area 6, Dover Air Force Base. *Environmental Science and Technology* 35, 261-269.

Shiklomanov I. A. (1997) *Comprehensive assessment of the freshwater resources of the world*. WMO and Stockholm Environmental Institut.

Sinke A., Heimovaara T., Tonnaer H., and v.Veen J. (1999) Promoting the acceptance of monitored natural attenuation. In *NATO/CCMS pilot study on contaminated land and groundwater*, pp. 32-37.

Slater G. F., Damster H. S., Sherwood-Lollar B., and Ahad J. (1999) Headspace analysis: A new application for isotopic characterisation of dissolved organic contaminants. *Environmental Science and Technology* 33, 190-194.

Slater G. F., Sherwood-Lollar B., Sleep B. E., and Edwards E. A. (2001) Variability in carbon isotopic fractionation during biodegradation of chlorinated ethenes: Implication for field applications. *Environmental Science and Technology* 35, 901-907.

Stehmeier L. G., Francis M. M., Jack T. R., Diegor E., Winsor L., and Abrajano T. A. (1999) Field and in vitro evidence for in-situ bioremediation using compound-specific $^{13}C/^{12}C$ ratio monitoring. *Organic Geochemistry* 30(8a), 821-833.

Sturchio N. C., Clausen J. L., Heraty L. J., Huang L., Holt B. D., and Abrajano A. J. (1998) Chlorine isotope investigation of natural attenuation of trichloroethene in an aerobic aquifer. *Environmental Science and Technology* 32(20), 3037-3042.

Sudicky E. A. (1986) A natural tracer experiment on solute transport in a sand aquifer: Spatial variability of hydraulic conductivity and its role in the dispersion process. *Water Resources Research* 22(13), 2069-2082.

Teutsch G. (1990) Stochastic groundwater transport simulations using replacement transfer functions (RTFs). *Geostatistical Methods: Recent Developments and Applications in Surface and Subsurface Hydrology*, 32-39.

Teutsch G., Hofmann B., and Ptak T. (1991) Non parametric simulation of groundwater transport processes in highly heterogeneous formations. *Int. Conf. and Workshop on Transport and Mass Exchange Processes in Sand and Gravel Aquifers*, 224-241.

Teutsch G. (1999) Controlled Reactive Zones (CORZO): The implementation of innovative plume control techniques for groundwater protection at contaminated sites. In *NATO/CCMS pilot study on contaminated land and groundwater*, pp. 43-52.

Teutsch G., Ptak T., Schwarz R., and Holder T. (2000) Ein neues integrales Verfahren zur Quantifizierung der Grundwasserimmission, Teil I: Beschreibung der Grundlagen. *Grundwasser* 4(5), 170-175.

**Thierrin J., Davis G. B., and Barber C.** (1995) A ground-water tracer test with deuterated compounds for monitoring in situ biodegradation and retardation of aromatic hydrocarbons. *Ground Water* 33(3), 469-475.

**Thierrin J., Davis G. B., Barber C., Patterson B. M., Probac F., Power T. R., and Lambert M.** (1993) Natural degradation rates of BTEX compounds and naphthalene in a sulphate reducing groundwater environment. *Hydrological Sciences* 38(4), 309-322.

**Travis C. C. and Doty C. B.** (1990) Can contaminated aquifers at Superfund Sites be remediated? *Environmental Science and Technology* 24(1), 1464-1466.

**USAirForce.** (1999) Natural attenuation of fuel hydrocarbons - performance and cost results from multiple Air Force demonstration sites, pp. 67. U.S. Air Force Center for Environmental Excellence.

**USDOE.** (1998) Technical guidance for the long-term monitoring of natural attenuation remedies at Department of Energy sites, pp. 22. U.S. Department of Energy, Office of Environmental Restoration.

**USEPA.** (1994) Methods for monitoring pump-and-treat performance, pp. 102. United States Environmental Protection Agency.

**USEPA.** (1997) Draft Region 4 suggested practice for evaluation of a site for natural attenuation. U.S. Environmental Protection Agency Region 4.

**USEPA.** (1999) Use of monitored natural attenuation at superfund, RCRA corrective action, and underground storage tank sites, pp. 32. Office of Solid Wast and Emergency Response.

**USEPA**. (2000) National priority site fact sheet - Love Canal, pp. 1. United States Environmental protection Agency.

**USEPA.** (2000) Semi-Annual Corrective Action Activity Report. U.S. EPA Office of Underground Storage Tanks.

**USEPA.** (2001) Cost analyses for selected groundwater cleanup projects: Pump and Treat Systems and Permeable Reactive Barriers, pp. 23. United States Environmental Protection Agency.

**Verschueren K.** (1983) *Handbook of environmental data on organic chemicals*. Van Nostrand Reinhold Company.

**Vogel T. M. and Grbic-Galic D.** (1986) Incorporation of oxygen from water into toluene and benzene during anaerobic fermentive transformation. *Applied and Environmental Microbiology* 52, 200-202.

**Vroblesky D. A. and Chapelle F. H.** (1994) Temporal and spatial changes of terminal electron-accepting processes in a petroleum hydrocarbon-contaminated aquifer and the significance for contaminant biodegradation. *Water Resources Research* 30(5), 1561-1570.

**Wakao N. and Smith J. M.** (1962) Diffusion in catalyst pellets. *Chemical Engineering Science* 17, 825-834.

**Ward J. A. M., Ahad J. M. E., Lacrampe-Couloume G., Slater G. F., Edwards E. A., and Sherwood Lollar B.** (2000) Hydrogen isotope fractionation during methanogenic degradation of toluene: Potential for direct verification of bioremediation. *Environmental Science and Technology* 34, 4577-4581.

**WDNR.** (1997) Interim Guidance for selection of natural attenuation for groundwater restoration and case closure under section nr. 726.05(2)(b), pp. 26. Wisconsin Department of Natural Resources.

**WDNR.** (1999) Interim Guidance on natural attenuation for petroleum releases, pp. 109. Wisconsin Department of Natural Resources.

**Weiner J. M. and Lovley D. R.** (1998) Anaerobic benzene degradation in petroleum-contaminated aquifer sediments after inculation with a benzene-oxidizing enrichment. *Applied and Environmental Microbiology* 64(2), 775-778.

**Wiedemeier T. H., Wilson J. T., Kampbell D. H., Miller R. N., and Hansen J. E.** (1995) Technical protocol for implementing intrinsic remediation with long-term monitoring for natural attenuation of fuel contaminent dissolved in groundwater, pp. 295. U.S. Air Force Center for Environmental Excellence.

**Wiedemeier T. H., Swanson M. A., Wilson J. T., Kampbell D. H., Miller R. N., and Hansen J. E.** (1996) Approximation of biodegradation rate constants for monoaromatic hydrocarbons (BTEX) in ground water. *Ground Water Monitoring and Remediation* 16(3), 186-194.

**Wiedemeier T. H., Swanson M. A., Moutoux D. E., Gordon E. K., Wilson J. T., Wilson B. H., Kambell D. H., Hansen J. E., Haas P., and Chapelle F. H.** (1997) Technical protocol for evaluating natural atenuation of chlorinated solvents in groundwater. Air Force Center for Environmental Excellence.

**Wiedemeier T. H. and Chapelle F. H.** (1998) Techical guidelines for evaluation monitored natural attenuation at naval and marine corps facilities. US Navy.

**Wiedemeier T. H., Swanson M. A., Moutoux D. E., Gordon E. K., Wilson J. T., Wilson B. H., Kampell D. H., Haas P. E., Miller R. N., Hansen J. E., and Chapelle F. H.** (1998) Technical protocol for evaluationg natural attenuation of chlorinated solvents in ground water, pp. 248. EPA Office of Research and Development.

**Wiedemeier T. H., Rifai H. S., Newell C. J., and Wilson J. T.** (1999) *Natural attenuation of fuels and chlorinated solvents in the subsurface*. Wiley.

**Wilson T. W., Cho J. S., and Wilson B. H.** (2000) Natural attenuation of MTBE in the subsurface under methanogenic conditions. U.S. Environmental Protection Agency.

**World Bank.** (1999) *Groundwater: Legal and policy perspectives: Proceedings of a World Bank seminar*. World Bank.

**Yalkowski S. H. and Valvani S. C.** (1979) Solubilities and partitioning - 2. Relationships between aqueous solubilities, partitioning coefficients and molecular surface areas of rigid aromatic hydrocarbons. *Journal of Chemical Engeneering Data* 24(2), 127-129.

**Yang X., Barden M., Mickelson G., Delwiche J., Portz E., Steinhermer C., Alvarez G., Hagerty D., Petrofske S., and Misky D.** (1995) Natural attenuation study in Wisconsin and Illinois, pp. 20.

**Yang X., Jeng C. Y., Kremesec V., Fisher B., and Cuurran L.** (1995) Natural attenuation as a remedial alternative. Amoco.

**Zamfirescu D. and Grathwohl P.** (1998) Schadstoffemission durch Desorption und Lösung standortspezifischer organischer Verbindungen im Schadenszentrum, Testfeld Süd. *Grundwasser* 3(4), 167-174.

**Zamfirescu D.** (2000) Release and fate of specific organic contaminants at a former gasworks site. Ph.D., Universität Tübingen.

**Zamfirescu D. and Grathwohl P.** (2001) Occurrence and attenuation of specific organic compounds in the groundwater plume at a former gasworks site. *Journal of Contaminant Hydrology* in print.

**Zheng C.** (1990) MT3D: A modular three-dimensional transport model for simulation of advection, dispersion and chemical reactions of contaminants in groundwater systems, pp. 170.

124

# 11 Appendix – Field data

This appendix presents the field data (organic solutes, inorganic solutes, physical groundwater parameters) which was measured at the former manufactured gas plant "Testfeld Süd" located in SW-Germany during the field experiments conducted for this thesis. The data shown is used for the mass flux and natural attenuation quantifications discussed in Chapters 4 and 5 of this thesis. The numerical mass flux quantification based on this data can be found in Chapter 7, whereas the reactive transport modelling at the MGP site is documented in Chapter 8.

Table 11.1 gives an overview of the duration and pumping rate of the pumping test, which were performed in two consecutive pumping campaigns in November 1999 and April 2000.

At well NT01 two pumping campaigns were conducted to investigate the influence of the extended pumping test on the geo-chemical conditions and contaminant distributions in the investigated aquifer system as discussed in more detail in Chapter 4 of this thesis.

Table 11.1: Overview of the pumping tests

| Well | Start | End | Duration [h] | Pumping rate [$m^3\ s^{-1}$] |
|---|---|---|---|---|
| B42 | 06/11/99 10:00 | 12/11/99 10:00 | 144 | 4.08E-03 |
| B41 | 16/11/99 10:00 | 20/11/98 10:00 | 96 | 4.16E-03 |
| P2 | 23/11/99 11:30 | 27/11/98 11:30 | 96 | 1.44E-03 |
| P1 | 30/11/98 11:00 | 04/12/98 11:00 | 96 | 4.85E-03 |
| NT01 [1] | 13/04/99 11:00 | 16/04/99 00:30 | 61.5 | 2.95E-03 |
| B72 | 21/04/99 11:00 | 23/04/99 12:15 | 49.25 | 1.03E-04 |
| B73 | 27/04/99 11:00 | 30/04/99 11:50 | 72.83 | 2.33E-03 |
| B2069 | 03/05/99 11:45 | 08/05/99 12:00 | 120.25 | 2.52E-03 |
| NT01 [2] | 10/05/99 11:15 | 15/05/99 12:05 | 120.83 | 3.46E-03 |

[1] First pumping campaign
[2] Second pumping campaign performed 24 days after the first

## 11.1 Organic solute concentrations

### 11.1.1 Well B42

| Detection limit | < 0.01 | < 0.01 | < 0.01 | < 0.01 | < 0.01 | < 0.01 | < 0.01 | < 0.01 | < 0.01 | < 0.01 | < 0.01 | < 0.01 | < 0.01 |
|---|---|---|---|---|---|---|---|---|---|---|---|---|---|
| Pumping time | Benzene | Toluene | Ethylbenzene | p-Xylene | o-Xylene | Iso-PB | PB | 1,3,5-TMB | 1,2,4-TMB | BF | 1,2,3-TMB | Indane | Indane |
| [s] | [µg l$^{-1}$] | [µg l$^{-1}$] | [µg l$^{-1}$] | [µg l$^{-1}$] | [µg l$^{-1}$] | [µg l$^{-1}$] | [µg l$^{-1}$] | [µg l$^{-1}$] | [µg l$^{-1}$] | [µg l$^{-1}$] | [µg l$^{-1}$] | [µg l$^{-1}$] | [µg l$^{-1}$] |
| 300 | n.d. | 1.42 | 0.08 | 0.22 | n.d. | 0.45 | 0.14 | 0.04 | 0.03 | n.d. | n.d. | n.d. | 0.52 |
| 2700 | n.d. | 0.34 | 0.07 | 0.17 | n.d. | 0.57 | 0.17 | 0.04 | 0.02 | n.d. | 0.38 | n.d. | 0.37 |
| 5400 | n.d. | 0.27 | 0.06 | 0.19 | n.d. | 0.76 | 0.18 | 0.05 | 0.03 | n.d. | 0.40 | n.d. | 0.40 |
| 12600 | 0.19 | 0.78 | 0.09 | 0.17 | 0.05 | 1.43 | 0.18 | 0.07 | 0.05 | n.d. | 0.01 | n.d. | 0.42 |
| 21600 | 0.37 | 0.74 | 0.10 | 0.18 | 0.05 | 2.26 | 0.21 | 0.08 | 0.05 | n.d. | n.d. | n.d. | 0.43 |
| 36000 | 0.79 | 0.75 | 0.09 | 0.20 | n.d. | 2.49 | 0.20 | 0.07 | 0.05 | n.d. | 0.01 | n.d. | 0.39 |
| 48600 | 1.30 | 0.67 | 0.09 | 0.17 | n.d. | 2.78 | 0.21 | 0.07 | 0.05 | n.d. | n.d. | n.d. | 0.39 |
| 68400 | 2.24 | 0.66 | 0.10 | 0.19 | n.d. | 3.20 | 0.22 | 0.08 | 0.05 | n.d. | n.d. | n.d. | 0.39 |
| 86400 | 3.22 | 0.67 | 0.10 | 0.20 | 0.08 | 3.33 | 0.23 | 0.08 | 0.06 | n.d. | n.d. | n.d. | 0.41 |
| 111600 | 4.61 | 0.65 | 0.10 | 0.20 | 0.08 | 3.62 | 0.26 | 0.10 | 0.07 | n.d. | n.d. | n.d. | 0.36 |
| 136800 | 6.09 | 0.66 | 0.12 | 0.20 | 0.09 | 3.80 | 0.26 | 0.09 | 0.07 | n.d. | n.d. | n.d. | 0.42 |
| 165600 | 8.18 | 0.69 | 0.18 | 0.25 | 0.09 | 4.26 | 0.28 | 0.10 | 0.08 | n.d. | n.d. | n.d. | 0.40 |
| 194400 | 8.25 | 0.13 | 0.16 | 0.22 | 0.08 | 3.51 | 0.24 | 0.09 | 0.07 | n.d. | n.d. | n.d. | 0.37 |
| 226800 | 10.60 | 0.14 | 0.24 | 0.24 | 0.05 | 3.65 | 0.26 | 0.10 | 0.07 | n.d. | n.d. | n.d. | 0.38 |
| 259200 | 12.11 | 0.13 | 0.32 | 0.27 | 0.09 | 3.41 | 0.31 | 0.10 | 0.08 | n.d. | n.d. | n.d. | 0.37 |
| 298800 | 15.09 | 0.15 | 0.52 | 0.30 | 0.10 | 3.44 | 0.33 | 0.10 | 0.07 | n.d. | n.d. | n.d. | 0.34 |
| 338400 | 16.56 | 0.15 | 0.75 | 0.34 | 0.08 | 3.35 | 0.35 | 0.09 | 0.06 | n.d. | n.d. | n.d. | 0.29 |
| 385200 | 19.11 | 0.13 | 1.09 | 0.41 | 0.11 | 3.35 | 0.32 | 0.10 | 0.07 | n.d. | n.d. | n.d. | 0.33 |
| 432000 | 22.27 | 0.13 | 1.57 | 0.46 | 0.14 | 3.13 | 0.38 | 0.10 | 0.08 | n.d. | 0.02 | n.d. | 0.36 |
| 468900 | 23.81 | 0.12 | 1.93 | 0.48 | 0.12 | 3.41 | 0.42 | 0.10 | 0.07 | n.d. | 0.02 | n.d. | 0.39 |
| 518400 | 25.00 | 0.13 | 2.34 | 0.50 | 0.12 | 3.03 | 0.71 | 0.15 | 0.11 | n.d. | 0.03 | n.d. | 0.07 |
| n.d. = no detect | | | | | | | | | | | | | |

Table 11.2. Concentration-time series of petroleum hydrocarbons at well B42

Table 11.3: Concentration-time series of polycyclic aromatic hydrocarbons at well B42

| Detection limit | < 0.02 | < 0.02 | < 0.02 | < 0.02 | < 0.02 | < 0.02 | < 0.02 | < 0.02 | < 0.02 | < 0.02 | < 0.02 | < 0.02 | < 0.02 | < 0.02 | < 0.02 |
|---|---|---|---|---|---|---|---|---|---|---|---|---|---|---|---|
| Pumping time | NAP | ACY | ACE | FLR | PHE | ANT | FLN | PYR | B(a)A | CHR | B(b.k)F | B(a)P | Indeno | D(ah)A | B(ghi)P |
| [s] | [µg l$^{-1}$] | [µg l$^{-1}$] | [µg l$^{-1}$] | [µg l$^{-1}$] | [µg l$^{-1}$] | [µg l$^{-1}$] | [µg l$^{-1}$] | [µg l$^{-1}$] | [µg l$^{-1}$] | [µg l$^{-1}$] | [µg l$^{-1}$] | [µg l$^{-1}$] | [µg l$^{-1}$] | [µg l$^{-1}$] | [µg l$^{-1}$] |
| 300 | 0.46 | 3.93 | 154.56 | n.d. | 0.06 | 0.33 | 0.11 | 0.08 | 0.05 | 0.07 | n.d. | n.d. | n.d. | n.d. | n.d. |
| 2700 | 0.12 | 4.66 | 188.49 | n.d. | 0.05 | 0.40 | 0.06 | 0.03 | n.d. | n.d. | n.d. | n.d. | n.d. | n.d. | n.d. |
| 5400 | 0.11 | 4.91 | 197.86 | n.d. | 0.04 | 0.44 | 0.05 | 0.03 | n.d. | n.d. | n.d. | n.d. | n.d. | n.d. | n.d. |
| 12600 | 0.11 | 5.00 | 199.99 | n.d. | 0.04 | 0.44 | 0.05 | 0.03 | n.d. | n.d. | n.d. | n.d. | n.d. | n.d. | n.d. |
| 21600 | 0.13 | 5.24 | 213.60 | n.d. | 0.04 | 0.46 | 0.06 | 0.02 | n.d. | n.d. | n.d. | n.d. | n.d. | n.d. | n.d. |
| 36000 | 0.12 | 5.68 | 224.15 | n.d. | 0.03 | 0.47 | 0.06 | 0.02 | n.d. | n.d. | n.d. | n.d. | n.d. | n.d. | n.d. |
| 48600 | 0.13 | 5.51 | 231.36 | n.d. | 0.04 | 0.48 | 0.06 | 0.03 | n.d. | n.d. | n.d. | n.d. | n.d. | n.d. | n.d. |
| 68400 | 0.13 | 5.66 | 231.32 | n.d. | 0.04 | 0.50 | 0.06 | 0.02 | n.d. | n.d. | n.d. | n.d. | n.d. | n.d. | n.d. |
| 86400 | 0.13 | 5.97 | 245.37 | n.d. | 0.05 | 0.50 | 0.06 | 0.02 | n.d. | n.d. | n.d. | n.d. | n.d. | n.d. | n.d. |
| 111600 | 0.13 | 5.86 | 248.37 | n.d. | 0.05 | 0.47 | 0.07 | 0.02 | n.d. | n.d. | n.d. | n.d. | n.d. | n.d. | n.d. |
| 136800 | 0.14 | 5.58 | 251.00 | n.d. | 0.07 | 0.47 | 0.06 | 0.02 | n.d. | n.d. | n.d. | n.d. | n.d. | n.d. | n.d. |
| 165600 | 0.14 | 6.18 | 260.22 | n.d. | 0.03 | 0.49 | 0.07 | 0.02 | n.d. | n.d. | n.d. | n.d. | n.d. | n.d. | n.d. |
| 194400 | 0.14 | 4.88 | 246.25 | n.d. | 0.04 | 0.40 | 0.06 | 0.02 | n.d. | n.d. | n.d. | n.d. | n.d. | n.d. | n.d. |
| 226800 | 0.14 | 4.79 | 251.87 | n.d. | 0.03 | 0.40 | 0.06 | 0.02 | n.d. | n.d. | 0.02 | n.d. | n.d. | n.d. | n.d. |
| 259200 | 0.15 | 5.14 | 248.91 | n.d. | 0.05 | 0.42 | 0.07 | 0.02 | n.d. | n.d. | n.d. | n.d. | n.d. | n.d. | n.d. |
| 298800 | 0.15 | 5.21 | 253.65 | n.d. | 0.04 | 0.43 | 0.07 | 0.02 | n.d. | n.d. | 0.01 | n.d. | n.d. | n.d. | n.d. |
| 338400 | 0.15 | 5.13 | 251.25 | n.d. | 0.06 | 0.41 | 0.07 | 0.02 | n.d. | n.d. | n.d. | n.d. | n.d. | n.d. | n.d. |
| 385200 | 0.15 | 5.26 | 256.93 | n.d. | 0.03 | 0.40 | 0.07 | 0.02 | n.d. | n.d. | 0.01 | n.d. | n.d. | n.d. | n.d. |
| 432000 | 0.15 | 4.83 | 244.08 | n.d. | 0.05 | 0.38 | 0.07 | 0.02 | n.d. | n.d. | n.d. | n.d. | n.d. | n.d. | n.d. |
| 468900 | 0.15 | 5.19 | 249.61 | n.d. | 0.05 | 0.39 | 0.07 | 0.02 | n.d. | n.d. | n.d. | n.d. | n.d. | n.d. | n.d. |
| 518400 | 0.16 | 5.19 | 261.76 | n.d. | 0.06 | 0.40 | 0.07 | 0.02 | n.d. | n.d. | n.d. | n.d. | n.d. | n.d. | n.d. |

n.d. = no detect

## 11.1.2  Well P2

| Detection limit | < 0.01 | < 0.01 | < 0.01 | < 0.01 | < 0.01 | < 0.01 | < 0.01 | < 0.01 | < 0.01 | < 0.01 | < 0.01 | < 0.01 | < 0.01 |
|---|---|---|---|---|---|---|---|---|---|---|---|---|---|
| Pumping time | Benzene | Toluene | Ethylbenzene | p-Xylene | o-Xylene | Iso-PB | PB | 1,3,5-TMB | 1,2,4-TMB | BF | 1,2,3-TMB | Indane | Indane |
| [s] | $[\mu g\, l^{-1}]$ | $[\mu g\, l^{-1}]$ | $[\mu g\, l^{-1}]$ | $[\mu g\, l^{-1}]$ | $[\mu g\, l^{-1}]$ | $[\mu g\, l^{-1}]$ | $[\mu g\, l^{-1}]$ | $[\mu g\, l^{-1}]$ | $[\mu g\, l^{-1}]$ | $[\mu g\, l^{-1}]$ | $[\mu g\, l^{-1}]$ | $[\mu g\, l^{-1}]$ | $[\mu g\, l^{-1}]$ |
| 300 | 0.85 | 2.07 | 1.75 | 4.34 | 1.73 | 0.59 | 0.24 | 1.92 | 3.12 | 2.66 | 0.97 | 5.89 | 16.53 |
| 7200 | 0.42 | 0.95 | 0.66 | 1.77 | 0.64 | 0.52 | 0.17 | 0.83 | 1.16 | 1.07 | 0.40 | 2.63 | 6.28 |
| 14400 | 0.60 | 0.78 | 0.44 | 1.22 | 0.51 | 0.53 | 0.15 | 0.59 | 0.95 | 0.74 | 0.29 | 1.87 | 4.45 |
| 28800 | 2.47 | 0.46 | 0.35 | 0.90 | 0.39 | 0.62 | 0.17 | 0.45 | 0.66 | 0.51 | 0.19 | 1.45 | 2.91 |
| 57600 | 6.52 | 0.37 | 0.37 | 0.76 | 0.23 | 0.87 | 0.19 | 0.33 | 0.45 | 0.36 | 0.13 | 1.10 | 2.12 |
| 86400 | 8.85 | 0.20 | 0.43 | 0.44 | 0.24 | 0.93 | 0.27 | 0.26 | 0.32 | 0.19 | 0.09 | 0.77 | 1.20 |
| 122400 | 12.57 | 0.21 | 0.61 | 0.56 | 0.17 | 1.27 | 0.20 | 0.17 | 0.24 | 0.20 | 0.07 | 0.68 | 1.13 |
| 172800 | 16.28 | 0.28 | 0.98 | 0.62 | 0.14 | 1.47 | 0.27 | 0.19 | 0.20 | 0.21 | 0.07 | 0.64 | 1.16 |
| 223200 | 19.19 | 0.30 | 1.35 | 0.66 | 0.18 | 1.90 | 0.25 | 0.15 | 0.17 | 0.15 | 0.05 | 1.40 | 0.91 |
| 284400 | 20.54 | 0.29 | 1.62 | 0.68 | 0.16 | 1.94 | 0.39 | 0.16 | 0.17 | 0.18 | 0.06 | 1.51 | 0.88 |
| 345600 | 21.43 | 0.24 | 1.75 | 0.69 | 0.21 | 2.25 | 0.31 | 0.11 | 0.13 | 0.13 | 0.05 | 1.37 | 0.80 |

n.d. = no detect

| Detection limit | < 0.02 | < 0.02 | < 0.02 | < 0.02 | < 0.02 | < 0.02 | < 0.02 | < 0.02 | < 0.02 | < 0.02 | < 0.02 | < 0.02 | < 0.02 | < 0.02 | < 0.02 |
|---|---|---|---|---|---|---|---|---|---|---|---|---|---|---|---|
| Pumping time | NAP | ACY | ACE | FLR | PHE | ANT | FLN | PYR | B(a)A | CHR | B(b.k)F | B(a)P | Indeno | D(ah)A | B(ghi)P |
| [s] | $[\mu g\, l^{-1}]$ | $[\mu g\, l^{-1}]$ | $[\mu g\, l^{-1}]$ | $[\mu g\, l^{-1}]$ | $[\mu g\, l^{-1}]$ | $[\mu g\, l^{-1}]$ | $[\mu g\, l^{-1}]$ | $[\mu g\, l^{-1}]$ | $[\mu g\, l^{-1}]$ | $[\mu g\, l^{-1}]$ | $[\mu g\, l^{-1}]$ | $[\mu g\, l^{-1}]$ | $[\mu g\, l^{-1}]$ | $[\mu g\, l^{-1}]$ | $[\mu g\, l^{-1}]$ |
| 300 | 156.64 | 4.24 | 92.58 | 2.70 | 2.29 | 0.52 | 0.36 | 0.22 | 0.05 | 0.05 | 0.06 | n.d. | n.d. | n.d. | n.d. |
| 7200 | 47.82 | 5.40 | 211.31 | 1.49 | 1.19 | 0.33 | 0.26 | 0.15 | 0.12 | 0.13 | 0.28 | 0.17 | n.d. | n.d. | 0.13 |
| 14400 | 38.56 | 6.24 | 267.91 | 1.30 | 0.96 | 0.27 | 0.13 | 0.06 | 0.03 | 0.04 | 0.07 | 0.06 | n.d. | n.d. | n.d. |
| 28800 | 23.70 | 6.34 | 283.53 | 1.11 | 0.80 | 0.27 | 0.12 | 0.05 | n.d. | n.d. | 0.06 | n.d. | n.d. | n.d. | n.d. |
| 57600 | 14.28 | 6.57 | 292.72 | 0.74 | 0.66 | 0.26 | 0.11 | 0.04 | n.d. | n.d. | n.d. | n.d. | n.d. | n.d. | n.d. |
| 86400 | 9.82 | 6.20 | 295.29 | 0.60 | 0.60 | 0.25 | 0.10 | 0.04 | n.d. | n.d. | n.d. | n.d. | n.d. | n.d. | n.d. |
| 122400 | 7.70 | 6.44 | 300.29 | 0.52 | 0.55 | 0.26 | 0.10 | 0.03 | n.d. | n.d. | n.d. | n.d. | n.d. | n.d. | n.d. |
| 172800 | 5.93 | 6.90 | 298.27 | 0.44 | 0.44 | 0.24 | 0.07 | 0.02 | n.d. | n.d. | n.d. | n.d. | n.d. | n.d. | n.d. |
| 223200 | 4.65 | 6.34 | 293.21 | 0.40 | 0.40 | 0.23 | 0.09 | 0.02 | n.d. | n.d. | n.d. | n.d. | n.d. | n.d. | n.d. |
| 284400 | 3.82 | 6.17 | 296.00 | 0.39 | 0.37 | 0.23 | 0.08 | 0.02 | n.d. | n.d. | n.d. | n.d. | n.d. | n.d. | n.d. |
| 345600 | 3.21 | 6.03 | 296.44 | 0.40 | 0.31 | 0.20 | 0.09 | 0.02 | n.d. | n.d. | n.d. | n.d. | n.d. | n.d. | n.d. |

n.d. = no detect

Table 11.4: Concentration-time series of petroleum hydrocarbons at well P2 (left)

Table 11.5: Concentration-time series of polycyclic aromatic hydrocarbons at well P2 (right)

### 11.1.3 Well B41

At well B41 no petroleum hydrocarbons could be detected.

Table 11.6: Concentration-time series of polycyclic aromatic hydrocarbons at well B41

| Detection limit | < 0.02 | < 0.02 | < 0.02 | < 0.02 | < 0.02 | < 0.02 | < 0.02 | < 0.02 | < 0.02 | < 0.02 | < 0.02 | < 0.02 | < 0.02 | < 0.02 | < 0.02 |
|---|---|---|---|---|---|---|---|---|---|---|---|---|---|---|---|
| Pumping time | NAP | ACY | ACE | FLR | PHE | ANT | FLN | PYR | B(a)A | CHR | B(b.k)F | B(a)P | Indeno | D(ah)A | B(ghi)P |
| [s] | [µg l-1] | [µg l-1] | [µg l-1] | [µg l-1] | [µg l-1] | [µg l-1] | [µg l-1] | [µg l-1] | [µg l-1] | [µg l-1] | [µg l-1] | [µg l-1] | [µg l-1] | [µg l-1] | [µg l-1] |
| 300 | 0.03 | 0.12 | 4.46 | n.d. | 0.09 | 0.03 | 0.12 | 0.11 | 0.04 | 0.10 | n.d. | n.d. | n.d. | n.d. | n.d. |
| 1800 | 0.02 | 0.07 | 2.40 | n.d. | 0.03 | 0.01 | n.d. | n.d. | n.d. | n.d. | n.d. | n.d. | n.d. | n.d. | n.d. |
| 4500 | 0.03 | 0.07 | 2.11 | n.d. | 0.03 | 0.01 | n.d. | n.d. | n.d. | n.d. | n.d. | n.d. | n.d. | n.d. | n.d. |
| 10800 | 0.03 | 0.06 | 2.03 | n.d. | 0.02 | 0.01 | n.d. | n.d. | n.d. | n.d. | n.d. | n.d. | n.d. | n.d. | n.d. |
| 17100 | 0.03 | 0.06 | 2.10 | n.d. | 0.02 | 0.02 | n.d. | n.d. | n.d. | n.d. | n.d. | n.d. | n.d. | n.d. | n.d. |
| 28800 | 0.03 | 0.06 | 2.10 | n.d. | 0.02 | 0.02 | n.d. | n.d. | n.d. | n.d. | n.d. | n.d. | n.d. | n.d. | n.d. |
| 37800 | 0.03 | 0.07 | 2.19 | n.d. | 0.02 | 0.02 | n.d. | n.d. | n.d. | n.d. | n.d. | n.d. | n.d. | n.d. | n.d. |
| 50400 | 0.03 | 0.07 | 2.23 | n.d. | 0.02 | 0.01 | n.d. | n.d. | n.d. | n.d. | n.d. | n.d. | n.d. | n.d. | n.d. |
| 68400 | 0.03 | 0.07 | 2.33 | n.d. | 0.03 | 0.01 | n.d. | n.d. | n.d. | n.d. | n.d. | n.d. | n.d. | n.d. | n.d. |
| 86400 | 0.03 | 0.08 | 2.64 | n.d. | 0.03 | 0.01 | n.d. | n.d. | n.d. | n.d. | n.d. | n.d. | n.d. | n.d. | n.d. |
| 106200 | 0.03 | 0.09 | 3.05 | n.d. | n.d. | n.d. | n.d. | n.d. | n.d. | n.d. | n.d. | n.d. | n.d. | n.d. | n.d. |
| 129600 | 0.03 | 0.10 | 3.79 | n.d. | n.d. | n.d. | n.d. | n.d. | n.d. | n.d. | n.d. | n.d. | n.d. | n.d. | n.d. |
| 154800 | 0.04 | 0.12 | 4.44 | n.d. | n.d. | n.d. | n.d. | n.d. | n.d. | n.d. | n.d. | n.d. | n.d. | n.d. | n.d. |
| 180000 | 0.03 | 0.14 | 5.32 | n.d. | 0.02 | n.d. | n.d. | n.d. | n.d. | n.d. | n.d. | n.d. | n.d. | n.d. | n.d. |
| 208800 | 0.03 | 0.15 | 6.31 | n.d. | n.d. | n.d. | n.d. | n.d. | n.d. | n.d. | n.d. | n.d. | n.d. | n.d. | n.d. |
| 241200 | 0.03 | 0.19 | 7.83 | n.d. | n.d. | n.d. | n.d. | n.d. | n.d. | n.d. | n.d. | n.d. | n.d. | n.d. | n.d. |
| 273600 | 0.06 | 0.21 | 9.22 | n.d. | 0.03 | n.d. | n.d. | n.d. | n.d. | n.d. | n.d. | n.d. | n.d. | n.d. | n.d. |
| 302400 | 0.14 | 0.54 | 23.78 | 0.02 | 0.06 | 0.04 | n.d. | n.d. | n.d. | n.d. | n.d. | n.d. | n.d. | n.d. | n.d. |
| 345600 | 0.07 | 0.27 | 12.46 | n.d. | 0.03 | 0.02 | n.d. | n.d. | n.d. | n.d. | n.d. | n.d. | n.d. | n.d. | n.d. |

n.d. = no detect

11.1.4  Well P1

At well P1 no petroleum hydrocarbons could be detected.

| Detection limit | < 0.02 | < 0.02 | < 0.02 | < 0.02 | < 0.02 | < 0.02 | < 0.02 | < 0.02 | < 0.02 | < 0.02 | < 0.02 | < 0.02 | < 0.02 | < 0.02 | < 0.02 |
|---|---|---|---|---|---|---|---|---|---|---|---|---|---|---|---|
| Pumping time | NAP | ACY | ACE | FLR | PHE | ANT | FLN | PYR | B(a)A | CHR | B(b.k)F | B(a)P | Indeno | D(ah)A | B(ghi)P |
| [s] | $[\mu g\ l^{-1}]$ | $[\mu g\ l^{-1}]$ | $[\mu g\ l^{-1}]$ | $[\mu g\ l^{-1}]$ | $[\mu g\ l^{-1}]$ | $[\mu g\ l^{-1}]$ | $[\mu g\ l^{-1}]$ | $[\mu g\ l^{-1}]$ | $[\mu g\ l^{-1}]$ | $[\mu g\ l^{-1}]$ | $[\mu g\ l^{-1}]$ | $[\mu g\ l^{-1}]$ | $[\mu g\ l^{-1}]$ | $[\mu g\ l^{-1}]$ | $[\mu g\ l^{-1}]$ |
| 300 | 1.06 | 0.18 | 1.74 | 0.06 | 0.13 | 0.02 | n.d. | n.d. | n.d. | n.d. | n.d. | n.d. | n.d. | n.d. | n.d. |
| 1800 | 0.53 | 0.11 | 0.91 | 0.04 | 0.14 | 0.05 | 0.16 | 0.16 | n.d. | 0.09 | 0.01 | 0.07 | n.d. | n.d. | n.d. |
| 4500 | 0.48 | 0.1 | 0.67 | 0.05 | 0.07 | 0.02 | n.d. | n.d. | n.d. | n.d. | n.d. | n.d. | n.d. | n.d. | n.d. |
| 10800 | 0.41 | 0.1 | 0.67 | 0.05 | 0.08 | n.d. | n.d. | n.d. | n.d. | n.d. | n.d. | n.d. | n.d. | n.d. | n.d. |
| 17100 | 0.34 | 0.08 | 0.62 | 0.05 | 0.06 | n.d. | n.d. | n.d. | n.d. | n.d. | n.d. | n.d. | n.d. | n.d. | n.d. |
| 28800 | 0.26 | 0.07 | 0.46 | 0.04 | 0.06 | n.d. | n.d. | n.d. | n.d. | n.d. | n.d. | n.d. | n.d. | n.d. | n.d. |
| 37800 | 0.29 | 0.06 | 0.52 | 0.04 | 0.04 | n.d. | n.d. | n.d. | n.d. | n.d. | n.d. | n.d. | n.d. | n.d. | n.d. |
| 50400 | 0.27 | 0.07 | 0.56 | 0.04 | 0.05 | n.d. | n.d. | n.d. | n.d. | n.d. | n.d. | n.d. | n.d. | n.d. | n.d. |
| 68400 | 0.22 | 0.06 | 0.46 | 0.04 | 0.07 | n.d. | n.d. | n.d. | n.d. | n.d. | n.d. | n.d. | n.d. | n.d. | n.d. |
| 86400 | 0.22 | 0.06 | 0.45 | 0.04 | 0.05 | n.d. | n.d. | n.d. | n.d. | n.d. | n.d. | n.d. | n.d. | n.d. | n.d. |
| 106200 | 0.19 | 0.05 | 0.48 | n.d. | 0.04 | n.d. | n.d. | n.d. | n.d. | n.d. | n.d. | n.d. | n.d. | n.d. | n.d. |
| 129600 | 0.19 | 0.04 | 0.38 | n.d. | 0.04 | n.d. | n.d. | n.d. | n.d. | n.d. | n.d. | n.d. | n.d. | n.d. | n.d. |
| 154800 | 0.15 | 0.04 | 0.37 | n.d. | n.d. | n.d. | n.d. | n.d. | n.d. | n.d. | n.d. | n.d. | n.d. | n.d. | n.d. |
| 180000 | 0.14 | 0.03 | 0.38 | n.d. | n.d. | n.d. | n.d. | n.d. | n.d. | n.d. | n.d. | n.d. | n.d. | n.d. | n.d. |
| 208800 | 0.15 | 0.04 | 0.36 | n.d. | n.d. | n.d. | n.d. | 0.11 | n.d. | n.d. | n.d. | n.d. | n.d. | n.d. | n.d. |
| 241200 | 0.16 | 0.04 | 0.45 | n.d. | n.d. | n.d. | n.d. | 0.11 | n.d. | n.d. | n.d. | n.d. | n.d. | n.d. | n.d. |
| 273600 | 0.15 | 0.03 | 0.39 | n.d. | n.d. | n.d. | n.d. | 0.12 | n.d. | n.d. | n.d. | n.d. | n.d. | n.d. | n.d. |
| 309600 | 0.15 | 0.03 | 0.43 | n.d. | n.d. | n.d. | n.d. | 0.12 | n.d. | n.d. | n.d. | n.d. | n.d. | n.d. | n.d. |
| 345600 | 0.15 | 0.04 | 0.38 | n.d. | n.d. | n.d. | n.d. | 0.12 | n.d. | n.d. | n.d. | n.d. | n.d. | n.d. | n.d. |
| n.d. = no detect | | | | | | | | | | | | | | | |

11.1.5  Well NT01 – First campaign

| Detection limit | < 0.01 | < 0.01 | < 0.01 | < 0.01 | < 0.01 | < 0.01 | < 0.01 | < 0.01 | < 0.01 | < 0.01 | < 0.01 | < 0.01 | < 0.01 |
|---|---|---|---|---|---|---|---|---|---|---|---|---|---|
| Pumping time | Benzene | Toluene | Ethylbenzene | p-Xylene | o-Xylene | Iso-PB | PB | 1,3,5-TMB | 1,2,4-TMB | BF | 1,2,3-TMB | Indane | Indane |
| [s] | [µg l$^{-1}$] | [µg l$^{-1}$] | [µg l$^{-1}$] | [µg l$^{-1}$] | [µg l$^{-1}$] | [µg l$^{-1}$] | [µg l$^{-1}$] | [µg l$^{-1}$] | [µg l$^{-1}$] | [µg l$^{-1}$] | [µg l$^{-1}$] | [µg l$^{-1}$] | [µg l$^{-1}$] |
| 900 | n.d. | 0.10 | 0.08 | 0.33 | 0.03 | 0.80 | 0.11 | 0.11 | 0.07 | 0.10 | 0.05 | 0.16 | 0.23 |
| 1800 | n.d. | 0.09 | 0.06 | 0.28 | n.d. | 0.71 | 0.09 | 0.09 | 0.09 | 0.03 | 0.02 | 0.10 | 0.11 |
| 2700 | n.d. | 0.09 | 0.06 | 0.27 | n.d. | 0.68 | 0.09 | 0.04 | 0.06 | 0.03 | 0.03 | 0.08 | 0.10 |
| 3600 | n.d. | 0.09 | 0.06 | 0.28 | n.d. | 0.72 | 0.09 | 0.09 | 0.08 | 0.03 | 0.03 | 0.09 | 0.11 |
| 5400 | n.d. | 0.08 | 0.06 | 0.27 | n.d. | 0.69 | 0.09 | 0.09 | 0.08 | 0.03 | 0.02 | 0.06 | 0.08 |
| 7200 | n.d. | 0.07 | 0.06 | 0.25 | n.d. | 0.62 | 0.08 | 0.09 | 0.08 | 0.08 | 0.03 | n.d. | 0.09 |
| 9000 | 0.05 | 0.13 | 0.12 | 0.30 | 0.07 | 0.68 | 0.14 | 0.16 | 0.14 | 0.06 | 0.10 | n.d. | 0.17 |
| 11700 | n.d. | 0.07 | 0.06 | 0.26 | n.d. | 0.64 | 0.08 | 0.09 | 0.08 | 0.02 | 0.03 | n.d. | 0.11 |
| 14400 | n.d. | 0.07 | 0.06 | 0.26 | n.d. | 0.65 | 0.09 | 0.09 | 0.08 | 0.03 | 0.03 | n.d. | 0.11 |
| 17100 | n.d. | 0.07 | 0.06 | 0.25 | n.d. | 0.62 | 0.08 | 0.09 | 0.08 | 0.02 | n.d. | n.d. | 0.10 |
| 20700 | n.d. | 0.05 | 0.05 | 0.20 | n.d. | 0.50 | 0.07 | 0.07 | 0.07 | 0.39 | n.d. | n.d. | 0.11 |
| 24300 | n.d. | 0.05 | 0.05 | 0.21 | n.d. | 0.52 | 0.07 | 0.07 | 0.06 | 0.18 | n.d. | n.d. | 0.07 |
| 27900 | n.d. | 0.05 | 0.05 | 0.20 | n.d. | 0.51 | 0.07 | 0.07 | 0.06 | 0.13 | n.d. | n.d. | 0.07 |
| 32400 | n.d. | 0.05 | 0.05 | 0.20 | n.d. | 0.52 | 0.07 | 0.07 | 0.06 | 0.13 | n.d. | n.d. | 0.06 |
| 36000 | n.d. | 0.09 | 0.06 | 0.21 | 0.03 | 0.54 | 0.08 | 0.08 | 0.08 | 0.08 | n.d. | n.d. | 0.13 |
| 41400 | n.d. | 0.08 | 0.05 | 0.21 | n.d. | 0.53 | 0.07 | 0.07 | 0.07 | 0.02 | n.d. | n.d. | 0.07 |
| 45900 | n.d. | 0.08 | 0.05 | 0.20 | n.d. | 0.52 | 0.07 | 0.09 | 0.06 | 0.01 | n.d. | n.d. | 0.07 |
| 51300 | n.d. | 0.07 | 0.05 | 0.20 | n.d. | 0.52 | 0.07 | 0.07 | 0.06 | 0.02 | n.d. | n.d. | 0.07 |
| 70812 | n.d. | 0.07 | 0.05 | 0.20 | n.d. | 0.52 | 0.07 | 0.07 | 0.06 | 0.02 | n.d. | n.d. | 0.08 |
| 77400 | n.d. | 0.07 | 0.06 | 0.21 | 0.02 | 0.66 | 0.08 | 0.09 | 0.08 | 0.07 | n.d. | n.d. | 0.12 |
| 84600 | n.d. | 0.07 | 0.06 | 0.21 | n.d. | 0.65 | 0.08 | 0.08 | 0.07 | 0.02 | n.d. | n.d. | 0.08 |
| 91800 | n.d. | 0.07 | 0.05 | 0.20 | n.d. | 0.66 | 0.07 | 0.08 | 0.07 | 0.02 | n.d. | n.d. | 0.09 |
| 99000 | n.d. | 0.07 | 0.06 | 0.21 | 0.02 | 0.66 | 0.08 | 0.08 | 0.08 | 0.03 | n.d. | n.d. | 0.08 |
| 107100 | n.d. | 0.07 | 0.06 | 0.20 | n.d. | 0.64 | 0.07 | 0.08 | 0.07 | 0.02 | n.d. | n.d. | 0.07 |
| 117288 | n.d. | 0.08 | 0.07 | 0.22 | 0.04 | 0.62 | 0.09 | 0.10 | 0.09 | 0.12 | n.d. | n.d. | 0.13 |
| 123300 | n.d. | 0.07 | 0.06 | 0.21 | 0.03 | 0.60 | 0.08 | 0.09 | 0.08 | 0.03 | n.d. | n.d. | 0.08 |
| 132300 | n.d. | 0.07 | 0.06 | 0.21 | 0.03 | 0.61 | 0.08 | 0.09 | 0.08 | 0.03 | n.d. | n.d. | 0.08 |
| 159300 | n.d. | 0.07 | 0.06 | 0.20 | 0.02 | 0.60 | 0.08 | 0.09 | 0.08 | 0.03 | n.d. | n.d. | 0.08 |
| 169200 | n.d. | 0.07 | 0.06 | 0.22 | 0.03 | 0.64 | 0.08 | 0.09 | 0.08 | 0.03 | n.d. | n.d. | 0.08 |
| 179100 | n.d. | 0.08 | 0.07 | 0.22 | 0.03 | 0.64 | 0.09 | 0.09 | 0.08 | 0.08 | 0.01 | n.d. | 0.13 |
| 189900 | n.d. | 0.07 | 0.06 | 0.21 | 0.02 | 0.61 | 0.08 | 0.09 | 0.08 | 0.02 | n.d. | n.d. | 0.08 |
| 200700 | n.d. | 0.07 | 0.06 | 0.21 | 0.02 | 0.63 | 0.08 | 0.09 | 0.08 | 0.02 | n.d. | n.d. | 0.08 |
| 211500 | n.d. | 0.07 | 0.06 | 0.22 | 0.02 | 0.65 | 0.08 | 0.09 | 0.08 | 0.01 | n.d. | n.d. | 0.07 |
| 221400 | n.d. | 0.07 | 0.06 | 0.21 | 0.02 | 0.63 | 0.08 | 0.09 | 0.07 | 0.02 | n.d. | n.d. | 0.07 |
| n.d. = no detect | | | | | | | | | | | | | |

Table 11.8: Concentration-time series of petroleum hydrocarbons at well NT01 – First campaign

| Detection limit<br>Pumping time<br>[s] | < 0.02<br>NAP<br>[µg l⁻¹] | < 0.02<br>ACY<br>[µg l⁻¹] | < 0.02<br>ACE<br>[µg l⁻¹] | < 0.02<br>FLR<br>[µg l⁻¹] | < 0.02<br>PHE<br>[µg l⁻¹] | < 0.02<br>ANT<br>[µg l⁻¹] | < 0.02<br>FLN<br>[µg l⁻¹] | < 0.02<br>PYR<br>[µg l⁻¹] | < 0.02<br>B(a)A<br>[µg l⁻¹] | < 0.02<br>CHR<br>[µg l⁻¹] | < 0.02<br>B(b.k)F<br>[µg l⁻¹] | < 0.02<br>B(a)P<br>[µg l⁻¹] | < 0.02<br>Indeno<br>[µg l⁻¹] | < 0.02<br>D(ah)A<br>[µg l⁻¹] | < 0.02<br>B(ghi)P<br>[µg l⁻¹] |
|---|---|---|---|---|---|---|---|---|---|---|---|---|---|---|---|
| 900 | 1.43 | 3.38 | 157.32 | 0.21 | 0.58 | 0.16 | 0.14 | 0.07 | n.d. | n.d. | 0.11 | n.d. | n.d. | n.d. | n.d. |
| 1800 | 1.40 | 4.12 | 194.99 | 0.24 | 0.64 | 0.14 | 0.14 | 0.06 | n.d. | n.d. | 0.06 | n.d. | n.d. | n.d. | n.d. |
| 2700 | 1.21 | 4.19 | 197.86 | 0.23 | 0.61 | 0.15 | 0.14 | 0.06 | n.d. | n.d. | 0.08 | n.d. | n.d. | n.d. | n.d. |
| 3600 | 1.01 | 3.66 | 175.08 | 0.21 | 0.62 | 0.11 | 0.14 | 0.06 | n.d. | n.d. | n.d. | n.d. | n.d. | n.d. | n.d. |
| 5400 | 0.95 | 4.00 | 192.75 | 0.23 | 0.61 | 0.12 | 0.12 | 0.05 | n.d. | n.d. | 0.04 | n.d. | n.d. | n.d. | n.d. |
| 7200 | 0.90 | 4.25 | 201.41 | 0.23 | 0.65 | 0.13 | 0.15 | 0.07 | n.d. | n.d. | 0.08 | n.d. | n.d. | n.d. | n.d. |
| 9000 | 0.84 | 3.99 | 195.05 | 0.21 | 0.56 | 0.12 | 0.11 | 0.05 | n.d. | n.d. | 0.04 | n.d. | n.d. | n.d. | n.d. |
| 11700 | 0.63 | 4.12 | 196.23 | 0.22 | 0.60 | 0.12 | 0.13 | 0.06 | n.d. | n.d. | 0.00 | n.d. | n.d. | n.d. | n.d. |
| 14400 | 0.59 | 3.89 | 191.50 | 0.21 | 0.55 | 0.11 | 0.11 | 0.04 | n.d. | n.d. | 0.07 | n.d. | n.d. | n.d. | n.d. |
| 17100 | 0.56 | 3.85 | 191.72 | 0.21 | 0.53 | 0.11 | 0.11 | 0.05 | n.d. | n.d. | 0.06 | n.d. | n.d. | n.d. | n.d. |
| 20700 | 0.54 | 3.99 | 193.24 | 0.22 | 0.63 | 0.13 | 0.14 | 0.06 | n.d. | n.d. | n.d. | n.d. | n.d. | n.d. | n.d. |
| 24300 | 0.51 | 4.08 | 198.48 | 0.21 | 0.53 | 0.11 | 0.10 | 0.03 | n.d. | n.d. | 0.05 | n.d. | n.d. | n.d. | n.d. |
| 27900 | 0.48 | 3.93 | 194.54 | 0.23 | 0.66 | 0.15 | 0.13 | 0.05 | n.d. | n.d. | n.d. | n.d. | n.d. | n.d. | n.d. |
| 32400 | 0.46 | 3.98 | 191.53 | 0.23 | 0.74 | 0.15 | 0.14 | 0.07 | n.d. | n.d. | n.d. | n.d. | n.d. | n.d. | n.d. |
| 36000 | 0.44 | 4.01 | 195.16 | 0.21 | 0.53 | 0.14 | 0.12 | 0.04 | n.d. | n.d. | 0.06 | n.d. | n.d. | n.d. | n.d. |
| 41400 | 0.41 | 3.92 | 191.57 | 0.18 | 0.42 | 0.11 | 0.08 | 0.03 | n.d. | n.d. | 0.05 | n.d. | n.d. | n.d. | n.d. |
| 45900 | 0.39 | 3.87 | 189.88 | 0.20 | 0.55 | 0.13 | 0.11 | 0.05 | n.d. | n.d. | n.d. | n.d. | n.d. | n.d. | n.d. |
| 51300 | 0.38 | 3.98 | 191.11 | 0.20 | 0.60 | 0.14 | 0.13 | 0.05 | n.d. | n.d. | n.d. | n.d. | n.d. | n.d. | n.d. |
| 70812 | 0.34 | 3.70 | 187.79 | 0.20 | 0.53 | 0.12 | 0.13 | 0.05 | n.d. | n.d. | n.d. | n.d. | n.d. | n.d. | n.d. |
| 77400 | 0.33 | 3.87 | 187.47 | 0.18 | 0.45 | 0.13 | 0.09 | 0.04 | n.d. | n.d. | n.d. | n.d. | n.d. | n.d. | n.d. |
| 84600 | 0.33 | 3.79 | 180.47 | 0.21 | 0.64 | 0.15 | 0.13 | 0.07 | n.d. | n.d. | n.d. | n.d. | n.d. | n.d. | n.d. |
| 91800 | 0.31 | 3.76 | 183.60 | 0.18 | 0.41 | 0.12 | 0.08 | 0.03 | n.d. | n.d. | n.d. | n.d. | n.d. | n.d. | n.d. |
| 99000 | 0.32 | 3.87 | 187.94 | 0.20 | 0.55 | 0.12 | 0.11 | 0.04 | n.d. | n.d. | n.d. | n.d. | n.d. | n.d. | n.d. |
| 107100 | 0.29 | 3.76 | 184.82 | 0.18 | 0.44 | 0.13 | 0.09 | 0.04 | n.d. | n.d. | n.d. | n.d. | n.d. | n.d. | n.d. |
| 117288 | 0.30 | 3.81 | 187.01 | 0.20 | 0.54 | 0.15 | 0.13 | 0.05 | n.d. | n.d. | n.d. | n.d. | n.d. | n.d. | n.d. |
| 123300 | 0.30 | 3.77 | 189.61 | 0.21 | 0.61 | 0.16 | 0.15 | 0.06 | n.d. | n.d. | n.d. | n.d. | n.d. | n.d. | n.d. |
| 132300 | 0.29 | 3.71 | 187.17 | 0.19 | 0.54 | 0.13 | 0.11 | 0.04 | n.d. | n.d. | n.d. | n.d. | n.d. | n.d. | n.d. |
| 159300 | 0.27 | 3.58 | 178.31 | 0.18 | 0.46 | 0.11 | 0.09 | 0.04 | n.d. | n.d. | n.d. | n.d. | n.d. | n.d. | n.d. |
| 169200 | 0.26 | 3.71 | 182.99 | 0.17 | 0.47 | 0.12 | 0.10 | 0.04 | n.d. | n.d. | n.d. | n.d. | n.d. | n.d. | n.d. |
| 179100 | 0.25 | 3.64 | 180.46 | 0.17 | 0.40 | 0.09 | 0.08 | 0.03 | n.d. | n.d. | n.d. | n.d. | n.d. | n.d. | n.d. |
| 189900 | 0.26 | 3.65 | 184.06 | 0.20 | 0.64 | 0.15 | 0.13 | 0.06 | n.d. | n.d. | n.d. | n.d. | n.d. | n.d. | n.d. |
| 200700 | 0.24 | 3.58 | 178.63 | 0.19 | 0.50 | 0.10 | 0.10 | 0.04 | n.d. | n.d. | n.d. | n.d. | n.d. | n.d. | n.d. |
| 211500 | 0.25 | 3.57 | 179.74 | 0.19 | 0.60 | 0.12 | 0.13 | 0.06 | n.d. | n.d. | n.d. | n.d. | n.d. | n.d. | n.d. |
| 221400 | 0.24 | 3.60 | 181.03 | 0.15 | 0.41 | 0.11 | 0.09 | 0.03 | n.d. | n.d. | n.d. | n.d. | n.d. | n.d. | n.d. |

n.d. = no detect

Table 11.9. Concentration-time series of polycyclic aromatic hydrocarbons at well NT01 – First campaign

Table 11.10: Concentration-time series of petroleum hydrocarbons at well NT01 – Second campaign

| Detection limit | < 0.01 | < 0.01 | < 0.01 | < 0.01 | < 0.01 | < 0.01 | < 0.01 | < 0.01 | < 0.01 | < 0.01 | < 0.01 | < 0.01 | < 0.01 |
|---|---|---|---|---|---|---|---|---|---|---|---|---|---|
| Pumping time | Benzene | Toluene | Ethyl-benzene | p-Xylene | o-Xylene | Iso-PB | PB | 1,3,5-TMB | 1,2,4-TMB | BF | 1,2,3-TMB | Indane | Indane |
| [s] | [µg l$^{-1}$] | [µg l$^{-1}$] | [µg l$^{-1}$] | [µg l$^{-1}$] | [µg l$^{-1}$] | [µg l$^{-1}$] | [µg l$^{-1}$] | [µg l$^{-1}$] | [µg l$^{-1}$] | [µg l$^{-1}$] | [µg l$^{-1}$] | [µg l$^{-1}$] | [µg l$^{-1}$] |
| 299 | n.d. | 0.06 | 0.04 | 0.21 | n.d. | 0.52 | 0.08 | 0.08 | 0.07 | 0.06 | 0.03 | n.d. | 0.10 |
| 1800 | n.d. | 0.06 | 0.04 | 0.22 | n.d. | 0.54 | 0.08 | 0.08 | 0.07 | 0.02 | 0.03 | n.d. | 0.07 |
| 3600 | n.d. | 0.06 | 0.04 | 0.21 | n.d. | 0.52 | 0.07 | 0.08 | 0.06 | 0.02 | 0.03 | n.d. | 0.06 |
| 6300 | n.d. | 0.06 | 0.04 | 0.22 | n.d. | 0.53 | 0.07 | 0.08 | 0.07 | 0.02 | 0.03 | n.d. | 0.06 |
| 9000 | n.d. | 0.06 | 0.05 | 0.22 | n.d. | 0.55 | 0.07 | 0.08 | 0.07 | 0.02 | 0.03 | n.d. | 0.06 |
| 12600 | n.d. | 0.07 | 0.05 | 0.23 | 0.03 | 0.55 | 0.08 | 0.09 | 0.08 | 0.09 | 0.05 | n.d. | 0.10 |
| 17100 | n.d. | 0.05 | 0.05 | 0.22 | n.d. | 0.52 | 0.07 | 0.08 | 0.07 | 0.03 | 0.03 | n.d. | 0.07 |
| 21600 | n.d. | 0.05 | 0.05 | 0.22 | n.d. | 0.53 | 0.08 | 0.09 | 0.07 | 0.03 | 0.03 | n.d. | 0.06 |
| 27000 | n.d. | 0.05 | 0.04 | 0.22 | n.d. | 0.54 | 0.07 | 0.09 | 0.07 | 0.03 | 0.03 | n.d. | 0.06 |
| 32400 | n.d. | 0.06 | 0.05 | 0.23 | n.d. | 0.55 | 0.08 | 0.09 | 0.07 | 0.02 | 0.03 | n.d. | 0.06 |
| 38700 | n.d. | 0.07 | 0.06 | 0.24 | 0.03 | 0.63 | 0.09 | 0.10 | 0.08 | 0.11 | 0.05 | n.d. | 0.11 |
| 46512 | n.d. | 0.06 | 0.05 | 0.23 | 0.02 | 0.62 | 0.08 | 0.09 | 0.07 | 0.04 | 0.04 | n.d. | 0.07 |
| 69300 | n.d. | 0.06 | 0.05 | 0.22 | n.d. | 0.62 | 0.08 | 0.09 | 0.07 | 0.03 | 0.03 | n.d. | 0.07 |
| 80100 | n.d. | 0.06 | 0.05 | 0.23 | n.d. | 0.63 | 0.08 | 0.09 | 0.07 | 0.03 | 0.03 | n.d. | 0.06 |
| 90000 | n.d. | 0.06 | 0.05 | 0.22 | n.d. | 0.63 | 0.08 | 0.09 | 0.07 | 0.03 | 0.03 | n.d. | 0.05 |
| 98100 | n.d. | 0.06 | 0.04 | 0.21 | n.d. | 0.59 | 0.07 | 0.09 | 0.07 | 0.07 | 0.03 | n.d. | 0.10 |
| 108900 | n.d. | 0.06 | 0.04 | 0.20 | n.d. | 0.58 | 0.07 | 0.08 | 0.07 | 0.02 | 0.03 | n.d. | 0.06 |
| 119700 | n.d. | 0.06 | 0.04 | 0.21 | n.d. | 0.60 | 0.07 | 0.08 | 0.07 | 0.02 | 0.03 | n.d. | 0.06 |
| 131400 | n.d. | 0.06 | 0.04 | 0.20 | n.d. | 0.58 | 0.07 | 0.08 | 0.07 | 0.02 | 0.03 | n.d. | 0.06 |
| 156600 | n.d. | 0.06 | 0.04 | 0.20 | n.d. | 0.58 | 0.07 | 0.08 | 0.07 | 0.02 | 0.03 | n.d. | 0.06 |
| 170100 | n.d. | 0.06 | 0.05 | 0.20 | n.d. | 0.57 | 0.07 | 0.08 | 0.07 | 0.09 | 0.04 | n.d. | 0.10 |
| 183600 | n.d. | 0.05 | 0.04 | 0.20 | n.d. | 0.56 | 0.07 | 0.08 | 0.06 | 0.03 | 0.03 | n.d. | 0.06 |
| 199800 | n.d. | 0.06 | 0.04 | 0.20 | n.d. | 0.57 | 0.07 | 0.08 | 0.06 | 0.03 | 0.03 | n.d. | 0.07 |
| 213300 | n.d. | 0.05 | 0.04 | 0.19 | n.d. | 0.56 | 0.07 | 0.08 | 0.06 | 0.03 | 0.03 | n.d. | 0.07 |
| 243900 | n.d. | 0.05 | 0.04 | 0.18 | n.d. | 0.54 | 0.06 | 0.08 | 0.06 | 0.03 | 0.03 | n.d. | 0.05 |
| 261900 | n.d. | 0.06 | 0.04 | 0.18 | n.d. | 0.51 | 0.07 | 0.08 | 0.07 | 0.04 | 0.04 | n.d. | 0.09 |
| 276588 | n.d. | 0.05 | 0.04 | 0.19 | n.d. | 0.55 | 0.07 | 0.08 | 0.07 | 0.02 | 0.03 | n.d. | 0.05 |
| 296100 | n.d. | 0.06 | 0.04 | 0.20 | n.d. | 0.58 | 0.07 | 0.08 | 0.07 | 0.01 | 0.03 | n.d. | 0.05 |
| 334800 | n.d. | 0.05 | 0.04 | 0.19 | n.d. | 0.56 | 0.07 | 0.08 | 0.07 | 0.02 | 0.03 | n.d. | 0.06 |
| 352800 | n.d. | 0.06 | 0.05 | 0.20 | n.d. | 0.58 | 0.07 | 0.08 | 0.07 | 0.02 | 0.03 | n.d. | 0.05 |
| 373500 | n.d. | 0.05 | 0.04 | 0.18 | n.d. | 0.55 | 0.06 | 0.08 | 0.07 | 0.06 | 0.03 | n.d. | 0.09 |
| 392112 | n.d. | 0.05 | 0.04 | 0.16 | n.d. | 0.53 | 0.06 | 0.07 | 0.06 | 0.01 | 0.03 | n.d. | 0.05 |
| 434988 | n.d. | 0.05 | 0.04 | 0.18 | n.d. | 0.52 | 0.07 | 0.08 | 0.07 | 0.08 | 0.03 | n.d. | 0.08 |

n.d. = no detect

Table 11.11: Concentration-time series of polycyclic aromatic hydrocarbons at well NT01 – Second campaign

| Detection limit | < 0.02 | < 0.02 | < 0.02 | < 0.02 | < 0.02 | < 0.02 | < 0.02 | < 0.02 | < 0.02 | < 0.02 | < 0.02 | < 0.02 | < 0.02 | < 0.02 | < 0.02 |
|---|---|---|---|---|---|---|---|---|---|---|---|---|---|---|---|
| Pumping time | NAP | ACY | ACE | FLR | PHE | ANT | FLN | PYR | B(a)A | CHR | B(b.k)F | B(a)P | Indeno | D(ah)A | B(ghi)P |
| [s] | [µg l$^{-1}$] | [µg l$^{-1}$] | [µg l$^{-1}$] | [µg l$^{-1}$] | [µg l$^{-1}$] | [µg l$^{-1}$] | [µg l$^{-1}$] | [µg l$^{-1}$] | [µg l$^{-1}$] | [µg l$^{-1}$] | [µg l$^{-1}$] | [µg l$^{-1}$] | [µg l$^{-1}$] | [µg l$^{-1}$] | [µg l$^{-1}$] |
| 299 | 0.30 | 5.06 | 184.84 | 0.19 | 0.37 | 0.30 | 0.11 | 0.05 | 0.06 | 0.04 | 0.10 | 0.00 | 0.07 | 0.00 | 0.17 |
| 1800 | 0.24 | 5.58 | 189.04 | 0.14 | 0.31 | 0.27 | 0.11 | 0.04 | 0.00 | 0.00 | 0.04 | 0.00 | 0.00 | 0.00 | 0.10 |
| 3600 | 0.23 | 4.89 | 186.83 | 0.21 | 0.42 | 0.29 | 0.13 | 0.05 | 0.00 | 0.00 | 0.05 | 0.00 | 0.00 | 0.00 | 0.06 |
| 6300 | 0.21 | 5.40 | 186.02 | 0.20 | 0.39 | 0.27 | 0.13 | 0.05 | 0.00 | 0.00 | 0.02 | 0.00 | 0.00 | 0.00 | 0.05 |
| 9000 | 0.19 | 5.54 | 188.18 | 0.15 | 0.29 | 0.26 | 0.09 | 0.03 | 0.00 | 0.00 | 0.03 | 0.00 | 0.00 | 0.00 | 0.00 |
| 12600 | 0.18 | 5.17 | 183.43 | 0.37 | 0.38 | 0.28 | 0.15 | 0.06 | 0.00 | 0.00 | 0.03 | 0.00 | 0.00 | 0.00 | 0.00 |
| 17100 | 0.19 | 5.32 | 183.82 | 0.15 | 0.27 | 0.25 | 0.08 | 0.03 | 0.00 | 0.00 | 0.02 | 0.00 | 0.00 | 0.00 | 0.00 |
| 21600 | 0.17 | 5.28 | 184.99 | 0.13 | 0.24 | 0.26 | 0.08 | 0.03 | 0.00 | 0.00 | 0.01 | 0.00 | 0.00 | 0.00 | 0.00 |
| 27000 | 0.17 | 5.25 | 184.12 | 0.17 | 0.33 | 0.25 | 0.11 | 0.04 | 0.00 | 0.00 | 0.00 | 0.00 | 0.00 | 0.00 | 0.00 |
| 32400 | 0.16 | 5.68 | 181.89 | 0.15 | 0.27 | 0.26 | 0.08 | 0.02 | 0.00 | 0.00 | 0.04 | 0.00 | 0.00 | 0.00 | 0.00 |
| 38700 | 0.16 | 5.81 | 184.69 | 0.14 | 0.28 | 0.25 | 0.08 | 0.02 | 0.00 | 0.00 | 0.00 | 0.00 | 0.00 | 0.00 | 0.00 |
| 46512 | 0.16 | 5.30 | 184.18 | 0.11 | 0.21 | 0.23 | 0.07 | 0.02 | 0.00 | 0.00 | 0.00 | 0.00 | 0.00 | 0.00 | 0.00 |
| 69300 | 0.12 | 4.89 | 156.89 | 0.07 | 0.16 | 0.19 | 0.05 | 0.01 | 0.00 | 0.00 | 0.01 | 0.00 | 0.00 | 0.00 | 0.00 |
| 80100 | 0.14 | 4.85 | 159.17 | 0.11 | 0.20 | 0.21 | 0.06 | 0.02 | 0.00 | 0.00 | 0.00 | 0.00 | 0.00 | 0.00 | 0.00 |
| 90000 | 0.13 | 4.08 | 148.63 | 0.22 | 0.14 | 0.18 | 0.05 | 0.01 | 0.00 | 0.00 | 0.01 | 0.00 | 0.00 | 0.00 | 0.00 |
| 98100 | 0.12 | 4.76 | 155.34 | 0.08 | 0.15 | 0.20 | 0.05 | 0.02 | 0.00 | 0.00 | 0.00 | 0.00 | 0.00 | 0.00 | 0.00 |
| 108900 | 0.11 | 3.86 | 144.20 | 0.18 | 0.12 | 0.16 | 0.04 | 0.00 | 0.00 | 0.00 | 0.02 | 0.00 | 0.00 | 0.00 | 0.00 |
| 119700 | 0.12 | 4.74 | 158.35 | 0.14 | 0.13 | 0.18 | 0.04 | 0.01 | 0.00 | 0.00 | 0.00 | 0.00 | 0.00 | 0.00 | 0.00 |
| 131400 | 0.13 | 5.25 | 172.06 | 0.22 | 0.14 | 0.19 | 0.05 | 0.00 | 0.00 | 0.00 | 0.03 | 0.00 | 0.00 | 0.00 | 0.00 |
| 156600 | 0.16 | 4.92 | 160.34 | 0.38 | 0.32 | 0.24 | 0.09 | 0.03 | 0.00 | 0.00 | 0.01 | 0.00 | 0.00 | 0.00 | 0.00 |
| 170100 | 0.12 | 4.99 | 163.14 | 0.07 | 0.14 | 0.20 | 0.06 | 0.01 | 0.00 | 0.00 | 0.00 | 0.00 | 0.00 | 0.00 | 0.00 |
| 183600 | 0.15 | 4.36 | 157.74 | 0.35 | 0.30 | 0.23 | 0.08 | 0.03 | 0.00 | 0.00 | 0.01 | 0.00 | 0.00 | 0.00 | 0.00 |
| 199800 | 0.12 | 5.77 | 162.93 | 0.25 | 0.18 | 0.20 | 0.05 | 0.01 | 0.00 | 0.00 | 0.00 | 0.00 | 0.00 | 0.00 | 0.00 |
| 213300 | 0.12 | 5.41 | 161.34 | 0.23 | 0.16 | 0.19 | 0.05 | 0.01 | 0.00 | 0.00 | 0.00 | 0.00 | 0.00 | 0.00 | 0.00 |
| 243900 | 0.11 | 5.13 | 149.16 | 0.07 | 0.15 | 0.18 | 0.05 | 0.00 | 0.00 | 0.00 | 0.03 | 0.00 | 0.00 | 0.00 | 0.00 |
| 261900 | 0.10 | 3.62 | 117.88 | 0.04 | 0.09 | 0.11 | 0.03 | 0.00 | 0.00 | 0.00 | 0.00 | 0.00 | 0.00 | 0.00 | 0.00 |
| 276588 | 0.12 | 5.39 | 161.49 | 0.08 | 0.17 | 0.19 | 0.05 | 0.01 | 0.00 | 0.00 | 0.00 | 0.00 | 0.00 | 0.00 | 0.00 |
| 296100 | 0.12 | 5.57 | 171.46 | 0.24 | 0.17 | 0.20 | 0.05 | 0.00 | 0.00 | 0.00 | 0.00 | 0.00 | 0.00 | 0.00 | 0.00 |
| 334800 | 0.14 | 4.97 | 171.43 | 0.25 | 0.17 | 0.21 | 0.05 | 0.01 | 0.00 | 0.00 | 0.00 | 0.00 | 0.00 | 0.00 | 0.00 |
| 352800 | 0.14 | 5.98 | 166.31 | 0.11 | 0.23 | 0.21 | 0.06 | 0.02 | 0.00 | 0.00 | 0.00 | 0.00 | 0.00 | 0.00 | 0.00 |
| 373500 | 0.13 | 5.46 | 157.29 | 0.08 | 0.16 | 0.19 | 0.06 | 0.02 | 0.00 | 0.00 | 0.00 | 0.00 | 0.00 | 0.00 | 0.00 |
| 434988 | 0.10 | 5.06 | 144.63 | 0.14 | 0.11 | 0.17 | 0.04 | 0.00 | 0.00 | 0.00 | 0.00 | 0.00 | 0.00 | 0.00 | 0.00 |

n.d. = no detect

Table 11.12: Concentration-time series of petroleum hydrocarbons at well B73

| Detection limit | < 0.01 | < 0.01 | < 0.01 | < 0.01 | < 0.01 | < 0.01 | < 0.01 | < 0.01 | < 0.01 | < 0.01 | < 0.01 | < 0.01 | < 0.01 |
|---|---|---|---|---|---|---|---|---|---|---|---|---|---|
| Pumping time | Benzene | Toluene | Ethylbenzene | p-Xylene | o-Xylene | Iso-PB | PB | 1,3,5-TMB | 1,2,4-TMB | BF | 1,2,3-TMB | Indane | Indane |
| [s] | [µg l$^{-1}$] | [µg l$^{-1}$] | [µg l$^{-1}$] | [µg l$^{-1}$] | [µg l$^{-1}$] | [µg l$^{-1}$] | [µg l$^{-1}$] | [µg l$^{-1}$] | [µg l$^{-1}$] | [µg l$^{-1}$] | [µg l$^{-1}$] | [µg l$^{-1}$] | [µg l$^{-1}$] |
| 900 | n.d. | n.d. | n.d. | 0.02 | n.d. | 0.02 | n.d. | n.d. | n.d. | 0.02 | n.d. | n.d. | 0.03 |
| 1800 | n.d. | n.d. | n.d. | 0.02 | n.d. | 0.02 | n.d. | n.d. | 0.01 | n.d. | n.d. | 0.07 | 0.01 |
| 3600 | n.d. | n.d. | n.d. | n.d. | n.d. | 0.03 | n.d. | n.d. | n.d. | n.d. | n.d. | 0.06 | 0.01 |
| 5400 | n.d. | n.d. | n.d. | n.d. | n.d. | 0.03 | n.d. | n.d. | n.d. | n.d. | n.d. | 0.06 | n.d. |
| 7200 | n.d. | n.d. | n.d. | n.d. | n.d. | 0.04 | n.d. | n.d. | n.d. | n.d. | n.d. | 0.04 | n.d. |
| 9000 | n.d. | n.d. | n.d. | n.d. | n.d. | 0.03 | n.d. | n.d. | n.d. | 0.02 | n.d. | n.d. | n.d. |
| 12600 | n.d. | n.d. | n.d. | n.d. | n.d. | 0.03 | n.d. | n.d. | n.d. | n.d. | n.d. | n.d. | n.d. |
| 15012 | n.d. | n.d. | n.d. | n.d. | n.d. | 0.04 | n.d. | n.d. | n.d. | n.d. | n.d. | n.d. | n.d. |
| 16812 | n.d. | n.d. | n.d. | n.d. | n.d. | 0.04 | n.d. | n.d. | n.d. | n.d. | n.d. | n.d. | n.d. |
| 19800 | n.d. | n.d. | n.d. | n.d. | n.d. | 0.04 | n.d. | n.d. | n.d. | n.d. | n.d. | n.d. | n.d. |
| 23400 | n.d. | n.d. | n.d. | 0.02 | n.d. | 0.06 | n.d. | n.d. | n.d. | 0.02 | n.d. | n.d. | 0.02 |
| 27000 | n.d. | n.d. | n.d. | 0.02 | n.d. | 0.07 | n.d. | n.d. | n.d. | n.d. | n.d. | n.d. | n.d. |
| 32400 | n.d. | n.d. | n.d. | 0.02 | n.d. | 0.07 | n.d. | n.d. | 0.01 | n.d. | n.d. | n.d. | n.d. |
| 36900 | n.d. | n.d. | n.d. | 0.02 | n.d. | 0.07 | n.d. | n.d. | n.d. | n.d. | n.d. | n.d. | n.d. |
| 42300 | n.d. | n.d. | n.d. | 0.02 | n.d. | 0.07 | n.d. | n.d. | n.d. | n.d. | n.d. | n.d. | n.d. |
| 47700 | n.d. | n.d. | n.d. | 0.04 | n.d. | 0.09 | 0.01 | n.d. | n.d. | 0.17 | 0.01 | n.d. | n.d. |
| 53100 | n.d. | n.d. | n.d. | n.d. | n.d. | 0.06 | n.d. | n.d. | n.d. | n.d. | n.d. | n.d. | n.d. |
| 74412 | n.d. | n.d. | n.d. | n.d. | n.d. | 0.06 | n.d. | n.d. | n.d. | n.d. | n.d. | n.d. | n.d. |
| 80100 | n.d. | n.d. | n.d. | n.d. | n.d. | 0.07 | n.d. | n.d. | n.d. | n.d. | n.d. | n.d. | n.d. |
| 87300 | n.d. | n.d. | n.d. | 0.02 | n.d. | 0.10 | n.d. | n.d. | n.d. | n.d. | n.d. | n.d. | n.d. |
| 95400 | n.d. | n.d. | n.d. | 0.03 | n.d. | 0.11 | 0.01 | n.d. | 0.01 | 0.04 | n.d. | n.d. | 0.02 |
| 102600 | n.d. | n.d. | n.d. | 0.03 | n.d. | 0.10 | n.d. | n.d. | n.d. | n.d. | n.d. | n.d. | n.d. |
| 110700 | n.d. | n.d. | n.d. | 0.03 | n.d. | 0.10 | n.d. | n.d. | n.d. | n.d. | n.d. | n.d. | n.d. |
| 119700 | n.d. | n.d. | n.d. | 0.03 | n.d. | 0.10 | n.d. | n.d. | n.d. | n.d. | n.d. | n.d. | n.d. |
| 128700 | n.d. | n.d. | n.d. | 0.03 | n.d. | 0.11 | n.d. | n.d. | n.d. | n.d. | n.d. | n.d. | n.d. |
| 137988 | 0.02 | 0.04 | 0.05 | 0.06 | n.d. | 0.13 | 0.03 | 0.02 | 0.01 | 0.04 | n.d. | n.d. | 0.03 |
| 157500 | n.d. | n.d. | n.d. | 0.03 | n.d. | 0.10 | n.d. | n.d. | n.d. | n.d. | n.d. | n.d. | n.d. |
| 169200 | n.d. | n.d. | n.d. | 0.03 | n.d. | 0.10 | n.d. | n.d. | n.d. | n.d. | n.d. | n.d. | n.d. |
| 179388 | n.d. | n.d. | n.d. | 0.03 | n.d. | 0.11 | n.d. | n.d. | n.d. | n.d. | n.d. | n.d. | n.d. |
| 189900 | n.d. | n.d. | n.d. | 0.03 | n.d. | 0.11 | n.d. | n.d. | n.d. | n.d. | n.d. | n.d. | n.d. |
| 200700 | n.d. | n.d. | n.d. | 0.04 | n.d. | 0.12 | n.d. | n.d. | 0.01 | 0.04 | n.d. | n.d. | 0.02 |
| 212400 | n.d. | n.d. | n.d. | 0.04 | n.d. | 0.12 | n.d. | n.d. | n.d. | n.d. | n.d. | n.d. | n.d. |
| 249300 | n.d. | n.d. | n.d. | 0.05 | n.d. | 0.14 | n.d. | n.d. | 0.01 | n.d. | n.d. | n.d. | n.d. |
| 262188 | n.d. | n.d. | n.d. | 0.05 | n.d. | 0.13 | n.d. | n.d. | 0.01 | n.d. | n.d. | n.d. | n.d. |
| n.d. = no detect | | | | | | | | | | | | | |

| Detection limit | < 0.02 | < 0.02 | < 0.02 | < 0.02 | < 0.02 | < 0.02 | < 0.02 | < 0.02 | < 0.02 | < 0.02 | < 0.02 | < 0.02 | < 0.02 | < 0.02 | < 0.02 |
|---|---|---|---|---|---|---|---|---|---|---|---|---|---|---|---|
| Pumping time | NAP | ACY | ACE | FLR | PHE | ANT | FLN | PYR | B(a)A | CHR | B(b.k)F | B(a)P | Indeno | D(ah)A | B(ghi)P |
| [s] | [$\mu$g l$^{-1}$] | [$\mu$g l$^{-1}$] | [$\mu$g l$^{-1}$] | [$\mu$g l$^{-1}$] | [$\mu$g l$^{-1}$] | [$\mu$g l$^{-1}$] | [$\mu$g l$^{-1}$] | [$\mu$g l$^{-1}$] | [$\mu$g l$^{-1}$] | [$\mu$g l$^{-1}$] | [$\mu$g l$^{-1}$] | [$\mu$g l$^{-1}$] | [$\mu$g l$^{-1}$] | [$\mu$g l$^{-1}$] | [$\mu$g l$^{-1}$] |
| 900 | 1.11 | 0.09 | 2.91 | 0.19 | 0.38 | 0.00 | 0.04 | 0.00 | 0.00 | 0.00 | 0.03 | 0.00 | 0.00 | 0.00 | 0.00 |
| 1800 | 0.94 | 0.09 | 3.28 | 0.30 | 0.55 | 0.00 | 0.05 | 0.02 | 0.00 | 0.00 | 0.00 | 0.00 | 0.00 | 0.00 | 0.00 |
| 3600 | 0.77 | 0.10 | 3.46 | 0.38 | 0.93 | 0.00 | 0.28 | 0.15 | 0.00 | 0.00 | 0.03 | 0.00 | 0.00 | 0.00 | 0.00 |
| 5400 | 0.67 | 0.09 | 3.08 | 0.21 | 0.46 | 0.00 | 0.05 | 0.00 | 0.00 | 0.00 | 0.00 | 0.00 | 0.00 | 0.00 | 0.00 |
| 7200 | 0.58 | 0.10 | 3.02 | 0.14 | 0.30 | 0.00 | 0.00 | 0.00 | 0.00 | 0.00 | 0.00 | 0.00 | 0.00 | 0.00 | 0.00 |
| 9000 | 0.54 | 0.10 | 3.31 | 0.14 | 0.38 | 0.00 | 0.00 | 0.00 | 0.00 | 0.00 | 0.00 | 0.00 | 0.00 | 0.00 | 0.00 |
| 12600 | 0.48 | 0.11 | 3.59 | 0.22 | 0.45 | 0.00 | 0.04 | 0.00 | 0.00 | 0.00 | 0.00 | 0.00 | 0.00 | 0.00 | 0.00 |
| 16812 | 0.43 | 0.11 | 3.90 | 0.10 | 0.41 | 0.00 | 0.04 | 0.00 | 0.00 | 0.00 | 0.00 | 0.00 | 0.00 | 0.00 | 0.00 |
| 19800 | 0.44 | 0.13 | 4.09 | 0.08 | 0.33 | 0.00 | 0.00 | 0.00 | 0.00 | 0.00 | 0.00 | 0.00 | 0.00 | 0.00 | 0.00 |
| 23400 | 0.39 | 0.15 | 4.36 | 0.12 | 0.34 | 0.00 | 0.00 | 0.00 | 0.00 | 0.00 | 0.00 | 0.00 | 0.00 | 0.00 | 0.00 |
| 27000 | 0.36 | 0.13 | 4.55 | 0.05 | 0.25 | 0.00 | 0.00 | 0.00 | 0.00 | 0.00 | 0.05 | 0.00 | 0.00 | 0.00 | 0.00 |
| 32400 | 0.35 | 0.15 | 4.92 | 0.05 | 0.25 | 0.00 | 0.00 | 0.00 | 0.00 | 0.00 | 0.00 | 0.00 | 0.00 | 0.00 | 0.00 |
| 36900 | 0.33 | 0.15 | 5.16 | 0.04 | 0.18 | 0.00 | 0.00 | 0.00 | 0.00 | 0.00 | 0.05 | 0.00 | 0.00 | 0.00 | 0.00 |
| 42300 | 0.32 | 0.18 | 5.54 | 0.03 | 0.19 | 0.00 | 0.00 | 0.00 | 0.00 | 0.00 | 0.00 | 0.00 | 0.00 | 0.00 | 0.00 |
| 47700 | 0.30 | 0.17 | 5.76 | 0.05 | 0.19 | 0.00 | 0.00 | 0.00 | 0.00 | 0.00 | 0.00 | 0.00 | 0.00 | 0.00 | 0.00 |
| 53100 | 0.29 | 0.18 | 6.17 | 0.05 | 0.18 | 0.00 | 0.00 | 0.00 | 0.00 | 0.00 | 0.00 | 0.00 | 0.00 | 0.00 | 0.00 |
| 74412 | 0.27 | 0.25 | 7.56 | 0.04 | 0.20 | 0.00 | 0.00 | 0.00 | 0.00 | 0.00 | 0.00 | 0.00 | 0.00 | 0.00 | 0.00 |
| 80100 | 0.27 | 0.22 | 7.89 | 0.06 | 0.16 | 0.00 | 0.00 | 0.00 | 0.00 | 0.00 | 0.00 | 0.00 | 0.00 | 0.00 | 0.00 |
| 87300 | 0.26 | 0.26 | 8.17 | 0.05 | 0.20 | 0.00 | 0.00 | 0.00 | 0.00 | 0.00 | 0.00 | 0.00 | 0.00 | 0.00 | 0.00 |
| 95400 | 0.26 | 0.26 | 8.50 | 0.07 | 0.17 | 0.00 | 0.00 | 0.00 | 0.00 | 0.00 | 0.09 | 0.00 | 0.00 | 0.00 | 0.00 |
| 102600 | 0.25 | 0.25 | 8.85 | 0.05 | 0.23 | 0.00 | 0.00 | 0.00 | 0.00 | 0.00 | 0.09 | 0.00 | 0.00 | 0.00 | 0.00 |
| 110700 | 0.25 | 0.29 | 9.28 | 0.04 | 0.22 | 0.00 | 0.00 | 0.00 | 0.00 | 0.00 | 0.00 | 0.00 | 0.00 | 0.00 | 0.00 |
| 119700 | 0.25 | 0.29 | 9.90 | 0.08 | 0.23 | 0.00 | 0.00 | 0.00 | 0.00 | 0.00 | 0.00 | 0.00 | 0.00 | 0.00 | 0.00 |
| 128700 | 0.24 | 0.29 | 10.03 | 0.00 | 0.17 | 0.00 | 0.00 | 0.00 | 0.00 | 0.00 | 0.00 | 0.00 | 0.00 | 0.00 | 0.00 |
| 137988 | 0.23 | 0.31 | 10.46 | 0.04 | 0.18 | 0.00 | 0.00 | 0.00 | 0.00 | 0.00 | 0.00 | 0.00 | 0.00 | 0.00 | 0.00 |
| 157500 | 0.24 | 0.35 | 11.76 | 0.09 | 0.26 | 0.00 | 0.00 | 0.00 | 0.00 | 0.00 | 0.00 | 0.00 | 0.00 | 0.00 | 0.00 |
| 169200 | 0.16 | 0.33 | 11.70 | 0.03 | 0.14 | 0.00 | 0.00 | 0.00 | 0.00 | 0.00 | 0.00 | 0.00 | 0.00 | 0.00 | 0.00 |
| 179388 | 0.29 | 0.33 | 11.46 | 0.06 | 0.20 | 0.00 | 0.00 | 0.00 | 0.00 | 0.00 | 0.00 | 0.00 | 0.00 | 0.00 | 0.00 |
| 189900 | 0.18 | 0.37 | 12.43 | 0.06 | 0.21 | 0.00 | 0.00 | 0.00 | 0.00 | 0.00 | 0.00 | 0.00 | 0.00 | 0.00 | 0.00 |
| 200700 | 0.24 | 0.36 | 13.10 | 0.09 | 0.29 | 0.00 | 0.00 | 0.00 | 0.00 | 0.00 | 0.00 | 0.00 | 0.00 | 0.00 | 0.00 |
| 212400 | 0.18 | 0.38 | 13.16 | 0.07 | 0.20 | 0.00 | 0.00 | 0.00 | 0.00 | 0.00 | 0.00 | 0.00 | 0.00 | 0.00 | 0.00 |
| 249300 | 0.16 | 0.39 | 14.45 | 0.06 | 0.24 | 0.00 | 0.00 | 0.00 | 0.00 | 0.00 | 0.05 | 0.00 | 0.00 | 0.00 | 0.00 |
| 262188 | 0.16 | 0.45 | 15.28 | 0.07 | 0.21 | 0.00 | 0.00 | 0.00 | 0.00 | 0.00 | 0.00 | 0.00 | 0.00 | 0.00 | 0.00 |
| n.d. = no detect | | | | | | | | | | | | | | | |

Table 11.13: Concentration-time series of polycyclic aromatic hydrocarbons at well B73

## 11.1.8  Well B72

| Detection limit | < 0.01 | < 0.01 | < 0.01 | < 0.01 | < 0.01 | < 0.01 | < 0.01 | < 0.01 | < 0.01 | < 0.01 | < 0.01 | < 0.01 | < 0.01 |
|---|---|---|---|---|---|---|---|---|---|---|---|---|---|
| Pumping time | Benzene | Toluene | Ethylbenzene | p-Xylene | o-Xylene | Iso-PB | PB | 1,3,5-TMB | 1,2,4-TMB | BF | 1,2,3-TMB | Indane | Indane |
| [s] | [µg l$^{-1}$] | [µg l$^{-1}$] | [µg l$^{-1}$] | [µg l$^{-1}$] | [µg l$^{-1}$] | [µg l$^{-1}$] | [µg l$^{-1}$] | [µg l$^{-1}$] | [µg l$^{-1}$] | [µg l$^{-1}$] | [µg l$^{-1}$] | [µg l$^{-1}$] | [µg l$^{-1}$] |
| 299 | 0.03 | 0.15 | 0.06 | 0.17 | 0.08 | n.d. | n.d. | 0.01 | n.d. | 0.01 | n.d. | n.d. | 0.02 |
| 1800 | 0.02 | 0.08 | 0.05 | 0.15 | 0.08 | n.d. | n.d. | 0.02 | 0.02 | n.d. | n.d. | n.d. | 0.02 |
| 5400 | 0.01 | 0.05 | 0.03 | 0.10 | 0.06 | n.d. | n.d. | 0.01 | n.d. | n.d. | n.d. | n.d. | n.d. |
| 12600 | n.d. | 0.04 | 0.03 | 0.10 | 0.05 | n.d. | n.d. | 0.01 | n.d. | n.d. | n.d. | n.d. | n.d. |
| 22788 | n.d. | 0.02 | 0.02 | 0.08 | 0.04 | n.d. | n.d. | 0.01 | 0.01 | n.d. | n.d. | n.d. | n.d. |
| 35100 | n.d. | 0.03 | n.d. | 0.06 | 0.04 | 0.02 | n.d. | n.d. | n.d. | n.d. | n.d. | n.d. | n.d. |
| 50400 | n.d. | 0.02 | n.d. | 0.06 | 0.03 | 0.02 | n.d. | 0.02 | n.d. | n.d. | n.d. | n.d. | n.d. |
| 68400 | n.d. | n.d. | n.d. | 0.05 | 0.02 | n.d. | n.d. | 0.02 | n.d. | n.d. | n.d. | n.d. | n.d. |
| 91188 | n.d. | n.d. | n.d. | 0.05 | 0.03 | n.d. | n.d. | 0.02 | n.d. | n.d. | n.d. | n.d. | n.d. |
| 110700 | n.d. | n.d. | n.d. | 0.03 | n.d. | n.d. | n.d. | 0.01 | n.d. | n.d. | n.d. | n.d. | n.d. |
| 177300 | n.d. | n.d. | n.d. | 0.04 | 0.02 | n.d. | n.d. | n.d. | n.d. | n.d. | n.d. | n.d. | n.d. |
| n.d. = no detect | | | | | | | | | | | | | |

| Detection limit | < 0.02 | < 0.02 | < 0.02 | < 0.02 | < 0.02 | < 0.02 | < 0.02 | < 0.02 | < 0.02 | < 0.02 | < 0.02 | < 0.02 | < 0.02 | < 0.02 |
|---|---|---|---|---|---|---|---|---|---|---|---|---|---|---|
| Pumping time | NAP | ACY | ACE | FLR | PHE | ANT | FLN | PYR | B(a)A | CHR | B(b.k)F | B(a)P | Indeno | D(ah)A | B(ghi)P |
| [s] | [µg l$^{-1}$] | [µg l$^{-1}$] | [µg l$^{-1}$] | [µg l$^{-1}$] | [µg l$^{-1}$] | [µg l$^{-1}$] | [µg l$^{-1}$] | [µg l$^{-1}$] | [µg l$^{-1}$] | [µg l$^{-1}$] | [µg l$^{-1}$] | [µg l$^{-1}$] | [µg l$^{-1}$] | [µg l$^{-1}$] |
| 299 | 0.94 | 0.08 | 1.30 | 0.16 | 0.74 | 0.00 | 0.24 | 0.16 | 0.25 | 0.09 | 0.12 | 0.00 | 0.00 | 0.00 | 0.00 |
| 1800 | 0.90 | 0.06 | 1.24 | 0.20 | 0.89 | 0.00 | 0.28 | 0.16 | 0.00 | 0.00 | 0.10 | 0.00 | 0.00 | 0.00 | 0.00 |
| 5400 | 0.77 | 0.06 | 1.23 | 0.21 | 0.78 | 0.00 | 0.23 | 0.13 | 0.00 | 0.00 | 0.05 | 0.00 | 0.00 | 0.00 | 0.00 |
| 12600 | 0.63 | 0.05 | 1.15 | 0.11 | 0.81 | 0.00 | 0.18 | 0.12 | 0.00 | 0.00 | 0.00 | 0.00 | 0.00 | 0.00 | 0.00 |
| 22788 | 0.52 | 0.04 | 0.98 | 0.10 | 0.61 | 0.00 | 0.17 | 0.11 | 0.00 | 0.00 | 0.03 | 0.00 | 0.00 | 0.00 | 0.00 |
| 35100 | 0.48 | 0.03 | 1.01 | 0.09 | 0.56 | 0.00 | 0.15 | 0.07 | 0.00 | 0.00 | 0.00 | 0.00 | 0.00 | 0.00 | 0.00 |
| 50400 | 0.45 | 0.04 | 1.00 | 0.08 | 0.46 | 0.00 | 0.11 | 0.07 | 0.00 | 0.00 | 0.00 | 0.00 | 0.00 | 0.00 | 0.00 |
| 68400 | 0.40 | 0.03 | 0.94 | 0.05 | 0.38 | 0.00 | 0.10 | 0.06 | 0.00 | 0.00 | 0.00 | 0.00 | 0.00 | 0.00 | 0.00 |
| 110700 | 0.33 | 0.03 | 0.76 | 0.06 | 0.37 | 0.00 | 0.07 | 0.06 | 0.00 | 0.00 | 0.00 | 0.00 | 0.00 | 0.00 | 0.00 |
| 177300 | 0.31 | 0.02 | 0.73 | 0.03 | 0.22 | 0.00 | 0.04 | 0.04 | 0.00 | 0.00 | 0.00 | 0.00 | 0.00 | 0.00 | 0.00 |
| n.d. = no detect | | | | | | | | | | | | | | |

Table 11.14: Concentration-time series of petroleum hydrocarbons at well B72 (left)
Table 11.15: Concentration-time series of polycyclic aromatic hydrocarbons at well B73 (right)

| Detection limit | < 0.01 | < 0.01 | < 0.01 | < 0.01 | < 0.01 | < 0.01 | < 0.01 | < 0.01 | < 0.01 | < 0.01 | < 0.01 | < 0.01 | < 0.01 |
|---|---|---|---|---|---|---|---|---|---|---|---|---|---|
| Pumping time | Benzene | Toluene | Ethylbenzene | p-Xylene | o-Xylene | Iso-PB | PB | 1,3,5-TMB | 1,2,4-TMB | BF | 1,2,3-TMB | Indane | Indane |
| [s] | [µg l$^{-1}$] | [µg l$^{-1}$] | [µg l$^{-1}$] | [µg l$^{-1}$] | [µg l$^{-1}$] | [µg l$^{-1}$] | [µg l$^{-1}$] | [µg l$^{-1}$] | [µg l$^{-1}$] | [µg l$^{-1}$] | [µg l$^{-1}$] | [µg l$^{-1}$] | [µg l$^{-1}$] |
| 1188 | n.d. | 0.03 | n.d. | 0.04 | 0.03 | n.d. | n.d. | n.d. | n.d. | 0.02 | n.d. | n.d. | n.d. |
| 2700 | n.d. | n.d. | n.d. | 0.03 | n.d. | n.d. | n.d. | n.d. | n.d. | n.d. | n.d. | n.d. | n.d. |
| 4500 | n.d. | n.d. | n.d. | n.d. | n.d. | n.d. | n.d. | n.d. | n.d. | n.d. | n.d. | n.d. | n.d. |
| 7200 | n.d. | n.d. | n.d. | n.d. | n.d. | n.d. | n.d. | n.d. | n.d. | n.d. | n.d. | n.d. | n.d. |
| 10800 | n.d. | n.d. | n.d. | n.d. | n.d. | n.d. | n.d. | n.d. | n.d. | n.d. | n.d. | n.d. | n.d. |
| 15300 | n.d. | n.d. | n.d. | n.d. | n.d. | n.d. | n.d. | n.d. | n.d. | n.d. | n.d. | n.d. | n.d. |
| 20700 | n.d. | n.d. | n.d. | n.d. | n.d. | n.d. | n.d. | n.d. | n.d. | n.d. | n.d. | n.d. | n.d. |
| 25200 | n.d. | n.d. | n.d. | n.d. | n.d. | n.d. | n.d. | n.d. | n.d. | n.d. | n.d. | n.d. | n.d. |
| 32112 | n.d. | n.d. | n.d. | n.d. | n.d. | n.d. | n.d. | n.d. | n.d. | n.d. | n.d. | n.d. | n.d. |
| 38700 | n.d. | n.d. | n.d. | n.d. | n.d. | n.d. | n.d. | n.d. | n.d. | n.d. | n.d. | n.d. | n.d. |
| 45000 | n.d. | n.d. | n.d. | n.d. | n.d. | n.d. | n.d. | n.d. | n.d. | n.d. | n.d. | n.d. | n.d. |
| 70200 | n.d. | n.d. | n.d. | n.d. | n.d. | n.d. | n.d. | n.d. | n.d. | n.d. | n.d. | n.d. | n.d. |
| 79200 | n.d. | n.d. | n.d. | n.d. | n.d. | n.d. | n.d. | n.d. | n.d. | n.d. | n.d. | n.d. | n.d. |
| 89100 | n.d. | n.d. | n.d. | n.d. | n.d. | n.d. | n.d. | n.d. | n.d. | n.d. | n.d. | n.d. | n.d. |
| 100800 | n.d. | n.d. | n.d. | n.d. | n.d. | n.d. | n.d. | n.d. | n.d. | n.d. | n.d. | n.d. | n.d. |
| 112212 | n.d. | n.d. | n.d. | n.d. | n.d. | n.d. | n.d. | n.d. | n.d. | n.d. | n.d. | n.d. | n.d. |
| 122400 | n.d. | n.d. | n.d. | n.d. | n.d. | n.d. | n.d. | n.d. | n.d. | n.d. | n.d. | n.d. | n.d. |
| 134100 | n.d. | n.d. | n.d. | n.d. | n.d. | n.d. | n.d. | n.d. | n.d. | n.d. | n.d. | n.d. | n.d. |
| 160200 | n.d. | n.d. | n.d. | n.d. | n.d. | n.d. | n.d. | n.d. | n.d. | n.d. | n.d. | n.d. | n.d. |
| 177012 | 0.03 | n.d. | n.d. | n.d. | n.d. | n.d. | n.d. | n.d. | n.d. | n.d. | n.d. | n.d. | n.d. |
| 189000 | 0.03 | n.d. | n.d. | n.d. | n.d. | n.d. | n.d. | n.d. | n.d. | n.d. | n.d. | n.d. | n.d. |
| 203400 | 0.04 | n.d. | n.d. | n.d. | n.d. | n.d. | n.d. | n.d. | n.d. | n.d. | n.d. | n.d. | n.d. |
| 219600 | 0.06 | n.d. | n.d. | n.d. | n.d. | n.d. | n.d. | n.d. | n.d. | n.d. | n.d. | n.d. | n.d. |
| 237888 | 0.08 | n.d. | n.d. | n.d. | n.d. | n.d. | n.d. | n.d. | n.d. | n.d. | n.d. | n.d. | n.d. |
| 252000 | 0.08 | n.d. | n.d. | n.d. | n.d. | n.d. | n.d. | n.d. | n.d. | n.d. | n.d. | n.d. | n.d. |
| 269100 | 0.10 | n.d. | n.d. | n.d. | n.d. | n.d. | n.d. | n.d. | n.d. | n.d. | n.d. | n.d. | n.d. |
| 287100 | 0.15 | n.d. | n.d. | n.d. | n.d. | n.d. | n.d. | n.d. | n.d. | 0.01 | n.d. | n.d. | n.d. |
| 326088 | 0.20 | n.d. | n.d. | n.d. | n.d. | n.d. | n.d. | n.d. | n.d. | n.d. | n.d. | n.d. | n.d. |
| 343800 | 0.22 | n.d. | n.d. | n.d. | n.d. | n.d. | n.d. | n.d. | n.d. | n.d. | n.d. | n.d. | n.d. |
| 364500 | 0.26 | n.d. | n.d. | n.d. | n.d. | n.d. | n.d. | n.d. | n.d. | 0.01 | n.d. | n.d. | n.d. |
| 385200 | 0.29 | n.d. | n.d. | n.d. | n.d. | n.d. | n.d. | n.d. | n.d. | n.d. | n.d. | n.d. | n.d. |
| 432900 | 0.36 | n.d. | n.d. | n.d. | n.d. | n.d. | n.d. | n.d. | n.d. | n.d. | n.d. | n.d. | n.d. |
| n.d. = no detect | | | | | | | | | | | | | |

Table 11.16: Concentration-time series of petroleum hydrocarbons at well B2069

Table 11.17: Concentration-time series of polycyclic aromatic hydrocarbons at well B2069

| Detection limit | < 0.02 | < 0.02 | < 0.02 | < 0.02 | < 0.02 | < 0.02 | < 0.02 | < 0.02 | < 0.02 | < 0.02 | < 0.02 | < 0.02 | < 0.02 | < 0.02 | < 0.02 |
|---|---|---|---|---|---|---|---|---|---|---|---|---|---|---|---|
| Pumping time | NAP | ACY | ACE | FLR | PHE | ANT | FLN | PYR | B(a)A | CHR | B(b.k)F | B(a)P | Indeno | D(ah)A | B(ghi)P |
| [s] | [µg l$^{-1}$] | [µg l$^{-1}$] | [µg l$^{-1}$] | [µg l$^{-1}$] | [µg l$^{-1}$] | [µg l$^{-1}$] | [µg l$^{-1}$] | [µg l$^{-1}$] | [µg l$^{-1}$] | [µg l$^{-1}$] | [µg l$^{-1}$] | [µg l$^{-1}$] | [µg l$^{-1}$] | [µg l$^{-1}$] | [µg l$^{-1}$] |
| 1188 | 0.52 | 0.08 | 1.58 | 0.09 | 0.51 | n.d. | 0.07 | 0.04 | n.d. | n.d. | 0.25 | n.d. | n.d. | n.d. | n.d. |
| 2700 | 0.41 | 0.05 | 1.23 | 0.05 | 0.40 | n.d. | 0.06 | 0.04 | n.d. | n.d. | 0.15 | n.d. | n.d. | n.d. | n.d. |
| 4500 | 0.34 | 0.05 | 1.20 | 0.00 | 0.37 | n.d. | 0.04 | 0.03 | n.d. | n.d. | 0.12 | n.d. | n.d. | n.d. | n.d. |
| 7200 | 0.29 | 0.05 | 1.37 | 0.06 | 0.47 | n.d. | n.d. | n.d. | n.d. | n.d. | 0.24 | n.d. | n.d. | n.d. | n.d. |
| 10800 | 0.27 | 0.05 | 1.43 | 0.17 | 0.62 | n.d. | n.d. | n.d. | n.d. | n.d. | 0.09 | n.d. | n.d. | n.d. | n.d. |
| 15300 | 0.23 | 0.03 | 1.19 | 0.07 | 0.41 | n.d. | n.d. | n.d. | n.d. | n.d. | 0.06 | n.d. | n.d. | n.d. | n.d. |
| 20700 | 0.21 | 0.03 | 1.02 | 0.07 | 0.23 | n.d. | n.d. | n.d. | n.d. | n.d. | 0.05 | n.d. | n.d. | n.d. | n.d. |
| 25200 | 0.19 | 0.03 | 0.88 | 0.03 | 0.24 | n.d. | n.d. | n.d. | n.d. | n.d. | n.d. | n.d. | n.d. | n.d. | n.d. |
| 32112 | 0.16 | 0.02 | 0.99 | 0.05 | 0.29 | n.d. | n.d. | n.d. | n.d. | n.d. | n.d. | n.d. | n.d. | n.d. | n.d. |
| 38700 | 0.18 | 0.03 | 0.97 | 0.05 | 0.24 | n.d. | n.d. | n.d. | n.d. | n.d. | 0.05 | n.d. | n.d. | n.d. | n.d. |
| 45000 | 0.16 | 0.03 | 1.16 | 0.06 | 0.36 | n.d. | n.d. | n.d. | n.d. | n.d. | 0.06 | n.d. | n.d. | n.d. | n.d. |
| 70200 | 0.12 | n.d. | 0.56 | n.d. | 0.25 | n.d. | n.d. | n.d. | n.d. | n.d. | 0.00 | n.d. | n.d. | n.d. | n.d. |
| 79200 | 0.12 | n.d. | 0.59 | n.d. | 0.11 | n.d. | n.d. | n.d. | n.d. | n.d. | 0.05 | n.d. | n.d. | n.d. | n.d. |
| 89100 | 0.12 | n.d. | 0.75 | n.d. | 0.12 | n.d. | n.d. | n.d. | n.d. | n.d. | 0.03 | n.d. | n.d. | n.d. | n.d. |
| 100800 | 0.12 | n.d. | 0.82 | n.d. | 0.13 | n.d. | n.d. | n.d. | n.d. | n.d. | 0.04 | n.d. | n.d. | n.d. | n.d. |
| 112212 | 0.11 | n.d. | 0.62 | n.d. | 0.17 | n.d. | n.d. | n.d. | n.d. | n.d. | n.d. | n.d. | n.d. | n.d. | n.d. |
| 122400 | 0.10 | n.d. | 0.62 | n.d. | 0.17 | n.d. | n.d. | n.d. | n.d. | n.d. | n.d. | n.d. | n.d. | n.d. | n.d. |
| 134100 | 0.10 | n.d. | 0.65 | n.d. | 0.16 | n.d. | n.d. | n.d. | n.d. | n.d. | n.d. | n.d. | n.d. | n.d. | n.d. |
| 160200 | 0.10 | n.d. | 0.70 | n.d. | 0.27 | n.d. | n.d. | n.d. | n.d. | n.d. | 0.04 | n.d. | n.d. | n.d. | n.d. |
| 177012 | 0.11 | 0.03 | 1.00 | 0.05 | 0.25 | n.d. | n.d. | n.d. | n.d. | n.d. | 0.05 | n.d. | n.d. | n.d. | n.d. |
| 189000 | 0.10 | n.d. | 0.81 | n.d. | 0.23 | n.d. | n.d. | n.d. | n.d. | n.d. | n.d. | n.d. | n.d. | n.d. | n.d. |
| 203400 | 0.09 | n.d. | 0.55 | n.d. | 0.16 | n.d. | n.d. | n.d. | n.d. | n.d. | n.d. | n.d. | n.d. | n.d. | n.d. |
| 219600 | 0.09 | n.d. | 0.50 | n.d. | 0.19 | n.d. | n.d. | n.d. | n.d. | n.d. | n.d. | n.d. | n.d. | n.d. | n.d. |
| 237888 | 0.10 | 0.02 | 0.73 | 0.06 | 0.17 | n.d. | n.d. | n.d. | n.d. | n.d. | n.d. | n.d. | n.d. | n.d. | n.d. |
| 252000 | 0.10 | n.d. | 0.67 | n.d. | 0.17 | n.d. | n.d. | n.d. | n.d. | n.d. | n.d. | n.d. | n.d. | n.d. | n.d. |
| 269100 | 0.08 | n.d. | 0.45 | n.d. | 0.11 | n.d. | n.d. | n.d. | n.d. | n.d. | n.d. | n.d. | n.d. | n.d. | n.d. |
| 287100 | 0.07 | n.d. | 0.44 | n.d. | 0.10 | n.d. | n.d. | n.d. | n.d. | n.d. | n.d. | n.d. | n.d. | n.d. | n.d. |
| 326088 | 0.08 | n.d. | 0.50 | n.d. | 0.15 | n.d. | n.d. | n.d. | n.d. | n.d. | n.d. | n.d. | n.d. | n.d. | n.d. |
| 343800 | 0.09 | n.d. | 0.83 | n.d. | 0.29 | n.d. | n.d. | n.d. | n.d. | n.d. | n.d. | n.d. | n.d. | n.d. | n.d. |
| 364500 | 0.09 | 0.03 | 0.83 | 0.04 | 0.28 | n.d. | n.d. | n.d. | n.d. | n.d. | n.d. | n.d. | n.d. | n.d. | n.d. |
| 385200 | 0.10 | n.d. | 0.80 | n.d. | 0.25 | n.d. | n.d. | n.d. | n.d. | n.d. | n.d. | n.d. | n.d. | n.d. | n.d. |
| 432900 | 0.07 | n.d. | 0.59 | n.d. | 0.20 | n.d. | n.d. | n.d. | n.d. | n.d. | n.d. | n.d. | n.d. | n.d. | n.d. |

n.d. = no detect

## 11.2 Anorganic solute concentrations

### 11.2.1 Well B42

| Detection limit | < 1.0 | < 1.0 | < 1.0 | < 1.0 | < 1.0 | < 1.0 | < 1.0 | < 0.1 | < 0.1 | < 0.1 | < 0.1 | < 0.2 | < 0.1 |
|---|---|---|---|---|---|---|---|---|---|---|---|---|---|
| Pumping time | Sulfate | Chloride | Nitrate | Fluorine | Nitrit | Phosphate | Bromimine | Calcium | Magnesium | Sodium | Potassium | Iron (II)[1] | Manganese (II)[1] |
| [s] | [mg l$^{-1}$] | [mg l$^{-1}$] | [mg l$^{-1}$] | [mg l$^{-1}$] | [mg l$^{-1}$] | [mg l$^{-1}$] | [mg l$^{-1}$] | [mg l$^{-1}$] | [mg l$^{-1}$] | [mg l$^{-1}$] | [mg l$^{-1}$] | [mg l$^{-1}$] | [mg l$^{-1}$] |
| 300 | 244.02 | 98.05 | n.d. | n.d. | n.d. | n.d. | n.d. | 245.00 | 53.00 | 46.45 | 12.30 | 4.47 | 0.46 |
| 2700 | 254.08 | 96.64 | n.d. | n.d. | n.d. | n.d. | n.d. | 254.00 | 53.00 | 47.00 | 11.70 | 4.52 | 0.43 |
| 5400 | 254.97 | 98.64 | n.d. | n.d. | n.d. | n.d. | n.d. | 251.00 | 53.00 | 46.55 | 11.50 | 5.53 | 0.41 |
| 12600 | 250.20 | 101.65 | n.d. | n.d. | n.d. | n.d. | n.d. | 252.00 | 54.00 | 47.25 | 11.30 | 4.35 | 0.36 |
| 21600 | 262.10 | 109.82 | n.d. | n.d. | n.d. | n.d. | n.d. | 259.00 | 54.00 | 44.60 | 11.20 | 3.17 | 0.36 |
| 36000 | 259.54 | 103.90 | n.d. | n.d. | n.d. | n.d. | n.d. | 258.00 | 56.00 | 49.65 | 11.10 | 4.13 | 0.38 |
| 48600 | 275.13 | 108.84 | n.d. | n.d. | n.d. | n.d. | n.d. | 262.00 | 57.00 | 57.90 | 11.90 | 3.18 | 0.41 |
| 68400 | 285.94 | 109.58 | n.d. | n.d. | n.d. | n.d. | n.d. | 260.00 | 54.00 | 51.05 | 11.80 | 4.62 | 0.35 |
| 86400 | 311.34 | 114.33 | n.d. | n.d. | n.d. | n.d. | n.d. | 272.00 | 59.00 | 44.50 | 11.70 |  | 0.36 |
| 111600 | 341.78 | 121.69 | n.d. | n.d. | n.d. | n.d. | n.d. | 269.00 | 59.00 | 43.75 | 11.40 | 4.25 | 0.37 |
| 136800 | 351.71 | 120.86 | n.d. | n.d. | n.d. | n.d. | n.d. | 282.00 | 60.00 | 47.75 | 11.20 | 4.44 | 0.39 |
| 165600 | 361.52 | 127.99 | n.d. | n.d. | n.d. | n.d. | n.d. | 292.00 | 63.00 | 54.75 | 11.30 | 4.94 | 0.39 |
| 194400 | 336.14 | 117.11 | n.d. | n.d. | n.d. | n.d. | n.d. | 279.00 | 60.00 | 50.20 | 11.80 |  |  |
| 226800 | 393.15 | 132.65 | n.d. | n.d. | n.d. | n.d. | n.d. | 296.00 | 61.00 | 57.95 | 11.80 | 5.20 | 0.43 |
| 259200 | 401.06 | 137.18 | n.d. | n.d. | n.d. | n.d. | n.d. | 304.00 | 63.00 | 57.45 | 11.50 | 4.78 | 0.45 |
| 298800 | 400.56 | 128.12 | n.d. | n.d. | n.d. | n.d. | n.d. | 295.00 | 61.00 | 56.95 | 11.00 | 4.69 | 0.44 |
| 338400 | 400.41 | 140.05 | n.d. | n.d. | n.d. | n.d. | n.d. | 305.00 | 62.00 | 67.15 | 12.00 | 4.74 | 0.46 |
| 385200 | 422.47 | 148.01 | n.d. | n.d. | n.d. | n.d. | n.d. | 308.00 | 62.00 | 70.25 | 11.70 | 5.77 | 0.48 |
| 432000 | 430.50 | 155.69 | n.d. | n.d. | n.d. | n.d. | n.d. | 313.00 | 64.00 | 68.00 | 11.40 | 4.90 | 0.50 |
| 468900 | 435.19 | 160.55 | n.d. | n.d. | n.d. | n.d. | n.d. | 320.00 | 63.00 | 70.80 | 11.10 | 6.16 | 0.49 |

n.d. = no detect

[1] = Samples have not been sufficiently acidified and precipitation occured

Table 11.18: Concentration-time series of inorganic solutes at well B42

| Detection limit | < 1.0 | < 1.0 | < 1.0 | < 1.0 | < 1.0 | < 1.0 | < 1.0 | < 0.1 | < 0.1 | < 0.1 | < 0.1 | < 0.2 | < 0.1 |
|---|---|---|---|---|---|---|---|---|---|---|---|---|---|
| Pumping time | Sulfate | Chloride | Nitrate | Fluorine | Nitrit | Phosphate | Bromimine | Calcium | Magnesium | Sodium | Potassium | Iron (II)[1] | Manganese (II)[1] |
| [s] | [mg l$^{-1}$] | [mg l$^{-1}$] | [mg l$^{-1}$] | [mg l$^{-1}$] | [mg l$^{-1}$] | [mg l$^{-1}$] | [mg l$^{-1}$] | [mg l$^{-1}$] | [mg l$^{-1}$] | [mg l$^{-1}$] | [mg l$^{-1}$] | [mg l$^{-1}$] | [mg l$^{-1}$] |
| 300 | 510.83 | 186.43 | n.d. | n.d. | n.d. | n.d. | n.d. | 385.00 | 73.00 | 128.50 | 14.20 | 10.17 | 0.58 |
| 37800 | 498.55 | 176.60 | n.d. | n.d. | n.d. | n.d. | n.d. | 375.00 | 71.00 | 139.50 | 14.00 | 14.80 | 0.57 |
| 88200 | 496.16 | 176.59 | n.d. | n.d. | n.d. | n.d. | n.d. | 370.00 | 70.00 | 136.50 | 14.10 | 11.81 | 0.54 |
| 199800 | 476.41 | 160.95 | n.d. | n.d. | n.d. | n.d. | n.d. | 365.00 | 70.00 | 125.00 | 14.10 | 7.81 | 0.51 |
| 225000 | 508.63 | 210.88 | n.d. | n.d. | n.d. | n.d. | n.d. | 367.00 | 70.00 | 134.00 | 13.80 | 12.07 | 0.52 |
| 261000 | 496.36 | 205.80 | n.d. | n.d. | n.d. | n.d. | n.d. | 366.00 | 70.00 | 136.50 | 13.70 | 8.60 | 0.50 |
| n.d. = no detect | | | | | | | | | | | | | |
| [1] = Samples have not been sufficiently acidified and precipitation occured | | | | | | | | | | | | | |

Table 11.19: Concentration-time series of inorganic solutes at well P2

| Detection limit | < 1.0 | < 1.0 | < 1.0 | < 1.0 | < 1.0 | < 1.0 | < 1.0 | < 0.1 | < 0.1 | < 0.1 | < 0.1 | < 0.2 | < 0.1 |
|---|---|---|---|---|---|---|---|---|---|---|---|---|---|
| Pumping time | Sulfate | Chloride | Nitrate | Fluorine | Nitrit | Phosphate | Bromimine | Calcium | Magnesium | Sodium | Potassium | Iron (II)[1] | Manganese (II)[1] |
| [s] | [mg l$^{-1}$] | [mg l$^{-1}$] | [mg l$^{-1}$] | [mg l$^{-1}$] | [mg l$^{-1}$] | [mg l$^{-1}$] | [mg l$^{-1}$] | [mg l$^{-1}$] | [mg l$^{-1}$] | [mg l$^{-1}$] | [mg l$^{-1}$] | [mg l$^{-1}$] | [mg l$^{-1}$] |
| 300 | 383.54 | 204.91 | 1.79 | n.d. | n.d. | n.d. | n.d. | 294.00 | 41.00 | 164.00 | 20.20 | 3.45 | 1.18 |
| 1800 | 360.58 | 179.08 | 2.05 | n.d. | n.d. | n.d. | n.d. | 282.00 | 39.00 | 150.50 | 18.40 | 2.58 | 1.12 |
| 4500 | 362.28 | 178.45 | 2.36 | n.d. | n.d. | n.d. | n.d. | 281.00 | 38.00 | 150.50 | 18.60 | 5.63 | 1.09 |
| 10800 | 362.08 | 178.87 | 1.98 | n.d. | n.d. | n.d. | n.d. | 281.00 | 38.00 | 152.00 | 17.90 | 2.72 | 1.10 |
| 17100 | 362.12 | 180.70 | 2.22 | n.d. | n.d. | n.d. | n.d. | 281.00 | 38.00 | 150.50 | 17.90 | 2.88 | 1.13 |
| 28800 | 365.99 | 183.86 | 2.57 | n.d. | n.d. | n.d. | n.d. | 284.00 | 39.00 | 149.00 | 18.10 | 2.90 | 1.16 |
| 37800 | 359.78 | 184.28 | 1.87 | n.d. | n.d. | n.d. | n.d. | 283.00 | 38.00 | 149.00 | 17.90 | 2.98 | 1.19 |
| 50400 | 365.76 | 185.36 | 1.93 | n.d. | n.d. | n.d. | n.d. | 278.00 | 39.00 | 150.00 | 18.10 | 3.03 | 1.22 |
| 68400 | 371.79 | 190.43 | 2.08 | n.d. | n.d. | n.d. | n.d. | 286.00 | 40.00 | 159.50 | 18.50 | 3.10 | 1.29 |
| 86400 | 376.87 | 193.35 | 1.73 | n.d. | n.d. | n.d. | n.d. | 289.00 | 39.00 | 158.50 | 18.90 | 3.25 | 1.37 |
| 106200 | 388.42 | 204.55 | 1.20 | n.d. | n.d. | n.d. | n.d. | 282.00 | 41.00 | 164.00 | 19.30 | 3.48 | 1.52 |
| 129600 | 397.56 | 211.69 | 1.38 | n.d. | n.d. | n.d. | n.d. | 289.00 | 42.00 | 167.50 | 19.50 | 3.72 | 1.62 |
| 154800 | 406.03 | 214.28 | 0.86 | n.d. | n.d. | n.d. | n.d. | 301.00 | 42.00 | 169.00 | 19.70 | 3.91 | 1.71 |
| 180000 | 406.99 | 215.64 | 0.96 | n.d. | n.d. | n.d. | n.d. | 299.00 | 42.00 | 171.50 | 19.80 | 4.08 | 1.84 |
| 208800 | 413.07 | 216.97 | n.d. | n.d. | n.d. | n.d. | n.d. | 301.00 | 42.00 | 175.00 | 20.00 | 4.07 | 1.84 |
| 241200 | 378.38 | 236.78 | 0.73 | n.d. | n.d. | n.d. | n.d. | 298.00 | 43.00 | 174.50 | 20.10 | 4.24 | 1.92 |
| 273600 | 397.59 | 240.78 | n.d. | n.d. | n.d. | n.d. | n.d. | 300.00 | 43.00 | 176.50 | 20.40 | 4.24 | 1.81 |
| 302400 | 397.76 | 235.51 | 0.77 | n.d. | n.d. | n.d. | n.d. | 305.00 | 44.00 | 180.50 | 20.20 | 4.24 | 1.86 |
| 345600 | 400.53 | 237.02 | 0.44 | n.d. | n.d. | n.d. | n.d. | 303.00 | 44.00 | 184.50 | 14.40 | 2.94 | 1.94 |
| n.d. = no detect | | | | | | | | | | | | | |
| [1] = Samples have not been sufficiently acidified and precipitation occured | | | | | | | | | | | | | |

Table 11.20: Concentration-time series of inorganic solutes at well B41

| Detection limit | < 1.0 | < 1.0 | < 1.0 | < 1.0 | < 1.0 | < 1.0 | < 1.0 | < 0.1 | < 0.1 | < 0.1 | < 0.1 | < 0.2 | < 0.1 |
|---|---|---|---|---|---|---|---|---|---|---|---|---|---|
| Pumping time | Sulfate | Chloride | Nitrate | Fluorine | Nitrit | Phosphate | Bromimine | Calcium | Magnesium | Sodium | Potassium | Iron (II)[1] | Manganese (II)[1] |
| [s] | [mg l$^{-1}$] | [mg l$^{-1}$] | [mg l$^{-1}$] | [mg l$^{-1}$] | [mg l$^{-1}$] | [mg l$^{-1}$] | [mg l$^{-1}$] | [mg l$^{-1}$] | [mg l$^{-1}$] | [mg l$^{-1}$] | [mg l$^{-1}$] | [mg l$^{-1}$] | [mg l$^{-1}$] |
| 300 | 269.86 | 84.81 | 1.86 | n.d. | n.d. | n.d. | n.d. | 196.00 | 33.00 | 70.50 | 10.00 | 0.60 | 0.24 |
| 1800 | 275.96 | 100.96 | 1.79 | n.d. | n.d. | n.d. | n.d. | 201.00 | 34.00 | 73.00 | 10.00 | 0.95 | 0.32 |
| 4500 | 272.82 | 103.73 | 1.59 | n.d. | n.d. | n.d. | n.d. | 208.00 | 35.00 | 70.00 | 10.20 | 1.02 | 0.36 |
| 10800 | 268.90 | 97.31 | 1.43 | n.d. | n.d. | n.d. | n.d. | 204.00 | 34.00 | 66.50 | 10.30 | 1.11 | 0.42 |
| 17100 | 275.56 | 101.72 | 1.27 | n.d. | n.d. | n.d. | n.d. | 207.00 | 35.00 | 70.50 | 10.80 | 1.12 | 0.44 |
| 28800 | 278.32 | 103.12 | 1.35 | n.d. | n.d. | n.d. | n.d. | 208.00 | 35.00 | 68.50 | 11.00 | 1.31 | 0.47 |
| 37800 | 277.91 | 103.29 | 1.28 | n.d. | n.d. | n.d. | n.d. | 208.00 | 35.00 | 67.00 | 11.10 | 1.46 | 0.50 |
| 50400 | 291.53 | 109.15 | 1.21 | n.d. | n.d. | n.d. | n.d. | 216.00 | 35.00 | 74.50 | 11.50 | 1.51 | 0.51 |
| 68400 | 292.28 | 112.56 | 1.35 | n.d. | n.d. | n.d. | n.d. | 218.00 | 36.00 | 79.00 | 11.80 | 1.69 | 0.57 |
| 86400 | 287.64 | 111.10 | 1.42 | n.d. | n.d. | n.d. | n.d. | 215.00 | 35.00 | 77.00 | 11.70 | 1.79 | 0.60 |
| 106200 | 293.35 | 115.48 | 1.67 | n.d. | n.d. | n.d. | n.d. | 220.00 | 36.00 | 78.50 | 12.10 | 2.08 | 0.67 |
| 129600 | 305.22 | 123.30 | 1.49 | n.d. | n.d. | n.d. | n.d. | 226.00 | 37.00 | 89.00 | 12.60 | 2.42 | 0.72 |
| 154800 | 308.77 | 133.35 | 1.09 | n.d. | n.d. | n.d. | n.d. | 229.00 | 37.00 | 96.00 | 13.20 | 2.67 | 0.79 |
| 180000 | 300.44 | 124.24 | 1.20 | n.d. | n.d. | n.d. | n.d. | 228.00 | 37.00 | 94.50 | 13.00 | 2.67 | 0.81 |
| 208800 | 311.47 | 138.57 | n.d. | n.d. | n.d. | n.d. | n.d. | 229.00 | 37.00 | 89.50 | 13.20 | 2.48 | 0.76 |
| 241200 | 313.65 | 139.81 | 1.08 | n.d. | n.d. | n.d. | n.d. | 235.00 | 38.00 | 93.00 | 13.50 | 2.65 | 0.81 |
| 273600 | 322.61 | 145.03 | 1.03 | n.d. | n.d. | n.d. | n.d. | 238.00 | 39.00 | 95.00 | 13.60 | 2.60 | 0.79 |
| 309600 | 3.14 | 145.36 | 0.97 | n.d. | n.d. | n.d. | n.d. | 238.00 | 39.00 | 102.50 | 13.60 | 2.65 | 0.78 |
| 345600 | 322.41 | 151.93 | n.d. | n.d. | n.d. | n.d. | n.d. | 245.00 | 40.00 | 108.00 | 14.00 | 2.77 | 0.80 |
| n.d. = no detect | | | | | | | | | | | | | |
| [1] = Samples have not been sufficiently acidified and precipitation occured | | | | | | | | | | | | | |

Table 11.21: Concentration-time series of inorganic solutes at well P1

## 11.2.5  Well NT01 – First campaign

Table 11.22: Concentration-time series of inorganic solutes at well NT01 – First campaign

| Detection limit Pumping time [s] | < 0.1 Calcium [mg l⁻¹] | < 0.1 Magnesium [mg l⁻¹] | < 0.1 Sodium [mg l⁻¹] | < 0.1 Potassium [mg l⁻¹] | < 0.2 Iron (II) [mg l⁻¹] | < 0.1 Manganese (II) [mg l⁻¹] |
|---|---|---|---|---|---|---|
| 900 | 292.00 | 64.00 | 82.65 | 12.90 | 9.21 | 0.64 |
| 1800 | 297.00 | 65.00 | 86.30 | 12.80 | 9.30 | 0.68 |
| 2700 | 298.00 | 64.00 | 83.80 | 12.80 | 9.38 | 0.75 |
| 3600 | 296.00 | 64.00 | 85.10 | 12.90 | 8.54 | 0.86 |
| 5400 | 288.00 | 64.00 | 86.35 | 13.00 | 9.25 | 0.81 |
| 7200 | 298.00 | 64.00 | 88.70 | 13.00 | 9.39 | 0.81 |
| 9000 | 299.00 | 64.00 | 83.00 | 12.70 | 9.59 | 0.77 |
| 11700 | 295.00 | 65.00 | 84.20 | 12.70 | 9.72 | 0.82 |
| 14400 | 300.00 | 63.00 | 80.90 | 13.00 | 9.69 | 0.79 |
| 17100 | 290.00 | 63.00 | 83.65 | 12.60 | 9.22 | 0.88 |
| 20700 | 290.00 | 63.00 | 83.25 | 12.60 | 9.78 | 0.79 |
| 24300 | 297.00 | 64.00 | 83.30 | 12.50 | 9.87 | 0.71 |
| 27900 | 328.00 | 64.00 | 82.40 | 13.00 | 9.53 | 0.75 |
| 32400 | 292.00 | 64.00 | 84.20 | 12.90 | 9.59 | 0.66 |
| 36000 | 297.00 | 64.00 | 84.80 | 12.80 | 9.62 | 0.72 |
| 41400 | 288.00 | 63.00 | 83.25 | 12.90 | 9.69 | 0.74 |
| 45900 | 291.00 | 63.00 | 82.40 | 12.80 | 9.51 | 0.80 |
| 51300 | 291.00 | 64.00 | 79.65 | 12.50 | 9.93 | 0.80 |
| 70812 | 293.00 | 63.00 | 80.15 | 12.60 | 9.77 | 0.75 |
| 77400 | 287.00 | 63.00 | 83.25 | 12.50 | 9.82 | 0.73 |
| 84600 | 288.00 | 63.00 | 81.65 | 12.70 | 9.83 | 0.72 |
| 91800 | 287.00 | 63.00 | 86.55 | 12.70 | 9.92 | 0.75 |
| 99000 | 283.00 | 62.00 | 84.05 | 12.60 | 9.87 | 0.73 |
| 107100 | 290.00 | 63.00 | 85.65 | 12.70 | 9.64 | 0.75 |
| 117288 | 292.00 | 63.00 | 80.55 | 12.40 | 9.28 | 0.69 |
| 123300 | 289.00 | 64.00 | 78.00 | 12.70 | 9.65 | 0.69 |
| 132300 | 295.00 | 64.00 | 78.25 | 12.80 | 9.88 | 0.67 |
| 159300 | 293.00 | 63.00 | 81.00 | 12.70 | 9.89 | 0.68 |
| 169200 | 283.00 | 63.00 | 78.35 | 12.70 | 10.08 | 0.63 |
| 179100 | 286.00 | 63.00 | 77.15 | 12.70 | 9.97 | 0.59 |
| 189900 | 284.00 | 63.00 | 77.70 | 12.70 | 9.92 | 0.61 |
| 200700 | 284.00 | 63.00 | 77.20 | 12.60 | 9.89 | 0.58 |
| 211500 | 286.00 | 63.00 | 76.85 | 12.60 | 9.79 | 0.65 |
| 221400 | 286.00 | 63.00 | 78.40 | 12.80 | 9.85 | 0.66 |

n.d. = no detect

11.2.6  Well NT01 – Second campaign

| Detection limit | < 1.0 | < 1.0 | < 1.0 | < 1.0 | < 1.0 | < 1.0 | < 1.0 | < 0.1 | < 0.1 | < 0.1 | < 0.1 | < 0.2 | < 0.1 |
|---|---|---|---|---|---|---|---|---|---|---|---|---|---|
| Pumping time | Sulfate | Chloride | Nitrate | Fluorine | Nitrit | Phosphate | Bromimine | Calcium | Magnesium | Sodium | Potassium | Iron (II) | Manganese (II) |
| [s] | [mg l$^{-1}$] | [mg l$^{-1}$] | [mg l$^{-1}$] | [mg l$^{-1}$] | [mg l$^{-1}$] | [mg l$^{-1}$] | [mg l$^{-1}$] | [mg l$^{-1}$] | [mg l$^{-1}$] | [mg l$^{-1}$] | [mg l$^{-1}$] | [mg l$^{-1}$] | [mg l$^{-1}$] |
| 300 | 408.59 | 154.61 | 3.28 | n.d. | n.d. | n.d. | n.d. | 293.00 | 60.00 | 85.50 | 13.00 | 10.53 | 0.68 |
| 1800 | 399.09 | 147.64 | 1.48 | n.d. | n.d. | n.d. | n.d. | 281.00 | 57.00 | 79.45 | 13.20 | 10.36 | 0.70 |
| 3600 | 399.21 | 147.28 | n.d. | n.d. | n.d. | n.d. | n.d. | 273.00 | 57.00 | 81.65 | 12.20 | 11.58 | 0.71 |
| 6300 | 396.01 | 147.77 | 1.55 | n.d. | n.d. | n.d. | n.d. | 285.00 | 58.00 | 81.65 | 12.30 | 10.26 | 0.71 |
| 9000 | 400.58 | 147.95 | n.d. | n.d. | n.d. | n.d. | n.d. | 283.00 | 56.00 | 92.85 | 13.10 | 11.13 | 0.70 |
| 12600 | 395.39 | 147.17 | n.d. | n.d. | n.d. | n.d. | n.d. | 286.00 | 58.00 | 84.65 | 13.10 | 10.54 | 0.69 |
| 17100 | 401.02 | 147.84 | 2.61 | n.d. | n.d. | n.d. | n.d. | 277.00 | 58.00 | 79.65 | 12.70 | 11.22 | 0.70 |
| 21600 | 390.94 | 146.54 | n.d. | n.d. | n.d. | n.d. | n.d. | 280.00 | 56.00 | 86.50 | 12.50 | 10.63 | 0.70 |
| 27000 | 399.82 | 147.75 | 2.55 | n.d. | n.d. | n.d. | n.d. | 278.00 | 57.00 | 83.75 | 12.50 | 10.54 | 0.68 |
| 32400 | 395.74 | 148.32 | 1.73 | n.d. | n.d. | n.d. | n.d. | 275.00 | 56.00 | 82.90 | 13.00 | 10.55 | 0.69 |
| 38700 | 392.85 | 148.31 | n.d. | n.d. | n.d. | n.d. | n.d. | 281.00 | 57.00 | 85.45 | 12.90 | 10.99 | 0.69 |
| 46512 | 392.56 | 147.49 | n.d. | n.d. | n.d. | n.d. | n.d. | 272.00 | 58.00 | 84.45 | 12.60 | 10.49 | 0.69 |
| 69300 | 400.26 | 152.08 | n.d. | n.d. | n.d. | n.d. | n.d. | 285.00 | 57.00 | 85.95 | 12.70 | 10.69 | 0.69 |
| 80100 | 398.12 | 149.00 | 1.88 | n.d. | n.d. | n.d. | n.d. | 285.00 | 57.00 | 86.40 | 12.60 | 10.72 | 0.70 |
| 90000 | 389.93 | 149.33 | n.d. | n.d. | n.d. | n.d. | n.d. | 277.00 | 55.00 | 82.80 | 12.60 | 10.38 | 0.62 |
| 98100 | 390.26 | 149.09 | n.d. | n.d. | n.d. | n.d. | n.d. | 277.00 | 56.00 | 84.75 | 12.30 | 10.94 | 0.61 |
| 108900 | 392.77 | 148.67 | n.d. | n.d. | n.d. | n.d. | n.d. | 281.00 | 55.00 | 82.00 | 12.40 | 10.37 | 0.64 |
| 119700 | 389.40 | 148.46 | n.d. | n.d. | n.d. | n.d. | n.d. | 273.00 | 54.00 | 81.65 | 12.20 | 10.05 | 0.66 |
| 131400 | 392.04 | 155.58 | 2.36 | n.d. | n.d. | n.d. | n.d. | 278.00 | 55.00 | 78.90 | 12.20 | 9.90 | 0.68 |
| 156600 | 390.82 | 149.55 | n.d. | n.d. | n.d. | n.d. | n.d. | 265.00 | 55.00 | 80.60 | 12.30 | 9.95 | 0.65 |
| 170100 | 388.56 | 149.99 | n.d. | n.d. | n.d. | n.d. | n.d. | 285.00 | 57.00 | 85.40 | 12.40 | 9.77 | 0.67 |
| 183600 | 385.65 | 149.00 | n.d. | n.d. | n.d. | n.d. | n.d. | 284.00 | 55.00 | 82.10 | 12.70 | 10.40 | 0.67 |
| 199800 | 386.12 | 149.03 | n.d. | n.d. | n.d. | n.d. | n.d. | 286.00 | 55.00 | 80.15 | 12.40 | 9.70 | 0.67 |
| 213300 | 388.92 | 149.27 | n.d. | n.d. | n.d. | n.d. | n.d. | 283.00 | 55.00 | 81.55 | 12.40 | 9.65 | 0.67 |
| 243900 | 387.73 | 150.10 | n.d. | n.d. | n.d. | n.d. | n.d. | 277.00 | 55.00 | 79.40 | 12.40 | 9.90 | 0.66 |
| 261900 | 378.98 | 145.84 | n.d. | n.d. | n.d. | n.d. | n.d. | 277.00 | 54.00 | 81.40 | 12.60 | 9.80 | 0.66 |
| 276588 | 379.28 | 145.79 | n.d. | n.d. | n.d. | n.d. | n.d. | 286.00 | 55.00 | 81.60 | 12.60 | 9.80 | 0.65 |
| 296100 | 383.12 | 147.42 | n.d. | n.d. | n.d. | n.d. | n.d. | 279.00 | 54.00 | 82.30 | 12.70 | 9.65 | 0.65 |
| 334800 | 382.03 | 148.13 | n.d. | n.d. | n.d. | n.d. | n.d. | 273.00 | 54.00 | 83.80 | 12.80 | 9.65 | 0.63 |
| 352800 | 385.61 | 149.47 | n.d. | n.d. | n.d. | n.d. | n.d. | 278.00 | 54.00 | 81.15 | 12.40 | 9.55 | 0.63 |
| 373500 | 387.50 | 150.96 | n.d. | n.d. | n.d. | n.d. | n.d. | 283.00 | 59.00 | 81.75 | 12.80 | 9.50 | 0.62 |
| 392112 | 388.87 | 151.65 | n.d. | n.d. | n.d. | n.d. | n.d. | 271.00 | 53.00 | 79.30 | 12.90 | 9.70 | 0.63 |
| 434988 | 384.29 | 150.01 | n.d. | n.d. | n.d. | n.d. | n.d. | 281.00 | 57.00 | 83.70 | 13.00 | 9.60 | 0.61 |
| n.d. = no detect | | | | | | | | | | | | | |

Table 11.23: Concentration-time series of inorganic solutes at well NT01 – Second campaign

| Detection limit | < 1.0 | < 1.0 | < 1.0 | < 1.0 | < 1.0 | < 1.0 | < 1.0 | < 0.1 | < 0.1 | < 0.1 | < 0.1 | < 0.2 | < 0.1 |
|---|---|---|---|---|---|---|---|---|---|---|---|---|---|
| Pumping time | Sulfate | Chloride | Nitrate | Fluorine | Nitrit | Phosphate | Bromimine | Calcium | Magnesium | Sodium | Potassium | Iron (II) | Manganese (II) |
| [s] | [mg l$^{-1}$] | [mg l$^{-1}$] | [mg l$^{-1}$] | [mg l$^{-1}$] | [mg l$^{-1}$] | [mg l$^{-1}$] | [mg l$^{-1}$] | [mg l$^{-1}$] | [mg l$^{-1}$] | [mg l$^{-1}$] | [mg l$^{-1}$] | [mg l$^{-1}$] | [mg l$^{-1}$] |
| 900 | 342.53 | 208.89 | n.d. | n.d. | n.d. | n.d. | n.d. | 276.00 | 69.00 | 156.00 | 43.50 | 12.34 | 1.30 |
| 1800 | 348.93 | 212.57 | n.d. | n.d. | n.d. | n.d. | n.d. | 266.00 | 66.00 | 147.40 | 40.50 | 11.86 | 1.31 |
| 3600 | 360.80 | 219.44 | n.d. | n.d. | n.d. | n.d. | n.d. | 261.00 | 64.00 | 165.50 | 40.00 | 11.63 | 1.35 |
| 5400 | 369.07 | 221.52 | n.d. | n.d. | n.d. | n.d. | n.d. | 266.00 | 65.00 | 176.70 | 39.50 | 11.63 | 1.37 |
| 7200 | 374.57 | 226.28 | n.d. | n.d. | n.d. | n.d. | n.d. | 265.00 | 65.00 | 154.50 | 37.50 | 11.74 | 1.34 |
| 9000 | 378.40 | 224.11 | n.d. | n.d. | n.d. | n.d. | n.d. | 280.00 | 64.00 | 168.80 | 37.50 | 11.53 | 1.31 |
| 12600 | 387.16 | 224.27 | n.d. | n.d. | n.d. | n.d. | n.d. | 282.00 | 63.00 | 170.40 | 37.00 | 11.33 | 1.33 |
| 15012 | 388.16 | 224.85 | n.d. | n.d. | n.d. | n.d. | n.d. | 284.00 | 63.00 | 172.70 | 37.50 | 11.15 | 1.41 |
| 16812 | 391.17 | 224.78 | n.d. | n.d. | n.d. | n.d. | n.d. | 286.00 | 64.00 | 170.70 | 36.50 | 11.38 | 1.44 |
| 19800 | 391.93 | 223.93 | n.d. | n.d. | n.d. | n.d. | n.d. | 288.00 | 63.00 | 169.10 | 38.50 | 11.42 | 1.48 |
| 23400 | 396.82 | 224.31 | n.d. | n.d. | n.d. | n.d. | n.d. | 306.00 | 64.00 | 151.20 | 37.00 | 11.42 | 1.48 |
| 27000 | 402.06 | 225.11 | n.d. | n.d. | n.d. | n.d. | n.d. | 297.00 | 64.00 | 156.50 | 45.50 | 11.06 | 1.47 |
| 32400 | 408.89 | 229.52 | n.d. | n.d. | n.d. | n.d. | n.d. | 313.00 | 66.00 | 156.80 | 36.50 | 10.91 | 1.51 |
| 36900 | 408.29 | 229.23 | n.d. | n.d. | n.d. | n.d. | n.d. | 312.00 | 64.00 | 165.10 | 36.00 | 10.90 | 1.51 |
| 42300 | 411.54 | 229.15 | n.d. | n.d. | n.d. | n.d. | n.d. | 324.00 | 62.00 | 154.50 | 36.00 | 10.92 | 1.53 |
| 47700 | 411.08 | 227.68 | n.d. | n.d. | n.d. | n.d. | n.d. | 298.00 | 64.00 | 175.40 | 36.50 | 10.78 | 1.51 |
| 53100 | 412.73 | 228.02 | n.d. | n.d. | n.d. | n.d. | n.d. | 295.00 | 63.00 | 165.90 | 32.00 | 11.22 | 1.47 |
| 74412 | 414.08 | 226.74 | n.d. | n.d. | n.d. | n.d. | n.d. | 306.00 | 63.00 | 149.00 | 34.00 | 10.95 | 1.48 |
| 80100 | 417.86 | 227.68 | n.d. | n.d. | n.d. | n.d. | n.d. | 299.00 | 64.00 | 163.40 | 34.00 | 10.76 | 1.46 |
| 87300 | 417.66 | 226.20 | n.d. | n.d. | n.d. | n.d. | n.d. | 308.00 | 65.00 | 154.70 | 36.50 | 10.74 | 1.46 |
| 95400 | 419.24 | 226.77 | n.d. | n.d. | n.d. | n.d. | n.d. | 300.00 | 64.00 | 162.60 | 37.00 | 11.29 | 1.48 |
| 102600 | 422.04 | 226.44 | n.d. | n.d. | n.d. | n.d. | n.d. | 308.00 | 64.00 | 140.70 | 35.00 | 10.83 | 1.49 |
| 110700 | 419.83 | 225.21 | n.d. | n.d. | n.d. | n.d. | n.d. | 313.00 | 64.00 | 155.70 | 36.00 | 11.08 | 1.49 |
| 119700 | 423.19 | 224.86 | n.d. | n.d. | n.d. | n.d. | n.d. | 308.00 | 64.00 | 163.40 | 36.50 | 10.18 | 1.51 |
| 128700 | 424.05 | 224.00 | n.d. | n.d. | n.d. | n.d. | n.d. | 316.00 | 66.00 | 164.10 | 37.50 | 10.46 | 1.44 |
| 137988 | 424.36 | 222.86 | n.d. | n.d. | n.d. | n.d. | n.d. | 319.00 | 65.00 | 147.00 | 40.50 | 10.80 | 1.43 |
| 157500 | 421.26 | 222.46 | n.d. | n.d. | n.d. | n.d. | n.d. | 296.00 | 64.00 | 145.90 | 38.00 | 10.59 | 1.43 |
| 169200 | 429.73 | 222.33 | n.d. | n.d. | n.d. | n.d. | n.d. | 302.00 | 65.00 | 149.00 | 39.50 | 11.42 | 1.44 |
| 179388 | 417.27 | 216.97 | n.d. | n.d. | n.d. | n.d. | n.d. | 316.00 | 65.00 | 126.10 | 30.40 | 10.52 | 1.47 |
| 189900 | 412.78 | 215.11 | n.d. | n.d. | n.d. | n.d. | n.d. | 309.00 | 63.00 | 124.90 | 28.00 | 10.59 | 1.47 |
| 200700 | 422.22 | 217.61 | n.d. | n.d. | n.d. | n.d. | n.d. | 308.00 | 62.00 | 123.30 | 27.80 | 10.15 | 1.49 |
| 212400 | 421.06 | 216.52 | n.d. | n.d. | n.d. | n.d. | n.d. | 317.00 | 62.00 | 124.00 | 28.40 | 10.60 | 1.50 |
| 249300 | 422.11 | 215.62 | n.d. | n.d. | n.d. | n.d. | n.d. | 313.00 | 62.00 | 120.70 | 28.20 | 10.15 | 1.52 |
| 262188 | 418.22 | 211.16 | n.d. | n.d. | n.d. | n.d. | n.d. | 312.00 | 62.00 | 117.40 | 28.20 | 10.21 | 1.51 |
| n.d. = no detect | | | | | | | | | | | | | |

| Detection limit | < 1.0 | < 1.0 | < 1.0 | < 1.0 | < 1.0 | < 1.0 | < 1.0 | < 0.1 | < 0.1 | < 0.1 | < 0.1 | < 0.2 | < 0.1 |
|---|---|---|---|---|---|---|---|---|---|---|---|---|---|
| Pumping time | Sulfate | Chloride | Nitrate | Fluorine | Nitrit | Phosphate | Bromimine | Calcium | Magnesium | Sodium | Potassium | Iron (II) | Manganese (II) |
| [s] | [mg l$^{-1}$] | [mg l$^{-1}$] | [mg l$^{-1}$] | [mg l$^{-1}$] | [mg l$^{-1}$] | [mg l$^{-1}$] | [mg l$^{-1}$] | [mg l$^{-1}$] | [mg l$^{-1}$] | [mg l$^{-1}$] | [mg l$^{-1}$] | [mg l$^{-1}$] | [mg l$^{-1}$] |
| 299 | 57.66 | 28.71 | 4.10 | n.d. | n.d. | n.d. | n.d. | 163.00 | 52.00 | 32.80 | 35.50 | 4.50 | 0.28 |
| 1800 | 65.62 | 23.73 | n.d. | n.d. | n.d. | n.d. | n.d. | 240.00 | 79.00 | 37.55 | 55.00 | 5.48 | 0.39 |
| 5400 | 56.46 | 28.52 | n.d. | n.d. | n.d. | n.d. | n.d. | 232.00 | 79.00 | 38.00 | 55.50 | 4.70 | 0.34 |
| 12600 | 53.66 | 33.40 | n.d. | n.d. | n.d. | n.d. | n.d. | 221.00 | 79.00 | 39.70 | 59.00 | 4.63 | 0.31 |
| 22788 | 51.89 | 33.67 | n.d. | n.d. | n.d. | n.d. | n.d. | 219.00 | 81.00 | 54.70 | 79.00 | 5.42 | 0.27 |
| 35100 | 56.81 | 35.13 | n.d. | n.d. | n.d. | n.d. | n.d. | 221.00 | 84.00 | 41.40 | 62.50 | 4.74 | 0.26 |
| 50400 | 55.09 | 35.83 | n.d. | n.d. | n.d. | n.d. | n.d. | 231.00 | 82.00 | 41.30 | 63.00 | 4.59 | 0.24 |
| 68400 | 55.42 | 36.11 | n.d. | n.d. | n.d. | n.d. | n.d. | 226.00 | 82.00 | 41.75 | 63.50 | 4.31 | 0.26 |
| 91188 | 56.41 | 36.44 | n.d. | n.d. | n.d. | n.d. | n.d. | 222.00 | 82.00 | 41.35 | 63.50 | 5.47 | 0.29 |
| 110700 | 53.76 | 36.64 | n.d. | n.d. | n.d. | n.d. | n.d. | 216.00 | 82.00 | 42.00 | 63.50 | 4.35 | 0.24 |
| 177300 | 53.03 | 37.67 | n.d. | n.d. | n.d. | n.d. | n.d. | 208.00 | 82.00 | 48.00 | 73.50 | 4.31 | 0.23 |
| n.d. = no detect | | | | | | | | | | | | | |

Table 11.24: Concentration-time series of inorganic solutes at well B72

| Detection limit | < 1.0 | < 1.0 | < 1.0 | < 1.0 | < 1.0 | < 1.0 | < 1.0 | < 0.1 | < 0.1 | < 0.1 | < 0.1 | < 0.2 | < 0.1 |
|---|---|---|---|---|---|---|---|---|---|---|---|---|---|
| Pumping time | Sulfate | Chloride | Nitrate | Fluorine | Nitrit | Phosphate | Bromimine | Calcium | Magnesium | Sodium | Potassium | Iron (II) | Manganese (II) |
| [s] | [mg l$^{-1}$] | [mg l$^{-1}$] | [mg l$^{-1}$] | [mg l$^{-1}$] | [mg l$^{-1}$] | [mg l$^{-1}$] | [mg l$^{-1}$] | [mg l$^{-1}$] | [mg l$^{-1}$] | [mg l$^{-1}$] | [mg l$^{-1}$] | [mg l$^{-1}$] | [mg l$^{-1}$] |
| 1188 | 494.86 | 179.37 | 6.24 | n.d. | n.d. | n.d. | n.d. | 325.00 | 47.00 | 134.00 | 20.00 | 6.76 | 0.98 |
| 2700 | 432.68 | 179.13 | 4.73 | n.d. | n.d. | n.d. | n.d. | 311.00 | 43.50 | 115.30 | 21.60 | 5.24 | 0.90 |
| 4500 | 413.44 | 180.88 | 5.03 | n.d. | n.d. | n.d. | n.d. | 287.00 | 42.00 | 129.50 | 19.20 | 4.85 | 0.86 |
| 7200 | 381.39 | 172.74 | 4.00 | n.d. | n.d. | n.d. | n.d. | 279.00 | 39.50 | 128.40 | 19.60 | 4.52 | 0.83 |
| 10800 | 371.58 | 173.61 | 4.01 | n.d. | n.d. | n.d. | n.d. | 272.00 | 39.00 | 134.50 | 19.60 | 4.22 | 0.78 |
| 15300 | 357.51 | 171.06 | 3.74 | n.d. | n.d. | n.d. | n.d. | 255.00 | 38.50 | 129.50 | 19.70 | 4.10 | 0.80 |
| 20700 | 353.59 | 172.68 | 3.53 | n.d. | n.d. | n.d. | n.d. | 261.00 | 39.00 | 137.20 | 19.00 | 3.92 | 0.73 |
| 25200 | 354.55 | 172.46 | 3.66 | n.d. | n.d. | n.d. | n.d. | 263.00 | 37.50 | 134.20 | 19.10 | 3.90 | 0.70 |
| 32112 | 348.40 | 171.29 | 2.79 | n.d. | n.d. | n.d. | n.d. | 264.00 | 38.50 | 131.30 | 19.30 | 3.86 | 0.66 |
| 38700 | 340.65 | 169.02 | 2.69 | n.d. | n.d. | n.d. | n.d. | 249.00 | 37.00 | 130.80 | 19.20 | 3.80 | 0.70 |
| 45000 | 335.88 | 167.95 | 4.50 | n.d. | n.d. | n.d. | n.d. | 258.00 | 39.00 | 140.20 | 21.20 | 3.78 | 0.69 |
| 70200 | 321.64 | 162.97 | 2.07 | n.d. | n.d. | n.d. | n.d. | 256.00 | 37.50 | 127.40 | 20.00 | 3.74 | 0.68 |
| 79200 | 318.66 | 162.07 | 2.23 | n.d. | n.d. | n.d. | n.d. | 244.00 | 35.50 | 127.10 | 20.80 | 3.70 | 0.65 |
| 89100 | 312.38 | 158.13 | 1.84 | n.d. | n.d. | n.d. | n.d. | 259.00 | 35.50 | 126.20 | 20.40 | 3.72 | 0.59 |
| 100800 | 303.70 | 162.66 | 1.98 | n.d. | n.d. | n.d. | n.d. | 255.00 | 35.50 | 118.50 | 20.00 | 3.55 | 0.56 |
| 112212 | 303.56 | 154.48 | 1.50 | n.d. | n.d. | n.d. | n.d. | 245.00 | 35.50 | 119.80 | 20.20 | 3.51 | 0.56 |
| 122400 | 299.77 | 152.42 | n.d. | n.d. | n.d. | n.d. | n.d. | 252.00 | 35.50 | 113.50 | 18.60 | 3.60 | 0.53 |
| 134100 | 299.48 | 151.76 | 1.51 | n.d. | n.d. | n.d. | n.d. | 248.00 | 34.50 | 113.10 | 19.40 | 3.31 | 0.51 |
| 160200 | 299.61 | 151.02 | 1.22 | n.d. | n.d. | n.d. | n.d. | 203.00 | 34.00 | 107.70 | 20.40 | 3.40 | 0.53 |
| 177012 | 298.88 | 149.92 | n.d. | n.d. | n.d. | n.d. | n.d. | 220.00 | 34.00 | 111.00 | 19.20 | 3.45 | 0.65 |
| 189000 | 291.40 | 148.48 | n.d. | n.d. | n.d. | n.d. | n.d. | 204.00 | 33.50 | 115.60 | 20.00 | 3.42 | 0.63 |
| 203400 | 293.38 | 147.28 | n.d. | n.d. | n.d. | n.d. | n.d. | 208.00 | 34.50 | 115.40 | 19.40 | 3.41 | 0.61 |
| 219600 | 293.04 | 146.53 | n.d. | n.d. | n.d. | n.d. | n.d. | 220.00 | 34.00 | 109.30 | 19.80 | 3.30 | 0.61 |
| 237888 | 291.30 | 145.11 | n.d. | n.d. | n.d. | n.d. | n.d. | 222.00 | 33.50 | 106.70 | 18.80 | 3.33 | 0.59 |
| 252000 | 291.00 | 145.93 | 1.03 | n.d. | n.d. | n.d. | n.d. | 211.00 | 33.50 | 104.30 | 19.20 | 3.23 | 0.57 |
| 269100 | 291.72 | 146.02 | 0.99 | n.d. | n.d. | n.d. | n.d. | 207.00 | 33.00 | 102.70 | 18.40 | 3.23 | 0.58 |
| 287100 | 289.89 | 144.50 | n.d. | n.d. | n.d. | n.d. | n.d. | 213.00 | 34.00 | 102.50 | 18.80 | 3.20 | 0.54 |
| 326088 | 288.67 | 143.85 | n.d. | n.d. | n.d. | n.d. | n.d. | 195.00 | 33.00 | 100.50 | 19.20 | 3.25 | 0.49 |
| 343800 | 287.67 | 142.79 | n.d. | n.d. | n.d. | n.d. | n.d. | 203.00 | 34.50 | 98.50 | 19.00 | 3.17 | 0.58 |
| 364500 | 286.56 | 142.41 | n.d. | n.d. | n.d. | n.d. | n.d. | 213.00 | 32.50 | 97.50 | 18.80 | 3.14 | 0.57 |
| 385200 | 285.72 | 141.62 | n.d. | n.d. | n.d. | n.d. | n.d. | 220.00 | 32.00 | 98.10 | 18.40 | 3.08 | 0.57 |
| 432900 | 284.81 | 140.48 | n.d. | n.d. | n.d. | n.d. | n.d. | 219.00 | 32.50 | 96.70 | 18.40 | 3.31 | 0.60 |
| n.d. = no detect | | | | | | | | | | | | | |

Table 11.25: Concentration-time series of inorganic solutes at well B2069

## 11.3 Physical field parameters

### 11.3.1 Well B42

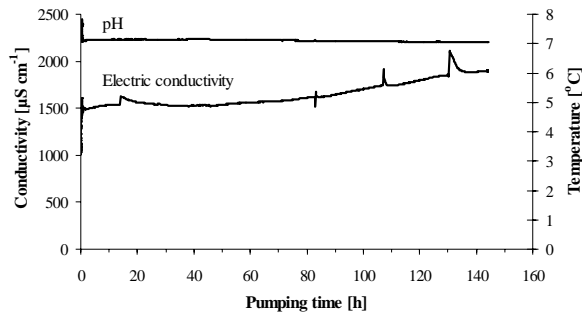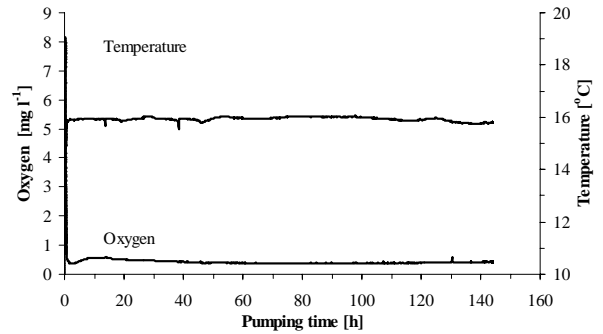Figure 11.1: Time series of electric conductivity and temperature at well B42

Figure 11.2: Time series of oxygen and temperature at well B42

### 11.3.2 Well P2

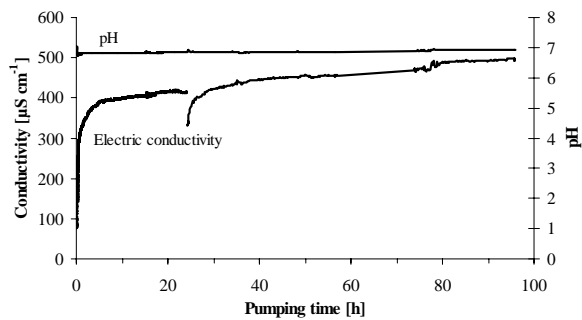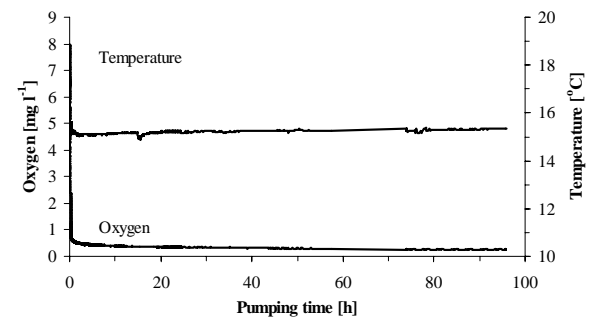Figure 11.3: Time series electric conductivity and pH at well P2

Figure 11.4: Time series of oxygen content and temperature at well P2

### 11.3.3 Well B41

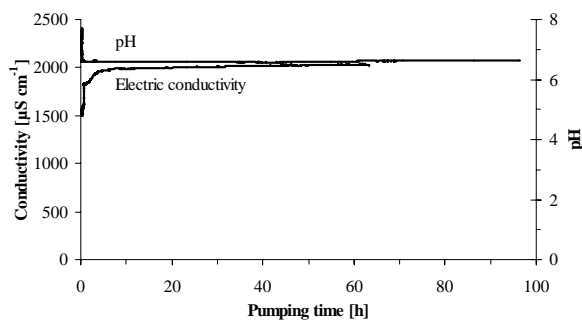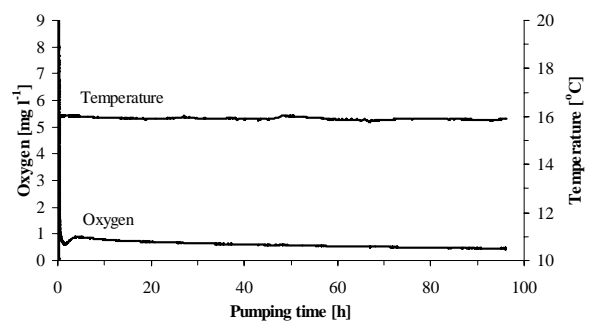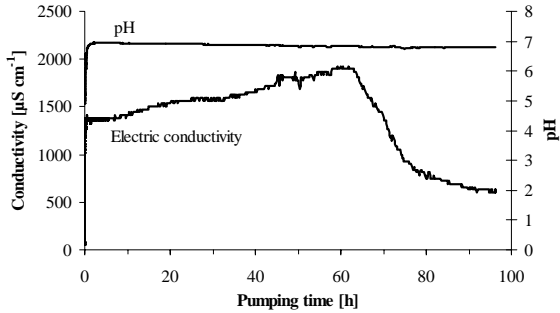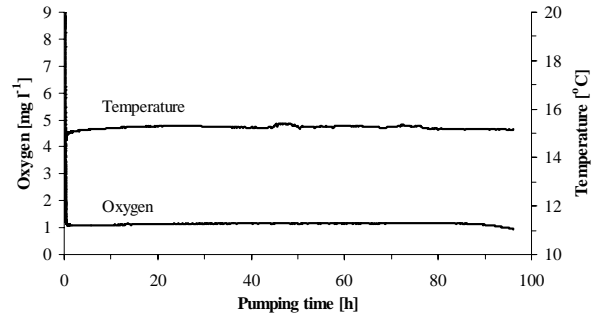Figure 11.5: Time series of electric conductivity and pH at well B41

Figure 11.6: Time series of oxygen and temperature at well B41

149

## 11.3.4 Well P1

Figure 11.7: Time series of electric conductivity and pH at well P1



Figure 11.8: Time series of oxygen and temperature at well P1



## 11.3.5 Well NT01 – First campaign

Figure 11.9: Time series of electric conductivity and pH at well NT01 during the first pumping campaign
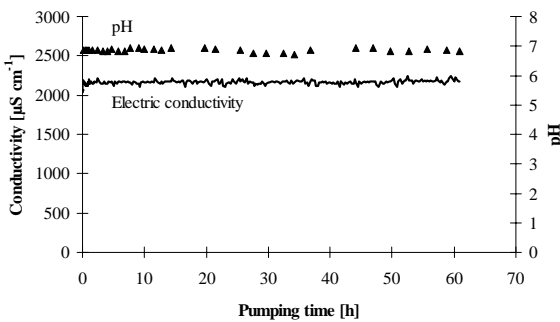


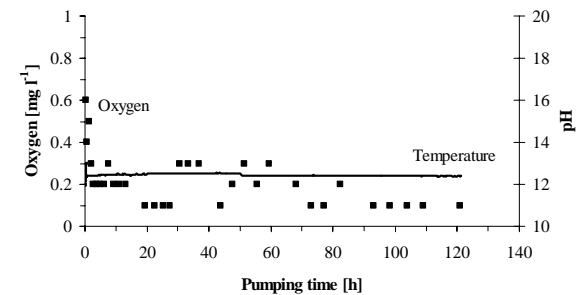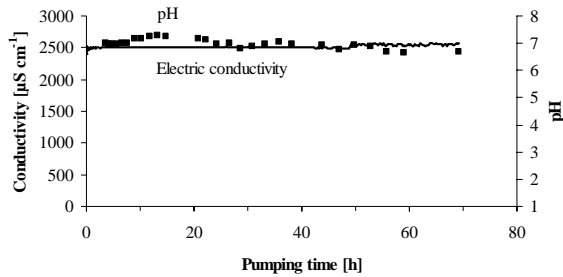Figure 11.10: Time series of oxygen and temperature at well NT01 during the first pumping campaign
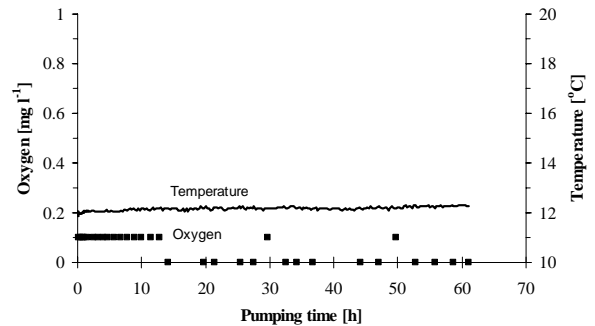


## 11.3.6 Well NT01 – Second Campaign

Figure 11.11: Time series of electric conductivity and pH at well NT01 during the second pumping campaign
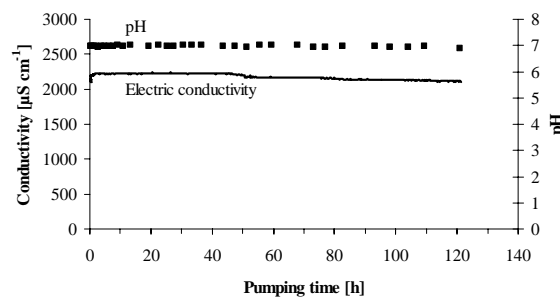


Figure 11.12: Time series of oxygen and temperature at well NT01 during the second pumping campaign

## 11.3.7 Well B73

Figure 11.13: Time series of electric conductivity and pH at well B73
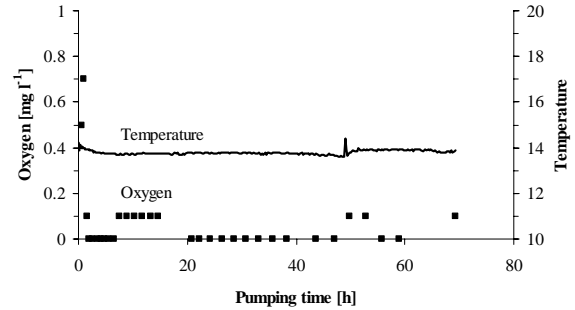


Figure 11.14: Time series of oxygen and temperature at well B73



## 11.3.8 Well B72

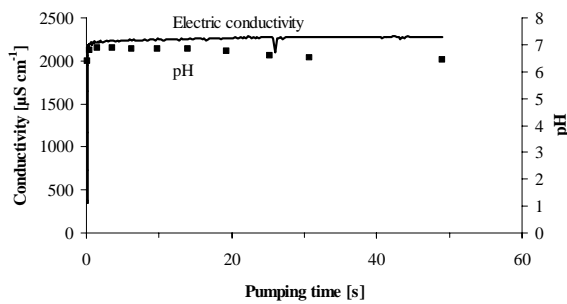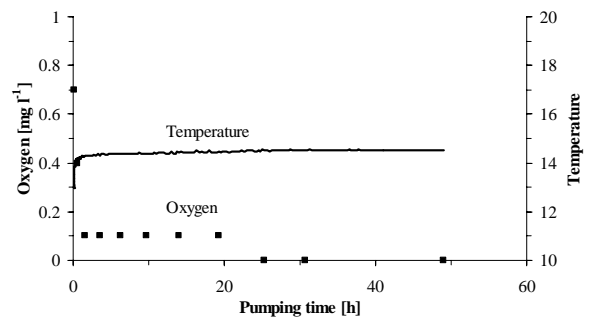Figure 11.15: Time series of electric conductivity and pH at well B72



Figure 11.16: Time series of oxygen and temperature at well B72



## 11.3.9 Well B2069

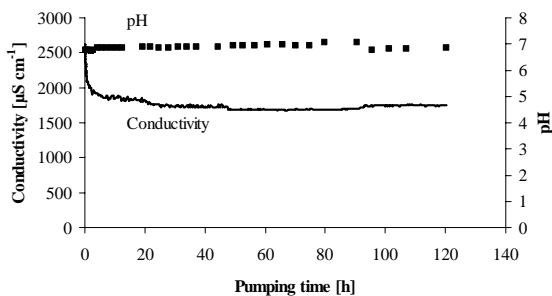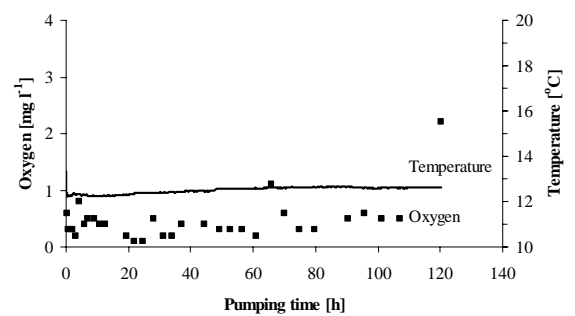Figure 11.17: Time series of electric conductivity and pH at well B2069



Figure 11.18: Time series of oxygen and temperature at well B2069

152

| | |
|---|---|
| Name, Vorname: | Bockelmann, Mark <u>Alexander</u> |
| Geburtsdatum: | 23.01.1974 |
| Geburtsort: | Hamburg |

## Bildungsgang

08/1985 - 06/1993:   Besuch des Heilwig-Gymnasiums Hamburg, Abschluss: Abitur

10/1994 - 08/1997:   Studium der Geoökologie an der Universität Bayreuth, Abschluss: Vordiplom-Geoökologie

09/1997 – 07/1998:   Studium der Environmental Sciences an der University of East Anglia, Abschluss: Master of Science in Environmental Sciences

Thema der Master Thesis:

*Trace elements in groundwater, surface and drinking water in a calcareous catchment in the UK*

01/1999 - 08/2001:   wissenschaftlicher Mitarbeiter im DFG-SSP 546 an der Eberhard Karls Universität Tübingen

bis 08/2001:   Promotion am Institut und Museum für Geologie und Paläontologie der Universität Tübingen (Arbeitsbereich Angewandte Geologie, Prof. Dr. Georg Teutsch)